Quality Assurance of
Superficial Hyperthermia Treatments

Quality assurance of superficial hyperthermia treatments
M. de Bruijne
PhD thesis Erasmus University Rotterdam – with summary in Dutch
ISBN 978-90-6464-492-4

Quality Assurance of
Superficial Hyperthermia Treatments

Kwaliteitsborging van oppervlakkige hyperthermie behandelingen

Proefschrift

ter verkrijging van de graad van doctor aan de

Erasmus Universiteit Rotterdam

op gezag van de rector magnificus

Prof.dr. H.G. Schmidt

en volgens besluit van het College voor Promoties.

De openbare verdediging zal plaatsvinden op

woensdag 21 september 2011 om 11.30 uur

door

Maarten de Bruijne

geboren te Ede

ERASMUS UNIVERSITEIT ROTTERDAM

Promotiecommissie

voor Pa

Contents

1
Introduction

Hyperthermia

Hyperthermia treatments

In hyperthermia, tumour-loaded tissue is heated to a supraphysiological level of 40-45 °C. Hyperthermia is a well-established adjuvant to radiotherapy and/or chemotherapy. Hyperthermia causes direct cytotoxicity and has effect on tumour blood flow and oxygenation, which may enhance the other treatment modality. Further, hyperthermia sensitizes cells to both radiotherapy and chemotherapy, among other things by inhibition of DNA repair processes. The efficacy of hyperthermia has been demonstrated in randomized trials for multiple cancer types [1-18].

Several heating techniques and devices exist to heat tumours at different sites: deep-regional and part-body hyperthermia, local hyperthermia, interstitial and endocavitary hyperthermia, and whole body hyperthermia [19]. The Erasmus MC – Daniel den Hoed Cancer Center has three treatment modes available, all of which use electromagnetic waves to heat tissue. Tumours in the pelvic region (deep hyperthermia) can be heated using the BSD-2000 system (BSD Medical, USA). The in-house developed Lucite cone applicator system can heat tumours at the body surface (superficial hyperthermia). Recently, also a specific system has been developed to heat tumours in the head and neck region [20].

The scope of this thesis is limited to superficial hyperthermia (SHT). Therefore, the next sections will focus on the clinical context and quality assurance of SHT treatments.

Superficial hyperthermia

The value of adding superficial hyperthermia to radiotherapy (RT) has been demonstrated for various tumour types in multiple randomized clinical trials. The results have been summarized in Table 1, and show significant improvements of clinical response in six out of seven trials. The greatest benefit of adding hyperthermia to radiotherapy is seen in previously irradiated patients. For example, previously irradiated patients in the study by Jones *et al*. [16] had a complete response (CR) rate of 24% in the no-HT arm versus 68% in the HT arm, and in the ESHO trial (published in [11]) the CR rates were 38% for re-RT alone, and 78% for re-RT + HT. Superficial hyperthermia is mostly applied in combination with radiotherapy in the treatment of locally advanced breast carcinoma [11,16], malignant melanoma [9], and advanced neck nodes [2,7].

During superficial hyperthermia, tumours and surrounding tissue at the body surface (in Rotterdam up to ~4 cm depth) are heated. The heating devices, or applicators, are antennas that emit non-ionizing electromagnetic fields in the frequency range of 300 – 915 MHz. One or multiple applicators are positioned on the body surface to cover the whole treatment area. A water layer, the waterbolus, is placed between the applicators and the
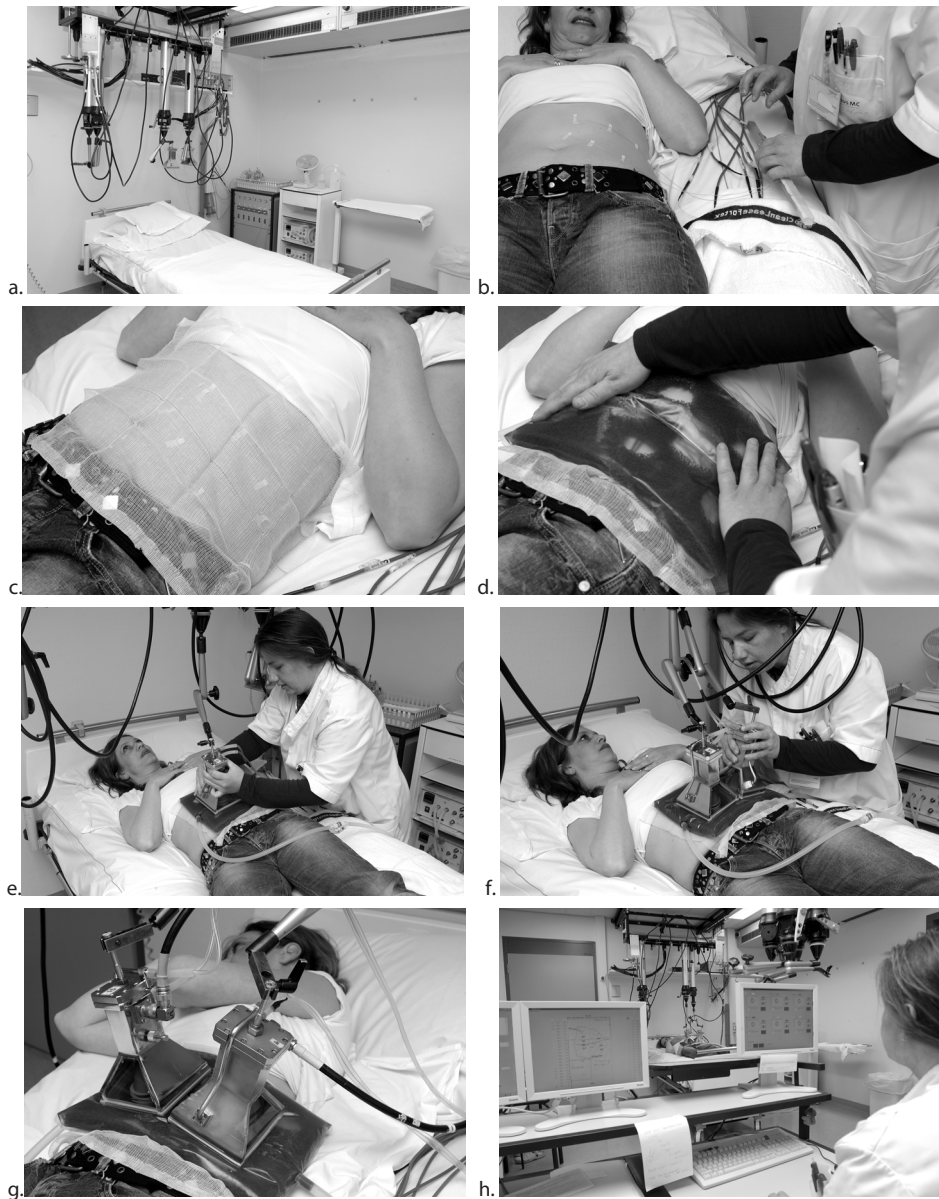
Figure 1. (a) Superficial hyperthermia equipment in the treatment room: bed, unipods for applicator positioning, thermometry probes, applicators, applicator perfusion unit, fan for patient's comfort, thermo-circulators for the water boli. (b-g) Example set-up of a 2×1 applicator array on the patient. (b) thermometry probes are attached to the skin and placed in the interstitial catheters (not shown). (c-d) The skin is covered with a wet gauze before the waterbolus is placed. (e-f) The applicators are positioned one by one. (g) The power cables are connected to the applicators. (h) Treatment from the perspective of the technician: on the left the monitors for tissue temperature observation and on the right the power steering user interface.

skin. Temperature sensors are placed on the skin and in interstitial catheters to observe the temperature distribution during treatments. The heating starts when power is applied to the applicators. The treatment room for superficial hyperthermia, the equipment and the setup of an applicator array are depicted in Figure 1.

Today, national guidelines prescribe reirradiation and hyperthermia for recurrent breast cancer in previously irradiated areas in the Netherlands [22]. Also, hyperthermia is considered a regular addition to radiotherapy for irresectable malignant melanoma. Because superficial hyperthermia is a local treatment, it usually will not enhance overall survival for these indications. However, as a palliative treatment it provides an important gain for patients because symptoms like ulceration, bleeding, severe pain, and the stress of watching a tumour grow at the body surface are relieved [23, 24].

Table 1. Results of published randomized clinical trials in superficial hyperthermia.

Study	Tumour	N	Endpoint	RT	RT + HT	Significant difference
Jones *et al.* (2005) [16]	Various [a]	122 patients	Complete response	42%	66%	Yes
International Collaborative Hyperthermia Group (1996) [11]	Breast cancer	308 patients	Complete response	41%	59%	Yes
Overgaard *et al.* (1995) [9]	Melanoma	128 lesions	Complete response	35%	62%	Yes
			2-year local control	28%	46%	Yes
Valdagni *et al.* (1994) [7]	Lymphnodes of head and neck tumours	41 patients	Complete response	41%	83%	Yes
			5-year local control	24%	69%	Yes
			5-year survival	0%	53%	Yes
Perez *et al.* (1991) [21]	Various [b]	236 patients	Complete response	30%	32%	No
Egawa *et al.* (1989) [18]	Various	92 patients	Response	63%	82%	Yes

(a) breast 65%, head and neck 13%; melanoma 10%; other 12%.
(b) breast 42%; head and neck 37%, melanoma 9%; other 12%.

Opportunities for improvement

Hyperthermia is a complex treatment, because prescription of a temperature distribution is not yet clinically realistic and because of the interaction of a number of tumour-, patient-, treatment- and equipment-related factors that all correlate with tumour control. Although the biological rationale for hyperthermia is well established, the anti-tumour mechanisms acting in vivo in different temperature ranges have not been quantified clearly. In addition, different treatment centres use different approaches (e.g. equipment, treatment schedule, thermometry), due to which clinical results are difficult to compare. This leads to a

situation where general agreement is still lacking on a number of aspects of the treatment. The main problem is that a generally applicable quality indicator which assures optimal treatment outcome, has not yet been defined. Even until this gold standard has been defined, a systematic identification of potential quality determinants can be made in order to set up a quality assurance framework for SHT.

Quality Assurance

Definition

Applying a general definition of Quality Assurance (QA) [25] to hyperthermia, it would read: a program for the systematic monitoring and evaluation of the various aspects of a treatment to ensure that standards of quality are being met. QA cannot absolutely guarantee the delivery of optimal quality treatments, but makes this more likely. Two key principles characterise QA: *fit for purpose* (a treatment or device should be suitable for the intended purpose) and *right first time* (mistakes should be eliminated).

Clemenhagen [26] states that QA in the clinic is a very simple process that deals with finding problems and fixing them: quality assurance is simply the systematization, documentation and assessment of certain evaluative activities and should be seen as a stimulus that makes these activities as rigorous and pertinent as possible.

QA guidelines for SHT

QA guidelines for superficial hyperthermia have been defined by the ESHO [27] and by the RTOG [28]. These guidelines cover the technical requirements of thermometry, applicators, waterbolus and data acquisition; clinical aspects are not fully covered. They were compiled about 20 years ago, and reflect the state of the art and the practical possibilities of the 1990s. Although many aspects of the guidelines are timeless, an update is recommended.

QA topics addressed in earlier studies

A number of studies stressed the significance of quality assurance in SHT and gave clear indications of quality determinants.

In a multivariate analysis of patient-, tumour- and treatment-related factors, Lee *et al*. [29] showed that adequate SAR[1] coverage was the most significant factor correlating with local tumour control. Adequate here was quantified as: at least 25% SAR coverage of the deepest and most peripheral portions of the tumour. They showed that even when the temperature of each catheter in tumour tissue had been above 43°C for at least 10 minutes, CR and duration of local control were significantly better when adequate SAR coverage was realised, see Table 2. Logically, the response rates were also significantly higher for patients

---

[1] Specific absorption rate (SAR) is a measure of the rate at which energy is absorbed by the body when exposed to a radio frequency electromagnetic field.

with adequate SAR coverage and high tumour temperatures, than for poor SAR coverage and lower tumour temperatures. Evidently, adequate SAR coverage is a prerequisite for good quality hyperthermia. A simple measure like matching the SAR characteristic of an applicator with a patient's target volume can make a big difference in terms of treatment outcome.

Table 2. Tumour response correlated with SAR coverage and minutes above 43°C [29]. The definition of t43 ≥ 10 minutes is that all tumour catheters had to have at least one hyperthermia session with temperatures above 43°C for at least 10 minutes. SAR coverage ≥ 25% means that the deepest and most distant portions of the tumour had at least 25% SAR coverage.

	SAR coverage < 25%	SAR coverage ≥ 25%
Complete response		
t43 < 10 minutes	18%	64%
t43 ≥ 10 minutes	55%	81%
Total	37%	76%
Local tumour control		
t43 < 10 minutes	6%	57%
t43 ≥ 10 minutes	34%	67%
Total	19%	64%

Rietveld *et al.* [30] compared the tissue temperatures measured below the conventional waveguide applicator (CWA) to those below the Lucite cone applicator (LCA). The latter is an improved design, which has a contiguous 50% SAR contour in array configurations as opposed to local SAR peaks when using conventional waveguide applicators in an array. The alternate use of CWAs and LCAs during treatment series showed that the mean tissue temperature was significantly higher for the LCA (Table 3). At the same time, the temperature difference between the centre and the periphery of the aperture nearly vanished: it was 0.43°C for the CWAs and about zero for the LCAs. These results clearly indicate that a better SAR coverage leads to higher and more homogeneous tissue temperatures in the clinic.

Table 3. Data from the clinical comparison of two antenna types: the conventional waveguide applicator (CWA) and the Lucite cone applicator (LCA) [30]. Explanation of the symbols and abbreviations: SD = standard deviation; P_{avg} = average applicator power; T_{avg} = average interstitial temperature; T_c = interstitial temperature centrally below the applicator aperture; T_p = interstitial temperature in the peripery of the applicator aperture; ΔT_{cp} = temperature difference between centre and periphery of the aperture.

	WGA	LCA	Difference (LCA – WGA)	
	Mean (SD)	Mean (SD)	Mean (SD)	*p*-value
P_{avg} (W)	48 (12)	62 (15)	14 (9)	<0.0001
T_{avg} (°C)	40.90 (0.69)	41.17 (0.55)	0.28 (0.4)	0.004
T_c (°C)	41.26 (0.64)	41.20 (0.59)	-0.03 (0.6)	0.8
T_p (°C)	40.77 (0.81)	41.20 (0.70)	0.43 (0.5)	0.0006
ΔT_{cp} (°C)	0.43 (0.92)	-0.05 (0.96)	-0.49 (0.7)	0.005

Van der Zee *et al.* [24] analysed the clinical results of patients who were treated with 433 and 2450 MHz applicators. They showed that the complete response rate was higher for the 433 MHz equipment, and especially for larger tumours (diameter > 3 cm) this difference was significant (Table 4). In addition, a multivariate regression analysis showed that duration of local control was influenced significantly by two factors: maximum tumour diameter ($\leq$ 3 cm and > 3 cm) and applicator frequency; again the 433 MHz equipment performed better. Further, it appeared that the 433 MHz treatments caused much less acute damage than the higher frequency. The advantage of using 433 MHz instead of 2450 MHz is that the penetration depth is larger at the lower frequency, which can be expected to result in adequate temperature increases in a larger part of the tumour volume. The lower number of burns at 433 MHz can be explained from the better control of skin surface temperatures by a perfused waterbolus, compared to the forced air cooling of the skin applied with the 2450 MHz applicators.

Table 4. Complete response rate in relation to applicator frequency [24]. Significant differences: 87% vs. 65%: $p = 0.017$; 91% vs. 31%: $p = 0.003$; 65% vs. 31%: $p = 0.024$.

	433 MHz equipment	2450 MHz equipment
Complete response	74%	58%
Max. tumour diameter $\leq$ 3 cm	87%	91%
Max. tumour diameter > 3 cm	65%	31%

The studies mentioned above highlight that an adequate hyperthermia technique is essential for clinical outcome. Adequate tissue heating can only be expected if the characteristics of the applicator or applicator array match the target volume. The key factors identified so far are: (*i*) good SAR coverage of the whole target area, (*ii*) sufficient penetration depth to achieve decent SAR coverage at depth and (*iii*) efficacious control of the skin cooling. The data in Table 4 indicate that the response rates for larger tumours, which are more difficult to heat, is significantly less than those of smaller tumours. In other words, heating technique still needs refinement before a target CR rate of 90% [24] for the whole patient population can be achieved.

QA topics addressed in this thesis

It is the goal of this thesis to investigate several critical aspects of superficial hyperthermia treatments, by means of modelling, experiments, treatment planning and data analysis. Within the scope of this thesis, the research effort was focused on three themes:

1. Identification of quality determinants in the technical application of superficial hyperthermia

In-depth knowledge of the functioning of heating equipment helps its efficacious application in the clinic. To gain this knowledge, the equipment can be characterised by measurements, its range of application can be explored by modelling studies, or a combination of modelling and experimentation can be performed.

Multiple quality topics were investigated. Following indications that waterbolus dimensions had an effect on the power absorption pattern of the LCA [31], this quality determinant was explored in great detail. Further, models were employed to generate a new guideline for the waterbolus temperature. Lastly, questions from the clinic were analysed by patient-specific treatment planning, e.g. to check the feasibility of treatment, or to choose an appropriate applicator set-up.

2. Reduction of variation in treatment approach and outcome

Subtle variations in the clinical and technical approach can make a difference in treatment efficacy. These are often obvious between centres, for example a different applicator system, treatment schedule, thermometry, patient selection, tumour coverage, or steering practice. Also within a centre differences may occur, because treatments are conducted by human operators.

One way to converge to a best common practice is to practice openness and transparency with regard to all aspects of the treatment. At Erasmus MC, all hyperthermia treatments are evaluated in a weekly, multidisciplinary patient discussion to counteract inter-individual variability. An intuitive presentation of treatment data was developed to allow time-efficient and effective evaluations, where all team members can fully participate. The patients indirectly benefit from the common experience of the team; in addition, the operators benefit from the peer review. To counteract variability at an international level, a review paper was published to share the experiences gained at Erasmus MC in the treatment of breast cancer recurrences with superficial hyperthermia.

3. (Re)definition of the goal of treatment

One problem in hyperthermia is that the mechanisms that explain its clinical effectiveness have not been fully understood and cannot be properly quantified (a situation that is common in more disciplines in medicine, e.g. pharmacy, psychotherapy). This problem can be circumvented by applying a treatment schedule and approach that was shown to be effective in a randomized trial. Multiple successful randomised trials are available to follow this approach in superficial hyperthermia [9,11].

In the USA, a randomised trial failed to show a benefit of hyperthermia in addition to radiotherapy in the 1990s [21]. This of course triggered a quality assurance discussion [32,33]. One idea that came out of this discussion was that prescribing a certain thermal dose should solve the problem. In 2005, the randomized trial by Jones et al. [16] showed that hyperthermia was effective, and in this trial a target dose of 10 equivalent minutes at 43°C was applied. This thermal dose was then, stronger than before, internationally propagated as a tool for quality assurance [34]. The virtue of the thermal dose parameter was tested on clinical Erasmus MC data, because resetting the goal of treatment is at the heart of clinical quality assurance.

Outline of the thesis

In the first part of this thesis, Chapters 2 and 3, the current practice and need for quality assurance is highlighted. Chapter 2 describes the state of the art of superficial hyperthermia for breast cancer recurrences at the Erasmus MC, with a special focus on the development of equipment and treatment schedule over the years, and the lessons learned. This chapter contains a compilation of published clinical results of reirradiaton and hyperthermia in recurrent breast cancer, which shows a wide range of reported CR rates: from 20 to 90%, whereas the reference point for CR rates in the Rotterdam group is 65 to 90%. This indicates the need to critically review, unify and further develop the heating techniques and clinical approaches to better assure quality in superficial hyperthermia clinics.

In Chapter 3, the general applicability of the CEM43°CT90 thermal dose parameter was tested on clinical data from the Rotterdam hyperthermia unit. This dose parameter was used in the randomized trial by Jones *et al.* [16], and thereafter embraced as a quality tool to prescribe hyperthermia. The concepts of setting a thermal dose target ("effective dose") and selecting patients by testing their heatability were scrutinized, because their general acceptance and implementation require that a benefit for the patient can be proven in multiple centres.

Chapters 4 to 6 aim at optimizing the current clinical practice, and focus on the waterbolus and evaluation of treatments. In Chapter 4 it is investigated how the waterbolus affects the power absorption pattern below a LCA. The effects of waterbolus area, thickness, length/width ratio, and asymmetric placement of the applicator were quantified. The finite difference time domain (FDTD) modelling results were backed up by phantom measurements. This resulted in a new clinical guideline for the waterbolus configuration, and initiated a redesign of the waterbolus.

Chapter 5 targets the waterbolus temperature. The waterbolus has two functions: coupling of electromagnetic waves into the body, and cooling of the skin surface to enable heating at depth. The cooling effect is controlled by setting a waterbolus temperature. The effect of waterbolus steering can only partly be observed in the clinic, due to sparse thermometry. An electromagnetic-thermal model was therefore set up to investigate optimal settings. Guideline temperatures were established for different target depths and applicator array dimensions.

A framework for the evaluation of treatments is presented in Chapter 6. Superficial hyperthermia treatments are controlled by a human operator, because automatic, closed-loop control is not yet possible. The steering performance and the overall quality of each treatment are discussed in a multidisciplinary team. To facilitate efficient evaluations, a compact and intuitive presentation of treatment data was introduced.

The last two chapters set new standards for future application of superficial hyperthermia. In Chapter 7, a quantitative validation of the predicted SAR distribution of superficial hyperthermia applicators is proposed. The increased clinical application of treatment planning requires a strict validation of applicator models. The common practice

is a qualitative evaluation of one or multiple 2D SAR cross sections. In Chapter 7 however, the full 3D SAR pattern of the applicators in clinical use was scanned using a state of the art measurement system and standardized phantoms. The measured profiles were compared with the model prediction using the gamma method, and their similarity was expressed in a numeric value, the gamma index. It quantifies the proven quality of an applicator model and thus provides a sound starting point for the interpretation of treatment plans. In addition, the ratio of modelled and measured power output indicates how applicator powers in the model should be translated to clinical amplifier powers and vice versa. This is relevant for the generation of overall SAR patterns of an antenna array, and for the calculation of temperature distributions in a patient.

The benefits of treatment planning in the clinical application of superficial hyperthermia are shown in Chapter 8. Model simulations may show a priori power absorption patterns, potential hot spots and estimated temperature distributions inside the patient. The clinical application of treatment plans therefore is virtually limitless: for example to find optimal applicator array configurations for individual patients, or to troubleshoot poor treatments.

In Chapter 9, links between the chapters are drawn, the value of the insights gained so far is discussed and a future outlook is provided. Chapter 10 summarizes the main conclusions.

References

[1]   Datta N, Bose A, Kapoor HK. Thermoradiotherapy in the management of carcinoma cervix (stage IIIB): A controlled clinical study. Indian Med Gaz 1987;121:68-71.

[2]   Valdagni R, Amichetti M, Pani G. Radical radiation alone versus radical radiation plus microwave hyperthermia for N3 (TNM-UICC) neck nodes: a prospective randomized clinical trial. Int J Radiat Oncol Biol Phys 1988;15:13-24.

[3]   Berdov BA, Menteshashvili GZ. Thermoradiotherapy of patients with locally advanced carcinoma of the rectum. Int J Hyperthermia 1990;6:881-890.

[4]   Kakehi M, Ueda K, Mukojima T, Hiraoka M, Seto O, Akanuma A, Nakatsugawa S. Multi-institutional clinical studies on hyperthermia combined with radiotherapy or chemotherapy in advanced cancer of deep-seated organs. Int J Hyperthermia 1990;6:719-740.

[5]   Sugimachi K, Kitamura K, Baba K, Ikebe M, Morita M, Matsuda H, Kuwano H. Hyperthermia combined with chemotherapy and irradiation for patients with carcinoma of the oesophagus--a prospective randomized trial. Int J Hyperthermia 1992;8:289-95.

[6]   You QS, Wang RZ, Suen GQ, Yan FC, Gao YJ, Cui SR, Zhao JH, Zhao TZ, Ding L. Combination preoperative radiation and endocavitary hyperthermia for rectal cancer: long-term results of 44 patients. Int J Hyperthermia 1993;9:19-24.

[7]   Valdagni R, Amichetti M. Report of long-term follow-up in a randomized trial comparing radiation therapy and radiation therapy plus hyperthermia to metastatic lymphnodes in stage IV head and neck patients. Int J Radiat Oncol Biol Phys 1994;28:163-169.

[8]   Kitamura K, Kuwano H, Watanabe M, Nozoe T, Yasuda M, Sumiyoshi K, Saku M, Sugimachi K. Prospective randomized study of hyperthermia combined with chemoradiotherapy for esophageal carcinoma. J Surg Oncol. 1995;60:55-58.

[9]   Overgaard J, Gonzalez Gonzalez D, Hulshof MC, Arcangeli G, Dahl O, Mella O, Bentzen SM. Randomised trial of hyperthermia as adjuvant to radiotherapy for recurrent or metastatic malignant melanoma. European Society for Hyperthermic Oncology. Lancet 1995;345:540-543.

[10] Colombo R, Da Pozzo LF, Lev A, Freschi M, Gallus G, Rigatti P. Neoadjuvant combined microwave induced local hyperthermia and topical chemotherapy versus chemotherapy alone for superficial bladder cancer. J Urol 1996;155:1227-1232.

[11] Vernon CC, Hand JW, Field SB, Machin D, Whaley JB, van der Zee J, van Putten WL, van Rhoon GC, van Dijk JD, González González D, Liu FF, Goodman P, Sherar M. Radiotherapy with or without hyperthermia in the treatment of superficial localized breast cancer: results from five randomized controlled trials. International Collaborative Hyperthermia Group. Int J Radiat Oncol Biol Phys 1996;35:731-744.

[12] Sneed PK, Stauffer PR, McDermott MW, Diederich CJ, Lamborn KR, Prados MD, Chang S, Weaver KA, Spry L, Malec MK, Lamb SA, Voss B, Davis RL, Wara WM, Larson DA, Phillips TL, Gutin PH. Survival benefit of hyperthermia in a prospective randomized trial of brachytherapy boost +/- hyperthermia for glioblastoma multiforme. Int J Radiat Oncol Biol Phys 1998;40:287-295.

[13] van der Zee J, González González D, van Rhoon GC, van Dijk JD, van Putten WL, Hart AA. Comparison of radiotherapy alone with radiotherapy plus hyperthermia in locally advanced pelvic tumours: a prospective, randomised, multicentre trial. Dutch Deep Hyperthermia Group. Lancet 2000;355:1119-1125.

[14] Harima Y, Nagata K, Harima K, Ostapenko VV, Tanaka Y, Sawada S. A randomized clinical trial of radiation therapy versus thermoradiotherapy in stage IIIB cervical carcinoma. Int J Hyperthermia 2001;17:97-105.

[15] Colombo R, Da Pozzo LF, Salonia A, Rigatti P, Leib Z, Baniel J, Caldarera E, Pavone-Macaluso M. Multicentric study comparing intravesical chemotherapy alone and with local microwave hyperthermia for prophylaxis of recurrence of superficial transitional cell carcinoma. J Clin Oncol 2003;21:4270-4276.

[16] Jones EL, Oleson JR, Prosnitz LR, Samulski TV, Vujaskovic Z, Yu D, Sanders LL, Dewhirst MW. Randomized trial of hyperthermia and radiation for superficial tumors. J Clin Oncol 2005;23:3079-3085.

[17] Issels RD, Lindner LH, Verweij J, Wust P, Reichardt P, Schem BC, Abdel-Rahman S, Daugaard S, Salat C, Wendtner CM, Vujaskovic Z, Wessalowski R, Jauch KW, Dürr HR, Ploner F, Baur-Melnyk A, Mansmann U,

Hiddemann W, Blay JY, Hohenberger P. Neo-adjuvant chemotherapy alone or with regional hyperthermia for localised high-risk soft-tissue sarcoma: a randomised phase 3 multicentre study. Lancet Oncol 2010;11:561-570.

[18] Egawa S, Tsukiyama I, Watanabe S, Ohno Y, Morita K, Tominaga S, Onoyama Y, Hashimoto S, Yanawaga S, Uehara S *et al*. A randomized clinical trial of hyperthermia and radiation versus radiation alone for superficially located cancers. J Jpn Soc Ther Radiol Oncol 1989;1:135-140.

[19] Wust P, Hildebrandt B, Sreenivasa G, Rau B, Gellermann J, Riess H, Felix R, Schlag PM. Hyperthermia in combined treatment of cancer. Lancet Oncol 2002;3:487-497.

[20] Paulides M. Development of a clinical head and neck hyperthermia applicator. PhD thesis, Erasmus University Rotterdam, 2007.

[21] Perez CA, Pajak T, Emami B, Hornback NB, Tupchong L, Rubin P. Randomized phase III study comparing irradiation and hyperthermia with irradiation alone in superficial measurable tumors. Final report by the Radiation Therapy Oncology Group. Am J Clin Oncol 1991;14:133-141.

[22] Dutch Association of Comprehensive Cancer Centres. Oncoline - Cancer clinical practice guidelines [internet]. 2010 [cited 2010 Aug 25]. Available from: http://www.oncoline.nl

[23] Bedwinek JM, Fineberg B, Lee J, Ocwieza M. Analysis of failures following local treatment of isolated local-regional recurrence of breast cancer. Int J Radiat Oncol Biol Phys 1981;7: 581-585.

[24] van der Zee J, van der Holt B, Rietveld PJ, Helle PA, Wijnmaalen AJ, van Putten WL, van Rhoon GC. Reirradiation combined with hyperthermia in recurrent breast cancer results in a worthwhile local palliation. Br J Cancer 1999;79:483-490.

[25] Wikipedia. [Internet]. 2010. Quality assurance. [cited 2010 July 15]. Available from: http://en.wikipedia.org/wiki/Quality_assurance

[26] Clemenhagen CJ. Quality assurance in the hospital – making it work. Can Med Assoc J 1985;133:17-19.

[27] Hand JW, Lagendijk JJ, Bach Andersen J, Bolomey JC. Quality assurance guidelines for ESHO protocols. Int J Hyperthermia 1989;5:421-428.

[28] Dewhirst MW, Phillips TL, Samulski TV, Stauffer P, Shrivastava P, Paliwal B, Pajak T, Gillim M, Sapozink M, Myerson R, *et al*. RTOG quality assurance guidelines for clinical trials using hyperthermia. Int J Radiat Oncol Biol Phys 1990;18:1249-1259.

[29] Lee HK, Antell AG, Perez CA, Straube WL, Ramachandran G, Myerson RJ, Emami B, Molmenti EP, Buckner A, Lockett MA. Superficial hyperthermia and irradiation for recurrent breast carcinoma of the chest wall: prognostic factors in 196 tumors. Int J Radiat Oncol Biol Phys 1998;40:365-375.

[30] Rietveld PJM, van Putten WLJ, van der Zee J, van Rhoon GC. Comparison of the clinical effectiveness of the 433 MHz Lucite cone applicator with that of a conventional waveguide applicator in applications of superficial hyperthermia. Int J Radiat Oncol Biol Phys 1999;43:681-687.

[31] van Rhoon GC, Rietveld PJM, van der Zee J. A 433 MHz Lucite cone waveguide applicator for superficial hyperthermia. Int J Hyperthermia 1998;14:13-27.

[32] Oleson JR. If we can't define the quality, can we assure it? Int J Radiat Oncol Biol Phys 1989;16:879.

[33] Perez CA, Gelliespie B, Pajak T, Hornback NB, Emami B, Rubin P. Quality assurance problems in clinical hyperthermia and their impact on therapeutic outcome: a report by the radiation therapy oncology group. Int J Radiation Oncology Biol Phys 1989;16:551-558.

[34] Jones EL, Thrall D, Dewhirst MW, Vujaskovic Z. Prospective thermal dosimetry: The key to hyperthermia's future. Int J Hyperthermia 2006;22:247-253.

2

Reirradiation combined with hyperthermia in breast cancer recurrences: overview of experience in Erasmus MC

Abstract

For superficial hyperthermia, a custom-built multi-applicator multi-amplifier superficial hyperthermia system operating at 433 MHz is utilized. Up to 6 Lucite cone applicators can be used simultaneously to treat an area of 600 cm^2. Temperatures are measured continuously with fibre optic multi-sensor probes. Hyperthermia treatment planning is used to support decision making with regard to treatment strategy for patients with non-standard clinical problems.

In 74% of our patients with recurrent breast cancer treated with a reirradiation scheme of 8 fractions of 4 Gy in 4 weeks combined with 4 or 8 hyperthermia treatments, a complete response is achieved. This is approximately twice as high as the CR rate following the same reirradation alone. The CR rate in tumours smaller than 3 cm is 80-90%, for larger tumours it is 65%. Hyperthermia appears beneficial for patients with microscopic residual tumour as well. To achieve high CR rates, it is important to heat the whole radiotherapy field, and to use an adequate heating technique.

Introduction

Reirradiation combined with hyperthermia is an effective treatment for recurrent breast cancer. Results from five randomised trials have shown that the complete response (CR) rate in breast cancer recurrences increases from 41% to 59% when hyperthermia is added to radiotherapy [1]. For the subgroup of patients treated within the ESHO 5-88 trial with a reirradiation schedule of 8 fractions of 4 Gy, applied twice weekly, the CR rate even increased from 38% after radiation alone to 78% after combined treatment.

In Rotterdam, the first patient with recurrent breast cancer was treated with hyperthermia in 1978. Over the years, many alterations were made in hyperthermia and thermometry equipment, in treatment procedure, registration and treatment scheme. In this review we take you through some of the history of hyperthermia in our department, and present the resulting treatment procedure and a summary of our clinical results.

History of equipment used

Heating equipment

In 1978 we started our clinical research on hyperthermia with the Pomp-Siemens whole body hyperthermia cabin which included several applicators for local hyperthermia [2]. These were condenser plates operating at 27 MHz and dipole antennas operating at 433 or 2450 MHz. With these applicators, originally designed for physiotherapy, we treated patients who were reirradiated for palliative reasons, among whom patients with recurrent breast cancer. The first applicators developed in our department were air-filled waveguides operating at 2450 MHz with aperture sizes of 8×4 and 8×6 cm^2. The rectangular shapes allowed us to use combinations of up to eight applicators at the same time. The number of amplifiers was still limited so that up to four applicators were coupled to one power supply, without the possibility to control power supply to the individual applicators. Surface cooling, when necessary, was performed by directing air currents under the applicators.

In 1985 we started using custom built water-filled waveguides operating at 433 MHz with a radiating opening of 10×10 cm^2. Until 1987 we could use maximally two applicators simultaneously, thereafter five and some time later six. Each applicator was supplied with independent power control [3]. These standard waveguides were replaced in 1996 by Lucite cone applicators (LCA), with a larger effective field size (EFS). The EFS of the LCA is approximately 100 cm^2, which is considerably larger than the 33 cm^2 of the standard waveguide [4]. The performance of both waveguide types was tested in the clinical setting by treating patients alternately by standard waveguides and LCA arrays. The average invasive temperature was 0.28°C higher with the LCA's than with the standard waveguides, which was primarily the result of higher temperatures in the periphery of the treatment
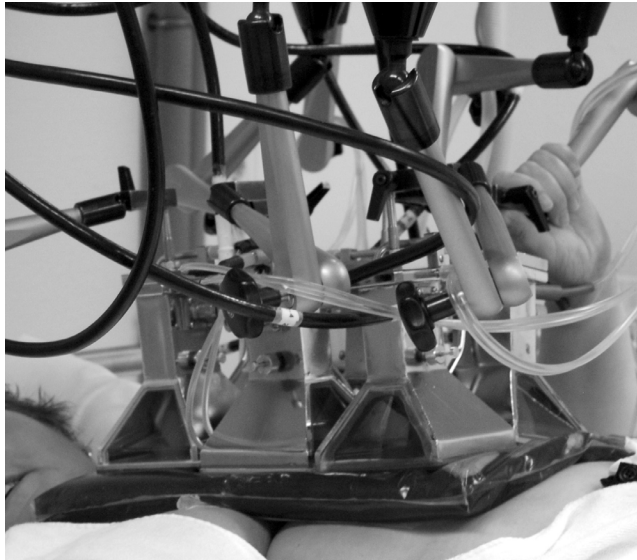
field. A perfused waterbolus was used with the 433 MHz waveguide applicators to control surface temperatures.

Waterbolus dimensions and selection of waterbolus temperature

The waterbolus placed between water-filled waveguides and skin (Figure 1) has two functions: improvement of coupling between the applicators and tissue and control of superficial temperature.

We investigated the effects of waterbolus configuration on the EFS of the LCA [5]. Placement of the LCA near the waterbolus edge reduced the EFS considerably. With waterbolus heights of more than 2 cm the EFS became more sensitive to distance to the waterbolus edge. Based on the results, the guideline now is that the height of the waterbolus should not exceed 2 cm and the waterbolus should extend the LCA aperture at least 2.5 cm, especially at the Lucite windows.

The two main parameters used for optimizing the temperature distribution are the electromagnetic power and the waterbolus temperature. A 3-D model was set up to simulate an abstraction of the treatment. In the model a convection coefficient for the waterbolus to skin surface was employed, which was measured for waterboluses of different sizes. The effect of perfusion and fat layer thickness were investigated in a layered model. The performance of the general model was verified against clinical data. The model was found to predict the temperature distribution well on a global view, and was used to set up guidelines, specific for our equipment, for the waterbolus temperature selection for various target depths and applicator arrays [6].

Figure 1. Close-up of the applicators placed above the thoracic wall, on top of the perfused waterbolus.

Thermometry

We started with thermocouples, either single sensor probes within a needle, or multi-sensor probes within a catheter. These probes had to be placed perpendicular to the direction of the electric field (E-field) and temperatures were measured every 5 minutes with the power shut off. Since 1987 temperatures are measured continuously during treatments by a 24-channel fiber-optic system, with which five multi-sensor probes (up to four sensors) and four single sensor probes are available (Takaoka FT1210). Closed-tip catheters are placed interstitially immediately before the first treatment and left in place till after the last treatment. The aim is to have both interstitial and superficial thermometry under each applicator. Usually, these catheters cause no clinical problems [7].

Use of hyperthermia treatment planning

Hyperthermia treatment planning tools have a significant potential to further improve the quality of hyperthermia treatments, by providing insight into the 3-D absorbed power distributions. In some patients with non-standard clinical problems, SEMCAD-X [8] hyperthermia treatment planning was successfully used to support decision making with regard to the treatment strategy [9]. Two cases are shortly described here.

A patient with recurrent breast cancer had undergone open heart surgery in the past, and sternal cerclage wires were within the target volume for hyperthermia. Treatment planning showed that the distortion of the electromagnetic field by the cerclage wires was neglectable with the E-field direction perpendicular to the cerclage wires. This patient was treated without problems with the applicator configuration advised by the planning.

The tumour of a patient with a recurrent breast cancer in the infraclavicular region was located at a depth of 37 to 54 mm below the skin, which is beyond the superficial system's standard maximum target depth of 40 mm. However, the subcutaneous fat layer in this patient was above average: 29 mm. Because the effective conductivity of fatty tissue is relatively low, it could be anticipated that power absorption in the fat layer would be limited, and that the remaining power at depth would be sufficient within the tumour. This was confirmed by hyperthermia treatment planning, and during hyperthermia treatment the intratumour temperature reached therapeutic levels.

Treatment scheme

When we started combining reirradiation with hyperthermia, the tolerance limits for reirradiation were not known. We started cautiously, with total doses of 12-25 Gy, in fraction sizes of 2 to 4 Gy. To avoid thermotolerance, we chose a treatment scheme of hyperthermia twice weekly with at least 3-day intervals. In order to sensitize every radiation fraction, radiation was also given twice weekly, in fractions of 4 Gy. Hyperthermia was given after radiotherapy on the basis of experimental studies showing that maximum therapeutic benefit can be obtained with that sequence [10-14].

When we did the first evaluation of the results of reirradiation and hyperthermia in 97 patients with recurrent breast cancer, we found a large influence of the applied reirradiation dose on CR rate. With a total dose of less than 29 Gy the CR rate was 24%, while it was 58% after a dose of 30 to 32 Gy. Time till progression was median 4 months after a partial response (PR) and 26 months for CR [15]. The reirradiation schedule of eight fractions of 4 Gy appeared safe, effective and well tolerated and was therefore selected as the standard scheme.

In 1996 we had a capacity problem for superficial hyperthermia. Taking in mind the results of several published randomised studies comparing a low with a high number of hyperthermia treatments, usually one versus two treatments per week, which showed no difference in results [16-21], we decreased the number of hyperthermia sessions to four. The number of patients was insufficient to do a randomised trial ourselves and we planned to evaluate the results after treating a sufficient number of patients with the new schedule.

We did a first analysis of results in patients treated with four hyperthermia sessions in 2004 [22] and compared these to those in patients who received eight hyperthermia sessions: 40 patients received four and 132 patients eight hyperthermia treatments. For patients with a maximum tumour diameter ≤ 30 mm CR rate was 86% after eight treatments and 82% after four treatments (not significant). For patients with larger tumours, CR rate was 59% after eight treatments and 65% after four treatments (not significant). The preliminary conclusion is that a decrease in number of hyperthermia treatments does not lead to inferior results. On the other hand, the hoped-for decrease in hyperthermia toxicity was not observed as well. A problem with this comparison is that, at around the same time that we changed the number of hyperthermia treatments, we also replaced the standard waveguide with the Lucite Cone Applicator, with which we achieved average 0.28°C higher temperatures. Although it is unlikely that a 0.28°C higher temperature compensates for 240 minutes treatment duration, we will perform a detailed analysis of prognostic factors including thermal dose parameters in these patients.

Lessons learned

No electromagnetically induced hyperthermia in anesthetized patient

We started our clinical hyperthermia research with the idea to apply local hyperthermia during whole body hyperthermia, in order to achieve a more homogeneous temperature distribution. In the first patient in whom we tried whole body hyperthermia, it appeared that a core temperature > 40°C was not tolerated by the conscious patient. We therefore gave subsequent treatments under general anesthesia. During the third treatment, core temperature was increased to a temperature of 41.6°C and the recurrent tumour at the chest wall was simultaneously heated with 433 MHz. One of the thermometry probes suddenly showed a steep temperature increase to maximum 47°C. After the treatment, the patient

developed a severe third degree burn of the thoracic wall with a diameter of 100 mm and including ribs [23].

We have seen similar toxicity in two other patients who were treated under general anesthesia. During normothermic regional isolation perfusion of the leg for multiple skin metastases of malignant melanoma, local hyperthermia was given to one of the metastases. Hyperthermia was given with a 2450 MHz dipole antenna with a diameter of 80 mm and interstitial temperatures were average between 39.2 and 40.9°C. In two of three patients treated this way, in whom the measured maximum temperature had been 41.4 and 40.3°C, a third-degree burn developed.

Unnoticed hot spots resulting in toxicity can occur in conscious patients as well, at sites of decreased sensitivity due to previous surgery, but usually some sensation of pain limits the extent of the damage.

No stray irradiation near linear accelerator

For a short period of time, we treated our patients in an orthovoltage room which was located next to a linear accelerator. The microwave equipment at that time consisted of a circular field dipole antenna connected to a generator operating at 433 MHz. In the Netherlands, 433 MHz can be used without shielding. The linear accelerator was a CGR-MeV Sagittaire. We found that the stray microwave radiation, at intensities of about 0.4 mW/cm^2 in the control room of the accelerator interfered with the beam energy settings. The microwave interference caused an increase in beam energy. At maximum power output this was a change from 25.5 to 29.1 MeV [24]. The most practical solution to this problem was to transfer the hyperthermia treatment to another room.

Heating technique is important for treatment outcome

In the first evaluation of treatment results in the group of patients treated with eight fractions of 4 Gy and hyperthermia, we found a CR rate of 58% [15]. When we evaluated later a larger group of patients, the CR rate was 71%. A multivariate analysis showed that two factors were independent and significantly associated with local control probability: tumour size (maximum diameter ≤ 3 cm or > 3 cm) and used equipment (2450 MHz or 433 MHz equipment) [25]. The better overall results were the effect of a large improvement in CR rate in the larger tumours: 31% with 2450 MHz heating and 65% with 433 MHz heating. In tumours ≤ 3 cm the results of 2450 and 433 MHz heating were not different; approximately 90% CR. The CR rate achieved with 2450 MHz in the larger tumours was similar to the results of reirradiation with 8×4 Gy without hyperthermia: 28% in the RTOG study [26] and 38% in the ICHG study [1]. Apparently, 2450 MHz heating was inadequate for the larger tumours. A disadvantage of using 2450 MHz compared to 433 MHz is the smaller penetration depth and thereby a smaller heated volume. From this experience we learned that patients should not be accepted for hyperthermia treatment if we expect that we cannot adequately heat the whole target volume.

Whole reirradiation volume is target for hyperthermia

Until July 1987, the aim of treatment was to heat the macroscopic tumour. With that approach, we observed in a few patients tumour regrowth within the radiation field, outside the margin of the hyperthermia field. At the same time, there was no regrowth within the combined treated field. Since then we choose the applicator set-up such that the radiation field is widely covered.

Further experiences suggest that hyperthermia is an effective additional treatment for microscopic tumour. The patient population in which we found better outcomes after 433 MHz heating compared to 2450 MHz heating included total 15 patients with microscopic disease. Three patients treated with 2450 MHz equipment all developed in-field tumour regrowth 10-12 months after start treatment. In 12 patients treated with 433 MHz equipment only two in-field re-recurrences occurred, 10 and 13 months after start treatment. Three patients died with a locally controlled tumour after median 10 months and seven patients were still alive with a locally controlled tumour 16-70 months after treatment. This is a significant difference, suggesting that good-quality hyperthermia is effective here as well [25].

A tumour near the eye can be treated successfully

A patient was referred with a metastatic lesion of breast cancer in the lower eyelid, recurring after two radiation treatments with partially overlapping fields. The tumour was progressive under second-line hormonal therapy and she was unfit for chemotherapy. The first local treatment of this tumour had been irradical resection (positive surgical margins) and radiotherapy, 10×3 Gy plus boost of 10×2 Gy. The tumour recurred 9 months later at the margin of the radiotherapy field, was treated again with irradical surgery and 15×2 Gy. Four months later the tumour recurred again. With the patient two treatment options were discussed: surgery, including enucleation of the eye, or reirradiation with hyperthermia, with unknown risk of toxicity like eyelid fibrosis, retina damage, cataract and glaucoma. The patient preferred radiotherapy and hyperthermia. During radiotherapy the eyeball was shielded with a leaden contact lens. We applied eight fractions of 4 Gy and four hyperthermia treatments of 60 minutes. The tumour regressed fast with a complete regression established one week after the last treatment. During follow-up, local tumour control was maintained. The only side effect was a dry eye for which the patient used eyedrops. Vision was unchanged. The patient died 22 months after the last treatment owing to a cerebrovascular accident, unrelated to breast cancer [27].

No excessive toxicity in patients with tissue transfers

Between 1992 and 2009, 36 patients were treated on total 37 tissue transfers, including split skin grafts (15), transverse rectus abdominis myocutaneous (1), latissimus dorsi (14) or rhomboid (1) flaps or a combination of grafts and flaps. The guidelines for treating these patients were not different from those for other patients. Hyperthermia toxicity (according

to CTC-AE version 3) grade 2 (minimal medical intervention required, no interference with ADL (activities of daily life) occurred in four patients and grade 3 (surgical intervention required and/or interference with ADL) in three. The incidence of toxicity appears not much different from that observed in patients without tissue transfer and is acceptable [28].

Current treatment procedure

Patient selection

In the Netherlands, national guidelines prescribe reirradiation and hyperthermia for recurrent breast cancer after previous irradiation in the same area, when the expected survival is 6 months or more. This concerns inoperable tumours, irradically resected tumours (tumour positive surgical margins), or radically resected tumours with a high risk of re-recurrence (multifocal recurrences or second recurrences).

The aim of the treatment is a complete response, which means that it must be possible to heat the whole target volume. The target volume should be within 40 mm from the skin surface, but on occasion subcutaneous fat can be subtracted from this distance. It must be feasible to place the applicators parallel to the surface of the treatment area. When the area is larger than 20×30 cm^2, two (or more) hyperthermia applications are scheduled for one treatment. We consider a pacemaker a contraindication for hyperthermic treatment. Metallic implants larger than surgical clips may give problems, e.g. a portacath has to be removed. In case of doubt we will model a treatment with SEMCAD-X.

The patients receive a detailed explanation of the treatment procedure and information on their own role in monitoring the temperature distribution, specifically instructions concerning the mentioning of complaints induced by hot spots.

Preparation before first treatment

The treatment team of physician or nurse practitioner, physicist and technician examine the treatment area and decide which applicator set-up will be used. The aim is to cover the whole radiotherapy field with the footprint of the applicator array with an overlap of 1 cm all around. Thereafter the closed tip catheters are placed under local anaesthesia, with the aim to have interstitial thermometry under each of the applicators. The catheters are fixed to the skin with Histoacryl® tissue adhesive (B. Braun, Melsungen AG, Germany) and Tegaderm® transparent dressing (3M, USA). The interstitial length and depth of each catheter are measured. A life-size drawing of the treatment area is made on a transparent sheet including some anatomical landmarks (prominent bones, scars, and birth marks), the radiotherapy field margins, the location of macroscopic tumour, the location of the applicators, and the location of interstitial and superficial thermometry probes [29]. All necessary information is loaded into the computer program for treatment monitoring, steering and registration.

Figure 2. The superficial hyperthermia treatment set-up. The technician observes both the patient and the temperature and power information. The PC screens show, from left to right (left) the course of temperatures over time, per applicator; (middle) the drawing of the treated area with location of applicators and actual temperature per measuring site (details are shown in Figure 3), and (right) the power output per applicator.
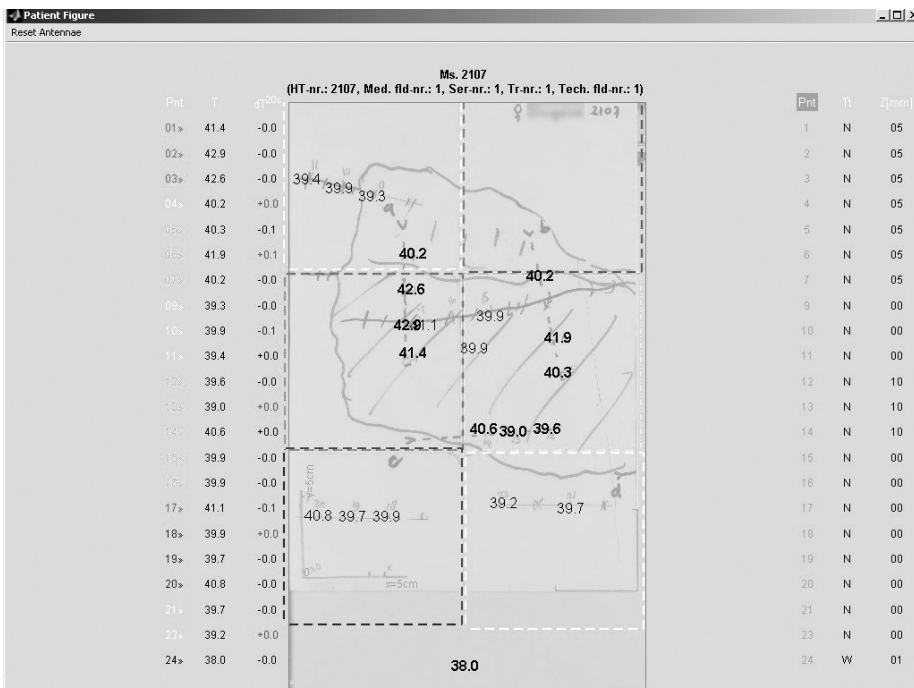
Figure 3. An example of the middle PC screen during treatment with the drawing of the ventral treatment area. The drawing shows the tumour tissue, the mastectomy scar, four interstitially placed catheters, the footprints of the applicators, and actual interstitial (in bold) and superficial temperatures.

Treatment

The patient is positioned on the treatment bed in a position as comfortable as possible, and up to 23 thermometry probes are placed within the catheters and on the skin. Multi-sensor probes with four measuring points at 20 mm spacing are placed in the catheters, some of the superficial probes are placed on scars. The applicator position is indicated on a gauze which is placed on the surface of the treatment area and then wetted. The waterbolus is placed such that it extends the planned position of the applicators with at least 25 mm. The waterbolus temperature is selected depending on the size of the waterbolus and the depth of the target volume. Usually the applicators are placed "clockwise": adjacent applicators have their E-field direction perpendicular to each other [4].

The treatment is administered by the technician. All necessary information is visible on PC screens during treatment: the position of all applicators and thermometry probes in relation to the patient's anatomy, the power output and reflected power per applicator, the course of temperature under each applicator and the current temperature at each measuring site (Figures 2 and 3). The first treatment starts with a power of 30 W per applicator. The increase of power per applicator depends on the steepness of temperature increase under the specific applicator. The aim is to have all interstitial temperatures above 40°C. An interstitial temperature of maximum 43°C is allowed during the first 30 minutes, thereafter maximum 44°C. In tumour tissue at a distance of more than 10 mm from normal tissue higher temperatures are allowed. The treatment duration is 60 minutes with power on.

Evaluation

Between treatments, the course of the previous treatment is discussed with the whole team and adjustments for the application of the next treatment determined. Special attention is paid to cold spots (average temperature below 40°C), treatment limiting hot spots, and the temperature distribution in depth. If a cold or a hot spot can be explained by the expected SAR distribution, the position of the applicators or their E-field direction is changed. If superficial temperatures were power-limiting during treatment, the waterbolus temperature is decreased. If the treatment quality is limited by tumour related pain, general stress or anxiety, appropriate medication will be given during subsequent treatments. A detailed description of this evaluation can be found in [30].

Results

Effect on tumour

Since we use 433 MHz for the application of hyperthermia, the results are rather stable. In 1999 we published a CR rate of 74% for the total group of patients treated with eight fractions of 4 Gy and eight hyperthermia treatments, 87% for patients with tumours smaller

than 30 mm and 65% for patients with larger tumours [25]. With the same reirradiation schedule combined with four hyperthermia treatments, the overall CR rate is 73%; 82% for small tumours and 65% for larger tumours [22]. The median duration of local tumour control is 32 months. In patients treated for a microscopic tumour residual, the local tumour control rate till death or date of last follow-up was 83% for the patients who received eight hyperthermia treatments and 84% for those receiving four hyperthermia treatments.

Toxicity

Acute radiation toxicity usually is no problem with this schedule with an incidence of epidermolysis in 11% of the patients [25]. In the randomised trial, no increase in radiation toxicity was found [1]. One case report even suggest a decrease in late toxicity (telangiectasis) with the addition of hyperthermia [31].

Hyperthermia toxicity is rather frequent in these patients. In 1999 we reported second-degree burns in 19% of the patients and third-degree burns in 7% and subcutaneous burns in 3% after eigth 433 MHz treatments. In 71 patients who received four treatments we observed second-degree burns in 31%, third-degree burns in 10% and subcutaneous burns in 7%. These side-effects usually are grade 2 or less according to the Common Terminology Criteria for Adverse Events version 3.0 [2006] scoring system. The hyperthermia-induced burns generally cause no pain because they occur at sites of decreased sensitivity.

Late radiation toxicity was evaluated in 121 patients treated with reirradiation (8×4 Gy) and hyperthermia (eight treatments) between 1992 and 2000. The overall incidence of late radiation toxicity was 12%: a skin ulcer in six patients, bone necrosis or fracture in seven patients, and both an ulcer and bone fracture in one patient. The incidence of late radiation toxicity however increased with longer follow-up durations. In 38 patients with a follow-up duration >3 years it was 18%, and in eight patients followed longer than 5 years it was 38%. The median follow-up of all patients was between 1 and 2 years [Van der Zee, unpubished results].

Discussion

In approximately three-quarter of our patients, reirradiation with eight fractions of 4 Gy combined with hyperthermia results in a CR, which lasts for a median duration of 32 months. In over 80% of the patients treated for microscopic disease, local tumour control lasts till death or date of last follow-up. We do not expect that a locally controlled chest wall recurrence will influence overall survival. Nevertheless, the absence of symptomatic local tumour can result in an improvement in quality of life [32]. In our view, the achievement of a partial response is less worthwhile, since regrowth is observed after median 4 months and we find it unlikely that hyperthermia influences time to progression.

That is the reason that we do not accept patients for hyperthermia treatment when we can heat only part of the target volume.

We have not included a test heating session in the patient selection procedure. Patients are selected on the basis of tumour location and extension in depth. We assume that a target volume can be adequately heated when the depth is limited to 4 cm from the skin surface and the applicators can be placed parallel to the surface over the whole target area. The results of the randomised trial of Jones *et al*., for which patients were eligible after a test treatment had shown "heatability" (the achievement of a hyperthermia dose of 0.5 CEM43°CT90) [33], has triggered us to evaluate retrospectively this thermal dose parameter in our patients. CR rates were the same for patients who were heatable and unheatable, and for patients who received less or more than 10 CEM43°CT90 during the whole treatment series [34].

Many clinical studies on hyperthermia in addition to radiotherapy included patients with recurrent breast cancer after previous irradiation. The results in this specific subgroup, however, are not always reported separately. Table 1 summarizes CR rates in this subgroup which are available from published experience [1,21,26,35-52]. This table includes three studies in which not all but the majority of patients were reirradiated, and one study reporting CR combined with partial response with >80% regression. Four studies included a control group treated with the same radiation alone: 3 randomised studies and one study in which patients with multiple lesions received radiation alone to 1 lesion and combined treatment to another. CR rates following reirradiation and hyperthermia vary widely, from 20% to 95%. This is not surprising, since the used radiotherapy schedule varies between studies and also within studies, and the prognostic variables of included patients will differ between studies as well. A summation of the data results in 61% CR after combined treatment and 32% after radiotherapy alone. In the majority of studies, hyperthermia is combined with radiotherapy only and applied after radiation. Unusual approaches are simultaneous combination of radiation and hyperthermia and the addition of chemotherapy. Myerson *et al*. [46] tested the simultaneous combination of radiotherapy and hyperthermia in 15 patients and achieved a CR in 79%. Feyerabend *et al*. [47] applied once weekly epirubicin and ifosfamide, simultaneously with hyperthermia, in the period of radiotherapy. Kouloulias *et al*. [48] applied once monthly liposomal doxorubicin 3 to 40 hours before hyperthermia, once during the perod of radiotherapy and 5 times thereafter. The complete response rates in the last two studies were lower than in all other studies: 22% and 20% respectively.

We find the schedule of 2 fractions of 4 Gy per week attractive in view of the palliative aim of the treatment. The overall duration of a treatment series is 3.5 weeks, during which period patients have to come to the hospital only twice weekly for around 2 hours, so the inconvenience is limited. On the other hand, the incidence of late toxicity can be expected to be lower with a radiation schedule with smaller fraction sizes [53,54]. Oldenburg *et al*. recently reported a 40% incidence of ≥ grade 3 toxicity at three years in 78 patients treated with 8 x 4 Gy and hyperthermia for microscopic disease [55]. In our patients it was 38% at

five years follow-up. For the majority of patients late toxicity will not be a problem in view of the limited overall survival, but for the patients with a longer expected overall survival smaller fraction sizes may be considered.

Table 1. Results of reirradiation and hyperthermia in recurrent breast cancer.

Reference	RT dose and scheme	HT technique and scheme	CR after RT (total n), %	CR after RT+HT (total n), %
35	F 2-2.5, T 20-30, 3/wk	A 2450, R-H, D 35-40, N 6-8		(15) 53%
36 *M *reRT 72%	F 3, T 30, 5/wk	A 2450, 915, R-H, D +45, N 4	(17) 35%	(28) 64%
37	F 4, T 24, 2/wk	A 433, R-H, D 60, N 6		(26) 77%
38 *R	F 2, T 35-75, 5/wk	MW or RF, D 40, N 4-8	(10) 40%	(9) 67%
39	F 4, T 32, 2/wk	A 200-700, R-H, D 60, N8		(30) 57%
40	F 2-2.5, T 20-80, mean 47	A 915, 2450, R-H, D 40, N mean 12		(20) 80%
41	F 3.5-4.5, T 30-41, 2-3/wk (7 pts T<30)	A 2450, R-H, D +45, N 3-10		(34) 65%
42	9 pts F 1.8-2, T 20-58 4 pts F 4, T 28-44	A 430,2450, 8 or 13.5, R-H, D 30-60, N 2-10, mean 6		CR+PR >80% (13) 92%
26 91 *R	F 4, T 32, 2/wk	A 915, R-H, D 60, N 8	<3 cm (10) 40% >3 cm (29) 28%	(13) 62% (29) 21%
43	F2-5, T 16-56, mean 29.4, 2-5/wk	A 300-1000, R-H, D 60, N 2-9, mean 5		(44) 41%
21	F 3, T 30, or F 2.3, T 34.5, 5/wk	A2450, 915, R-H, D +45, N 4, 3 or 6		(69) 71% ª
44	F 1.8-5.2, T 8-68, 2-5/wk ETD mean 42	A 915 patchwork, D 60, N 1-5, mean 1.3		(20) 95%
1 (ESHO) *R	F 4, T 32, 2/wk	A 433, R-H, D 60, N 4-8	(29) 38%	(27) 78%
1 (MRC-BrR) *R *reRT 81%	F 3.6, T 28.8, 4wk 28 pts T433 Gy	A 433, 2450, R-H, D 10+60, N 3	(59) 29%	(90) 57%
1 (PMH) *R *reRT 61%	F 1.8, T 32.4, 5/wk 13 pts T 51-60	A 915, R-H, D15+30, N 2	(16) 31%	(17) 29%
45 *reRT 51%	F1.8-2, T2-70, median 46.5, 5/wk, or F 4, T20-66, median 32, 2/wk	915 (few 60-130 or US), R-H, D +45, N 1-11 median 8		(178) 63%
25	F 4, T 32, 2/wk	A 2450, R-H, D 60, N 8 A 433, R-H, D 60, N 8	(24) 58%	(95) 74%
46	F 2-4, T 30, 3/wk	A 915 or US, R+H simultaneously, D 60, N 1-6 mean 3.3		(15) 79%
47	F 1.2-2, T 36-60, mean 45, 5-9/wk, *C	A 915, R-H, D 60, N 1-5 mean 3.9, HT simultaneously with chemotherapy		(18) 22%
48	F 1.8, T 30.5, 5/wk, *C	A 433, R-H, D 60, N 6, HT simultaneously with chemotherapy		(15) 20%
49	F 1.8-2, T 30-40, 5/wk	A 915, R-H, D 45, N 2-6		(24) 42%
50	F 1.8-2, T 12-74, median 43, 5/wk	A 8, 13.5, 430, 2450 or US, R-H, D 30-60, N 2-9 mean 4.5		(41) 56%
51	F ~2, T14-72, median 48, 5/wk	Multi-institutional review; no details on HT treatment reported		(36) 67%
52	F1.8-2, T20-60 mean 31.8	A 433, R-H, D +30, N median 6		(44) 66%
Summation			**(170) 32%**	**(974) 61%**

Legend to Table 1:
Reference: *M: matched lesions; *R: randomized study; *reRT: % of patients that was reirradiated; RT = radiotherapy.
RT dose and scheme: F = fraction size; T = total dose in Gy; n/wk = number of fractions per week; *C: treatment schedule included chemotherapy as well; ETD = equivalent total radiation dose based on linear quadratic model; HT = hyperthermia.
HT technique and scheme: A = application technique: microwave frequency, US = ultrasound, MW = microwave equipment and RF = radiofrequency equipment, not otherwise specified; R-H = HT after RT; D = duration per treatment in minutes (+: extra heating-up time); N = number of treatments.
CR after RT+HT: ª = no difference between 3 schemes

We are now investigating the potential use of predicted 3D-SAR (Specific Absorption Rate) coverage as a prognostic indicator for treatment outcome. Patient-specific treatment planning is done with SEMCAD X [8]. Predicted SAR-volume histograms, total absorbed energy per tissue type and calculated temperatures will be compared with measured temperatures, and we will analyse whether the predicted treatment quality correlates with treatment outcome. A correlation of predicted treatment quality with measured temperatures, and/or with clinical outcome, would allow to abandon interstitial thermometry, to prescribe treatments of a certain quality, and to apply reproducible treatments.

In conclusion: it is feasible to achieve CR rates of 65 to 90% in breast cancer recurrences when reirradiation is combined with hyperthermia. The burden to the patient can be limited to four 2-hour visits to the clinic. To achieve high CR rates, it is important to heat the whole radiotherapy field, and to choose an adequate heating technique. In special cases, hyperthermia treatment planning can be applied to support clinical decisions.

References

[1] International Collaborative Hyperthermia Group (CC Vernon, JW Hand, SB Field, D Machin, JB Whaley, J van der Zee, WLJ van Putten, GC van Rhoon, JDP van Dijk, D Gonzalez Gonzalez, F-F Liu, P Goodman and M Sherar). Radiotherapy with or without hyperthermia in the treatment of superficial localized breast cancer - results from five randomised controlled trials. Int J Radiation Oncology Biol Phys 1996, 35, 731-744.

[2] Reinhold HS, Van der Zee J, Faithfull NS, Van Rhoon GC, Wike-Hooley J, Utilization of the Pomp-Siemens hyperthermia cabin. Natl Cancer Inst Monogr 1982;61:371-375.

[3] Van Rhoon GC, Rietveld PJM , Van der Zee J. A 433 MHz Lucite Cone waveguide applicator for superficial hyperthermia. Int. J. Hyperthermia 14, 13-27, 1998.

[4] Rietveld PJM, Van Putten WLJ, Van der Zee J, Van Rhoon GC. Comparison of the clinical effectiveness of the 433 MHz Lucite Cone Applicator with that of a conventional wave guide applicator in applications of superficial hyperthermia. Int. J. Radiation Oncology Biol. Phys. 43, 681-687, 1999.

[5] De Bruijne M, Samaras T, Bakker JF, Van Rhoon GC. Effects of waterbolus size, shape and configuration on the SAR distribution pattern of the Lucite cone applicator. Int J Hyperthermia 2006;22:15-28.

[6] Van der Gaag ML, De Bruijne M, Samaras T, Van der Zee J, Van Rhoon GC. Development of a guideline for the water bolus temperature in superficial hyperthermia. Int J Hyperthermia 2006;22:637-656.

[7] J van der Zee, GC van Rhoon, MP Broekmeyer-Reurink, HS Reinhold. The use of implanted closed-tip catheters for the introduction of thermometry probes during local hyperthermia treatment series. Int. J. Hyperthermia 3, 337-345, 1987.

[8] SEMCAD Reference Manual. Zürich, Switzerland: Schmid & Partner Engineering AG; 2004. Accessed 24 November 2005. Available online at: http//www.semcad.com.

[9] De Bruijne M, Wielheesen DHM, Van der Zee J, Chavannes N, Van Rhoon GC. Benefits of superficial hyperthermia treatment planning: five case studies. Int J Hyperthermia 2007;23:417-429.

[10] Gillette EL, Ensley BA. Effect of heating order on radiation response of mouse tumor and skin. Int J Radiat Oncol Biol Phys 1979;5:209-213.

[11] Hill SA, Denekamp J. The response of six mouse tumours to combined heat and X rays: implications for therapy. Br J Radiol 1979;52:209-218.

[12] Hiraoka M, Miyakoshi J, Jo S, Takahashi M, Abe M. Effects of step-up and step-down heating combined with radiation on murine tumor and normal tissues. Jpn J Cancer Res 1987;78:63-67.

[13] Overgaard J, Overgaard M. Hyperthermia as an adjuvant to radiotherapy in the treatment of malignant melanoma. Int J Hyperthermia 1987;3:483-501.

[14] Van der Zee J, De Bruijne M, Van Rhoon GC. Letter to the Editor. Hyperthermia dose and schedule: no evidence yet for changing treatment design. Int J Hyperthermia 2006;22:433-447.

[15] Van der Zee J, Treurniet-Donker AD, The SK, Helle PA, Seldenrath JJ, Meerwaldt JH, Wijnmaalen AJ, Van den Berg AP, Van Rhoon GC, Broekmeyer-Reurink MP and Reinhold HS. Low dose reirradiation in combination with hyperthermia: a palliative treatment for patients with breast cancer recurring in previously irradiated areas. Int. J. Radiat. Biol. Phys. Oncol. 15, 1407-1413, 1988.

[16] Arcangeli G, Nervi C, Cividalli A, Lovisolo GA. Problem of sequence and fractionation in the clinical application of combined heat and radiation. Cancer Res 1984;44:4857s-4863s.

[17] Valdagni R. Two versus six hyperthermia tratments in combination with radical irradiation for fixed metastatic neck nodes: progress report. Recent Results Cancer Res 1988;107:123-128.

[18] Kapp DS, Petersen IA, Cox RS, Hahn GM, Fessenden P, Prionas SD, Lee ER, Meyer JL, Samulski TD, Bagshaw MA. Two or six hyperthermia treatments as an adjunct to radiation therapy yield similar tumor responses: results of a randomized trial. Int J Radiat Oncol Biol Phys 1990;19:1481-1495.

[19] Emami B, Myerson RJ, Cardenes H, Paris KG, Perez CA, Straube W, Leybovich L, Mildenberger M, Kuske RR, Devineni R, Kucik N. Combined hyperthermia and irradiation in the treatment of superficial tumors: results of a prospective randomized trial of hyperthermia fractionation (1/wk vs 2/wk). Int J Radiat Oncol Biol Phys 1992;24:145-152.

[20] Engin K, Tupchong L, Moylan DJ, Alexander GA, Waterman FM, Komarnicky L, Nerlinger RE, Leeper DB. Randomized trial of one versus two adjuvant hyperthermia treatments per week in patients with superficial tumours. Int J Hyperthermia 1993;9:327-340.

[21] Lindholm C-E, Kjellen E, Nilsson P, Weber L, Hill S. Prognostic factors for tumour response and skin damage to combined radiotherapy and hyperthermia in superficial recurrent breast carcinomas. Int J Hyperthermia 1995; 11:337-355.

[22] Van der Zee J, Mens JW, Graveland WJ, Verloop-van 't Hof EM, Van Rhoon GC. Comparison between 4 and 8 hyperthemia treatments combined with reirradiation for breast cancer. Presented at 9th International Congress on Hyperthermic Oncology, Saint Louis 2004.

[23] Van der Zee J, Van Rhoon GC, Wike-Hooley JL, Faithfull NS, Reinhold HS. Whole-body hyperthermia in cancer therapy: a report of a phase I-II study. Eur J Cancer Clin Oncol 1983;19:1189-1200.

[24] Van Rhoon GC, Van de Poel JA, Van der Heiden JA, Reinhold HS. Interference of 433 MHz microwaves with a megavoltage linear accelerator. Phys Med Biol 1984;29:719-723.

[25] J. van der Zee, B. van der Holt, P.J.M. Rietveld, P.A. Helle, A.J. Wijnmaalen, W.L.J. van Putten and G.C. van Rhoon. Reirradiation combined with hyperthermia in recurrent breast cancer results in a worthwhile local palliation. British J. Cancer, 1999; 79:483-490

[26] Perez CA, Pajak T, Emami B, Hornback NB, Tupchong L, Rubin P. Randomized phase III study comparing irradiation and hyperthermia with irradiation alone in superficial measurable tumors. Am J Clin Oncol 1991;14:133-141.

[27] J van der Zee, PCM Koper, RFM Jansen, KAJ de Winter, GC van Rhoon. Re-irradiation and hyperthermia for recurrent breast cancer in the orbital region: a case report. Int J Hyperthermia 2004;20:1-6.

[28] Linthorst M, Van Rhoon GC, Broekmeijer-Reurink MP, Drizdal T, Van der Zee J. The tolerance of skin transfers for reirradiation and hyperthermia. Presented at 26th Annual Meeting of the European Society for Hyperthermic Oncology, Rotterdam 2010.

[29] Broekmeyer-Reurink MP, Rietveld PJM, Van Rhoon GC, Van der Zee J. Some practical notes on documentation of superficial hyperthermia treatment, Int J Hyperthermia 1992;8:401-406.

[30] De Bruijne M, Van der Zee J, Ameziane A, Van Rhoon GC. Quality control of superficial hyperthermia by treatment evaluation. Int J Hyperthermia 2011;27:199-213.

[31] J. van der Zee, A.J. Wijnmaalen, J. Haveman, E. Woudstra and S.K. van der Ploeg. Hyperthermia may decrease the development of telangiectasia after radiotherapy. Int. J. Hyperthermia 14, 57-64, 1998.

[32] Liu F-F, Bezjak A, Levin W, Cooper B. Pintilie M, Sherar MD. Letter to the Editor. Assessment of palliation in women with recurrent breast cancer. Int J Hyperthermia 1996;12:825-826.

[33] Jones EL, Oleson JR, Prosnitz LR, Samulski TV, Vujaskovic Z, Yu D, Sanders LL, Dewhirst MW. Randomized trial of hyperthermia and radiation for superficial tumors. J Clin Oncol 2005;23:3079-3085.

[34] De Bruijne M, Van der Holt B, Van Rhoon GC, Van der Zee J. Evaluation of CEM43°CT90 thermal dose in superficial hyperthermia: a retrospective analysis. Strahlenther Onkol 2010;186:436-443.

[35] Fazekas JT, Nerlinger RE. Localized hyperthermia adjuvant to irradiation in superficial recurrent carcinomas: a preliminary report on 46 patients. Int J Radiat Oncol Biol Phys 1981;7:1457-1463.

[36] Lindholm C-E, Kjellen E, Nilsson P, Hertzman S. Microwave-induced hyperthermia and radiotherapy in human superficial tumours: clinical results with a comparative study of combined treatment versus radiotherapy alone. Int J Hyperthermia 1987;3:393-411.

[37] González González D, Van Dijk JDP, Blank LECM. Chestwall recurrences of breast cancer: results of combined treatment with radiation and hyperthermia. Radiotherapy and Oncology 1988;12:95-103.

[38] Egawa S, Tsukiyama I, Watanabe S, Ohno Y, Morita K, Tominaga S, Onoyama Y, Hashimoto S, Yanagawa S, Uehara S, Abe M, Mochizuki S, Sugiyama A, Inoue T. A randomized clinical trial of hyperthermia and radiation versus radiation alone for superficially located cancers. J Jpn Soc Ther Radio Oncol 1989;1:135-140.

[39] Dragovic J, Seydel HG, Sandhu T, Kolosvary A. Blough J. Local superficial hyperthermia in combination with low-dose radiation therapy for palliation of locally recurrent breast carcinoma. J Clin Oncol 1989;7:30-35.

[40] Li RY, Lin SY, Zhang TZ. Assessment of combined thermoradiotherapy in recurrent or advanced carcinoma of the breast. Adv Exp Med Biol 1990;267:521-523.

[41] Dubois JB, Hay M, Bordure G. Superficial microwave-induced hyperthermia in the treatment of chest wall recurrences in breast cancer. Cancer 1990;848-852.

[42] Masanuga S, Hiraoka M, Takahashi M, Jo S, Akuta K, Nishimura Y, Nagata Y, Abe M. Clinical results of thermoradiotherapy for locally advanced and/or recurrent breast cancer – comparison of results with radiotherapy alone. Int J Hyperthermia 1990;6:487-497.

[43] Phromratanapongse P, Steeves RA, Severson SB, Paliwal BR. Hyperthermia and irradiation for locally recurrent previously irradiated breast cancer. Strahlenther Onkol 1991;167:93-97.

[44] Engin K, Tupchong L, Waterman FM, Komarnicky L, Mansfield CM, Hussain N, Hoh LL, McFarlane JD, Leeper DB. Multiple field hyperthermia combined with radiotherapy in advanced carcinoma of the breast. Int J Hyperthermia 1994;10:587-603.

[45] Lee HK, Antell AG, Perez CA, Straube WL, Ramachandran G, Myerson RJ, Emami B, Molmenti EP, Buckner A, Lockett MA. Superficial hyperthermia and irradiation for recurrent breast carcinoma of the chest wall: prognostic factors in 196 tumors. Int J Radiat Oncol Biol Phys 1998;40:365-375.

[46] Myerson RJ, Straube WL, Moros EG, Emami BN, Lee HK, Perez CA, Taylor ME. Simultaneous superficial hyperthermia and external radiotherapy: report of thermal dosimetry and tolerance to treatment. Int J Hyperthermia 1999;15:251-266.

[47] Feyerabend T, Wiedemann GJ, Jäger B, Vesely H, Mahlmann B, Richter E. Local hyperthermia, radiation, and chemotherapy in recurrent breast cancer is feasible and effective except for inflammatory disease. Int J Radiat Oncol Biol Phys 2001;49:1317-1325.

[48] Kouloulias VE, Dardoufas CE, Kouvaris JR, Gennatas CS, Polyzos AK, Gogas HJ, Sandilos PH, Uzunoglu NK, Malas EG, Vlahos LJ. Liposomal doxorubicin in conjunction with reirradiation and local hyperthermia treatment in recurrent breast cancer: a phase I/II trial. Clin Canc Res 2002;8:374-382.

[49] Ben Yosef R, Vigler N, Inbar M, Vexler A. Hyperthermia combined with radiation therapy in the treatment of local recurrent cancer. IMAJ 2004;6:392-395.

[50] Li G, Mitsumori M, Ogura M, Horii N, Kawamura S, Masanuga S, Nagata Y, Hiraoka M. Local hyperthermia combined with external irradiation for regional recurrent breast carcinoma. Int J Clin Oncol 2004;9:179-183.

[51] Wahl AO, Rademaker A, Kiel KD, Jones EL, Marks LB, Croog V, McCormick BM, Hirsch A, Karkar MS, Motwani SB, Tereffe W, Yu T-K, Her D, Silverstein J, Kachnic LA, Kesslering C, Freedman GM, Small W. Multi-institutional review of repeat irradiation of chest wall and breast for recurrent breast cancer. Int J Radiat Oncol Biol Phys 2008;70:477-484.

[52] Gabriele P, Ferrara T, Baiotto B, Garibaldi E, Marini PG, Penduzzu G, Giovanni V, Bardati F, Guiot C. Radio hyperthermia for re-treatment of superficial tumours. Int J Hyperthermia 2009;25:189-198.

[53] Turesson I, Thames HD. Repair capacity and kinetics of human skin during fractionated therapy, erythema, desquamation, and telangiectasis after 3 and 5 year's follow-up. Radiotherapy and Oncology 1989;15:169-188.

[54] Emami B, Lyman J, Brown A, Coia L, Goitein M, Munzenrider JE, Shank B, Solin LJ, Wesson M. Tolerance of normal tissue to therapeutic irradiation. Int J Radiat Oncol Biol Phys 1991;21:109-122.

[55] Oldenborg S, Van Os RM, Van Rij CM, Crezee J, Van de Kamer JB, Rutgers EJT, Geijsen ED, Zum Vörde sive Vörding PJ, Koning CCE, Van Tienhoven G. Elective re-irradiation and hyperthermia following resection of persistent locoregional breast cancer: a retrospective study. Int J Hyperthermia 2010;26:136-144.

3

Evaluation of CEM43°CT90 thermal dose in superficial hyperthermia: a retrospective analysis

Abstract

Purpose: Prospective use of the CEM43°CT90 thermal dose parameter has been proposed for hyperthermia treatments. This study evaluates the CEM43°CT90 parameter by means of a retrospective analysis of recurrent breast cancer patients receiving reirradiation plus hyperthermia.

Methods and Materials: CEM43°CT90 was calculated for 72 patients who received 8×4 Gy reirradiation plus 8×1 hr hyperthermia for adenocarcinoma recurrences at the chest wall. Associations of prognostic factors CEM43°CT90 and tumour maximum diameter with endpoints complete response (CR), duration of local control (DLC), and survival (OS) were determined.

Results: A highly significant inverse association between CEM43°CT90 and tumour maximum diameter (ρ = -0.7, p < 1e-6) was found. The association between CR and CEM43°CT90 was not significant (p > 0.7). CEM43°CT90 was associated with DLC. Both CEM43°CT90 and tumour maximum diameter had a significant association with survival ($p \leq 0.01$). The association with thermal dose, when adjusted for tumour maximum diameter, was not significant for either CR, DLC or OS (p > 0.2).

Conclusions: In this retrospective study no clear CEM43°CT90 thermal dose targets or associations with clinical endpoints could be established.

Introduction

The identification of quality factors for hyperthermia (HT) treatments has been a central theme in hyperthermia research for the last twenty years. As the objective in hyperthermia treatments is to heat a tissue volume to 39-45°C, it is obvious to use thermal parameters to quantify hyperthermia quality. Over the years, more then twenty of such parameters have been proposed. They range from simple temperature statistics (e.g. minimum temperature, median temperature, temperature percentiles, etc.) to thermal iso-effect dose parameters, which convert the time-temperature data into an iso-effect dose [19]. Several of these have been shown to correlate significantly with complete response, duration of local control, and survival [2,8,14,16,20].

A thermal dose parameter that can be generally adopted should meet the principal requirements of a dose: it should relate to the biological response in a relevant manner, it is a well defined and measurable quantity, and it can be used as a proper means of comparison [7]. Apart from temperature and duration of treatment other factors may significantly affect the efficacy of hyperthermia treatments, for example: HT technique (e.g. applicator frequency [27], specific absorption rate coverage [15]), previous irradiation [10,11], tumour size [15,16,18,20,27] and histology [16,18]. Since hyperthermia is usually applied in combination with radiotherapy or chemotherapy, the dose and treatment scheme of the other modality will also influence clinical outcome [15,16]. Finally, the quality of the applied thermometry (number of measurement points, spatial distribution, etc.) is likely to affect the measured thermal dose [20]. The identification of a robust and generally applicable thermal dose parameter is therefore a daunting task.

The randomized trial by Jones *et al.* [11] was the first to prescribe thermal dose in human patients, using the CEM43°CT90 thermal dose parameter. A quantitative dose measure was introduced to test heatability (> 0.5 CEM43°CT90 during the first treatment) and for the minimum effective dose (≥ 10 CEM43°CT90 for the whole treatment series). In order to reach this effective dose, a variable number of treatments and variable treatment lengths were applied.

We are now at a point where several randomized clinical trials have demonstrated the significant improvement in clinical response when hyperthermia is added to radiotherapy, both in fixed schedules [10], and in flexible treatment series based on a CEM43°CT90 thermal dose [11]. At the same time there are still open questions. One is: is there a generally applicable minimum effective thermal dose for both approaches? If CEM43°CT90 meets the principal requirements of a dose, data obtained in fixed HT schedules should also reflect the effective thermal dose. To verify this hypothesis this study evaluates the CEM43°CT90 thermal dose parameter by means of a retrospective analysis in a homogeneous group of patients, all of whom received a fixed-schedule superficial HT treatment plus reirradiation for breast adenocarcinoma recurrences at the chest wall.

Material and methods

Patients and treatments

The analysis presented in this paper comprises 72 patients with locoregional breast cancer (adenocarcinoma) who received reirradiation (8×4 Gy, twice weekly) plus HT (60 minutes, after radiotherapy) in our clinic over a period of five years. For this group the same treatment schedule, techniques, and strategy were applied, and time-temperature and follow-up data were available. Table 1 details the tumour characteristics of the patients. Figure 1 shows the overall structure of the study.

Table 1. Characteristics of the adenocarcinoma chest wall recurrences (total 72 patients).

Number of separate tumour lesions in the HT field	
1	24 (33%)
2	13 (18%)
3	7 (10%)
4	1 (1%)
5	5 (7%)
6	6 (6%)
7	1 (1%)
8	4 (8%)
≥ 9	11 (15%)
Diameter of the largest lesion (max.tumour diameter, cm)	
0.0 – 1.0	12 (17%) *
1.1 – 2.0	12 (17%)
2.1 – 3.0	7 (10%)
3.1 – 4.0	4 (6%)
4.1 – 5.0	4 (6%)
5.1 – 6.0	4 (6%)
6.1 – 7.0	4 (6%)
7.1 – 8.0	5 (7%)
8.1 – 9.0	3 (4%)
9.1 – 10.0	2 (3%)
10.1 – 15.0	9 (13%)
15.1 – 20.0	4 (6%)
20.1 – 25.0	1 (1%)
25.1 – 30.0	1 (1%)
Maximum depth relative to skin surface (cm)	
1	17 (24%)
2	35 (49%)
3	12 (17%)
4	2 (3%)
5	2 (3%)
≥ 6	4 (6%)
Ulcerating tumour	
Yes	16 (22%)
No	56 (78%)

* = 6 patients have microscopic tumour
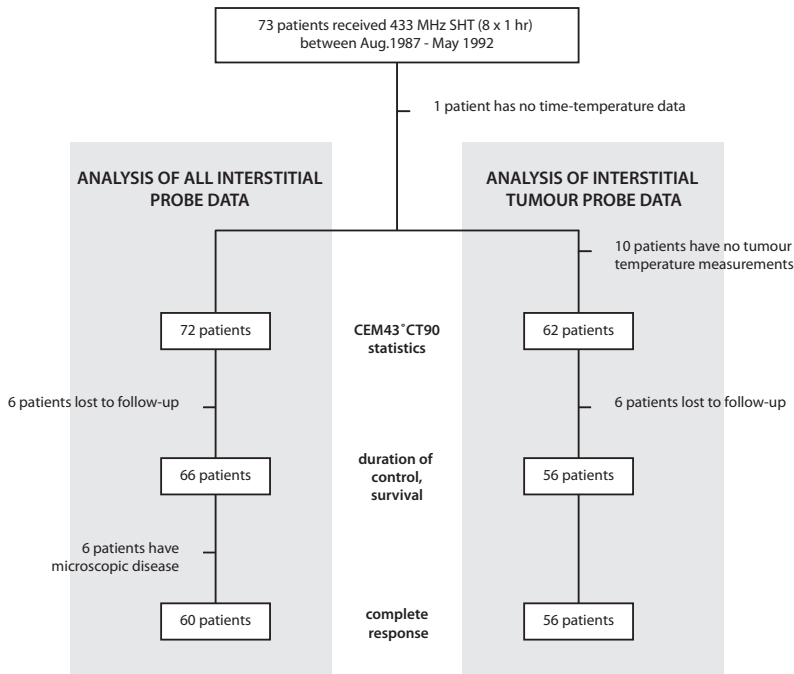
Figure 1. Overview of the retrospective analysis.

An array of one to five incoherently driven 433 MHz water-filled waveguide applicators [29] was applied on the patients. The applicator array extended the RT field at least 1 cm at all sides; patchwork heating or multiple applications per HT field did not occur. A temperature-controlled waterbolus was placed between the applicators and the skin. Interstitial and skin temperatures were measured using stationary single- and multi-sensor fibre-optic probes (24 channels). The distribution of temperature sensors over the target volume aimed at measuring interstitial temperatures below each applicator, for which a median of four catheters were introduced. For more details about the treatment and clinical results, see [26,27].

Prognostic factors

Two prognostic factors were tested: the thermal dose expressed as CEM43°CT90, and tumour maximum diameter. The latter, defined as the diameter of the largest tumour lesion in the treatment field, is a representative for tumour physiology, and was included because it proved to be the most significant factor associated with duration of local control in univariate analysis, and the only significant patient/tumour characteristic in multivariate analysis in a previous analysis of RT+HT in recurrent breast cancer [27].

Thermal dose

CEM43°CT90 represents the thermal iso-effect dose expressed in cumulative equivalent minutes at a reference temperature of 43°C, based on the low end of the temperature distribution (T90). For a review of the background and historical development of the thermal iso-effect dose concept, see [3,5,8]. Cumulative equivalent minutes (CEM) were calculated from the time/temperature data as follows [19]:

$$CEM\,43°CT90 = \sum_{i=1}^{n} t_i \cdot R^{(43-T90_i)}$$

where t_i is the time interval of the ith sample (t_i = 1.5 minutes), R the rate of cell killing ($R(T < 43°C) = ¼$, $R(T > 43°C) = ½$) [11,14,16,20]. $T90_i$ was determined by linear interpolation in temperature map i; the T90 rank r in the ordered n-element set of temperatures is $r = 0.1 \cdot (n+1)$ [21].

The iso-effect dose acquired over the whole treatment series (CEM43°CT90$_{tot}$) is the sum of the thermal dose per treatment (CEM43°CT90$_i$), corrected for treatments for which no data was available:

$$CEM\,43°CT90_{tot} = \frac{n_{given}}{n_{data}} \cdot \sum_{i=1}^{n_{data}} CEM\,43°CT90_i$$

where n_{given} is the number of treatments actually given and n_{data} the number for which time/temperature data was available.

In line with most thermal dose studies in literature [2,11,14,15,16,20], the analysis was limited to interstitially measured temperatures, since the value of measurements from probes placed between the skin and waterbolus was considered questionable [30].

Two sets of dose parameters were calculated from the clinical data. First, thermal dose was calculated from interstitial temperature measurements *in tumours only* (CEM43°CT90$_{TUMOUR}$). This agrees with the approach taken in other published studies [11,14,16], where the primary aim was to heat macroscopic tumour. Second, it was calculated from *all interstitially measured temperatures* (CEM43°CT90$_{ALL}$), reflecting the principle that heating macroscopic as well as microscopic tumour is a prerequisite for achieving a lasting clinical response [27].

Clinical response

The aim of the treatments was to achieve local tumour control [27]. A complete response (CR) was defined as a complete remission of all tumour lesions within the treatment field, observed twice with a time interval of at least four weeks. Duration of local control (DLC) was defined as the interval between the first treatment and the first observation of progression after achieving a CR. Overall survival (OS) was defined as the interval between the first treatment and the date of death.

Statistical analysis

Due to the skewed distribution of CEM43°CT90 and tumour maximum diameter values, their logarithms were included in the analysis of prognostic factors. To test for significance, logistic regression [9] was used for CR, and Cox regression [1] for DLC and OS. Kaplan-Meier curves [13] were constructed to illustrate DLC and OS. p values ≤ 0.01 were considered statistically significant, while p values ≤ 0.05 were denoted a trend.

Results

Thermal dose statistics

The cumulative distribution of the total thermal dose for CEM43°CT90$_{TUMOUR}$ and CEM43°CT90$_{ALL}$ are depicted in Figure 2. Figure 3 shows the connection between the number of temperature sensors and CEM43°CT90$_{TUMOUR}$ and CEM43°CT90$_{ALL}$ per treatment.
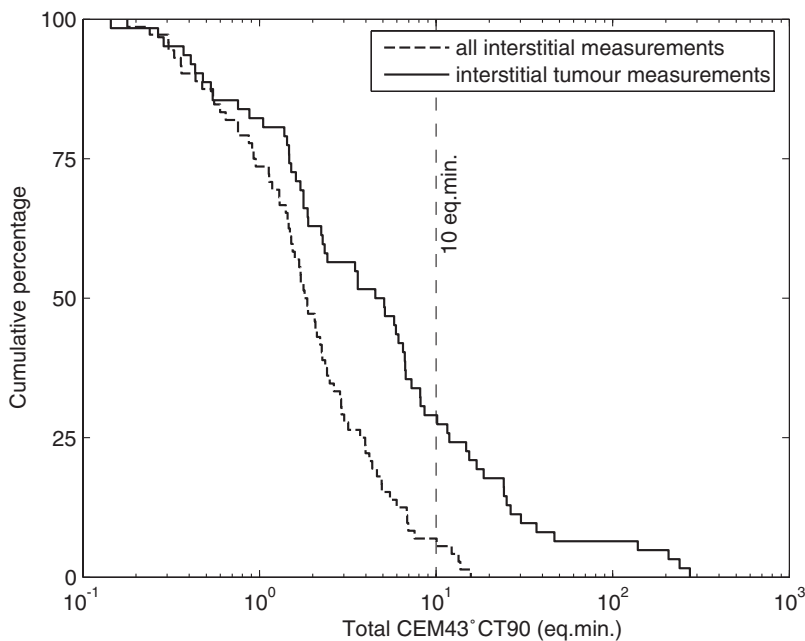
Figure 2. Cumulative distribution of the total thermal dose for all interstitial probe data (CEM43°CT90$_{ALL}$), and for the interstitial tumour probe data (CEM43°CT90$_{TUMOUR}$). CEM43°CT90$_{ALL}$ (median 1.8) was lower than CEM43°CT90$_{TUMOUR}$ (median 4.8). 29% of the patients obtained $\geq$10 CEM43°CT90$_{TUMOUR}$, and 7% of patients obtained $\geq$10 CEM43°CT90$_{ALL}$.

a.

b.
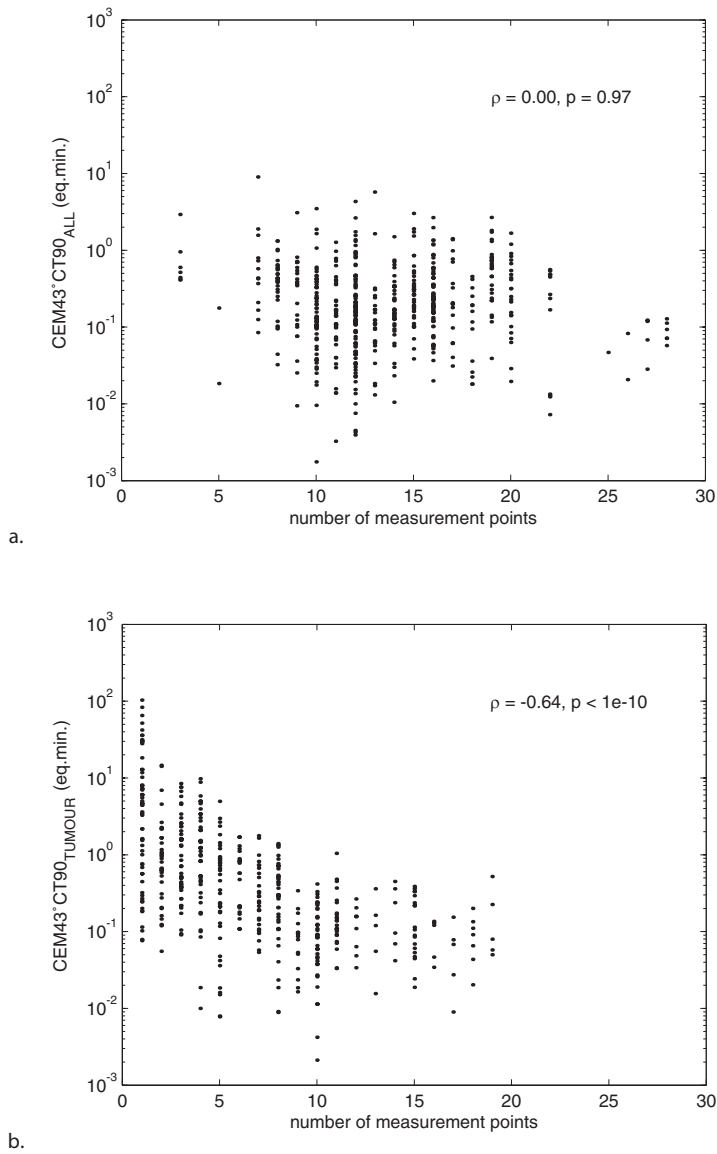
Figure 3. Illustration of the association between number of measurement points and thermal dose. (a) CEM43°CT90$_{ALL}$ (n = 550 treatments), (b) CEM43°CT90$_{TUMOUR}$ (n = 451 treatments). For CEM43°CT90$_{TUMOUR}$ Spearman's rank correlation was highly significant: ρ = -0.64 (p < 1e-10).

a.

b.
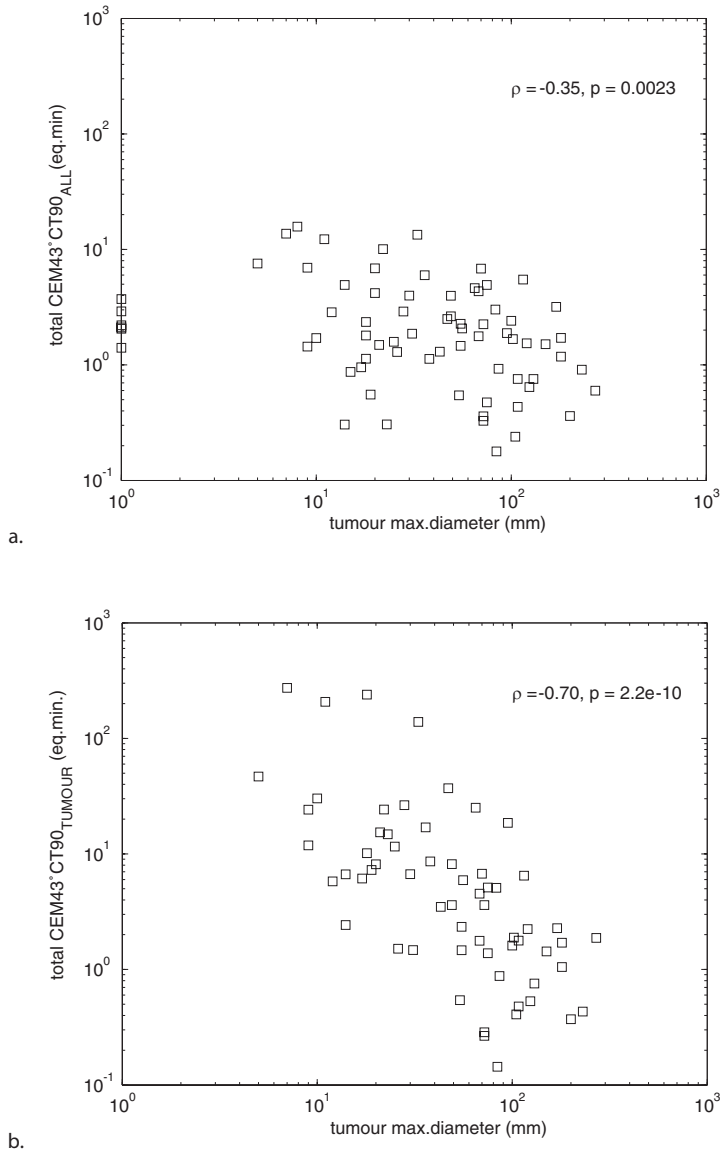
Figure 4. Illustration of the association between tumour maximum diameter and thermal dose. (a) total CEM43°CT90$_{ALL}$, (b) total CEM43°CT90$_{TUMOUR}$. For CEM43°CT90$_{TUMOUR}$ Spearman's rank correlation was −0.70 (p < 1e-6, n = 62); for CEM43°CT90$_{ALL}$ it was -0.35 (p = 0.002, n = 72).

Association between prognostic factors

As shown in Figure 4, a highly significant negative association was found between tumour maximum diameter and the thermal dose parameters.

Relation between prognostic variables and clinical response

Table 2 shows the univariate correlations between the thermal dose parameters and clinical response. No statistically significant dependence of complete response on $CEM43°CT90_{TUMOUR}$ or $CEM43°CT90_{ALL}$ was found. However, duration of local control was associated with $CEM43°CT90_{TUMOUR}$, and a significant relation between survival and $CEM43°CT90_{TUMOUR}$ was found. For $CEM43°CT90_{ALL}$ similar, but slightly less significant associations with DLC and OS were observed. Figure 5 illustrates these trends for duration of control and survival with Kaplan-Meier curves for equally sized clusters of low, medium and high $CEM43°CT90_{TUMOUR}$.

Table 2. Associations between (1) the logarithm of thermal dose and clinical response, (2) the logarithm of tumour maximum diameter and clinical response, and (3) the logarithm of $CEM43°CT90_{TUMOUR}$ thermal dose after adjustment for tumour maximum diameter, and clinical response.

| Parameter, endpoint	Odds ratio	Hazard ratio	95% confidence interval	P
1.a) $CEM43°CT90_{TUMOUR}$				
Complete response	1.03	-	0.70 - 1.49	0.89
Duration of local control	-	0.78	0.63 - 0.97	0.027
Survival	-	0.67	0.51 - 0.88	0.004
1.b) $CEM43°CT90_{ALL}$				
Complete response	0.89	-	0.50 - 1.58	0.70
Duration of local control	-	0.79	0.58 - 1.08	0.13
Survival	-	0.59	0.40 - 0.85	0.005
2) Tumor maximum diameter				
Complete response	0.66	-	0.34 - 1.30	0.23
Duration of local control	-	1.49	1.14 - 1.96	0.004
Survival	-	1.86	1.29 - 2.67	<0.001
3) $CEM43°CT90_{TUMOUR}$ adjusted for tumor maximum diameter				
Complete response	0.73	-	0.43 - 1.23	0.24
Duration of local control	-	0.83	0.62 - 1.11	0.21
Survival	-	0.81	0.56- 1.16	0.25

Also for tumour maximum diameter there was no significant correlation with CR. The hazard ratios for duration of local control and survival were strongly significant, indicating a poor prognosis for tumours with large maximum diameters. These correlations are illustrated in Figure 6, which plots Kaplan-Meier curves for equally sized clusters of small, medium and large tumour maximum diameter. It can be seen that the trends in Figure 6 for maximum diameter are the opposite of the trends in Figure 5 for thermal dose, as could be expected from the strong inverse association between the thermal dose parameters and tumour maximum diameter.

Finally, both prognostic factors were combined in a multivariate analysis. The results in Table 2 show that the association with thermal dose, when adjusted for tumour maximum diameter, was not significant for either CR, DLC or OS.
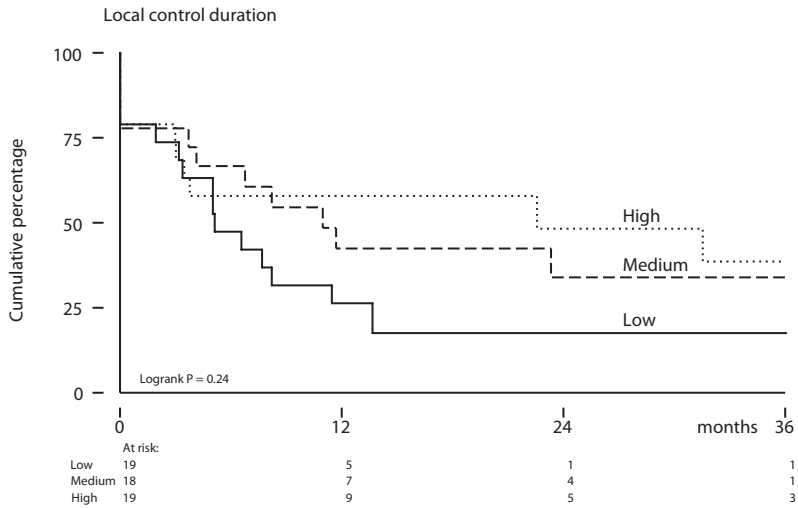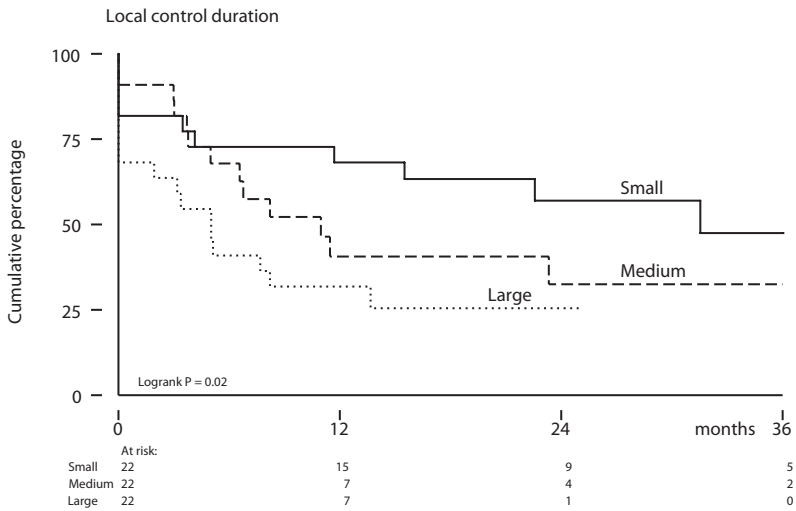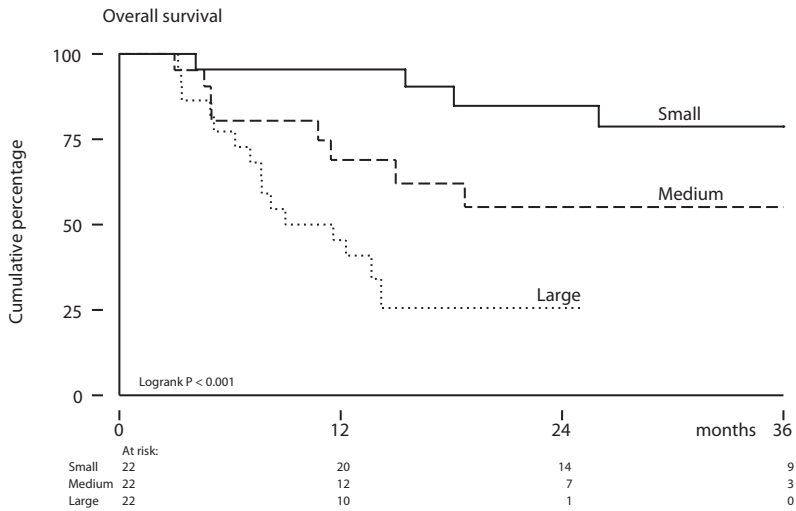

a.
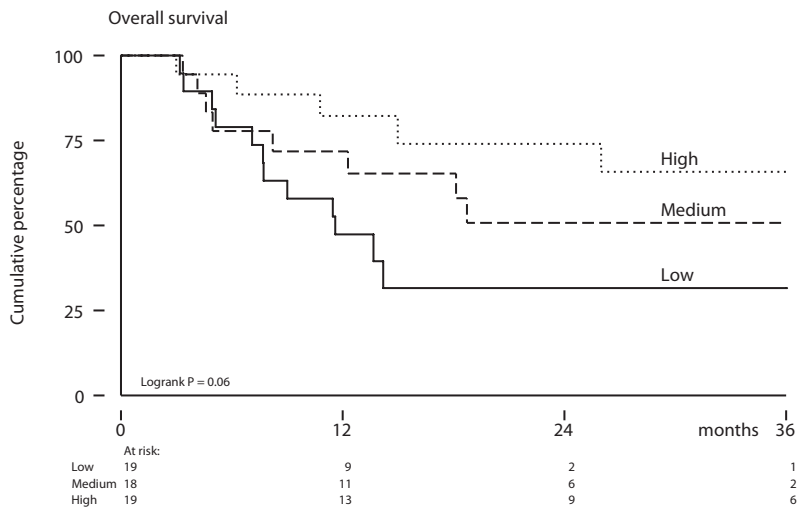
b.

Figure 5. Kaplan-Meier curves depicting (a) duration of local control, and (b) survival in relation to total thermal dose measured in tumour, for equally sized clusters of low (≤ 1.9), medium (1.9 – 8.6) and high (≥ 8.6) CEM43°CT90$_{TUMOUR}$.

Local control duration

Overall survival

Figure 6 Kaplan-Meier curves depicting (a) duration of local control and (b) survival in relation to tumour maximum diameter, for equally sized clusters of small (≤ 19 mm), medium (20 – 68 mm) and large (≥ 70 mm) maximum tumour diameters.

Discussion

Combined radiation and HT is a successful tool in the management of cancer [28]. For recurrent breast cancer in previously irradiated areas, CR rates double compared to RT alone (RT 24-38%; RT+HT 68-78%) [10,11]. These favourable results have been obtained both in schedules where the number and duration of treatments was fixed, and in schedules where HT duration was varied to reach a certain target dose. The current retrospective analysis was performed to investigate whether there is a relation between both approaches in terms of thermal dose.

The CR rate of 79% observed in the current analysis shows that the addition of HT was effective, as published CR rates for re-RT alone in comparable patient groups are 24-38% [10,11,17]. At the same time, however, our data showed no significant independent correlation ($p \geq 0.7$) between CEM43°CT90 and complete response. Three factors may explain the weak correlation. First, it must be stated that the high (79%) CR rate in the data studied makes the association more difficult to detect statistically, given the relatively limited number of patients included. Second, in principle CEM43°CT90 does not cover all mechanisms of action that are responsible for the supra-additive effect of RT plus HT. The equivalent minutes formulation of Sapareto and Dewey [19] of which CEM43°CT90 was derived basically describes heat cytotoxicity. Although this certainly is a mechanism, opinions are that inhibition of DNA damage repair, and improvements in tumour oxygenation are further responsible for the improved response when HT is added to RT [4,6,12,22-25]. Third, the interaction between tumour size, number of measurement points, and T90 temperatures may affect the ability of the CEM43°CT90 quantity to reflect the quality of heating, as will be discussed below.

Apart from the prospective trial by Jones *et al.* [11], several retrospective studies investigated CEM43°CT90$_{TUMOUR}$ [14,16] or an analogue [20] in breast cancer patients. Oleson *et al.* [16] and Kapp *et al.* [14] showed a significant correlation with CR. A significant correlation with duration of control has been reported by [14]. Sherar *et al.* [20] found a strong correlation with duration of control and overall survival. Details about tumour size and its effect were included in most studies [14,16,20]. In [16] tumour volume was a significant factor in their regression model. In [20] tumour area was significantly associated with survival, but not with CR or DLC. It must be mentioned that most studies [11,14,16] investigated thermal dose per lesion, whereas in this study the clinical response relates to the treatment field, which can contain multiple lesions.

Because of the low correlation with CR, no "effective thermal dose" value can be defined for the current dataset. Consequently, the published criteria of 0.5 CEM43°CT90 for heatability and 10 CEM43°CT90$_{TUMOUR}$ for effective dose [11,14] does not select the responders in our case, see Table 3. Apparently, quantitative thermal dose measures may have a different impact in different HT centres, due to e.g. differences in thermometer placement.

Table 3. Complete response rates for subgroups of patients who received less or more than 10 CEM43°CT90$_{TUMOUR}$ in total ("minimal effective dose"; $n = 56$), and for patients who achieved less or more than 0.5 CEM43°CT90$_{TUMOUR}$ during the first HT treatment ("heatability"; $n = 55$, one patient lacked temperature data of first treatment).

Criterion	Complete response
Total CEM43°CT90$_{TUMOUR}$ > 10	14/18 (78%)
Total CEM43°CT90$_{TUMOUR}$ ≤ 10	30/38 (79%)
CEM43°CT90$_{TUMOUR}$ first treatment > 0.5	20/25 (80%)
CEM43°CT90$_{TUMOUR}$ first treatment ≤ 0.5	24/30 (80%)

The univariate analysis revealed a trend for higher duration of control at higher CEM43°CT90, and a statistically significant correlation with survival. From a clinical point of view, no relation between thermal dose and survival should be expected, as the vast majority of patients with breast cancer recurrences have metastases elsewhere in the body. Sherar *et al.* [20] stated that there appears to be no biological rationale why the quality of local treatment would affect overall survival for disease of this type, and suggested that the association would not be caused by any direct effect of the HT treatment. We hypothesize that the trends towards better local control and survival for higher thermal doses in the current study can be explained from an underlying tumour selection mechanism, namely the inverse association between thermal dose and tumour maximum dimension.

Tumour properties and practical aspects with regard to thermometry and calculation of T90 may contribute to this. First, tumours with a large maximum diameter may represent the more aggressive, faster-growing tumours having better vascularized tissue sections [20], adding to the chances of measuring a low T90, thus a low thermal dose. Second, as the number of measurement points increases with tumour dimension, the sensitivity of T90 for low outliers will especially affect tumours with larger diameters. The significant inverse correlation between the number of measurement points and CEM43°CT90$_{TUMOUR}$ (Figure 3) reflects this sensitivity.

The general application of thermal dose benefits from robust definitions. The presented data showed that probe inclusion criteria and tumour maximum diameter affected CEM43°CT90 thermal doses. Site-specific thermal dose assessments may be a solution here. CEM43°C can be calculated per point from the full three-dimensional temperature distribution, which can be obtained by combining clinical temperature measurements with hyperthermia treatment planning. The tissue damage equations might also include the other main mechanisms of action in their formulation. Work is currently underway attempting to predict clinical response using treatment planning models.

Conclusion

Our data show a highly significant inverse association between thermal dose and tumour maximum diameter, while no significant association with CR was found. This indicates that CEM43°CT90 thermal dose needs further exploration before it is generally applicable across treatment centres.

References

[1]   Cox DR. Regression models and life tables. J R Stat Soc 1972;34:187-220.

[2]   Cox RS, Kapp DS. Correlation of thermal parameters with outcome in combined radiation therapy-hyperthermia trials. Int J Hyperthermia 1992;8:719-732.

[3]   Dewey WC. Arrhenius relationships from the molecule and cell to the clinic. Int J Hyperthermia 1994;10:457–83.

[4]   Dewhirst MW, Thrall D, Vujaskovic Z, *et al*. In reply to van der Zee *et al*. Int J Hyperthermia 2006;22:437-446.

[5]   Dewhirst MW, Viglianti BL, Lora-Michiels M, *et al*. Basic principles of thermal dosimetry and thermal thresholds for tissue damage from hyperthermia. Int J Hyperthermia 2003;19:267-294.

[6]   Dewhirst MW, Vujaskovic Z, Jones E, *et al*. Re-setting the biological rationale for thermal therapy. Int J Hyperthermia 2005;21:779-790.

[7]   Field SB, Raaphorst GP. Thermal Dose. In: Field SB, Hand JW, ed. An introduction to the practical aspects of clinical hyperthermia. London: Taylor & Francis, 1990:69-76.

[8]   Hand JW, Machin D, Vernon CC, *et al*. Analysis of thermal parameters obtained during phase III trials of hyperthermia as an adjunct to radiotherapy in the treatment of breast carcinoma. Int J Hyperthermia 1997;13:343-364.

[9]   Hosmer DW, Lemeshow S. Applied logistic regression. New York: John Wiley and Sons, 1989.

[10] International Collaborative Hyperthermia Group: Vernon CC, Hand JW, Field SB, *et al*. Radiotherapy with or without hyperthermia in the treatment of superficial localized breast cancer – Results from five randomized controlled trials. Int J Radiat Oncol Biol Phys 1996;39:731-744.

[11] Jones EL, Oleson JR, Prosnitz LR, *et al*. Randomized trial of hyperthermia and radiation for superficial tumors. J Clin Oncol 2005;23:3079-3085.

[12] Kampinga HH. Cell biological aspects of hyperthermia. Int J Hyperthermia 2008; 24(2):126-134.

[13] Kaplan E, Meier P. Nonparametric estimation from incomplete observations. J Am Stat Assoc 1958;53:457-481.

[14] Kapp DS, Cox RS. Thermal treatment parameters are most predictive of outcome in patients with single tumor nodules per treatment field in recurrent adenocarcinoma of the breast. Int J Radiat Oncol Biol Phys 1995;33:887-899.

[15] Lee HK, Antell AG, Perez CA, *et al*. Superficial hyperthermia and irradiation for recurrent breast carcinoma of the chest wall: prognostic factors in 196 tumors. Int J Radiat Oncol Biol Phys 1997;40:365-375.

[16] Oleson JR, Samulski TV, Leopold KA, *et al*. Sensitivity of hyperthermia trial outcomes to temperature and time: implications for thermal goals of treatment. Int J Radiat Oncol Biol Phys 1993;25:289-297.

[17] Perez CA, Gillespie B, Pajak T, *et al*. Quality assurance problems in clinical hyperthermia and their impact on therapeutic outcome: a report by the Radiation Therapy Oncology Group. Int J Radiat Oncol Biol Phys 1989;16:551-558.

[18] Perez CA, Pajak T, Emami B, *et al*. Randomized phase III study comparing irradiation and hyperthermia with irradiation alone in superficial measurable tumors. Final report by the Radiation Therapy Oncology Group. Am J Clin Oncol 1991;14:133-141.

[19] Sapareto SA, Dewey WC. Thermal dose determination in cancer therapy. Int J Radiat Oncol Biol Phys 1984;10:787-800.

[20] Sherar M, Liu FF, Pintilie M, *et al*. Relationship between thermal dose and outcome in thermoradiotherapy treatments for superficial recurrences of breast cancer: data from a phase III trial. Int J Radiat Oncol Biol Phys 1997;39:371-380.

[21] Snedecor GW, Cochran WG. Statistical Methods. 6th edn. Ames: Iowa State University Press, 1967:123-125.

[22] Song CW. Overview and conclusion. Int J Hyperthermia 2008;24(2):139-140.

[23] Song CW, Park HJ, Lee CK, *et al*. Implications of increased tumor blood flow and oxygenation caused by mild teperature hyperthermia in tumor treatment. Int J Hyperthermia 2005;21:761-767.

[24] Song CW, Park HJ, Li G, *et al.* Genetic, immunological and physiological aspects of hyperthermia. Int J Hyperthermia 2008;24(2):134-138.

[25] Sugahara T, van der Zee J, Kampinga HH, *et al.* Kadota Fund International Forum 2004. Application of thermal stress for the improvement of health, 15–18 June 2004, Awaji Yumebutai International Conference Center, Awaji Island, Hyogo, Japan. Final Report. Int J Hyperthermia 2008;24(2):123-125.

[26] van der Zee J, de Bruijne M, Ameziane A, *et al.* Reirradiation combined with hyperthermia in breast cancer recurrences – overview of experience in Erasmus MC. Int J Hyperthermia 2010;26:638-648.

[27] van der Zee J, van der Holt B, Rietveld PJ, *et al.* Reirradiation combined with hyperthermia in recurrent breast cancer results in a worthwhile local palliation. Br J Cancer 1999;79:483-90.

[28] van der Zee J, Vujaskovic Z, Kondo M, *et al.* The Kadota Fund International Forum 2004 – Clinical group consensus. Int J Hyperthermia 2008;24(2):111-122.

[29] van Rhoon GC, Rietveld PJ, van der Zee J. A 433 MHz Lucite cone waveguide applicator for superficial hyperthermia. Int J Hyperthermia 1998;14:13-27.

[30] Waterman FM. Invasive thermometry techniques. In: Seegenschmiedt MH, Fessenden P, Vernon CC, ed. Thermoradiotherapy and Thermochemotherapy, Volume 1: Biology, Physiology, and Physics. Berlin: Springer-Verlag, 1995:331-360.

Effects of waterbolus size, shape and configuration on the SAR distribution pattern of the Lucite cone applicator

Abstract

The effects of waterbolus dimensions and configuration on the effective field size (EFS) of the Lucite cone applicator (LCA) for superficial hyperthermia are presented. The goal of the research is to develop guidelines which mark out a subset of optimal LCA-waterbolus set-ups. The effects of variations in (*i*) waterbolus thickness, (*ii*) waterbolus area, (*iii*) waterbolus length/width ratio and (*iv*) eccentric placement of the applicator have been investigated in an FDTD model study. The prominent effects were verified with IR thermography measurements. An optimal EFS value of 80 cm² was found for waterbolus area of 200-400 cm². A small (10×10 cm²) waterbolus area restricts the EFS to 25% of the optimal value. The sensitivity to sub-optimal waterbolus area and length/width ratio increases with waterbolus height. Eccentric placement of the LCA near the waterbolus edge reduces the EFS to up to 50% of the optimal value. The IR measurements confirmed the model findings. Based on the results, the following guidelines for the clinical application of the LCA have been defined: the waterbolus (*i*) should extend the LCA aperture at least 2.5 cm, especially at the Lucite windows, and (*ii*) its height should not exceed 2 cm.

Introduction

Efforts directed at improvement of SAR distributions in superficial hyperthermia generally aim for a large effective field size (EFS) [1], good spatial control and sufficient penetration depth. The design of the Lucite cone applicator (LCA) represented a major improvement of the EFS to aperture area ratio [2]. In array configurations, the EFS of the LCAs proved to be contiguous, as opposed to arrays of conventional waveguide applicators [3,4]. A clinical study revealed the strength of the LCA concept in terms of temperature distributions: higher (+0.3°C) invasively measured temperatures and virtually no average temperature differences (< 0.05°C) between the central area and periphery under the antennae [5].

In applicator systems for superficial hyperthermia the waterbolus is used to control skin temperature and to improve coupling between the electromagnetic applicators and tissue. Although the waterbolus is an essential part of the complete hyperthermia set-up, its influence on the resulting SAR distribution and the eventual performance of the applicator generally receives limited attention. In their paper describing the LCA, Van Rhoon *et al.* [2] already noted the potential effect of waterbolus size and shape on the resulting SAR distribution. Their measurements indicated the possibility that advantages of the LCA may be counteracted by the application of an unfavourable waterbolus configuration. The authors indicated the need to further investigate the effects of waterbolus size and shape in a parametric study.

In order to assess quality assurance guidelines for the clinical application of superficial hyperthermia, the FDTD method was exploited to investigate the effect of waterbolus size and shape on the EFS of the Lucite cone applicator. In addition, for the key waterbolus parameters, model output was collated with IR measurements. In this paper it is demonstrated that not only a proper applicator design, but also the waterbolus configuration is one of the key factors determining the quality of a superficial hyperthermia treatment.

Materials and methods

Lucite cone applicator

The Lucite cone applicator is a water-filled waveguide applicator operating in TE_{10} mode at 433 MHz. The inner dimensions of the LCA horn aperture are 10×10 cm². The LCA, which is an evolution of the conventional water-filled waveguide applicator, uses two distinctive features to realize an EFS to radiating aperture ratio of up to 0.9: (*i*) the diverging sidewalls of the horn which are parallel to the E-field were replaced by Lucite, and (*ii*) a PVC cone was placed in the centre of the aperture. The design and the performance of the LCA has been reported in detail in literature [2-4]. A schematic top-view of the LCA is given in Figure 1(a); Figure 1(b) depicts a 3-D representation of the LCA.
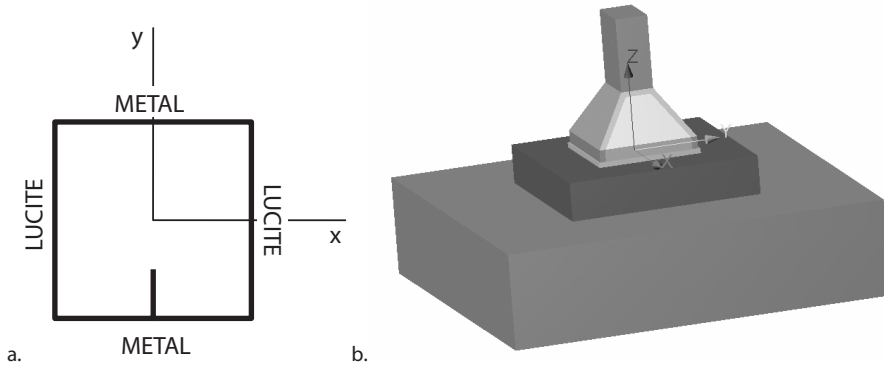
Figure 1. (a) Schematic representation of the LCA, showing the footprint of the antenna, the orientation of the feeding pin, and the lucite and brass sides of the horn aperture. (b) Configuration of the model: Lucite cone applicator, waterbolus and planar muscle-equivalent phantom.

Waterbolus parameters

The waterbolus is not an integral part of the LCA. Waterboli are available in several dimensions. This means that in clinical practice any combination of applicators and waterbolus may be applied.

Numerical calculations were carried out to study the effect of three parameters: (*i*) the waterbolus size, (*ii*) the waterbolus aspect ratio, defined as the ratio between dimensions parallel and perpendicular to the E-field , and (*iii*) an eccentric placement of the applicator onto the waterbolus. The waterbolus size comprises both thickness and area. The height was varied between 0 and 4 cm, to reflect the clinical range of the boli applied in our clinic. The area range encompasses the area of the boli applied in our clinic. Non-square waterboli (aspect ratio $\neq$ 1) were studied to take into account effects associated with the Lucite windows. Eccentric placement is relevant because in practical LCA array configurations applicators may touch the outer edge of the waterbolus and the extent of the waterbolus may be different at all sides.

All models consisted of a Lucite cone applicator (LCA), a brick-shaped waterbolus and a $40 \times 40 \times 10$ cm³ muscle-equivalent tissue phantom, as shown in Figure 1(b). The exact dimensions and alignment of the waterbolus varied with the parameter under study:

–   *waterbolus size*; assumed a square waterbolus area, ranging from the aperture size of the LCA horn (10×10 cm²) to the extent of the muscle phantom (40×40 cm²). The waterbolus was placed centrally under the LCA. Waterbolus height was 5, 10, 20 or 40 mm.
–   *waterbolus aspect ratio*; assumed a fixed waterbolus area of 250 or 500 cm². The aspect ratio ($AR = L_{\perp E} / L_{//E}$), that is the ratio of the waterbolus length and width, was set to

2/5, 2/4, 2/3, 2/2, 3/2, 4/2 and 5/2. The waterbolus was placed centrally under the LCA. Waterbolus height was 5, 10, 20 or 40 mm.

- *eccentric placement*; assumed a waterbolus area of 20×20 cm² and a height of 10, 20 or 40 mm. Starting from a configuration where the centre of the waterbolus was aligned with the centre of the LCA, the waterbolus was shifted 0, 25, or 50 mm parallel and/or perpendicular to the direction of the E-field.

FDTD model

The Finite Difference Time Domain (FDTD) method was used to calculate the electromagnetic energy deposition pattern. All simulations were performed with the SEMCAD FDTD simulation package (Schmid & Partner Engineering AG, Zürich, Switzerland). Using the solid modeling kernel of SEMCAD, the LCA, waterbolus and muscle phantom were implemented with their exact dimensions. As the PVC cone and the Lucite and brass walls of the LCA horn do not conform to the rectangular grid, staircasing effects are enevitable. However, the discretized models used a non-uniform mesh, allowing for local refinement. Moreover, a comparison of the current staircased model with an earlier split-cell implementation of the LCA [6] shows only marginal differences in the predicted SAR pattern (data not shown). Within the LCA volume, the grid step was restricted to 2 mm in all directions. Furthermore, the grid was refined at the boundaries of the source pin. Within the computational domain, the grid step varied between 1 and 10 mm, with a grading ratio of 1.5. The dimensions of the discretized model varied with the configuration, however the average model consisted of 1.5 million cells. The dielectric properties of the materials are listed in Table 1. A hard source between the wall of the waveguide and the source pin excited the E-field. The computational domain was terminated with Mur 2nd order boundary conditions.

Table 1. Dielectric parameters used in the FDTD simulations.

| Material	ε_r (-)	σ (S/m)
Lucite	2.59	$3 \cdot 10^{-3}$
PVC	2.2	$4 \cdot 10^{-3}$
De-ionized water	76	$1 \cdot 10^{-3}$
Muscle phantom	57	1.2

Experimental verification

For a selection of waterbolus configurations, the SAR distribution was measured at 1 cm depth in a 50×50×10 cm³ muscle-equivalent split phantom [7]. Gelatinous agar waterboli were composed of 87.8 weight% de-ionized water, 9.8 weight% formaldehyde solution (4%), and 2.4 weight% agar, and cut to a brick-shape. The experiments included the parameters waterbolus size and eccentric placement of the applicator. The effect of waterbolus size was measured for areas of 10×10, 15×15, 20×20 and 30×30 cm² and thicknesses of 8, 20 and 36 mm. The effect of eccentric placement was measured with a 20×20×4 cm³ waterbolus.

A net power of 200 W was applied to the applicator during 30 seconds, and the heating pattern was recorded with a TVS-600 infrared camera (Nippon Avionics Co. Ltd., Japan), within 10 seconds after power-off. A thermographic picture taken shortly before power-on, was substracted from the measured heating pattern in order to correct for inhomogeneities of the phantom surface temperatures and for reflections of heat sources in the phantom PVC foil cover. Another IR picture, taken during power-on, allows reconstruction of the exact position of the LCA within the image. Furthermore, measurement noise was filtered out with a 2D low-pass FIR filter, before normalizing the heating pattern and calculating the EFS.

Parameter evaluation

The effective field size (EFS) [1] was used as a quantitative measure for the evaluation and comparison of the different waterbolus configurations.
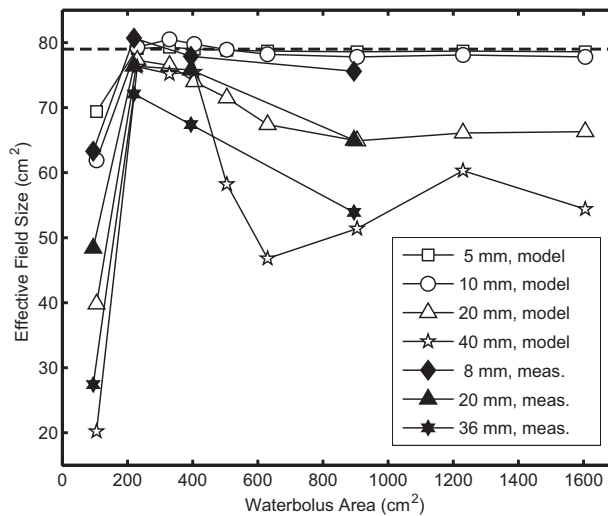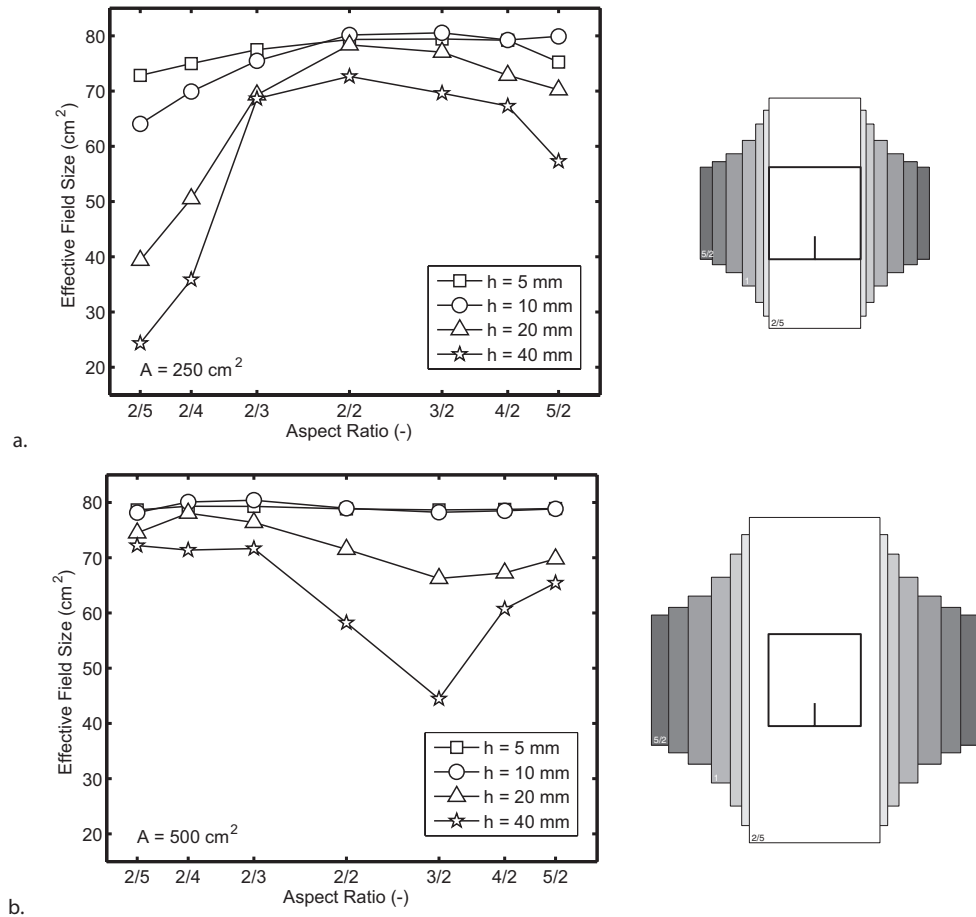

Figure 2. Effective Field Size as a function of square waterbolus area and waterbolus height. Results from measurements (black markers) and FDTD model (white markers). The dotted line indicates the calculated EFS in case no waterbolus is used.

Results I - FDTD parametric study

Waterbolus size

Figure 2 shows the predicted EFS for waterbolus dimensions ranging from 10×10 to 40×40 cm² and bolus heights of 5, 10, 20 and 40 mm. For comparison, the predicted EFS of the LCA without waterbolus is 79 cm². It was found that the sensitivity to waterbolus area

increases with waterbolus thickness. All thicknesses show an optimum EFS at areas between 200 and 400 cm². A waterbolus having the size of the LCA aperture (100 cm²) results in a drastic reduction of the EFS, which can be as high as 75% in case of the 40 mm thick bolus.

a.

b.

Figure 3. Effective Field Size as a function of waterbolus aspect ratio, for a bolus area of (a) 250 cm² and (b) 500 cm². Waterbolus height varies from 5 to 40 mm. The grey rectangles depict the extent of the waterboli relative to the LCA footprint (black icon).

Waterbolus Aspect Ratio.

Figure 3 shows the predicted EFS as a function of aspect ratio for waterbolus areas of 250 (Figure 3(a)) and 500 cm² (Figure 3(b)). For a waterbolus area of 250 cm² and an AR of 2/5, the long sides of the waterbolus touch the Lucite windows of the LCA horn. This leads to reduced EFS values for all waterbolus heights. When the waterbolus edges touch the brass sides of the horn (AR = 5/2), the reduction of the EFS is less pronounced.
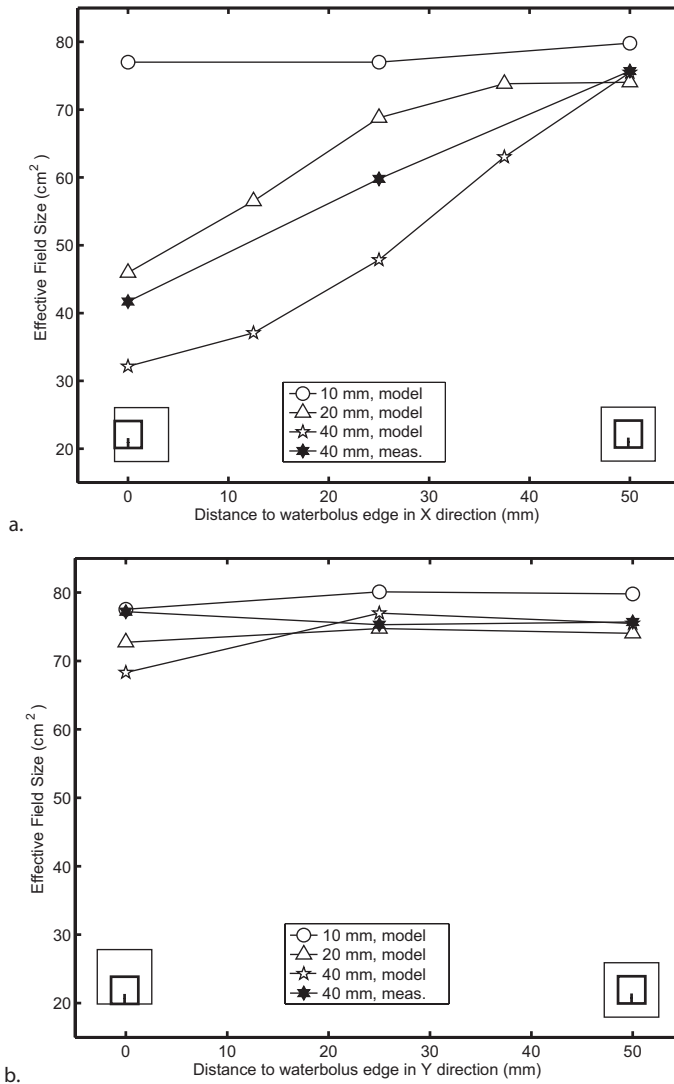
Figure 4. Effective Field Size as a function of distance to the waterbolus edge: effect of waterbolus shift in (a) x-direction, perpendicular to the E-field: bolus shifts towards Lucite window and (b) y-direction, parallel to the E-field: bolus shifts towards the brass wall of the horn.

The results for a waterbolus area of 500 cm² show that for the smaller waterbolus heights, the EFS value is not sensitive to changes in AR. Apparently, the EFS is influenced more by the absolute distance to the LCA edges than by the AR itself; an assumption that will be confirmed in the next paragraph. Furthermore, the thicker waterbolus layers are more prone to the effect of different ARs.

Eccentric placement of the applicator.

The effect of a waterbolus shift parallel or perpendicular to the direction of the E-field for bolus heights of 10, 20 and 40 mm is depicted in Figure 4(a) and 4(b), respectively. Figure 5 shows the relative SAR pattern at 1 cm depth for a waterbolus shift parallel and/or perpendicular to the direction of the E-field, for a bolus height of 40 mm. The diminishing of the EFS is most prominent for a thick (20-40 mm) waterbolus, as was also demonstrated in Figure 3. From Figures 3 and 4 it is clear that a shift of the waterbolus edge towards the brass wall of the applicator horn does not affect the normalised SAR pattern or the EFS appreciably. A shift of the waterbolus edge towards the Lucite windows of the LCA however clearly affects the normalised SAR distribution: when the edge of the bolus (nearly) touches the Lucite window, the typical elliptic 50% SAR/SAR$_{max}$ contour is reduced to a discoid shape, reducing the EFS value severely, see Figure 5.
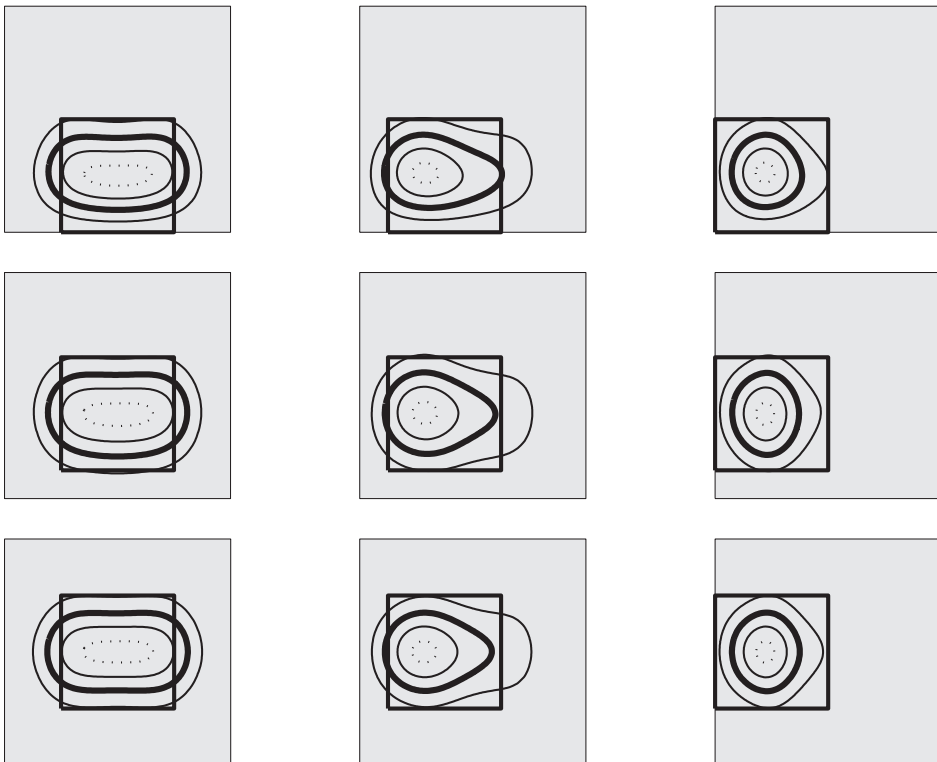
Figure 5. Calculated normalised SAR distributions at 1 cm depth in muscle-equivalent phantom illustrating the effect of waterbolus shifts of 0, 25 and 50 mm in two directions. Waterbolus dimensions: 20×20×4 cm³. The waterbolus area is depicted in grey; the black square indicates the LCA footprint; the contours indicate the 25% (outer solid line), 50% (bold line), 75% (inner solid line) and 95% (dotted line) SAR/SAR$_{max}$ contours.

Results II - SAR measurements

Waterbolus size

The measured average EFS values (n = 2-5) for different waterbolus areas and heights are depicted in Figure 2 and listed in Table 2, together with the corresponding predicted EFS values. The measurements closely reflect the changes in EFS as predicted by the model, both qualitatively and quantitatively. The measured EFS of the LCA without waterbolus is 77.8 ± 5.4 cm² (mean ± sd, n = 11). The EFS reaches the optimal value for a waterbolus area between 200 and 400 cm². Smaller waterboli (10×10 cm²) restrict the EFS. The sensitivity for a sub-optimal waterbolus area increases with waterbolus height.

Table 2. Measured and predicted Effective Field Size values (cm²) for several waterbolus heights and areas. Model values marked * have been linearly interpolated from the complete set of modelling results, to match the waterbolus height. Measurement values: mean ± sd (cm²).

Waterbolus height (cm)	Waterbolus area (cm²)							
	10×10		15×15		20×20		30×30	
	meas.	model	meas.	model	meas.	model	meas.	model
0.8	63.3±4.2 (n = 3)	64.9*	80.7±3.6 (n = 4)	79.2*	77.9±4.1 (n = 4)	79.5*	75.6± 3.9 (n = 3)	78.1*
2.0	48.4±2.5 (n = 4)	39.8	76.4±5.0 (n = 4)	77.3	75.8±6.3 (n = 5)	74.0	65.0±0.7 (n = 2)	64.9
3.6	27.4±0.7 (n = 4)	24.1*	72.1±9.2 (n = 4)	76.5*	67.4±5.8 (n = 4)	75.2*	53.9±0.9 (n = 4)	54.1*

Table 3. Measured and predicted EFS values (cm²) for waterbolus shifts in x- and y-direction. Waterbolus dimensions: 20×20×4 cm³. Measurement values: mean ± sd (cm²).

Waterbolus shift in y-direction (cm)	Waterbolus shift in x-direction (cm)					
	0.0		2.5		5.0	
	meas.	model	meas.	model	meas.	model
0.0	75.7±2.3 (n = 3)	75.5	59.8±1.8 (n = 3)	47.8	41.7±2.6 (n = 3)	32.1
2.5	75.3±3.2 (n = 3)	76.9	-	51.3	-	33.2
5.0	77.2±1.0 (n = 3)	68.3	-	20.2	38.7±4.6 (n = 3)	31.0

Eccentric placement of the applicator

Figure 4 and Table 3 show the measured effect of eccentric placement of the LCA, together with the modelled EFS values. Figure 6 depicts the measured (n = 3) and predicted 50% SAR/SAR_{max} contours for waterbolus shifts in both directions. Like the models, the measurements show a negligible sensitivity to a bolus shift in y-direction. Also, a bolus shift in x-direction results in asymmetric and, finally, circular EFS contours for shifts of 25 and 50 mm respectively, and consequently a reduction in EFS values. The effect of eccentric

placement is more pronounced in the models than in measurements, both in terms of decrease in EFS values (Figure 4, Table 3) and squeezing of the EFS contours (Figure 6).
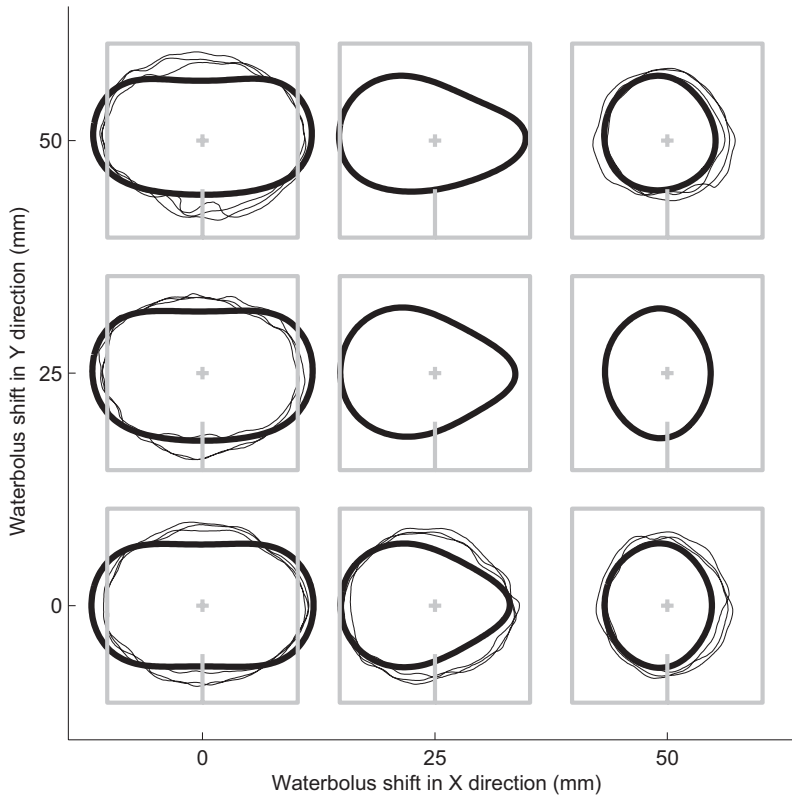
Figure 6. Measured (thin lines) and predicted (bold lines) 50% SAR/SAR$_{max}$ contours for waterbolus shifts of 0, 25 and 50 millimeters in both x- and y-direction. The grey lines indicate the LCA centre and footprint. Waterbolus dimensions: 20×20×4 cm^3.

Discussion

So far, reports on the optimization of waterbolus size and shape have been limited. In the field of deep hyperthermia, Hornsleth [8] related the bolus shape to a waterbolus edge effect causing local pain and to SAR performance parameters. In the field of superficial hyperthermia, several groups measured or calculated the effect of waterbolus thickness on the EFS, i.e. for the contact flexible microstrip applicator (CFMA, [9]) and the dual concentric conductor (DCC, [10]) applicator. Gelvich *et al.* [11] mathematically described spurious oscillations in the waterbolus and their disturbing effect on applicator SAR patterns. Hereafter, Neuman *et al.* [12] investigated how SAR patterns changed with

increasing bolus thickness, and reported that their observations could be evidence of the volume oscillations described by Gelvich. Where most authors focus on a critical value of the bolus thickness, Van Rhoon [2] reported the effects of both waterbolus thickness and shape on the EFS of the LCA.

In contrast to the DCC and CFMA applicators where the waterbolus is an integral part of the the applicator system and its length and width are fixed, the LCA utilizes a separate waterbolus, offering more flexibility in the applicator-waterbolus configuration. At the same time, it poses the question which range of waterbolus dimensions, shapes and applicator placement results in an optimal coupling between applicator and patient.

In this respect, the QA guidelines for ESHO protocols [1] are undersized. They mention that the presence of a bolus may cause significant changes to the EFS of an applicator and that the EFS recorded must be that corresponding to the clinical set-up. However, the LCA is used in a wide range of configurations, so a typical clinical set-up cannot be defined. At the same time, for the clinical application of a waterbolus, minimal restrictions with regard to waterbolus dimensions or applicator placement would be advantageous. Restrictions on thickness of the bolus layer can limit the ability to conform to anatomic features. Severe restrictions to waterbolus shape or applicator placement will not always be feasible in the clinic, or at least hamper the placement of an array of applicators. Therefore, we aim for a minimal set of guidelines that guarantee an acceptable SAR coverage, while leaving freedom of action for the hyperthermia technician.

The results presented in this work partially agree with earlier measurements by Van Rhoon *et al.* [2], who measured the influence of various thicknesses (0-3 cm) and two sizes (18×18 and 25×30 cm²) of the waterbolus on the resulting EFS. Both their work and the current models and measurements observe the highest EFS scores for a waterbolus area of about 18×18 cm². However, other trends delineated in their work are not reflected in the current measurements, nor in the model predictions. In contrast to results published in this paper, they found a low sensitivity to waterbolus height for a large (25×30 cm²) waterbolus area, and an EFS value measured with no waterbolus which is significantly lower than the optimal EFS score. The quantitative differences in reported EFS values are remarkable: for example, the earlier report found an overall maximum EFS = 103 cm², whereas in the current set of measurements, none of the repetitions exceeds 85.3 cm². The following factors may contribute to the observed differences:

–   The properties of the muscle-equivalent phantom differ between batches, even when they have been produced following the same receipe [7] and protocol. The differences may be ascribed to the fact that some ingredients (e.g. gelling agent, PE powder) were obtained from other manufacurers over the years, and to ageing effects. We cannot make a direct comparison of the phantom properties, as the actual permittivity and conductivity of the phantom tissue was not measured. However, to quantify the differences between phantoms we measured the EFS of an LCA placed directly on top of a phantom (no waterbolus) from a recent batch and from a previous batch. The

comparison revealed a significant difference between two sets of phantom layers: 73.5 ± 2.6 (n = 6) versus 82.8 ± 1.8 (n = 5) cm^2 (mean ± sd). Apparently, variations between batches account for at least 10% of the differences in EFS.

– The resolution of the TVS-600 infrared camera utilized in this work (236×320 pixels) is much higher than that of the former AGA thermograph (75×75 pixels [13]). The higher resolution permits a more accurate assessment of the EFS. Further, it allows for image processing steps that were not applied in the earlier work, e.g. low-pass filtering to suppress noise, and translation of pixels to millimeters by reconstructing the exact applicator position within the image.

– As the TVS-600 is more sensitive than the AGA thermograph, the duration of the power pulse in this study was considerably shorter than in the earlier work (30 sec at 200 W versus up to 90 sec at 100-300 W). Also, the time to measurement was shorter (10 sec versus 15 sec). In the current reasearch, the shorter power-pulse and time to measurement restrict the relative error in the half-width at half-power to < 1% [14]. On the other hand, the previous research violated the ESHO QA guidelines with respect to length of the power pulse.

– The LCA utilized in this work has been in clinical use for several years now, and there has been a slight modification of the waveguide back plane. Possibly this resulted in degraded applicator performance. However, our QA program does not provide an indication of the level of degradation in time.

In short, the measurement method has improved compared to the earlier measurements. Moreover, the current measurements are in line with the model predictions. However, given the fact that the LCA prototype, AGA thermograph and old phantoms were discarded, it is impossible to determine the relative contribution of the factors contributing to the differences in the results.

The role of spurious oscillations in the effects of waterbolus size and shape presented in this paper is not evident. According to Gelvich *et al.* [11] a water-filled horn applicator, like the LCA, cannot stimulate oscillations in the waterbolus.

Although spurious oscillations should not be fully excluded, the predominant effects described in this paper, restricted EFS values for set-ups where the waterbolus edge is close to the horn aperture, can be explained from the design of the LCA. The Lucite windows allow flaring of the E-field, which results in a large EFS to aperture ratio. In the absence of a watervolume in the periphery of the LCA aperture, flaring of the E-field is hampered, resulting in focusing of the SAR distribution: the SAR distribution is then similar to that of a conventional waveguide applicator. The Poynting vector plots in Figure 7 illustrate this behaviour: for a 20×20×4 cm^3 bolus, the power flow in the waterbolus is directed in the z-direction, whereas for the smaller 10×10×4 cm^3 bolus, the Poynting vectors are directed towards the centre of the LCA footprint, resulting in an accumulation of SAR at the centre and a circular 50% SAR/SAR$_{max}$ contour (Figure 7(e-f)).
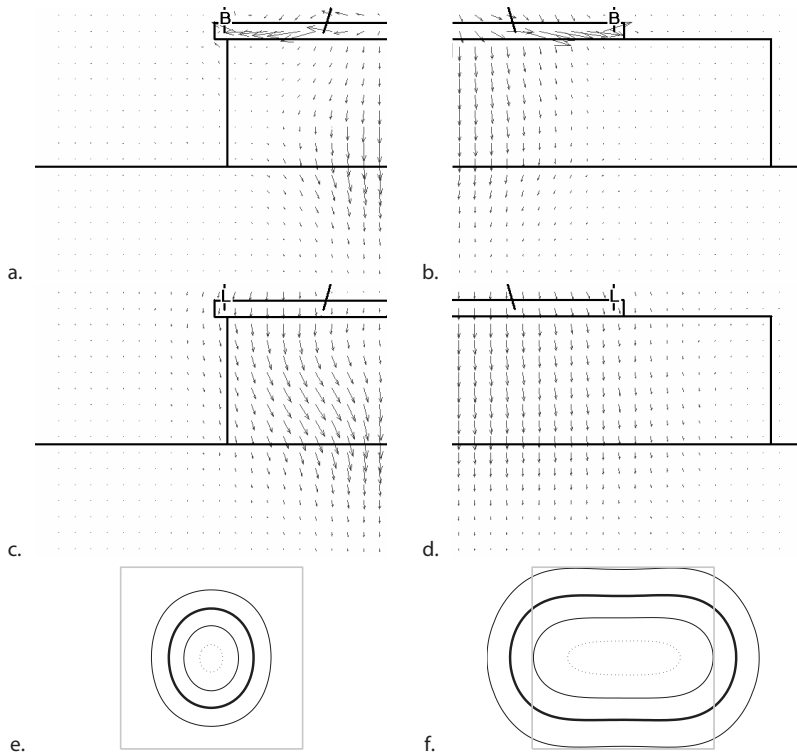
Figure 7. Illustration of SAR focusing when a small waterbolus is applied. Figures on the left (a,c,e) relate to a 10×10×4 cm³ waterbolus, on the right (b,d,f) to a 20×20×4 cm³ waterbolus. (a-d) depict Poynting vectors in the principal antenna planes: (a-b) YZ half-plane, parallel to, and (c-d) XZ half-plane, perpendicular to the E-field. L = lucite sidewall; B = brass sidewall. (e-f) the corresponding normalised SAR distributions at 1 cm depth: LCA footprint (grey) and 25% (thin), 50% (bold), 75% (thin) and 95% (dotted) contours.

In this parametric study, the brick-shape of the waterbolus is a premiss. The basic, rectangular shape favours simplicity of the model and facilitates interpretation of the waterbolus parameters under study. In the clinical situation however, the shape of the waterbolus is more complicated. A separate study comparing SAR patterns of more realistic, non-rectangular waterbolus edges to those of a brick-shaped bolus, is currently performed to determine the necessity of implementing a more complex waterbolus shape in treatment planning. So far, the brick-shape is considered appropriate for the deduction of QA guidelines for the application of the waterbolus.

The flat phantom set-up prescribed by the ESHO QA guidelines [1] that was adopted in this work basically provides a standard for the assessment of applicator performance in the lab. While it is suitable for the characterization of applicator performance and for inter-applicator comparisons, the clinical relevance of this shape is limited. In this respect, model investigations offer more opportunities to investigate applicator performance than

experiments. As an example, the modelling results in Figure 8 show that the waterbolus guidelines proposed in this paper also hold in a non-flat tissue configuration. This paper demonstrates that electromagnetic simulation is a useful tool for the systematic investigation of performance parameters of superficial hyperthermia applicators. A logical next stept is to exploit models to systematically investigate energy distributions in heterogeneous tissue configurations and antropomorphic shapes, which better reflect clinical practice.
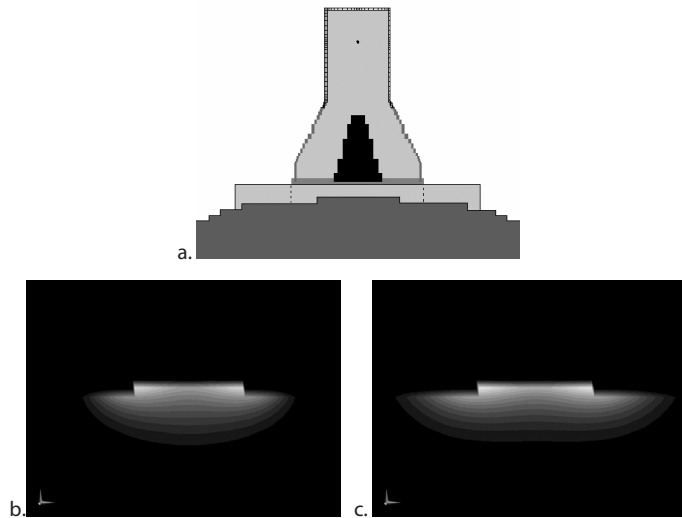
Figure 8. Example of the effect of the waterbolus on the SAR distribution in a non-flat shape. (a) Configuration: a small (10×10 cm², dotted) and a larger (20×20 cm²) waterbolus are applied on a sphere (staircased). (b-c) Normalized SAR on a linear scale in the y = 0 cross-section (perpendicular to the E-field). The smaller waterbolus (b) restricts the SAR distribution as compared to the larger bolus (c).

Conclusions

The effect of waterbolus size, shape and asymmetric configuration on the EFS of the LCA has been assessed in an FDTD model study. The model output has been verified against IR thermographic measurements. Two major trends can be deduced from the measurements and modeling results presented in this paper. First, the EFS is restricted in cases where a waterbolus edge is close to the LCA aperture. This effect is more obvious at the Lucite windows of the LCA, than it is at the metallic sides of the horn aperture. Second, restrictions in EFS are more evident with increasing waterbolus height. From the modeling results and the measurements, we deduce a minimal set of guidelines that are clinically feasible and ensure optimal (> 0.9·EFS_{max}) LCA performance: (*i*) the waterbolus edge should extend the LCA aperture in all directions and at least 2.5 cm at the Lucite windows, and (*ii*) the waterbolus height should not exceed 2 cm.

References

[1] Hand JW, Lagendijk JJW, Bach Andersen J, Bolomey JC. Quality assurance guidelines for ESHO protocols. Int J Hyperthermia 1989;5:421-428.

[2] Van Rhoon GC, Rietveld PJM, Van der Zee J. A 433 MHz Lucite cone waveguide applicator for superficial hyperthermia. Int J Hyperthermia 1998;14:13-27.

[3] Rietveld PJM, Lumori MLD, Hand JW, Prior MV, Van der Zee J, Van Rhoon GC. Effectiveness of the Gaussian beam model in predicting SAR distributions from the lucite cone applicator. Int J Hyperthermia 1998;14:293-308.

[4] Rietveld PJM, Lumori MLD, Van der Zee J, Van Rhoon GC. Quantitative evaluation of 2×2 arrays of Lucite cone applicators in flat layered phantoms usign Gaussian-beam-predicted and thermographically measured SAR distributions. Phys Med Biol 1998;43:2207-2220.

[5] Rietveld PJM, Van Putten WLJ, Van der Zee J, Van Rhoon GC. Comparison of the clinical effectiveness of the 433MHz lucite cone applicator with that of a conventional waveguide applicator in applicatons of superficial hyperthermia. Int J Radiat Oncol Biol Phys 1999;43:681-687.

[6] Samaras T, Rietveld PJM, Van Rhoon GC. Effectiveness of FDTD in predicting SAR distributions from the Lucite cone applicator. IEEE Trans Microwave Theory Techn 2000;48:2059-2063.

[7] Guy AW. Analysis of electromagnetic fields induced in biological tissues by thermographic studies on equivalent phantom models. IEEE Trans Microwave Theory Techn 1971;19:205-214.

[8] Hornsleth SN. Radiofrequency Regional Hyperthermia [dissertation]. Denmark: Aalborg University; 1996.

[9] Lamaitre G, Van Dijk JDP, Gelvich EA, Wiersma J, Schneider DJ. SAR characteristics of three types of Contact Flexible Microstrip Applicators for superficial hyperthermia. Int J Hyperthermia 1996;12:255-269.

[10] Rosetto F, Diederich CJ, Stauffer PR. Thermal and SAR characterization of multielement dual concentric conductor microwave applicators for hyperthermia, a theoretical investigation. Med Phys 2000;27:745-753.

[11] Gelvich EA, Mazokhin VN. Resonance effects in applicator water boluses and their influence on SAR distribution patterns. Int J Hyperthermia 2000;16:113-128.

[12] Neuman DG, Stauffer PR, Jacobsen S, Rosetto F. SAR pattern perturbations from resonance effects in water bolus layers used with superficial microwave hyperthermia applicators. Int J Hyperthermia 2002;18:180-193.

[13] Van Deursen JPB, Van Rhoon, GC. A low-cost interface for upgrading an AGA thermograph. Biomed Meas Infor Control 1987;2:10-13.

[14] Samaras T, Van Rhoon GC, Sahalos JN. Theoretical investigation of measurement procedures for the quality assurance of superficial hyperthermia applicators. Int J Hyperthermia 2002;18:416-425.

5

Development of a guideline for the waterbolus temperature in superficial hyperthermia

Abstract

Purpose: The research presented in this work investigates the influence of the waterbolus temperature on temperature distributions in tissue during superficial hyperthermia treatments using Lucite cone applicators. The goal of the research was to develop a guideline for the selection of the waterbolus temperature based on 3-D electromagnetic and thermal modelling.

Methods: A 3-D model was set up to simulate an abstraction of the treatment. In the model a convection coefficient for the waterbolus to skin surface was employed. In order to simulate the heat balance as realistically as possible, convection coefficients were measured for different waterboli, and ranged from 70 to 152 $W/(m^2K)$. The model was evaluated by simulating three clinical treatments and comparing the outcome of the model to clinical measurements.

Results: The model was found to predict the temperature distribution well on a global view; root mean square errors between 0.66 °C and 1.5 °C were found for the three treatments. For some temperature probes a deviation of 1.5 – 2.0 °C between measured and predicted temperature was found. These large deviations can be explained by local variations in cooling by blood vessels, tissue inhomogeneity, a varying convection coefficient of the waterbolus and of course the complexity of the anatomy.

Conclusions: The model was used to set up guidelines for the waterbolus temperature selection in clinical practice for the target depths and applicator arrays used in the Erasmus MC.

Introduction

In hyperthermic oncology, tissue is heated to a temperature between 40 °C and 43 °C by external means, commonly by electromagnetic (EM) energy absorption. In superficial hyperthermia, the two main parameters used for optimising the temperature distribution are the electromagnetic power and the waterbolus temperature. The dependence of the specific absorption rate (SAR) distribution on applicator type, waterbolus shape and size, and tissue configuration has been the subject of many experimental and theoretical studies. The exact thermal effect of the waterbolus on the other hand is less clear and has not been explored extensively. To optimise the temperature distribution during hyperthermia treatments and to obtain a more uniform approach among hyperthermia clinicians, guidelines for waterbolus temperatures are needed.

Even though the treatment is based on increasing tissue temperatures, thermal modelling has not been an important field of research in superficial hyperthermia. In the past, Lagendijk [1] provided a 1-D analytical model for calculating the temperature as a function of tissue depth. This model describes the steady-state temperatures due to electromagnetic heating, convective cooling by the waterbolus and conduction through tissue. However, the thermal balance of this model is not complete. Most importantly, the cooling effect of blood perfusion was not included in the model. Additionally, it used a value of 500 W/(m^{2}K) for the convection between the waterbolus and skin. This value is typical for a fluid flowing along a plate, but might not be correct for the convection between the skin and waterbolus. In the model, a constant Dirichlet boundary condition reflects the assumption that at some depth the tissue temperature will be at core body temperature: the temperature is set to 37 °C at 5 cm depth. Lacking the cooling effect of blood, however, this boundary condition primarily determines the temperature profiles predicted by the 1-D model.

Another model presented in literature is by Clegg *et al.* [2], which consists of a 3-D tissue geometry built from segmented CT data, to model the treatment of a specific patient. Perfusion and EM power were varied until the simulated temperatures were in agreement with the clinically measured temperatures. The model used a convective boundary at the waterbolus interface, but a convection coefficient was not given.

In this research convection coefficients of multiple waterbolus set-ups were measured, while the efficiencies of the applicators were investigated earlier by De Bruijne *et al.* [3]. These properties were implemented in a 3-D model, describing a general treatment with the Lucite cone applicator. The heating process was simulated using an electromagnetic and thermal solver. An important advantage of 3-D modelling over 1-D modelling is the implementation of the 3-D antenna pattern into the thermal model. To establish a guideline for selecting the waterbolus temperature in superficial hyperthermia, the predicted temperatures of the generic tissue configuration in the 3-D model were verified for three patient treatments.

Materials and Methods

The approach taken in this study is to establish a generic guideline for waterbolus temperature by simulating the effect of waterbolus temperature in a generalized three-layer anatomy. In order to achieve a realistic heat balance, the technical parameters (i.e. waterbolus convection coefficient, applicator efficiency) were measured. Additionally, the effect of perfusion and fat layer thickness were investigated in the layered model in a parameter study. Hereafter, the performance of the general model was verified against clinical data. Finally, a waterbolus temperature guideline was set up for each clinically relevant applicator configuration and target volume depth.

The Lucite cone applicator system

In the Erasmus MC-Daniel den Hoed Cancer Center, the Lucite cone applicator (LCA) is the standard antenna for superficial hyperthermia treatments. The LCA is a water-filled horn antenna operating at 433 MHz. The Lucite windows and the PVC cone of the LCA enhance the effective field size (EFS) of the applicator significantly. For a detailed description of the design, see Van Rhoon *et al.* [4]. The dimensions of the horn aperture are 100 mm by 100 mm. The LCAs can be combined in an array to heat arbitrary radiotherapy fields. The applicator target volume is defined as the target depth times the applicator array footprint. The maximum target depth of the LCA system is four centimetres.

A waterbolus is located between the applicator(s) and the skin surface to couple the electromagnetic field into the patient and to control the temperature of the upper tissue layer. In our clinic four waterboli of different sizes are used, matching a 1×1, 1×2, 2×2 and 2×3 applicator array. A recirculating heater (Polaron E3500, VG Microtech, UK) flushes the waterbolus with de-ionised water of a preset temperature. By changing the setpoint of the heater the hyperthermia technician can influence the temperature distribution in the patient: lowering its setpoint increases the cooling effect. Skin and invasive tissue temperatures are monitored using up to 24 simultaneous fibre optic thermometers (FT1310, Takaoka Electric MFG. CO. Ltd. Japan). In the clinic, a gauze is always placed between the waterbolus and the skin to prevent the skin from sticking to the bolus when removing it at the end of the treatment.

Convection coefficient measurements

The amount of energy transferred from the skin to the waterbolus by convection (q_{conv}) increases linearly with the convection coefficient (h), the surface area (A) and also with the temperature difference between the two surfaces ($T_{skin} - T_{waterbolus}$)

$$q_{conv} = hA(T_{skin} - T_{waterbolus}) \qquad (1)$$

As the effect of an increase in the convection coefficient gives the same result as an increase in temperature difference, it is imperative to use a realistic convection coefficient in the

model when investigating the influence of the waterbolus temperature. Therefore, the convection coefficients of the four different size waterboli that are currently in clinical use were measured.

In the model the convection coefficient h represents the total heat transfer from skin to bolus water. Thus, it includes the heat transfer by conduction through the two thin (~0.1 mm) layers in the waterbolus-skin interface: the polyurethane bolus envelope and the wet gauze. Due to their thinness, these layers are assumed to be a negligible impediment to the heat transfer across the interface. Therefore, convection is considered the predominant factor in the tissue-skin interface.

The waterbolus convection coefficients were determined empirically, by measuring the temperature rise in a block of superstuff phantom after placing a warm waterbolus on top if it, and subsequent thermal simulation of this experiment. During the experiments, 15 to 20 fibre optic thermometers were attached to the phantom surface. The gauze placed between the waterbolus and phantom surface was wetted to simulate the moistening effect of the patient's perspiration. The waterbolus was connected to a recirculating heater, which was set to a constant temperature of 30°C. The water temperature at the inflow of the bolus was measured using a fibre optic thermometer. The phantom was initially at room temperature (20°C). After placing the warm waterbolus on the phantom, the temperature was measured for 60 minutes.

In the thermal simulation, the top of a rectangular superstuff phantom (ρ = 1000 kg/m³, c_p = 3700 J/(kgK) and k = 0.535 W/(mK) [5]) was heated by a waterbolus through convection. The sides and bottom of the block were insulated. The initial phantom temperature was set to the average measured phantom temperature at t = 0 (room temperature). The temperatures in the top grid cell layer of the phantom, 0.5 mm beneath the waterbolus interface, were recorded to compare to the the measured profiles. For each measurement point, the convection coefficient and convective temperature were fitted in a graphical user interface, by projecting simulated temperature profiles on top of the measured profile, and tuning of the parameters until the simulated curve overlapped the measured profile (minimum step sizes: Δh_min = 1 W/(m²K), $\Delta\mathrm{T}_\mathrm{min}$ = 0.1 °C; total 366 simulated profiles). The best fit was assessed by visual inspection. Finally, the convection coefficient of a waterbolus was the average of the per-point convection coefficients.

The 3-D model

In order to simulate a superficial hyperthermia treatment, an LCA, a waterbolus and a block of tissue were implemented in the model (Figure 1). The waterbolus was 180 mm by 180 mm and had a thickness of 10 mm. These dimensions result in a maximum effective field size as investigated by De Bruijne *et al.* [6]. The tissue volume below the LCA was 300 mm by 300 mm, with a height of 100 mm and was made up of three different layers: skin, fat and muscle. The modelled thickness of the skin and fat layer was chosen after examining CT scans of the chest wall of eight representative patients. In all cases a skin thickness of

approximately 1 mm was found. However, the thickness of the fat layer varied from 5 mm to 30 mm for the eight patients, leading to the average thickness of 10 mm being implemented. The thickness of the muscle layer was extended to 89 mm in the model, to dampen the electromagnetic field. For the set-ups with an array of two, four and six applicators, the LCA in the single applicator model was duplicated and the tissue volume was extended to suit the applicator array. The model was electromagnetically and thermally simulated using the finite difference time domain (FDTD) simulation package SEMCAD [7].

The model was implemented in a non-uniform grid. Both the electromagnetic and thermal solver used this grid. The grid step varied between 1 and 10 mm. Inside the LCA horn and waveguide, the grid step was limited to 2 mm. At the source pin and in the skin layer the grid was refined to 1 mm. Outside the applicator target volume the grid step gradually increased. The grid for the single applicator had $3.5 \cdot 10^6$ cells in total for the EM simulation. To reduce computation time, the computational domain of the thermal simulation was restricted to the extent of the waterbolus plus 1 centimetre, see Figure 1. Sensitivity analysis determined that the difference between the full- and restricted domain simulated temperatures was less than 0.05 °C within the applicator target volume.
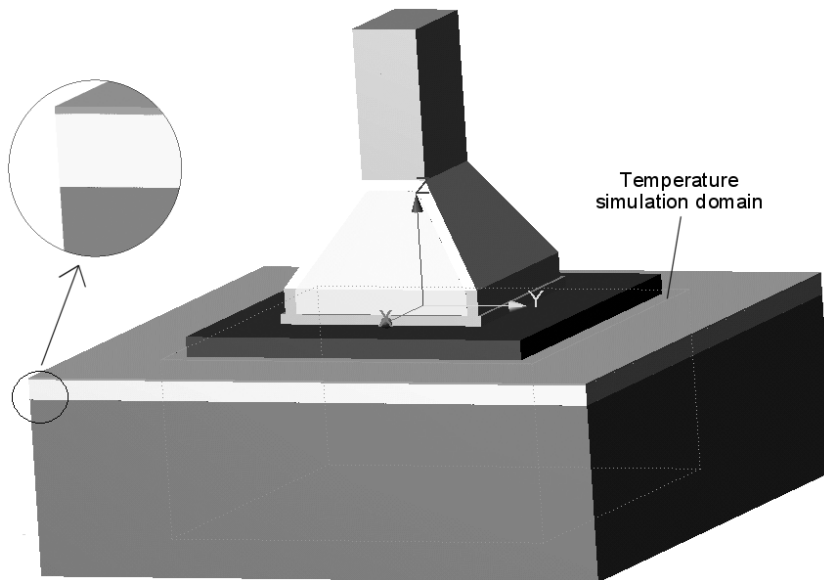
Figure 1. 3-D model used for simulating the superficial hyperthermia treatment. It employs an LCA, a waterbolus and a block of tissue consisting of a skin, fat and muscle layer.

Electromagnetic simulation

In the model the electromagnetic field was generated by an edge source element, which was implemented in the waveguide of the applicator. In measurements by de Bruijne *et al.* [3],

the LCAs were found to have an efficiency (100% · $P_{\text{absorbed in tissue}}$ / $P_{\text{delivered at connector}}$) between 32 and 39%, with an average value of 35%. An efficiency of 79% was measured for the cables connecting the LCAs to the amplifiers. For this reason 27.6% of the amplifier power was absorbed in the tissue. The SAR pattern of the LCA was calculated with the electric properties of the materials listed in Table 1. For the models with an array of incoherent applicators, the SAR patterns of the individual LCAs were added to give a total SAR pattern.

Table 1. Properties of materials used in the simulation. A range and average value is given for the perfusion rate (W). Average perfusion rates multiplied with the specific heat of blood lead to heatsink terms (B = W c_b).

Material	ε_r	σ (S/m)	ρ (kg/m³)	c (J/(kgK))	W (kg/(m³s))	B (W/m³K)	k_{eff} (W/(mK))
De-ionised water	80 [13]	0.046 [13]					
Lucite	2.6 [14]	0.003 [14]					
PVC	2.2 [14]	0.004 [14]					
Skin (wet)	49 [15]	0.68 [15]	1040 [16]	3662 [16]	2.3	8797.5	5.0
Fat	5.6 [15]	0.042 [15]	888 [16]	2387 [16]	0.54 (0.36 - 0.72) [9]	2065.5	1.2
Muscle	57 [15]	0.80 [15]	1050 [16]	3639 [16]	2.3 (0.45 - 4.00) [9]	8797.5	5.0 [10]
Blood			1043 [16]	3825 [16]			

Thermal simulation

The temperature distribution under an applicator array was calculated using the total SAR pattern and the convection coefficient of the array-specific waterbolus. The thermal model was simulated using the Bio-Heat Transfer Equation (BHTE) by Pennes [8], until steady-state was reached.

$$c\rho \frac{\partial T}{\partial t} + c_b W (T - T_b) = k\nabla^2 T + \rho\,SAR \tag{2}$$

Specific heat capacity, density and thermal conductivity of the tissue are denoted by c, ρ and k respectively. The temperature of the tissue is T and was initially set to 37 °C.

The term c_b W (T - T_b) represents the heat exchange due to blood perfusion, where c_b is the specific heat of blood, W is the mass flow rate of blood per unit volume of tissue and T_b is the blood temperature, which was set to 37 °C. Average perfusion rates for muscle and fat were taken from Lang *et al.* [9]. Skin was assumed to have the same perfusion as muscle. The perfusion rates W multiplied with the specific heat of blood c_b lead to heatsink terms B.

Blood flowing through vessels and arteries increases the effective thermal conductivity of the tissue. Therefore the intrinsic conductivity k was replaced by an effective conductivity k_{eff}. Gautherie [10] measured a value of k_{eff} = 5 W/(mK) in superficial layers in humans in vivo for temperatures above 42 °C. In this study this value was applied for muscle and skin. In fat the value for k_{eff} was scaled linearly with k_{eff} in muscle and the perfusion rates in fat and muscle, as shown in Equation 3.

$$k_{\text{eff,fat}} = k_{\text{eff,muscle}} \cdot \frac{W_{\text{fat}}}{W_{\text{muscle}}} \tag{3}$$

In clinical practice, the knowledge of a patient's vasculature is limited, as contrast enhanced CT scans are not standard. In addition, the general layout of the vessels may be affected by surgery and tumour infiltration. As the research objective was to develop a waterbolus guideline applicable to any location on the body, we followed the COMAC recommendation of combining the heatsink and effective conductivity [11]. As known from clinical experience, perfusion rates differ per patient and even vary between treatments of a patient. For this reason a variable perfusion was implemented: the heatsink terms and effective conductivities of all tissues (given in Table 1) were scaled with the same variable. This linear relation between the heatsink and effective conductivities was also assumed by Crezee [12].

All boundaries of the tissue domain in the model were insulated, except for the skin surface. This means that within the domain heat exchange to the environment occurred through two mechanisms. First, at the skin surface, a convective boundary accounted for heat exchange with the waterbolus and the environment. Second, energy was removed by the heatsink component. The computational domain was chosen large enough that the small amount of energy deposited at the boundaries could be removed by the heatsink term, virtually keeping the boundary at body temperature. The convection coefficients of the waterbolus were as measured in this research, while the temperature of the waterbolus was varied for the different simulations. For the skin to air interface, the contributions of natural convection (2.7 W/(m²K)) and radiation to the surroundings (5.0 W/(m²K)) [17] were summed to a total convection coefficient of 7.7 W/(m²K). The air temperature in the model was set to 20 °C.

Model verification

Treatment test cases
The three-layer model was verified using three clinical test cases. In all cases, a single applicator set-up was applied. In order to create a wide test range for the model, treatments on different anatomies with different waterbolus temperatures and electromagnetic power settings were selected. The clinical data included the steady-state amplifier power, the waterbolus temperature, the position of the temperature probes, and the temperature data from these probes. Inputs to the model were the amplifier power, waterbolus temperature and measured convection coefficient of the one-antenna waterbolus. As the perfusion rate of a patient is unknown, the values available from literature (Table 1) were taken as a starting point.

The clinically measured temperatures were then compared to the model prediction. The perfusion was scaled to minimize the mean square error (MSE)

$$\text{MSE} = \frac{1}{n-m} \sum_{i=1}^{n} (T_{i,\text{measured}} - T_{i,\text{simulated}})^2 \tag{4}$$

where $T_{i,measured}$ is the measured temperature of probe i, $T_{i,simulated}$ is the simulated temperature at the corresponding location of probe i and n is the total number of probes. Since only the perfusion was used for fitting, the number of fit parameters (m) was equal to 1. To fit blood perfusion, about 10 thermal simulations were run per patient, and MSE was plotted versus perfusion scaling factor. To pinpoint the minimum MSE, more simulations were run. The minimum perfusion scaling step size was 0.003.

The root of the MSE (RMSE), representing the spread of the temperature errors, is an indicator of the quality of the model. Another indicator is the perfusion rate at which the MSE was minimal. If the perfusion rate is outside the range specified in the literature [9,18], this is an indication that the factors contributing to the heat balance in the model were not realistic.

Parameter variations

Parameter variations were performed to gain qualitative insight in the patient-related parameters, namely thickness of the fat layer and perfusion rate. Both parameters were tested at a relatively low (36 °C) and high (42 °C) waterbolus temperature. The power to the applicator was adjusted such that the maximum temperature in the target volume was 43 °C.

A fat layer thickness of 10 mm was used for setting up the guideline. The thickness of this layer has an influence on the temperature profile, as in fat the EM absorption, thermal conduction and heatsink are lower than in muscle. Therefore, the temperature profiles resulting from 5, 10 and 20 mm fat layers were compared.

It is known that perfusion rates differ per patient and can even vary between treatments of a patient. The effect of perfusion variation on the temperature profiles was investigated by applying perfusion scaling factors of 0.5 and 1.0.

Development of clinical guidelines

When performing a hyperthermia treatment, our clinic aims at temperatures of 43 °C in the target volume. Temperatures between 40 °C and 43 °C are considered therapeutic, however a temperature close to 43 °C is assumed to be best. In clinical practice, target depths of 0 – 1, 0 – 2, 0 – 3, 0 – 4, 1 – 3, 1 – 4 and 2 – 4 centimetres are used.

In order to create clinical guidelines on selecting the waterbolus temperature, the temperature of the waterbolus in the model was varied, while the electromagnetic power was adjusted to keep a maximum tissue temperature of 43 °C. The values given in Table 1 were used for the heatsink terms and effective conductivities.

To maintain a safety margin, skin temperatures were not allowed to reach above 42.5 °C for all target depths, except the 0 – 1 centimetre target depth. In order to judge the quality of the tissue heating for the different waterbolus temperatures objectively, the average target volume temperature was determined as a function of the waterbolus temperature. Also, temperature volume histograms (TVH) were plotted. A TVH clearly shows the optimal waterbolus temperature: at the optimal waterbolus temperature the area

under the TVH is maximal. The waterbolus temperatures providing the highest overall temperatures in the target volume, while complying with the demand of a maximum skin temperature of 42.5 °C, were chosen as the optimal waterbolus temperature for that specific target region. These waterbolus temperatures are given in a table to make the guideline easily usable for hyperthermia physicians and technicians.

Results

Convection coefficient measurements

The convection coefficients for the four different waterboli applied with a wet gauze are shown in Table 2. For each configuration, the range of the measured convection coefficients and the number of measurement points for which a curve was fitted is given. The convection coefficient decreases for increasing size of the waterbolus: it ranges from 152 W/(m²K) for the smallest, to 70 W/(m²K) for the largest waterbolus. In the model, the convective temperature of the waterbolus was set to a value that produced the best fit, this was 0.1 – 1.0 °C below the measured temperature at the inflow of the waterbolus. An additional measurement showed that the application of a dry gauze between the bolus and the phantom resulted in a 23% lower convection coefficient than a wet gauze (54 vs. 70 W/(m²K), 6-antenna waterbolus).

Table 2. Measured convection coefficients for four different waterboli that are currently in clinical use, with a wet gauze between the waterbolus and muscle phantom. For each configuration the mean convection coefficient, its range and the number of measurement points in the waterbolus-muscle phantom interface are given.

Measurement case	mean h (W/(m²K))	range h (W/(m²K))	Number of measurement points
1-antenna bolus	152	78 – 320	20
2-antenna bolus	107	40 – 180	18
4-antenna bolus	91	28 – 180	18
6-antenna bolus	70	41 – 135	19

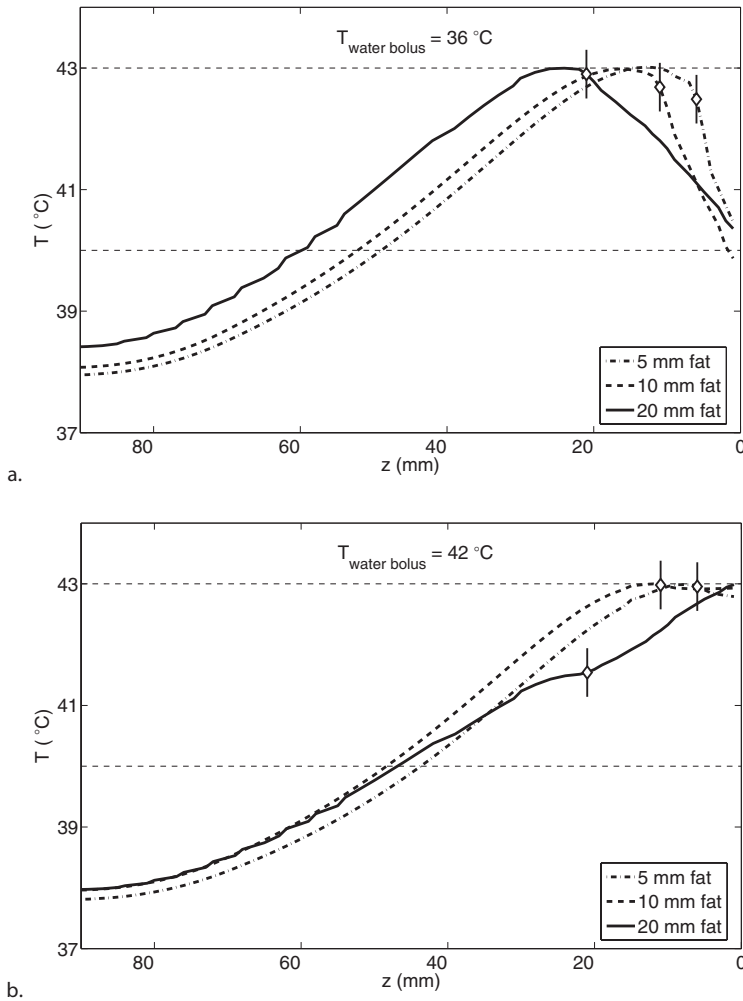### Verification of the 3-D model

Treatment test cases

The 3-layer model was tested by simulating the clinical treatments of three patients. The documented steady-state amplifier power and waterbolus temperature of these treatments were used as input to the simulations and are shown in Table 3. During the treatment of the third patient, the applied waterbolus temperature and amplifier power were both lower than during the treatment of the second patient. Nevertheless, the steady-state temperatures were just as high as in the other two test cases. Therefore it is clear that the perfusion rate of the third patient was lower than that of the second patient. The average heatsinks and effective conductivities given in Table 1 were multiplied with the perfusion scaling factors to minimize the MSE in every test case. All measured and simulated temperatures of the three

treatments can be compared using Table 3. The RMSE of the three test cases varied between 0.66 and 1.5 °C.

Table 3. Comparison between interstitially and superficially measured steady-state temperatures and simulated temperatures for the three test cases. Amplifier power and waterbolus temperature used during the treatments are given, as well as the perfusion scaling factor for each case. The RMSE of each test case is also given.

Case	Patient 1			Patient 2			Patient 3		
Amplifier power (W)	180			130			80		
Waterbolus temperature (°C)	35			40			38		
Perfusion scaling	1.05			1.09			0.54		
Invasive Probes (nr)	Probe depth (mm)	$T_{measured}$ (°C)	$T_{simulated}$ (°C)	Probe depth (mm)	$T_{measured}$ (°C)	$T_{simulated}$ (°C)	Probe depth (mm)	$T_{measured}$ (°C)	$T_{simulated}$ (°C)
1	19	41.2	40.3	3	40.5	41.0	17	39.6	41.7
2	30	42.3	40.9	7	41.6	41.6	18	40.0	42.2
3	28	42.4	41.9	7	41.7	41.7	12	40.8	42.2
4	15	42.7	42.6	5	40.1	41.3	4	43.0	40.3
5	10	43.4	41.9				7	42.2	40.7
6	10	40.5	42.4				12	43.8	42.1
7	7	40.3	41.4				12	43.1	42.2
8							7	42.7	41.0
Superficial probes		$T_{measured}$ (°C)	$T_{simulated}$ (°C)		$T_{measured}$ (°C)	$T_{simulated}$ (°C)		$T_{measured}$ (°C)	$T_{simulated}$ (°C)
		40.8	39.4		41.6	40.4		41.7	39.8
		40.0	39.4		41.9	40.9		41.2	39.6
		39.3	38.8		41.7	40.8		40.1	39.3
		39.1	38.7		41.0	40.2		39.7	39.6
		38.5	38.5		41.2	40.6		39.2	39.2
		38.6	38.8		41.2	40.7		39.7	39.7
		38.8	39.3		40.7	40.3		39.5	39.7
		38.8	39.3		41.0	40.7		38.8	39.5
		38.6	38.2		41.0	40.8		38.6	39.4
		38.3	38.9		40.9	40.9		38.4	39.5
		37.2	38.0		40.9	40.9		37.7	39.5
		38.2	39.3		41.2	41.4			
		37.1	38.7		40.3	40.6			
		37.0	38.7		40.5	40.9			
					40.1	40.8			
					40.6	41.4			
					39.9	40.8			
RMSE (°C)	1.02			0.66			1.50		

Figure 2. The effect of fat layer thickness for waterbolus temperatures of (a) 36 °C and (b) 42 °C. The marker indicates the fat-muscle interface. Z is the depth under the skin surface.

Parameter variation

To demonstrate the influence of the fat layer in the 3-D model, temperature profiles for fat layer thicknesses of 5, 10 and 20 mm are given for a waterbolus temperature of 36 °C in Figure 2(a), and for a waterbolus of 42 °C in Figure 2(b). Generally, the maximum temperature is located in the muscle, just below the fat layer. When the fat layer thickness varies, the maximum temperature shifts and stays in the muscle layer, see Figure 2(a). When the waterbolus cooling is limited, e.g. Figure 2(b), the temperature gradient in the fat layer flattens, and for thicker fat layers the maximum temperature shifts to the skin.
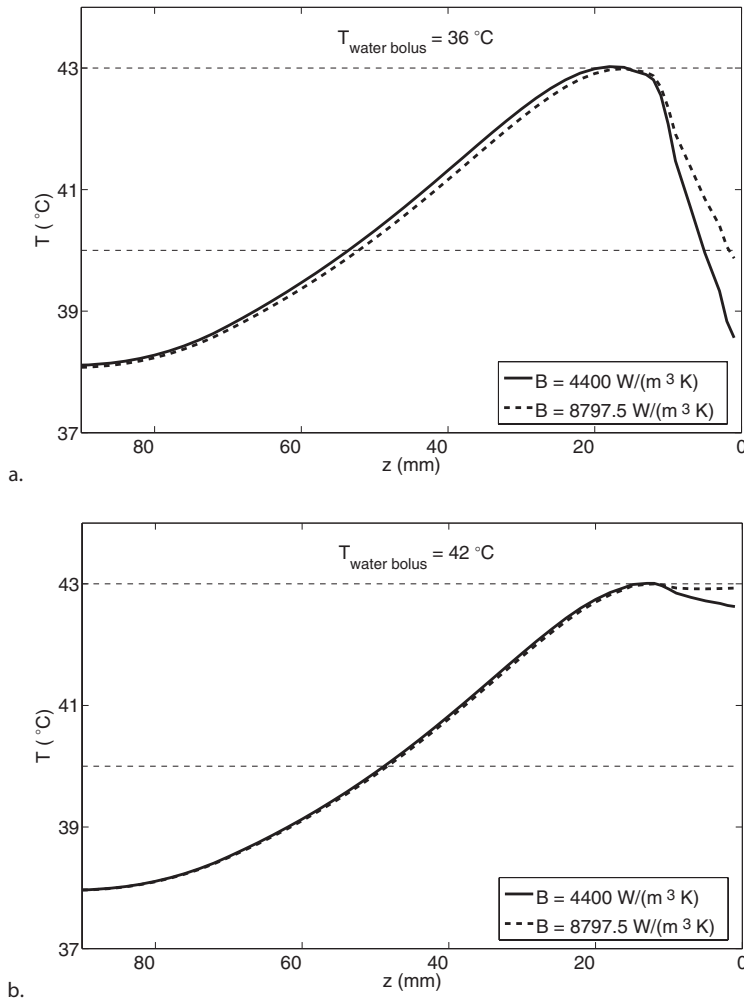
Figure 3. Tissue temperature as a function of depth in the centre of the volume for a perfusion scaling factor of 0.5 (solid line) and 1.0 (dotted line); the corresponding heatsink terms in muscle are indicated in the legend. The waterbolus temperatures are (a) 36 °C and (b) 42 °C.

To investigate the effect of a variation in perfusion, the coupled effective conductivity and heatsink terms were raised together with the electromagnetic power. This results in the temperature profiles given in Figure 3(a) for a waterbolus temperature of 36 °C and in 3(b) for 42 °C. The maximum temperature is located at nearly the same position and also the temperature profile at depth is almost the same for both perfusion rates, but the temperature profiles differ at the surface.
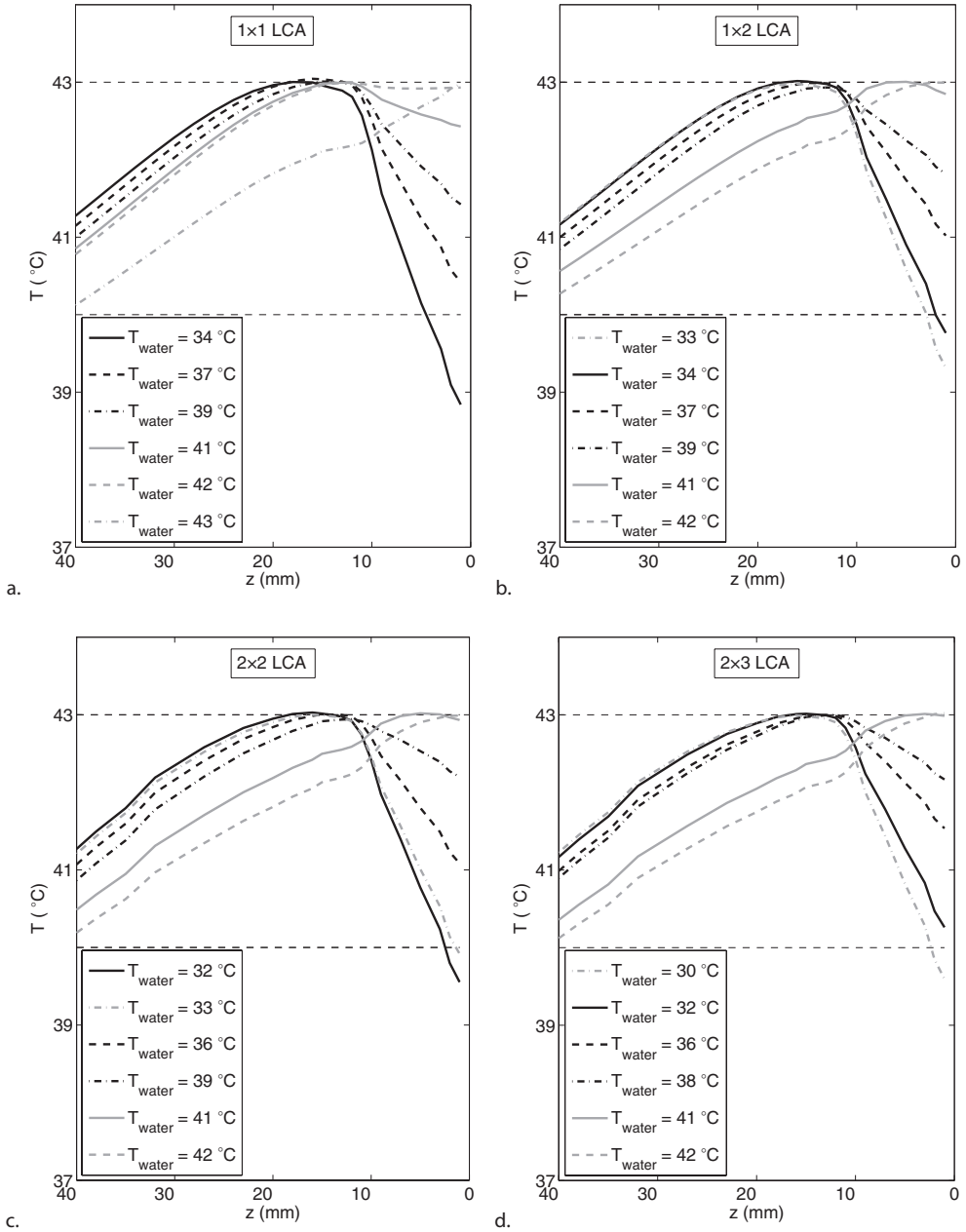
Figure 4. Tissue temperature as a function of depth under the skin surface using (a) a single applicator, (b) two applicators, (c) four applicators and (d) six applicators.
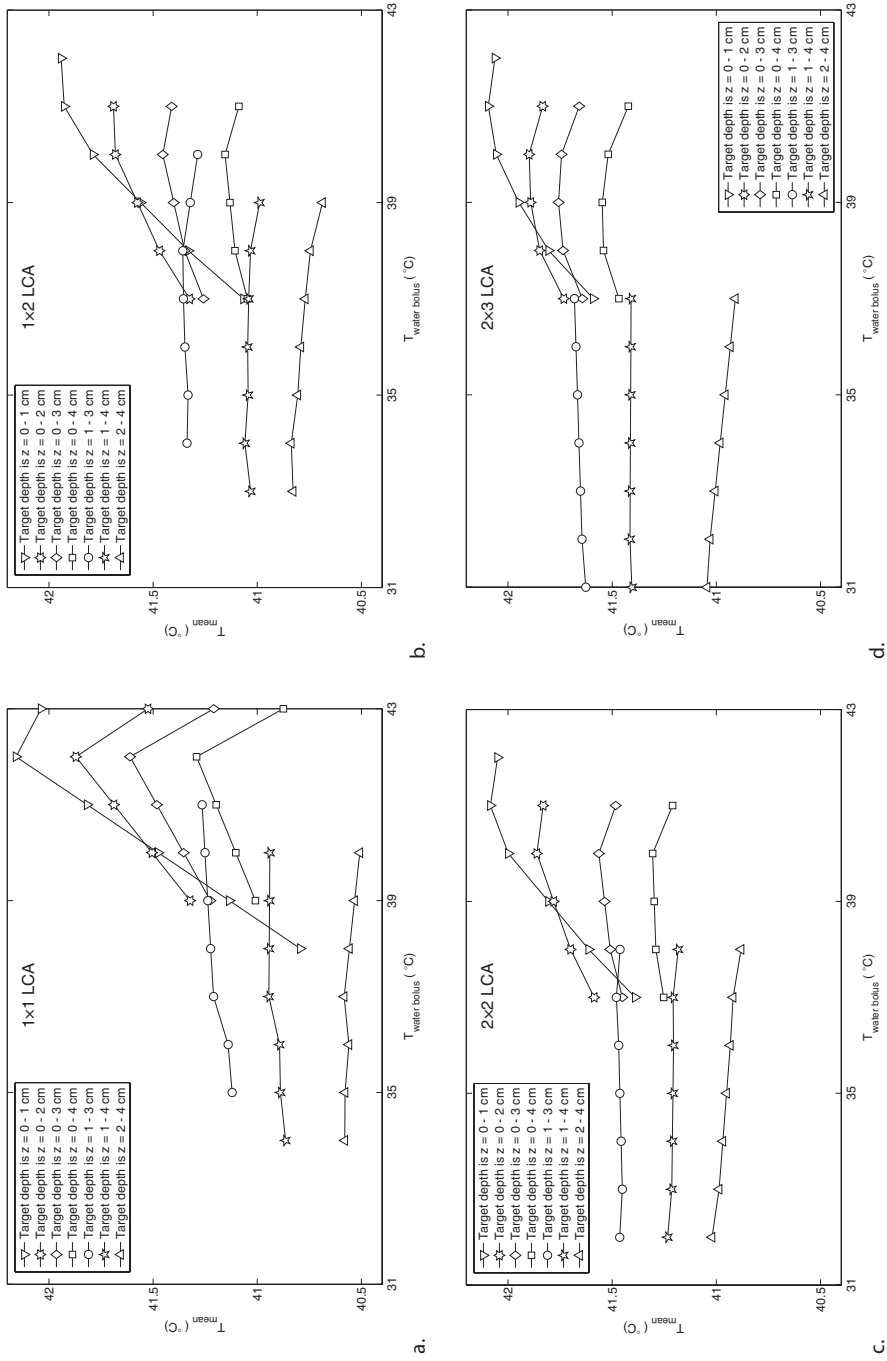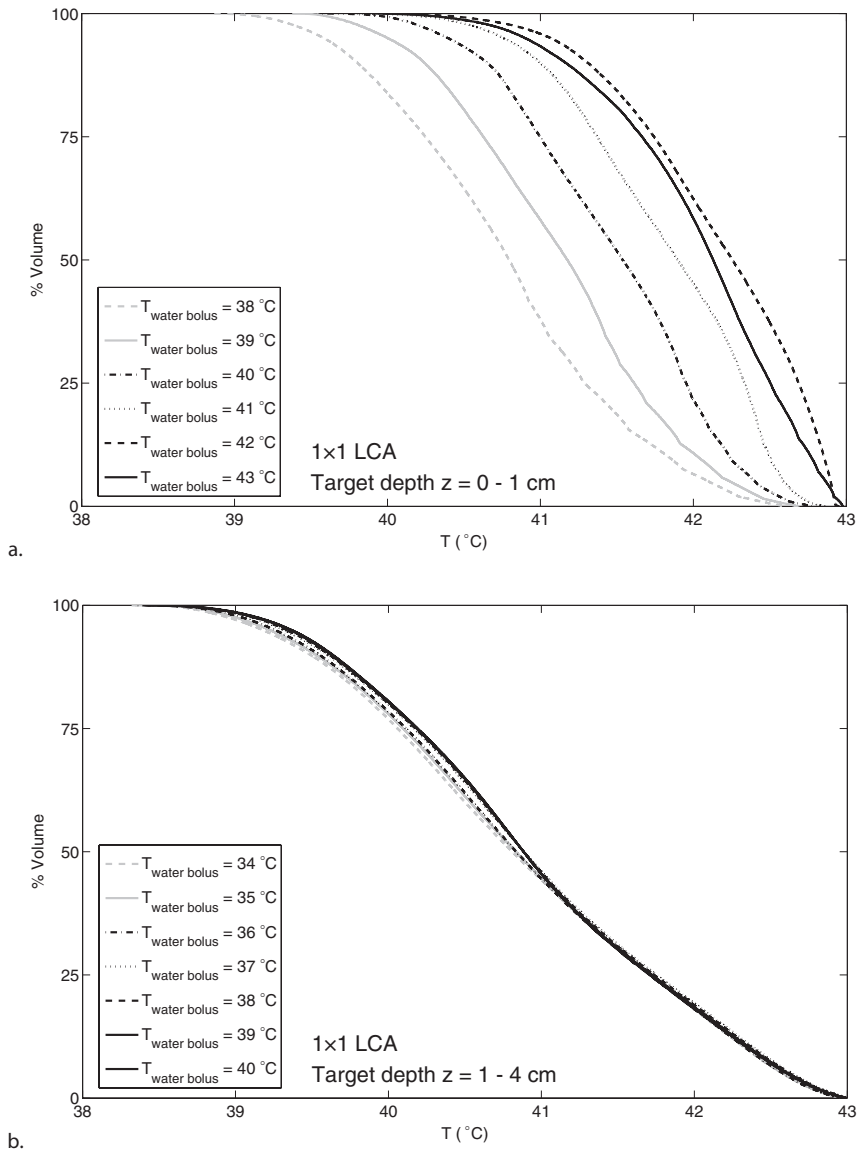
Figure 5. Mean target volume temperature as a function of water bolus temperature using (a) a single applicator, (b) two applicators, (c) four applicators and (d) six applicators.

a.

b.

**Figure 6.** Temperature volume histograms for a target depth of (a) 0 – 1 and (b) 1 – 4 centimetre in the single applicator set-up.

Clinical guideline

In Figures 4(a-d) the temperature profiles in the tissue are shown as a function of the depth under the skin surface for different waterbolus temperatures using a single, two, four and six LCAs respectively. For the single applicator set-up, shown in Figure 4(a), the temperature below the skin surface decreases rapidly when a waterbolus temperature of 43 °C is used. For a waterbolus of 42 °C the temperature profile is almost constant over the first centimetre below the skin. Comparing the waterbolus temperatures at which the skin temperatures are at ~40 °C in Figures 4(a-d) gives a clear view of the difference in temperature profiles between the four applicator arrays. These waterbolus temperatures are 36 °C, 34 °C, 33 °C and 31 °C for the single, two, four and six applicator array respectively.

The mean target volume temperature as a function of the waterbolus temperature is given in Figures 5(a-d) for the four different applicator set-ups. The deeper the target volume is located, the less influence the waterbolus temperature has on the mean temperature of the target volume. When the first centimetre below the skin is not part of the target volume, the differences in mean temperature become insignificant for a range of waterbolus temperatures. However, the guideline temperatures were chosen such that the waterbolus does not suppress the superficial temperatures too much (see Figure 5). If the target volume includes the upper centimetre, the curves show a more or less pronounced optimum. In some cases this optimum waterbolus temperature is not selected for the guideline because of skin temperatures above 42.5 °C. The TVHs in Figure 6 confirm the earlier observations: for a single applicator set-up, a waterbolus temperature of 42 °C is optimal for a target depth of 0 –1 cm, whereas for a target depth of 1 – 4 cm no optimal waterbolus temperature can be defined.

A distinct difference between Figures 4(a-d) is that the mean temperature becomes higher when the number of applicators increases. This can be explained by the contribution of neighbouring antennas, leading to higher SAR values at the edges of each antenna footprint for larger antenna arrays, see Figures 7(a) and (b).

Table 4 lists the waterbolus guideline: temperatures are given for every applicator array and target depth considered in this study. The guideline is based on the convection coefficients for a wet gauze. A dry gauze lowers the heat transfer of the waterbolus by about 23%. Therefore, especially at the beginning of a treatment when the patient does not yet perspire, a dry gauze could lead to a too rapid temperature rise of the skin. Consequently, the application of a wet gauze when setting up the applicator array is part of the guideline.

a.   b.
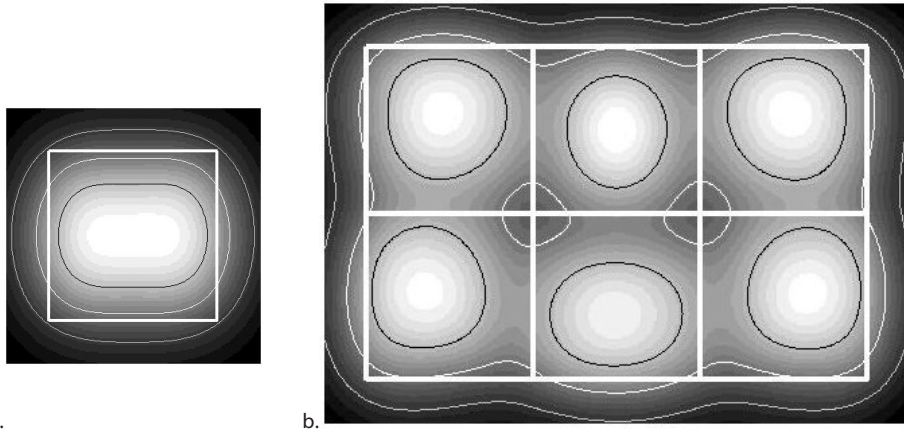
Figure 7. Illustration of increased SAR coverage below the footprint of an (a) 1x1 array and (b) 3x2 array of LCAs. Normalized SAR plots 12.5 mm below the skin surface. The thick white lines indicate the applicator footprint (aperture dimensions: 10×10 cm). The thin contours indicate 25% (grey), 50% (white), and 75% (black) SAR.

Table 4. Waterbolus temperature guideline for specified antenna array and target depth.

Target depth (cm)	1 antenna array	2 antenna array	4 antenna array	6 antenna array
0 – 1	42 °C	41 °C	41 °C	41 °C
0 – 2	41 °C	39 °C	39 °C	38 °C
0 – 3	41 °C	39 °C	39 °C	38 °C
0 – 4	41 °C	39 °C	39 °C	38 °C
1 – 3	39 °C	37 °C	36 °C	36 °C
1 – 4	37 °C	37 °C	36 °C	36 °C
2 – 4	37 °C	34 °C	33 °C	32 °C

When deriving the guideline, the effects of both perfusion and fat layer thickness were taken into consideration. Both phenomena can influence the temperature in the upper centimetre of the tissue. For example, at a constant waterbolus temperature, the temperature of the upper tissue layer may rise after an increase in perfusion was compensated by turning up the power (Figure 3). Therefore a safety margin was taken into account for all target depths except the 0 – 1 centimetre depth, to prevent superficial temperatures reaching above 42.5 °C. If the superficial temperatures are lower than desired, e.g. due to a non-average fat layer thickness or perfusion rate, the temperature of the waterbolus can be increased. Lowering the waterbolus temperature on the other hand is in our clinic not quickly possible, as the recirculator contains a heater but no device for cooling.

Discussion

The experimental procedure used to determine the waterbolus convection coefficients in this research is simple but effective. In the experiment the temperature was measured at the waterbolus to phantom interface. However, in the FDTD model the temperature of this interface is not defined. Instead, the temperature was recorded in the first grid cell below the interface. In theory this would result in a short delay in temperature response between the measurement and model prediction. However, the simulated profiles fitted the measurement (e.g. Figure 8), demonstrating that this delay is negligible.

The measurements presented in this paper show that the convection coefficient differs for the various size waterboli. In the clinic all waterboli are flushed using the same recirculating heater. Therefore the flow through a large waterbolus has a lower velocity than through a small waterbolus. Since convection increases with velocity, the small waterbolus has a higher convection coefficient than the large bolus.

Examples of waterbolus convection coefficients used in other studies are 45 W/(m²K) by Lang *et al*. [9], 100 W/(m²K) by Kumaradas and Sherar [19] and 500 W/(m²K) by Lagendijk [1]. As can be seen from Figure 8, the temperature profiles originating from the different convection coefficients vary significantly from the measured profile. The variation in literature values demonstrates that for a realistic implementation of the waterbolus in a thermal model using a convective boundary, the convection coefficient of the specific waterbolus system in use should be measured.
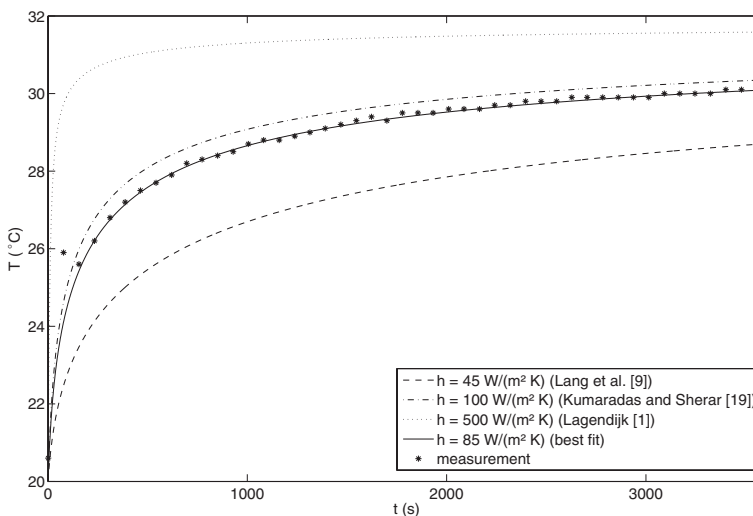

Figure 8. Example of measured and simulated temperature profiles for the convection coefficient of the 6-antenna waterbolus without a gauze. A simulation with a convection coefficient h = 85 W/(m²K) fits the measured profile best. Simulations with convection coefficients available from literature are plotted to demonstrate the effect of a too high or low convection value.

In steady-state, the bio-heat transfer equation shows that an increased heat loss by a higher perfusion can be compensated by SAR. At the skin surface however, the waterbolus also contributes to the thermal equilibrium. If the convective boundary at the skin surface remains constant, tuning the applicator power does not fully compensate a variation in perfusion at this location, see Figure 3. Therefore, to prevent over-heating of the skin under clinical conditions, it is recommended to decrease the waterbolus temperature when EM power is increased to compensate a perfusion increase.

The test cases were simulated using the known waterbolus temperature and amplifier power, and perfusion scaling was used to fit the temperature profiles such that the MSE was minimized. For the first two test cases the values for the heatsink terms in all tissues lie in the range mentioned by Lang *et al.* [9]. In the last case the heatsinks for skin and muscle are also in this range, however the heatsink in fat is below the range. For all three cases the perfusion rates for fat and muscle also agree with the ranges given by Feldmann [18]. The values for the effective conductivities used in the three test cases for the different types of tissue all lie between the intrinsic conductivities and values for the effective conductivity given by Crezee [20]. Little specific information about effective conductivities of different tissue types is given in literature. Since all parameters used in the model are either measured or given in literature, it can be concluded that the model is based on a realistic heat balance.

Temperature profiles predicted by the model are relatively smooth as the tissue is assumed to only have three planar layers. However, in clinical data relatively large differences in temperatures can be found over a small distance, a difference of more than 1.5 °C/cm is not unusual. For instance the temperature difference measured in the clinic between temperature probes 5 and 6 in test case 1 is 2.9 °C, while the distance between the probes was only 2 cm. These large temperature gradients over a small distance during treatments are responsible for the relatively large RMSE of the first, and especially third test case. There are several possible explanations for these large differences in temperatures. First of all, the model is a drastic simplification of the real anatomy. Although the values for the thicknesses of the skin and fat layer are in agreement with the findings of Kim and Park [21] for the mastectomy site, which represents the largest part of the superficial hyperthermia patients, the thickness of the three tissue layers will vary in reality and the layers will also never be flat. On top of that, there are always blood vessels, bony structures, scars or fibrotic areas present in the target volume. Secondly, the depths of the temperature probes are estimated by the hyperthermia physician and therefore not exact. The influence of the depth on the temperature is large, especially in the first centimetre as can be seen in Figure 9, where the temperature gradient is ~0.3 °C/mm. Lastly, skin temperature measurements may be affected by better contact of the temperature probe to the waterbolus than to the skin. Also the cooling effect of the waterbolus will vary over position, as was seen in the convection coefficient measurements. For the above reasons, it can be concluded that the observed differences are within the expected range.
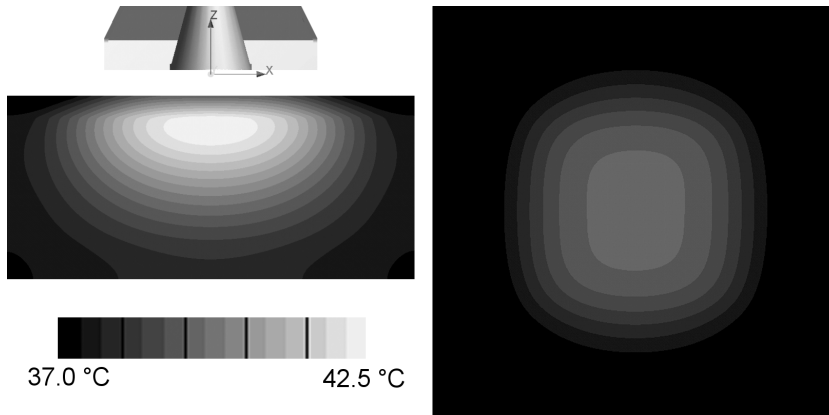
Figure 9. Temperature plots of the simulation of the treatment of the first patient with T_{water} = 35 °C. The left plot shows the temperatures in the x,z-cross-section where the temperature is maximum, at y = 0. The right plot depicts the skin temperatures. The LCA aperture (top left, width 10 cm) indicates dimensions.

The model of Kumaradas and Sherar [19] is one of the few superficial hyperthermia models in literature that compares simulated temperatures with measured temperatures. By scaling the power input, the simulated temperature was fit to the measured temperature at the location of a control probe. To implement perfusion in the model, the basal heatsink terms in skin, fat and muscle were multiplied with factors 2, 3 and 2 respectively to account for the increase in temperature of the different layers. The outcome of this was that the heatsink in muscle was lower than in fat, which is most unlikely, especially as the temperature in muscle was expected to be higher than in fat. In contrast, the perfusion in the current study was scaled to compensate for the applied applicator power, but the relation between the heatsink terms and effective conductivities of the different tissue types remained unaltered.

The model was used for setting up guidelines on selecting the waterbolus temperature in superficial hyperthermia treatments for four different applicator set-ups. The main differences between these guidelines are caused by the waterbolus convection coefficients. The interpretation of the temperature data was done in a fashion to create clear and clinically usable guidelines, with a safety margin for differences in perfusion and fat layer thickness. Two general points have to be taken into consideration.

Firstly, when the waterbolus temperature is set equal to or above the maximum allowed tissue temperature, the skin temperature will reach its limit at a low EM power input. In this case, effectively only the skin is heated, and the rest of the tissue will remain at a relatively low temperature, see for example the temperature profile for a waterbolus temperature of 43 °C in Figure 4(a). Thus, the temperature of the waterbolus should be set lower than the maximum allowed tissue temperature. Only in the rare occasion that the amplifier power is limited, the waterbolus can be used to assist the applicator in heating the tissue.

Secondly, when performing a hyperthermia treatment, the invasive temperature probes are usually located up to a depth of 10 - 15 mm. Thus, temperature measurements may not be available in deeper target regions. As a consequence, optimising the measured temperatures by tuning the waterbolus temperature may lead to limited heating at depth. This is clearly illustrated in Figure 4(d): compare the profiles for T_{water} = 41 - 42 °C to T_{water} = 30 - 38 °C. Hence when adjusting the waterbolus temperature, one should be aware of the limited observability of the overall temperature distribution in the target volume.

To compare the waterbolus temperatures proposed by the new guideline to current clinical practice in Rotterdam, the bolus temperature settings during 191 treatments between July 2004 and October 2005 were compiled, see Table 5. These clinical data reflect the temperature of the circulating water as indicated by the waterbath. Usually, the temperature at the inflow of the bolus is 0.5 - 1 °C lower than the waterbath temperature. Still, the new guideline proposes lower waterbolus temperatures than are used in current clinical practice. This can be explained by the aforementioned point: as most temperature probes were placed in the waterbolus-skin interface or in the very superficial tissue layers, striving to reach the target temperature (43 °C) at these probes will probably result in a higher waterbolus temperature than one would select based on the entire 3-D temperature distribution.

Although the guidelines in this research were developed for the 433 MHz LCA system, they can be of use for different applicators operating at the same frequency. However, one condition is that the convection coefficients for those systems are measured and lie in the same range as those presented in this paper.

Table 5. Overview of waterbath temperatures applied during 191 superficial hyperthermia treatments between July 2004 and October 2005 at the Erasmus MC.

Target depth (cm)	Waterbath temperature (°C)		n
	median	range	
0 - 1	43.0	41.0 - 43.0	12
0 - 2	42.0	40.0 - 43.5	91
0 - 3	41.0	40.0 - 42.0	39
0 - 4	40.0	35.0 - 41.0	31
1 - 3	40.0	37.0 - 41.5	10
1 - 4	36.0	36.0 - 39.0	4
2 - 4	40.0	40.0 - 40.0	4

Conclusions

The waterbolus convection coefficient measured in this research differed per bolus configuration; it depends on factors like the waterbolus geometry, the capacity of the circulation pump and the use of a gauze. Therefore, in order to realistically simulate the

waterbolus in a thermal model using a convective boundary, it is mandatory to measure the convection coefficients for each specific waterbolus set-up. Three test cases showed that the model presented in this study gives a good prediction of the global temperature distributions achieved during superficial hyperthermia treatments. Based on the model, a waterbolus temperature guideline for the LCA system was developed. The guideline specifies the optimal waterbolus temperature as predicted by the model, for four different set-ups and seven target depths.

References

[1] Lagendijk JJW. Thermal models: principles and implementation. In: Field SB, Hand JW, eds. An introduction to the practical aspects of clinical hyperthermia. London: Taylor and Francis; 1990. pp. 478–512.

[2] Clegg ST, Das SK, Fullar E, Anderson S, Blivin J, Oleson JR, Samulski TV. Hyperthermia treatment planning and temperature distribution reconstruction: a case study. Int J Hyperthermia 1996;12:65–76.

[3] De Bruijne M, Samaras T, Neufeld E, Chavannes N, Van Rhoon GC. Quantitative three-dimensional SAR validation of the Lucite cone applicator. In ESHO 2005 Book of abstracts, Graz, June 2005.

[4] Van Rhoon GC, Rietveld PJM, Van der Zee J. A 433 MHz Lucite cone waveguide applicator for superficial hyperthermia. Int J Hyperthermia 1998;14:13–27.

[5] Leonard JB, Foster KR, Athey TW. Thermal properties of tissue equivalent phantom materials. IEEE Trans Biomed Eng 1984;31:533–536.

[6] De Bruijne M, Samaras T, Bakker JF, Van Rhoon GC. Effects of water bolus size, shape and configuration on the SAR distribution pattern of the Lucite cone applicator. Int J Hyperthermia 2006;22: 15-28.

[7] SEMCAD Reference Manual. Zürich, Switzerland: Schmid & Partner Engineering AG; 2004. Accessed 24 November 2005. Available online at: http://www.semcad.com.

[8] Pennes HH. Analysis of tissue and arterial blood temperatures in the resting human forearm. J Appl Physiol 1998;85:5–34.

[9] Lang J, Erdmann B, Seebass M. Impact of nonlinear heat transfer on temperature control in regional hyperthermia. IEEE Trans Biomed Eng 1999;46:1129–1138.

[10] Gautherie M. Etude par thermométrie infrarouge des properties thermiques de tissues humains 'in vivo'. Influence de la température et de la vascularization. Revue Francaise d'Etudes Cliniques et Biologiques 1969; 14:885–901.

[11] Lagendijk JJW. COMAC-BME workshop on modelling and planning in hyperthermia. Conclusions subgroup thermal modelling. COMAC-BME Hyperthermia bulletin 4; 1990. pp 47-49.

[12] Crezee J, Lagendijk JJW. Experimental verification of bioheat transfer theories: measurement of temperature profiles around large artificial vessels in perfused tissue. Phys Med Biol 1990;35:905-923.

[13] Stogryn AP, Bull HT, Rubayi K, Iravanchy S. The microwave dielectric properties of sea and fresh water. Technical report. GenCorp Aerojet; 1995.

[14] Samaras T, Rietveld PJM, Van Rhoon GC. Effectiveness of FDTD in predicting SAR distributions from the Lucite cone applicator. IEEE Trans Microwave Theory Tech 2000;48:2059–2063.

[15] IFAC. Accessed 24 November 2005. Available online at: http://niremf.ifac.cnr.it/tissprop/htmlclie/htmlclie.htm.

[16] COMAC BME Task Group Report. Treatment planning and modelling in hyperthermia. Technical report. University of Rome; 1992.

[17] Fiala D, Lomas KJ, Stohrer M. Modelling in physiology, a computer model of human thermoregulation for a wide range of environmental conditions: the passive system. J Appl Physiol 1999;87:1957–1972.

[18] Feldmann HJ, Molls M, Hoederath A, Krümpelmann S, Sack H. Blood flow and steady state temperatures in deep-seated tumors and normal tissues. Int J Radiat Oncol Biol Phys 1992;23:1003-1008.

[19] Kumaradas JC, Sherar MD. Edge-element based finite element analysis of microwave hyperthermia treatments for superficial tumours on the chest wall. Int J Hyperthermia 2003;19:414–430.

[20] Crezee J, Lagendijk JJW. Temperature uniformity during hyperthermia: the impact of large vessels. Phys Med Biol 1992;37:1321-1337.

[21] Kim SM, Park JM. Normal and abnormal US findings at the mastectomy site. Radiographics 2004;24:357–365.

6

Quality control of superficial hyperthermia by treatment evaluation

Abstract

Steering of multi-element heating arrays for superficial hyperthermia (SHT) can be a challenge in the clinic. This is because the technician has to deal with a multiple-input multiple-output system, varying tissue dynamics and often, sparse tissue temperature data. In addition, patient feedback needs to be taken into account. Effective management of the steering task determines the quality of heating. Systematic evaluation is an effective tool to control the quality of treatments. The purpose of this manuscript is to report on a treatment evaluation flow developed for SHT at the Erasmus MC. This flow is used to secure the quality of steering as well as to stimulate general quality awareness in the hyperthermia team. All treatments are evaluated in a multidisciplinary discussion. Tools and methods were developed to enable effective and efficient evaluations.

The treatment evaluation sheet is a compact and intuitive representation of power and temperature data. Trend lines and a temperature-depth plot allow a quick analysis of the steering parameters and the heating profile within the target volume. In addition, the principal statistics of applicator power, waterbolus and tissue temperature values are given. Power steering data includes the number of switch off events, interruption time and the number of steering actions. A list of basic checks and reference values for clinical data support further the treatment evaluation.

These tools and the systematic treatment evaluations they facilitate, ultimately lead to consistent performance and fine tuning of the set-up and steering strategy for each individual patient.

Introduction

Clinical studies have shown that combined radiation and hyperthermia is an effective treatment method for malignancies at the surface of the body [1-3]. The objective of a superficial hyperthermia treatment is to heat a target volume to therapeutic temperatures of 40-45°C. Multi-element hyperthermia applicators have been developed to effectively heat large target volumes of superficial disease [4-11]. These can facilitate an optimum power deposition profile across the treatment volume by adapting the power of elements of the antenna array to minimise hot spots and tailor the local perfusion rate. Simultaneously, the temperature of the waterbolus layer between the skin and the applicator is adjusted to provide cooling of the skin surface.

The steering of applicator powers and waterbolus temperature can be a challenge in the clinic, because the technician needs to manage a multiple-input multiple-output system (Figure 1) where the tissue dynamics are time-varying and nonlinear. In addition, the temperature data is often from a limited number of sensors that incompletely measure the target volume. Furthermore, the technician must combine measured temperatures with patient feedback in the form of pain complaints and signs of discomfort. The optimum control strategy or maximum achievable temperature distribution for an individual case is often undefined. Effective management of the steering task determines the quality of heating. A too conservative approach using low powers may result in suboptimal temperatures, whereas a vigorous approach with fast power escalation may result in hot spots that require a prolonged period of reduced or zero power input. Both scenarios reduce the effectiveness of heating.

Automatic feedback control of applicator arrays has been proposed in several publications [12-17] and was shown to be effective in phantom models [12,14,18]. Such automatic feedback control systems rely on high-density thermal monitoring. When high-density thermometry is not available in the clinic, automatic feedback control based on measured temperatures only becomes less reliable. In this case, patient feedback becomes more important.

Automatic feedback control is not yet feasible in our clinic and in other clinics. The human factor may introduce inter-individual variability in control performance. To ensure the quality of steering and to stimulate general quality awareness in the hyperthermia team, all treatments are evaluated in multidisciplinary discussion sessions at Erasmus MC. It is our experience that the interpretation of the raw temperature and power data slows down the evaluation process. We therefore have developed a compact and intuitive representation of treatment data, to enable time-efficient and productive treatment evaluations. This treatment evaluation sheet and the treatment evaluation method are presented in this paper.
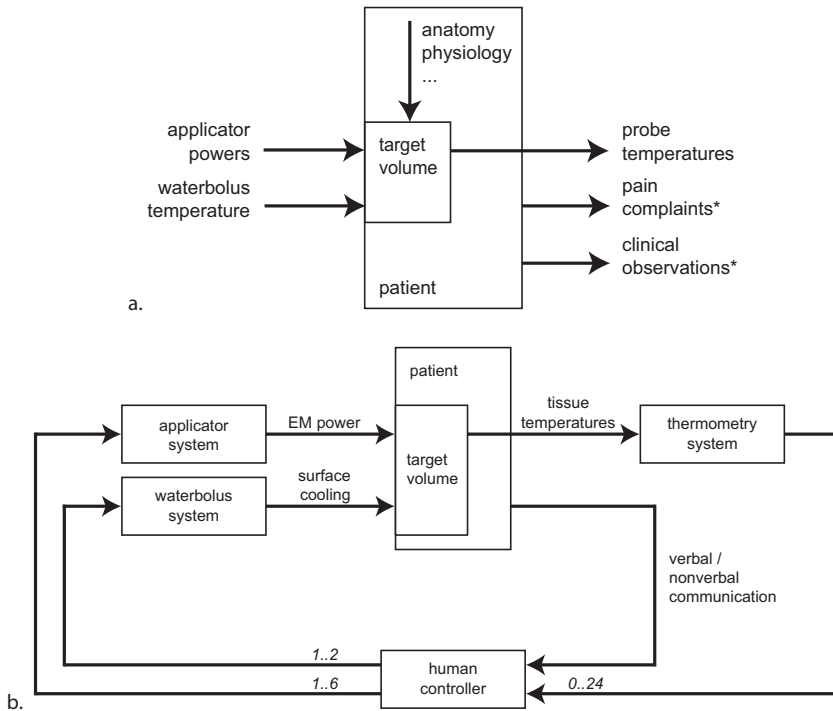
Figure 1. (a) Input-output schematic diagram of a superficial hyperthermia target volume. The patient-related factors are represented by the vertical arrow. The outputs marked * are subjective and not recorded by the data acquisistion system. (b) Closed-loop control in superficial hyperthermia where the human controller interprets tissue temperatures and patient feedback and steers the waterbolus temperature and applicator powers. Numbers in italic font represent the signal width and are specific to the circumstances at the Erasmus MC.

Hyperthermia treatment evaluation is rarely addressed in the literature. Our intention is to introduce this topic into the quality assurance framework, as it may be critical for the ultimate quality of treatments.

Materials & Methods

The evaluation flow as presented in this paper was especially developed for superficial hyperthermia treatments at Erasmus MC. Therefore, a brief description of the treatment approach and equipment used in this clinic is given here.

Patients and treatments

Superficial hyperthermia is used at Erasmus MC in the managment of breast carcinoma, melanoma, mesothelioma, and lymph nodes metastasis of head and neck squamous cell

carcinoma. For reirradiation cases, the hyperthermia target volume is the whole region at risk and encompasses the reirradiation field. For primary high dose radiotherapy cases (melanoma), the target volume is macroscopic tumour only. In general, the target volume has a depth of up to four centimetres.

The treatment duration is typically 60 minutes. The first 20 minutes are the heat-up period at the end of which the therapeutic temperature should be reached. The aim is to heat the whole target volume to 43°C, but temperatures between 40-43°C are still considered to be therapeutic. More details about the clinical approach can be found in [19-21].

Applicator system

A 433 MHz Lucite cone applicator (LCA) is the standard antenna for superficial hyperthermia at Erasmus MC (Figure 2). It is a water-filled horn applicator that has a high effective field size to aperture ratio due to its Lucite windows and a PVC cone in the horn [22]. The efficiency of this applicator is about 40% [23]. Six LCAs are available. The square aperture makes it easy to combine LCAs in an array. The size of the hyperthermia target volume and the shape of the anatomy determine the array configuration. This ranges from a single applicator (100 cm²) to a 2×3 array (600 cm²). For larger areas, two applications can be given successively ("technical fields"). Usually the electric field direction of adjacent applicators in the array is perpendicular for optimum SAR coverage [24]. The electric field directon is rotated 90° for subsequent treatments.
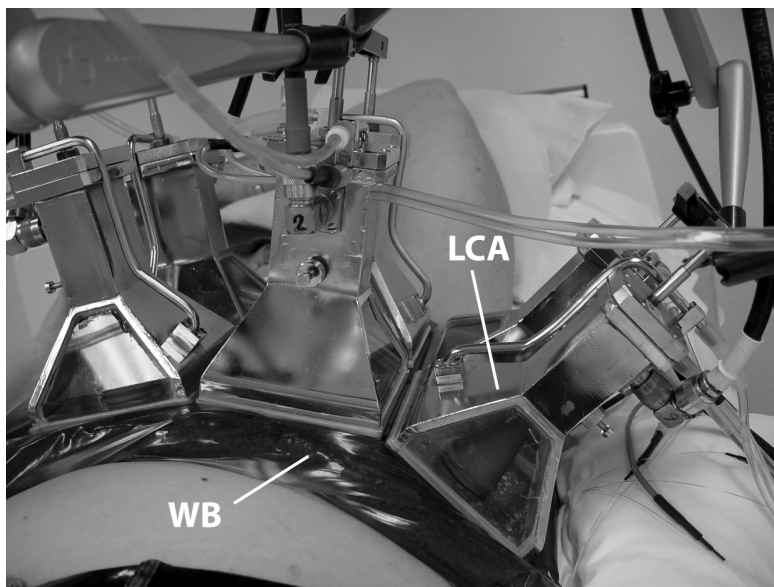
**Figure 2.** A 2×3 LCA array and waterbolus (WB) placed on the chest of a patient.
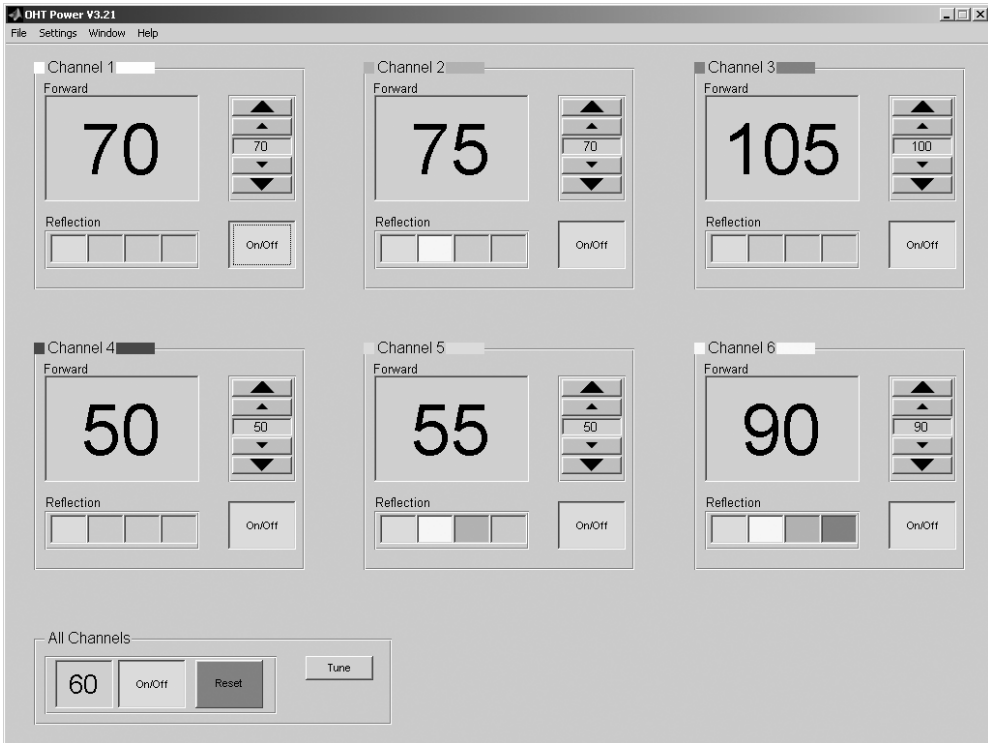
Figure 3. Screenshot of the graphical user interface for power steering. The measured forward power is indicated in large font and the power setpoint in small font. The reflected powers are represented graphically in a colour code (green <5%, yellow 5-10%, orange 10-15%, red >15% reflected power).

The applicators are fed by power amplifiers with non coherent sources (Pavoni Diffusion, Italy) [25]. The amplifiers deliver up to 200 Watts net incident power per LCA. The technician sets the power levels using a graphical user interface (GUI), see Figure 3. The interface shows the forward and reflected powers with a refresh rate of one second.

Waterbolus system

The function of the waterbolus is to couple the electromagnetic waves into the patient and to cool the skin. The waterbolus temperature is a steering parameter to control heating at depth: a lower waterbolus temperature allows deeper heating because more heat is drawn from the skin surface. A thermocirculator (Polaron E3500, Microtech, UK) flushes the waterbolus with de-ionized water of a set temperature. A sensor is placed in the waterbolus inlet to monitor the temperature. Several different sized waterboli are available for different LCA array configurations. Clinical guidelines have been developed for the optimal bolus application and for the selection of waterbolus temperature as a function of antenna array dimension and target depth [26-27].
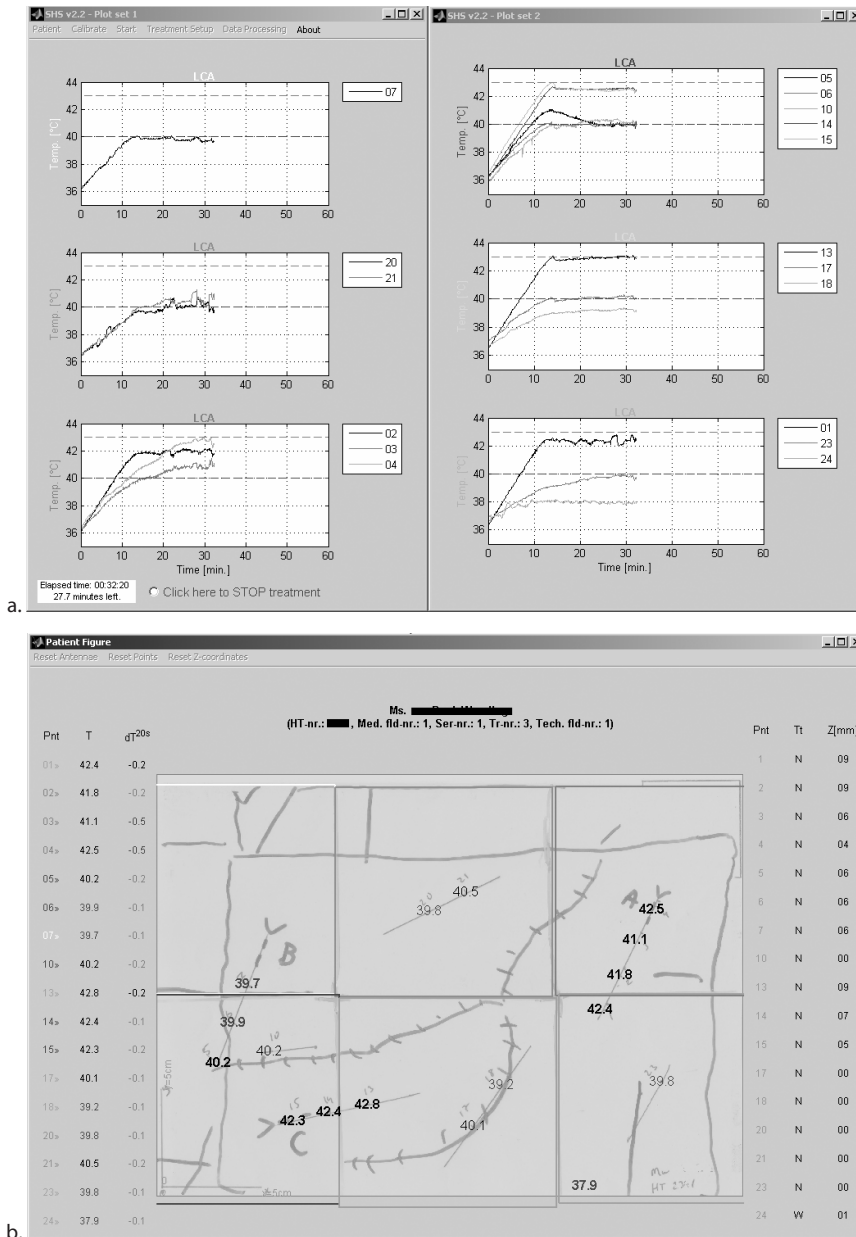
Figure 4. Screenshot of the temperature monitoring graphical user interface. On screen (a), temperature-time graphs for the sensors below each applicator are shown. On screen (b), the measured temperatures are mapped onto a sketch that includes anatomical features, the location of the tumour and scar tissue, apertures of the applicators, catheter tracks and margins of the radiation field. For each measurement point the tissue type, depth, temperature and temperature difference over 20 seconds is also shown.

Thermometry system

The temperatures are measured with single- and multi-sensor fibre-optic probes (accuracy 0.2°C) using a twenty-four channel Takaoka FT1310 fibre thermometry readout system (Takaoka Electric, Japan). These nonmetallic probes are attached to the skin or inserted into closed-tip interstitial catheters. The aim is to have both interstitial and superficial thermometry under each applicator. The probes are placed in the same location in consecutive treatments. During treatments, the hyperthermia operator monitors the interstitial and skin temperatures using a GUI, see Figure 4. The GUI shows time-temperature plots for measurement points below each LCA footprint and maps the temperatures onto a representation of the patient anatomy for ease of interpretation. Too high temperatures and steep temperature gradients are highlighted. The refresh rate of the temperature readings is three seconds.

Steering

Steering actions are based on the interpretation of measured temperatures and patient feedback. The actions are directed at achieving therapeutic temperatures (> 40°C) throughout the target volume. The maximum allowed tissue temperature is defined in a guideline [28] and differs per tissue type. It ranges from 43°C for normal tissue at first treatment to above 45°C for tumour tissue that is >2 cm distance from normal tissue. To prevent burns, pain complaints prevail over measured temperatures even if these are lower than allowed according to the guidelines.

At the start of the first treatment, the power is 30 W per applicator. This can be increased for later treatments. During the heat-up phase in the first 20 minutes, the target temperature rise is 0.25 to 1°C per minute and the applicator powers are increased in steps of 10 W to achieve this. Smaller steps may be applied if thermometry or tissue sensitivity is limited. After the heat-up phase, small power variations of 5-10 W per applicator are applied to optimize the temperature distribution and to prevent local temperature decreases. The initial waterbolus temperature is chosen according to the guideline table published in [27]. This temperature is varied in 0.5-1°C steps during waterbolus steering.

If temperatures exceed the upper limit, the applicator power is decreased in 5-10 Watt steps. In case of pain complaints, the technician determines systematically the applicator responsible. The most suspect applicator is switched off and the patient checked as to whether the pain disappears (i.e. power-related hot spot is removed). If the pain is relieved, the antenna is switched on again, but at a lower power level. If the pain does not disappear, it is switched on again to the previous power level and another applicator is switched off. Switching off one applicator at a time for a short period prevents a collapse of the temperature distribution.

Treatment evaluation

Patient discussion

At the start of each week, all treatments performed in the previous week are reviewed in the patient discussion session. Here all disciplines are represented: physicians, technicians and physicists. The basis for the discussion is the measured data presented in the treatment evaluation sheet and the clinical notes made during treatments. The focus is on three questions:

1. Was the aim of treatment achieved?
2. What were the limiting factors and anomalies?
3. Were there tangible indications on how next treatments could be improved for the particular patient?

The action points and issues that develop from the discussion are noted in the patient file. The discussion time needed per patient is typically four minutes, but can be up to about 10 minutes for special cases.

The primary aim is to optimize treatments for each individual patient. The patient discussion also stimulates the general quality awareness in the hyperthermia unit by serving as a peer review, encouraging interaction between disciplines and steepening the learning curve of new team members. Furthermore, it may initiate new research directions, equipment and procedure quality checks and fine tuning of the clinical guidelines, especially when subjects recur.

Treatment evaluation sheet

The treatment sheet summarizes the steering actions (i.e. applicator power and waterbolus temperature settings) and the resulting tissue temperatures in a compact and intuitive way (see Figure 5 for an example). In the graphs, the trend lines and temperature-depth plot enable a fast interpretation of a treatment. The numerical data allow a more in-depth analysis during treatment evaluations.

The treatment sheet is automatically generated as a single page portable document file (PDF). The treatment sheet repository can be browsed from any computer in the hyperthermia unit and can be used to inspect a patient's earlier treatments or similar treatments from other patients.

The treatment evaluation sheet consists of four sections: general treatment info, power data, waterbolus data, and tissue temperature data. Power and temperature statistics are reported both for the whole treatment duration (0-60 minutes) and for the steady-state period (20-60 minutes).

```
Patient       Ms XXXXXXX (XX-XX-XXXX)
HTnr          XXXX    Med.Field  1   Tech.Field  1   Series     1   Treatment   2

Operator      XXXXXXXXXXX
Start         13-Oct-2009 11:46:51
Duration      60.3 min

Power              Ch#1    Ch#2    Ch#3    Ch#4    Ch#5    Ch#6    Total
  ss mean (W)      68      36      64      58      58      67      351
  ss max (W)       74      39      78      73      73      76      404
  mean (W)         60      35      57      54      54      61      321
  max (W)          74      60      78      73      73      76      404
  #off switches     4       5       5       4       4       4
  time off (min)   5.2     8.1     4.5     4.3     4.4     4.4
  #steer.actions   17      12      16      15      14      14
```
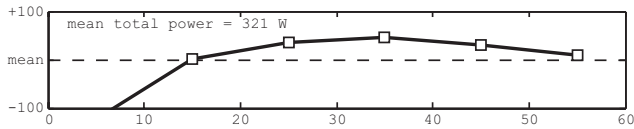


```
Waterbolus
  ss mean (°C)        38.0
  ss range (°C)       37.5    38.2
  mean (°C)           38.0
  range (°C)          37.2    39.4
```
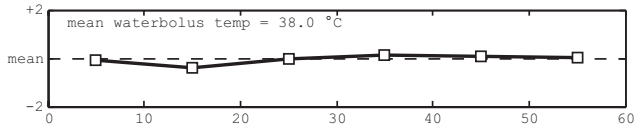


```
Temperature         Ch#1    Ch#2    Ch#3    Ch#4    Ch#5    Ch#6    Total
  #int.probes        5       1       0       2       2       0       10
  ss int.mean (°C)  41.3    40.1    NaN     41.0    41.0    NaN     41.1
  ss int.min (°C)   39.8    39.4    NaN     39.9    40.4    NaN     39.4
  ss int.max (°C)   42.6    40.3    NaN     42.1    41.7    NaN     42.6
  int.mean (°C)     40.9    39.8    NaN     40.6    40.5    NaN     40.6
  int.min (°C)      37.2    37.4    NaN     37.1    37.0    NaN     37.0
  int.max (°C)      42.6    40.3    NaN     42.1    41.7    NaN     42.6
  #sup.probes        0       2       3       2       0       1       8
  ss sup.mean (°C)  NaN     41.1    41.3    40.5    NaN     41.0    41.0
  ss sup.min (°C)   NaN     40.4    39.1    39.5    NaN     40.7    39.1
  ss sup.max (°C)   NaN     41.8    42.5    41.1    NaN     41.2    42.5
  sup.mean (°C)     NaN     40.8    40.9    40.1    NaN     40.7    40.6
  sup.min (°C)      NaN     38.2    37.2    37.9    NaN     38.6    37.2
  sup.max (°C)      NaN     41.8    42.5    41.1    NaN     41.2    42.5
```
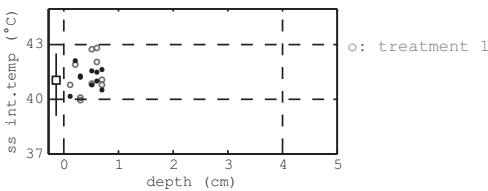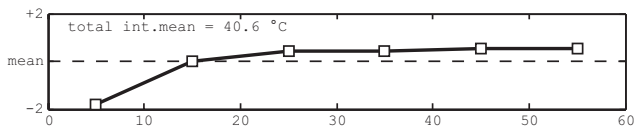


```
SHT report (v1.5), generated 13-Oct-2009 13:11:45
```

Figure 5. Example treatment evaluation sheet. Abbreviations: HT = hyperthermia; Ch = channel; ss = steady-state; int. = interstitial; sup. = superficial; NaN = not-a-number (no data available).

General treatment info

The general treatment information block contains the patient name and date of birth, the hyperthermia number, the number of the medical and technical field, the series number and the treatment number. Also the treatment date, the start time (power-on) and the treatment duration (power-on to power-off) is listed.

Power data

The power data block tabulates the average power and the maximum power per applicator. The last column gives this information for the total power (sum of all channels). The bottom lines mention the number of off-switching events per channel, the total time a channel has been switched off and the number of steering actions (power steps) per channel. Off-switching indicates that limiting factors (pain complaints, high tissue temperatures) have been encountered.

Below the text block is the trend line for the total applicator power. The trend line is centred along its mean value (indicated in the plot), and has a range of mean ± 100 Watts. Each marker in the trend line represents the 10 minute average value. In this way, the shape of the trend line can easily be compared between treatments. The trend lines for waterbolus and tissue temperatures are generated in a similar way, and have a range of mean ± 2 °C.

Waterbolus data

The average waterbolus temperature and its range are given and the trend line for waterbolus temperature is plotted.

Tissue temperature data

This is subdivided in two parts: interstitial and skin temperatures. Temperature statistics are given per applicator (columns Ch#1..6) and overall (Total). If no probes are available below an applicator's footprint, then not-a-number (NaN) values are shown. For each category the mean, minumum and maximum temperature is indicated.

The trend line indicates how the mean interstitial temperatures developed over time. The temperature-depth plot shows the mean interstitial temperatures during the steady-state period (one dot per measurement point) and the overall mean skin temperature (square marker) and its range during the steady-state period (line). For ease of interpretation, dashed lines indicate the depth of the target volume (0-4 cm in Figure 5), the target temperature (43°C) and the minimum therapeutic temperature (40°C). The temperature-depth plot allows the fast interpretation of therapeutic temperatures, heating at depth and the relation between skin temperatures and interstitial temperatures. Results of earlier treatments are indicated by coloured markers in this plot (see Figure 5).

Reference data

The reference for evaluation of tissue temperatures is the target (43°C), while values below 40°C are considered insufficient heating. For the waterbolus temperature, the reference value is prescribed by our guideline [27], taking into account the effective heating at depth. To create reference values for the evaluation of power steering values, the 2009 clinical data has been analysed (see Table 1). For example, an applicator power of 30 W is considered low and 85 W is high and for the number of steering actions this corresponds to 9 and 29.

Table 1. Power steering statistics based on a per applicator analysis of all treatments conducted in 2009 at Erasmus MC (196 treatments, 920 applicator·treatments).

Steering parameter	Steady-state mean power (Watt)	Number of switch off events	Time off (minutes)	Number of steering actions
Mean	56.4	3.7	2.7	17.8
10th percentile	30	1	0.1	9
25th percentile	42	1	0.4	12
Median	55	3	1.4	16
75th percentile	69	5	3.0	21
90th percentile	85	7	5.2	29

Basic checks

The following basic checks through the treatment sheet provide a systematic way to gain a complete impression of the treatment. The checks refer to the goal of treatment: to heat the whole target volume to the target temperature, unless limitations are met.

1. Is the data complete? Missing data is clearly indicated by not-a-number values, empty graphs, and messages like "No waterbolus data available". Reasons for incomplete data may be equipment out of order, datafiles not stored or stored in the wrong place and no thermometry applied.
2. Was the treatment duration 60 minutes? A shorter duration may indicate that the treatment was aborted due to serious pain complaints or discomfort.
3. How much power was applied to the patient? A steady-state mean power of less than 30 W per channel is unusual.
4. How many switch-off events were there? If there were no switch-off events, the power probably was not increased to the limit. Many switch-off events indicate trouble such as a restless patient, frequent pain complaints and severe power limiting hot spots.
5. What is the shape of the power trend line? Ideally, it is flat or slightly increasing in the steady-state period.
6. Was the waterbolus temperature stable and according to the guidelines and if waterbolus steering was applied, what was the effect?

7. What was the steady-state mean interstitial temperature? A mean interstitial temperature between 40-43°C is satisfactory. If it is below 40°C the temperature may not be therapeutic and the treatment strategy needs to be discussed.
8. What is the shape of the tissue temperature trend line? Ideally, it is stable at a therapeutic level in the steady-state period. Dips or a negative slope indicate severe limitations. A positive slope after the heat-up phase may indicate too cautious power steering.
9. What does the temperature-depth distribution look like? Poor heating at depth (or at the surface) shows that waterbolus steering should be applied. The temperature-depth plot also clearly indicates whether temperature measurements are available at the deeper sections of the target volume.
10. What was the treatment limiting factor? If there were no limiting issues such as power-related hot spots and limiting tissue temperatures that can be identified, heating might be enhanced.

Detail checks

In general, steering and control difficulties are indicated by a high number of off-switching events or steering actions, a significant off period, sub-therapeutic tissue temperatures and a drop of the power level towards the end of treatment. These difficulties often trace back to one or two applicators in the array. Therefore, a detailed analysis commonly focuses on the individual applicators. In addition to the treatment sheet, other sources of information such as time-temperature and time-power plots may be required for more detailed analyses.

Typical trend line and temperature-depth plot shapes

A quick inspection of the trend lines and temperature-depth plots often gives a first impression of the treatment and stimulates questions for evaluations. Common characteristic power, waterbolus and tissue temperature trend line shapes are described and illustrated in Figures 6, 7 and 8. These trend line shapes and possible checks and actions are discussed in Tables 2, 3 and 4, respectively. Common characteristic temperature-depth plots are shown in Figure 9.
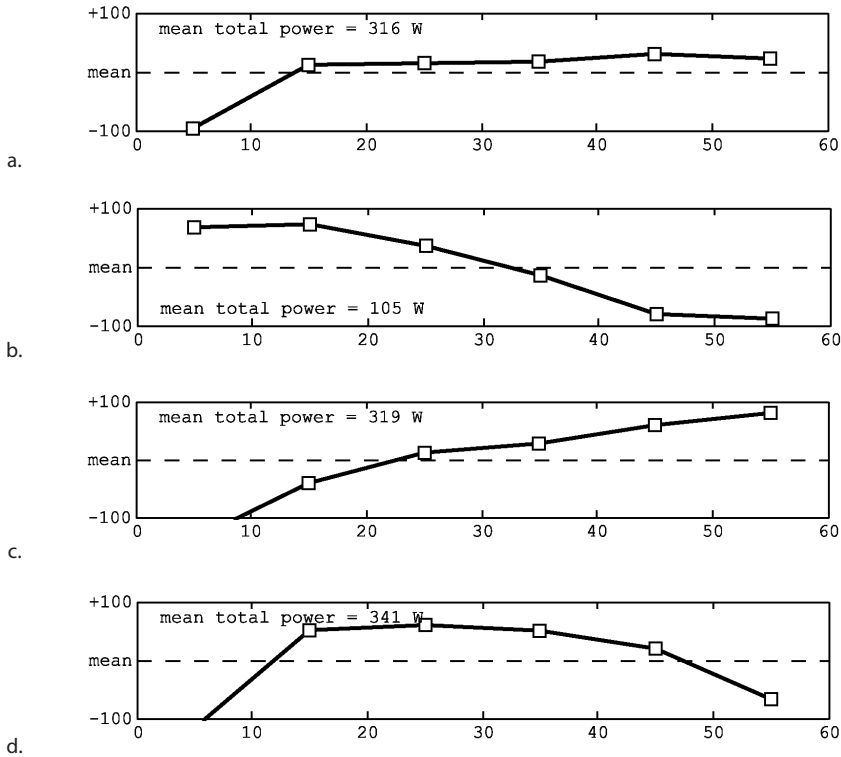
Figure 6. Characteristic shapes of the power trend line: (a) normal, (b) peak at beginning of treatment, (c) continuous increase and (d) decrease at the end of treatment.

Table 2. Characteristics of typical power trend line shapes, the related checks and possible actions for the next treatment.

Trend line shape	Characteristics	Checks and possible actions
Normal	The trend line rises to above the average within the first 20 minutes and remains there.	-
Peak at beginning of treatment	Peak in the trend line within the first half of the treatment.	Check if a too high start value or relatively large increments in power triggered early limitation events.
Continuous increase	The total power rises until the end of treatment.	Possibly the initial power and/or power increments were too modest. It may also reflect the willingness to treat in the upper therapeutic range with a tolerant patient.
Decrease at the end of treatment	The trend line slopes downwards in the second stage of the treatment.	This implies frequent off-switching due to pain complaints or limiting temperatures. The power build up in the first half may have been too fast.
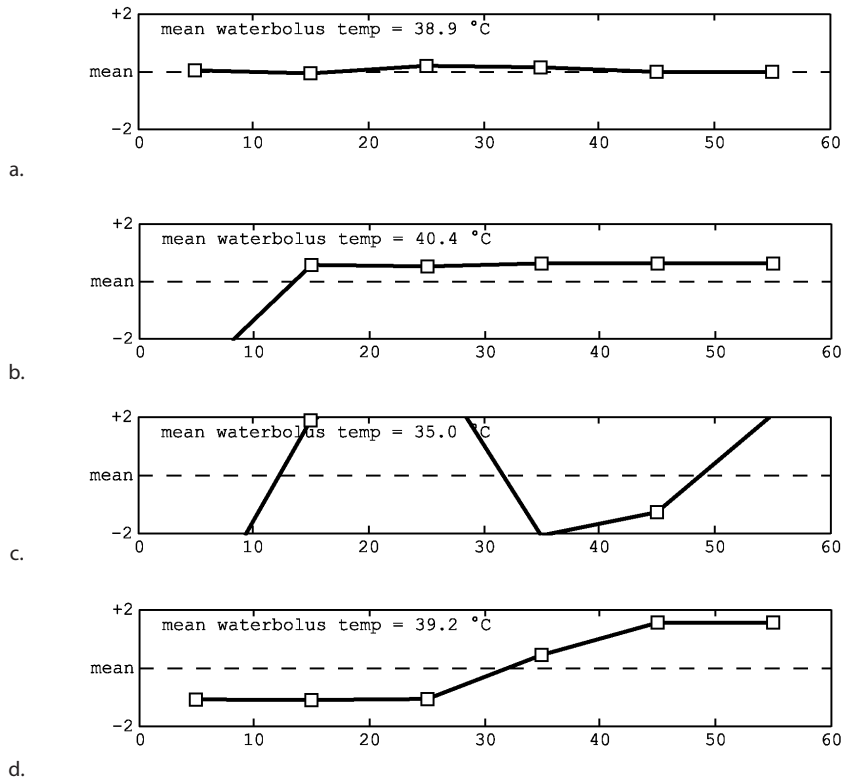
Figure 7. Characteristic shapes of the waterbolus trend line: (a) stable and normal, (b) low temperature at the start, (c) wavy and (d) steering.

Table 3. Characteristics of typical waterbolus temperature trend line shapes, the related checks and possible actions for the next treatment.

Trend line shape	Characteristics	Checks and possible actions
Stable and normal	The trend line shows little deviation from the mean.	-
Low temperature at the start	The temperature is far below average in the first 10-20 minutes.	Probably the waterbolus was not heated to the target temperature before the treatment, or the temperature probe was not correctly placed in the inlet.
Wavy	The trend line fluctuates up and down.	Possibly the treatment was interrupted and the waterbolus temporarily removed from the patient. Otherwise, check for malfunctioning of the equipment.
Steering	The trend line reflects the steering actions.	Check against the temperature data, if steering was effective.
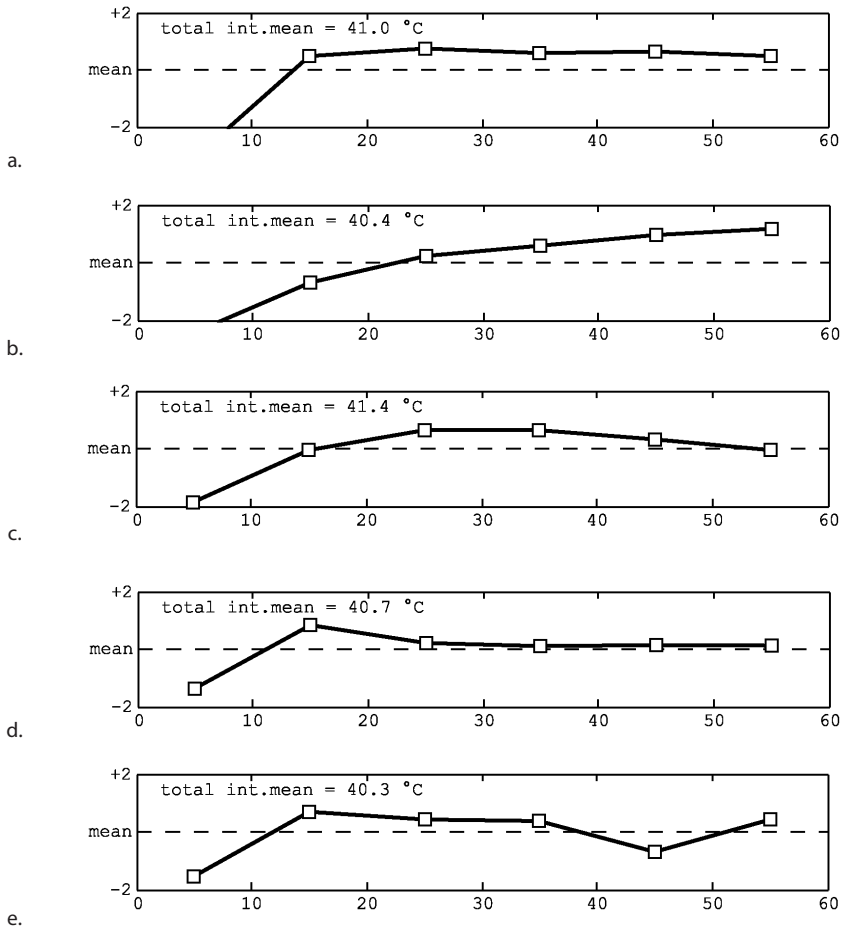
Figure 8. Characteristic shapes of the interstitial temperature trend line: (a) normal, stable, (b) increasing towards the end, (c) decline towards the end, (d) maximum in the early stages and (e) dip in the steady-state period.

Table 4. Characteristics of typical interstitial temperature trend line shapes, the related checks and possible actions during treatment evaluation.

Trend line shape	Characteristics	Checks and possible actions
Normal, stable	After 15-20 minutes the trend line settles to a steady-state at a temperature between 40-43°C.	-
Increasing towards the end	The trend line has a positive slope throughout the treatment.	Consider a higher start power or faster power build up.
Decline towards the end	The average interstitial temperature drops in the last 20 minutes.	Possibly limiting factors are handled with difficulty towards the end of treatment.
Maximum in the early stages	An initially fast rise is followed by a steady decline to or below the average temperature.	Consider a more gentle start of the treatment such that the temperature will not drop due to too early pain complaints.
Dip in the steady-state period	Dips in the holding state.	Dips often reflect severe limitations such as power off for several minutes, which may take more than 10 minutes to compensate for.
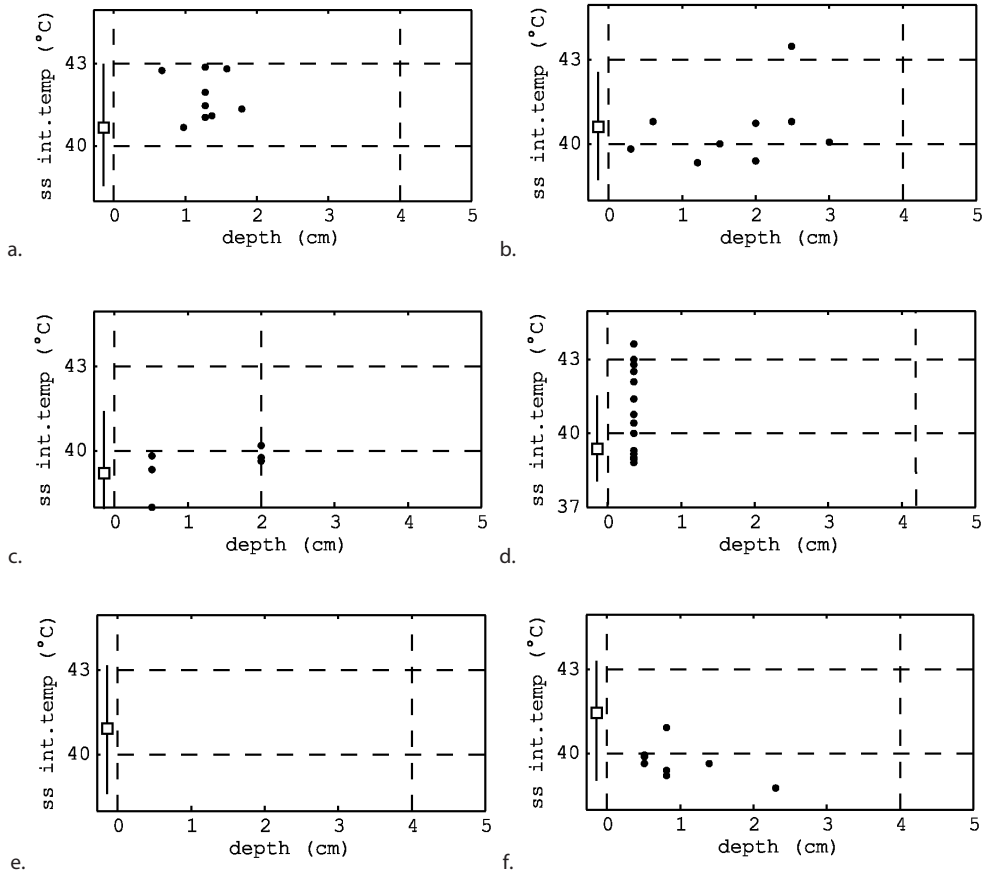
Figure 9. Examples of characteristic temperature-depth plots: (a) all temperatures therapeutic, (b) mix of therapeutic and subtherapeutic temperatures, (c) subtherapeutic temperatures, (d) available data only in the top layer with poor coverage at depth, (e) no interstitial data available and (f) relatively high surface and low interstitial temperatures indicating a too high waterbolus temperature.

Possible actions to optimize next treatments

Treatment evaluations aim at consistent or improved heating over the course of treatments. Apart from obvious cases, there is no rule-based translation of treatment characteristics into actions for improvement. The action points that roll out of the evaluation usually target:

–   Applicator set-up. The target volume may be covered by a different number of applicators and sometimes rearranging the array may be needed to avoid hot spots or to center an applicator directly above a region that is difficult to heat. The direction of the electric field may be changed by rotating the applicators. Different type applicators may be selected, preferably after a treatment planning case study [29].
–   Power build-up. The applicator power at start of treatment, the steps during the power increase and the target power in the steady state period may be redefined.
–   Waterbolus configuration. The waterbolus should follow the shape of the body and maintain contact with its surface. Adaptations of the waterbolus layer often aim at the prevention of air inclusions.
–   Waterbolus temperature. The guideline temperature is dropped if waterbolus steering is required to improve the temperature distribution.
–   Medication. Pain medication may be prescribed if pain complaints, restlessness or discomfort are not due to power-related high temperatures.
–   Application of treatment planning. Especially if there are doubts whether a target volume is able to be heated and thermometry is limited, treatment planning provides valuable additional information and may validate proposed changes in the treatment approach.

Discussion

Practical limitations: controllability and observability

In clinical practice, the ability to heat the whole target volume and to observe the temperatures often has its limitations. These two factors, controllability and observability, must be considered during treatment evaluation. A tissue-volume temperature is controllable if it is possible to heat it in a finite time by means of applicator power inputs and waterbolus temperature. Low power absorption values, high perfusion rates and power limiting hot spots may limit controllability. A tissue volume is observable if its temperature can be measured. Observability may be limited by the number of available probes or placement issues such as patient discomfort, anatomical constraints, and risk of infection. Note that degrees of controllability and observability may differ within the target volume. For example, both are good in a tissue section near a temperature probe placed centrally below an applicator, but both are poor at 4 cm depth where no interstitial probe can be placed.

In the clinic, it may not be possible to make sharp distinctions in the degree of controllability and observability. Therefore, we here focus on the four main cases, that are illustrated in Figure 10:

1. Good controllability, good observability – The ideal situation where we can heat the volume and observe it. If temperatures are too low, steering actions can directly improve the situation.
2. Good controllability, poor observability – In principle, tissue can be heated effectively if enough power is applied and the applicator set-up is appropriate. Patient feedback is important here, because it replaces measurements. We may conservatively increase applicator power as long as there are no pain complaints.
3. Poor controllability, good observability – where we know that we were not able to heat appropriately. To improve controllability, a different steering strategy or applicator set-up may be applied during the next treatment. The new approach can be evaluated because temperature data is available.
4. Poor controllability, poor observability – This is difficult as we cannot observe that achieving therapeutic temperatures is a problem. Treatment evaluation may end in pure speculation as measurement data is lacking. Below-average power input to the applicators may indicate suboptimal heating.
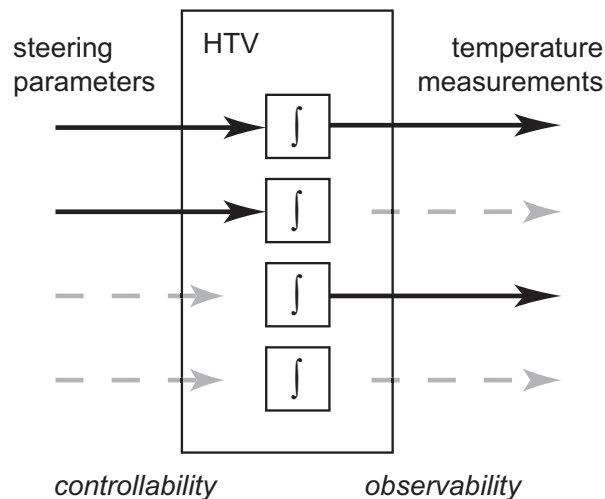
Figure 10. Schematic representation of the four main levels of controllability and observability in parts of the hyperthermia target volume (HTV). The blocks marked ∫ represent the tissue dynamics of a HTV subsection. From top to bottom: controllable and observable, controllable and poorly observable, poorly controllable and observable, poorly controllable and poorly observable.

It is tempting to focus on the available temperature data only and unintentionally apply that information also to poorly observable sections. For example, in an earlier study we found in our clinical data that limited observability of temperatures at depth led to too high waterbolus temperatures when compared to model output [27]. The evaluation sheet provides clues to take into account poor observability during treatment evaluations as it lists the number of measurement points below an applicator's footprint, prints not-a-number values if no data is available and the data point cloud in the temperature-depth plot clearly indicates coverage at depth.

Non-invasive thermometry greatly enhances observability. Magnetic resonance (MR) imaging is utilized to visualize 3D temperature distributions during deep heating [30-32]. For superficial hyperthermia MR imaging probably may not be an option, for economical and technical reasons. However, temperatures of the tissue top layer can be monitored by non-invasive radiometry [10,33]. The enhanced observability by non-invasive means also enables more advanced control [34-37].

Hyperthermia treatment planning (HTP) improves both observability and controllability, by showing the expected power distribution or temperature estimates inside the patient and its dependence on steering parameters, applicator set-up and anatomy. The potential of treatment planning in preparing superficial hyperthermia treatments was shown in [29]. Also during treatments, the HTP system may suggest steering actions, or show the effect of intended actions such as to reduce complaints [38]. The clinical merit of HTP optimized amplitude/phase settings in the heating of oesophageal cancer was evaluated by [39]. HTP-guided steering has been shown to be clinically feasible in deep hyperthermia [40].

Future directions

This paper reflects superficial hyperthermia treatment evaluation at Erasmus MC and although the basic idea can be transferred, the presented treatment evaluation sheet and methods may need adaptations in order to be appropriate for other centers and for other modes of application (e.g. thermal dose prescription, deep hyperthermia). For now, strict criteria for the judgement of treatment quality aspects are lacking. Systematic treatment evaluation however stimulates the exchange of personal opinions, the quantification of ideas and effects and eventually, the definition of more objective criteria for good quality hyperthermia treatments.

Besides the treatment sheet, other tools can facilitate treatment evaluations and the analysis of treatment efficacy. To make the course of a treatment fully transparent, the patient feedback, steering actions and measurement data can be visualized and preferably animated in one view, which offers play back functionality. HTP can play a major role in the evaluation of steering actions and what-if scenarios. Furthermore, the treatment data repository could be integrated into a database of clinical outcome for statistical analysis and data mining.

Quality assurance aspects

Currently, a human operator closes the control loop in virtually all hyperthermia clinics for reasons of safety and complexity of the steering task, combining patient feedback with measurements. Human control undeniably introduces a risk factor in terms of reproducibility between treatments and consistent performance. It might be one of the many factors underlying the large variability in response rates observed in for example reirradiation plus hyperthermia in recurrent breast cancer (21-95%, [20]). The presented treatment evaluation sheet and methods play a role in quality assurance in several ways. First, every patient is discussed before the next session in the multidisciplinary team. The sheet, which is projected on a screen during evaluation, allows a quick interpretation of the treatment data so that the team members who did not carry out the treatment can also fully participate in the discussion. The patient indirectly benefits from the common experience and knowledge of the team and the operators benefit from the peer review. The set of basic checks and the quantitative reference data provide a systematic framework for evaluation. Furthermore, the treatment sheets form a reference set for next treatments. The operator can always browse through them before of during treatments, to check and adjust the steering approach.

A final remark regarding quality assurance is that steering and treatment evaluation are not at all or only slightly addressed in the hyperthermia literature or in the published quality assurance guidelines [41-43]. We propose that the approach described here is merged with that of other clinics and subsequently the common denominator is added to the existing quality assurance guidelines.

Conclusion

A treatment summary sheet was developed for evaluation of superficial hyperthermia treatments. It allows a quick interpretation of a body of data, by graphic presentation of power and temperature trends, a temperature-depth plot, and basic statistics. The sheet, together with a set of basic checks and reference values, supports systematic treatment evaluations during weekly multidisciplinary patient discussions. This ultimately leads to a more consistent performance together with a fine tuned set-up and steering strategy for the individual patient.

References

[1] Overgaard J, Gonzalez Gonzalez D, Hulshof MCCM, Arcangeli G, Dahl O, Mella O, Bentzen SM. Randomised trial of hyperthermia as adjuvant to radiotherapy for recurrent or metastatic malignant melanoma. Lancet 1995;345:540-543.

[2] International Collaborative Hyperthermia Group: Vernon CC, Hand JW, Field SB, Machin D, Whaley JB, Van der Zee J, Van Putten WLJ, Van Rhoon GC, Van Dijk JDP, Gonzalez Gonzalez D, Liu F-F, Goodman P, Sherar M. Radiotherapy with or without hyperthermia in the treatment of superficial localized breast cancer - results from five randomised controlled trials. Int J Radiation Oncology Biol Phys 1996;35:731-744.

[3] Jones EL, Oleson JR, Prosnitz LR, Samulski TV, Vujaskovic Z, Yu D, Sanders LL, Dewhirst MW. Randomized trial of hyperthermia and radiation for superficial tumors. J Clin Oncol 2005;23:3079-3085.

[4] Rietveld PJM, Van Putten WLJ, Van der Zee J, Van Rhoon GC. Comparison of the clinical effectiveness of the 433 Mhz lucite cone applicator with that of a conventional waveguide applicator in applications of superficial hyperthermia. Int J Radiat Oncol Biol Phys 1999:43:681–687.

[5] Lee WM, Gelvich EA, Van der Baan P, Mazokhin VN, Van Rhoon GC. Assessment of the performance characteristics of a prototype 12-element capacitive contact flexible microstrip applicator (CFMA-12) for superficial hyperthermia. Int J Hyperthermia 2004;20:607–624.

[6] Diederich CJ, Stauffer PR. Pre-clinical evaluation of a microwave planar array applicator for superficial hyperthermia. Int J Hyperthermia 1993;9:227-246.

[7] Lee ER, Wilsey TR, Tarczy-Hornoch P, Kapp DS, Fessenden P, Lohrbach A, Prionas SD. Body conformable 915 MHz microstrip array applicators for large surface area hyperthermia. IEEE Trans Biomed Eng 1992;39:470–483.

[8] Samulski TV, Fessenden P, Lee ER, Kapp DS, Tanabe E, McEuen A. Spiral microstrip hyperthermia applicators: technical design and clinical performance. Int J Radiat Oncol Biol Phys 1990;18:233-42.

[9] Rossetto F, Stauffer PR. Theoretical characterization of dual concentric conductor microwave applicators for hyperthermia at 433 MHz. Int J Hyperthermia 2001;17:258-270.

[10] Jacobsen S, Stauffer PR, Neuman DG. Dual-mode antenna design for microwave heating and noninvasive thermometry of superficial tissue disease. IEEE Trans Biomed Eng 2000;47:1500–1509.

[11] Juang T, Stauffer PR, Neuman DG, Schlorff JL. Multilayer conformal applicator for microwave heating and brachytherapy treatment of superficial tissue disease. Int J Hyperthermia 2006;22:527-544.

[12] Johnson JE, Maccarini PF, Neuman D, Stauffer PR. Automatic temperature controller for multielement array hyperthermia systems. IEEE Trans Biomed Eng 2006;53:1006-1015.

[13] Arora D, Skliar M, Roemer RB. Model-predictive control of hyperthermia treatments. IEEE Trans Biomed Eng 2002;49:629-639.

[14] Zhou L, Fessenden P. Automation of temperature control for large-array microwave surface applicators. Int J Hyperthermia 1993;9:479-490.

[15] VanBaren P, Ebbini ES. Multipoint temperature control during hyperthermia treatments: theory and simulation. IEEE Trans Biomed Eng 1995;42:818-827.

[16] Potocki JK, Tharp HS. Reduced-order modeling for hyperthermia control. IEEE Trans Biomed Eng 1992;39:1265-1273.

[17] Cheng KS, Yuan Y, Li Z, Stauffer PR, Maccarini P, Joines WT, Dewhirst MW, Das SK. The performance of a reduced-order adaptive controller when used in multi-antenna hyperthermia treatments with nonlinear temperature-dependent perfusion. Phys Med Biol 2009;54:1979-1995.

[18] Kowalski ME, Jin J-M. A temperature-based feedback control system for electromagnetic phased-array hyperthermia: theory and simulation. Phys Med Biol 2003;48:633-651.

[19] Broekmeyer-Reurink MP, Rietveld PJM, Van Rhoon GC, Van der Zee J. Some practical notes on documentation of superficial hyperthermia treatment. Int J Hyperthermia 1992;8:401-406.

[20] van der Zee J, de Bruijne M, Mens JW, Ameziane A, Broekmeyer-Reurink MP, Drizdal T, Linthorst M, van Rhoon GC. Reirradiation combined with hyperthermia in breast cancer recurrences: overview of experience in Erasmus MC. Int J Hyperthermia 2010;26:638-648.

[21] Van der Zee J, Van Rhoon GC, Broekmeyer-Reurink MP, Reinhold HS. The use of implanted closed-tip catheters for the introduction of thermometry probes during local hyperthermia treatment series. Int J Hyperthermia 1987;3:337-345.

[22] Van Rhoon GC, Rietveld PJM, Van der Zee J. A 433 MHz Lucite Cone waveguide applicator for superficial hyperthermia. Int J Hyperthermia 1998;14:13-27.

[23] De Bruijne M, Samaras T, Chavannes N, Van Rhoon GC. Quantitative validation of the 3D SAR profile of hyperthermia applicators using the gamma method. Phys Med Biol 2007;52:3075-3088.

[24] Rietveld PJM, Lumori MLD, Van der Zee J, Van Rhoon GC. Quantitative evaluation of 2×2 arrays of Lucite cone applicators in flat layered phantoms using Gaussian beam predicted and thermographically measured SAR distributions. Phys Med Biol 1998;43:2207-2220.

[25] Bakker JF, Paulides MM, Westra AH, Schippers H, Van Rhoon GC. Design and test of a 434 MHz multi-channel amplifier system for targeted hyperthermia applicators. Int J Hyperthermia 2010;26:158-170.

[26] De Bruijne M, Samaras T, Bakker JF, van Rhoon GC. Effects of waterbolus size, shape and configuration on the SAR distribution pattern of the Lucite cone applicator. Int J Hyperthermia 2006;22:15–28.

[27] Van der Gaag ML, De Bruijne M, Samaras T, Van der Zee J, Van Rhoon GC. Development of a guideline for the water bolus temperature in superficial hyperthermia. Int J Hyperthermia 2006;22:637-656.

[28] [Erasmus MC guideline for superficial hyperthermia]. Erasmus MC – Daniel den Hoed Cancer Center, 2004. Dutch. (EMC-DDHCC internal report).

[29] De Bruijne M, Wielheesen D, Van der Zee J, Chavannes N, Van Rhoon GC. Benefits of superficial hyperthermia treatment planning: Five case studies. Int J Hyperthermia 2007;23:417-429.

[30] Gellermann J, Wlodarczyk W, Ganter H, Nadobny J, Fahling H, Seebass M, Felix R, Wust P. A practical approach to thermography in a hyperthermia/magnetic resonance hybrid system: validation in a heterogeneous phantom. Int J Radiat Oncol Biol Phys 2005;61:267–277.

[31] Gellerman J, Hildebrandt B, Issels R, Ganter H, Wlodarczyk W, Budach V, Felix R, Tunn P-U, Reichardt P, Wust P. Noninvasive magnetic resonance thermography of soft tissue sarcomas during regional hyperthermia - correlation with response and direct thermometry. Cancer 2006;107:1373–1382.

[32] Van Rhoon GC, Wust P. Introduction: Non-invasive thermometry for thermotherapy. Int J Hyperthermia 2005;21;489-495.

[33] Dubois L, Pribetich J, Fabre JJ, Chive M, Moschetto Y. Non-invasive microwave multifrequency radiometry used in microwave hyperthermia for bidimensional reconstruction of temperature patterns. Int J Hyperthermia 1993;9:415-431.

[34] Hutchinson E, Dahleh M, Hynynen K. The feasibility of MRI feedback control for intracavitary phased array hyperthermia treatments. Int J Hyperthermia 1998;14:39-56.

[35] Stakhursky VL, Arabe O, Cheng K-S, MacFall J, Maccarini P, Craciunescu O, Dewhirst M, Stauffer P, Das SK. Real-time MRI-guided hyperthermia treatment using a fast adaptive algorithm. Phys Med Biol 2009;54:2131–2145.

[36] Weihrauch M, Wust P, Weiser M, Nadobny J, Eisenhardt S, Budach V, Gellermann J. Adaptation of antenna profiles for control of MR guided hyperthermia (HT) in a hybrid MR-HT system. Med Phys 2007;34:4717-4725.

[37] Cheng KS, Dewhirst MW, Stauffer PR, Das S. Effective learning strategies for real-time image-guided adaptive control of multiple-source hyperthermia applicators. Med Phys 2010;37:1285-1297.

[38] Complaint-adaptive power density optimization as a tool for HTP-guided steering in deep hyperthermia treatment of pelvic tumors. Canters RAM, Franckena M, Van der Zee J, Van Rhoon GC. Phys Med Biol 2008;53:6799–6820.

[39] Kok HP, van Haaren PM, van de Kamer JB, Zum Vörde Sive Vörding PJ, Wiersma J, Hulshof MC, Geijsen ED, van Lanschot JJ, Crezee J. Prospective treatment planning to improve locoregional hyperthermia for oesophageal cancer. Int J Hyperthermia 2006;22:375-389.

[40] Franckena M, Canters R, Termorshuizen F, Van der Zee J, Van Rhoon G. Clinical implementation of hyperthermia treatment planning guided steering: A cross over trial to assess its current contribution to treatment quality. Int J Hyperthermia 2010;26:145-157.

[41] ESHO Quality Assurance Guidelines for Regional Hyperthermia. Lagendijk JJW, Van Rhoon GC, Hornsleth SN, Wust P, De Leeuw ACC, Schneider CJ, Van Dijk JDP, Van der Zee J, Van Heek-Romanowski R, Rahman SA, Gromoll C. Int J Hyperthermia 1998;14:125-133.

[42] RTOG quality assurance guidelines for clinical trials using hyperthermia. Dewhirst MW, Phillips TL, Samulski TV, Stauffer P, Shrivastava P, Paliwal B, Pajak T, Gillim M, Sapozink M, Myerson R, Waterman FM, Sapareto SA, Corry P, Cetas TC, Leeper DB, Fessenden P, Kapp D, Oleson JR, Emami B. Int J Radiat Oncol Biol Phys 1990;18:1249-1259.

[43] Hand JW, Lagendijk JJ, Bach Andersen J, Bolomey JC. Quality assurance guidelines for ESHO protocols. Int J Hyperthermia 1989;5:421-428.

7

Quantitative validation of the 3D SAR profile of hyperthermia applicators using the gamma method

Abstract

For quality assurance of hyperthermia treatment planning systems, quantitative validation of the electromagnetic model of an applicator is essential. The objective of this study was to validate an FDTD model implementation of the Lucite cone applicator (LCA) for superficial hyperthermia. The validation involved (*i*) the assessment of the match between the predicted and measured 3D SAR distribution, and (*ii*) assessment of the ratio between model power and real-world power. The 3D SAR distribution of seven LCAs was scanned in a phantom bath using the DASY4 dosimetric measurement system. The same set-up was modelled in SEMCAD X. The match between the predicted and the measured SAR distribution was quantified with the gamma method, which combines distance-to-agreement and dose-difference criteria. Good quantitative agreement was observed: more than 95% of the measurement points met the acceptance criteria 2 mm / 2% for all applicators. The ratio between measured and predicted power absorption ranged from 0.75 to 0.92 (mean 0.85). This study shows that quantitative validation of hyperthermia applicator models is feasible and is worth to be considered as a part of hyperthermia quality assurance procedures.

Introduction

Hyperthermia (HT) treatment planning systems have a wide range of application: they are used to optimize the treatment strategy to individual patients, to characterize hyperthermia applicator systems, to develop quality assurance guidelines, and to design new antenna systems. Treatment planning in hyperthermia is a two step process that involves the computation of 3D specific absorption rate (SAR) and temperature distributions by computer models. Advances in computer technology and development of sophisticated 3D electromagnetic and thermal models have made integration of treatment planning in clinical routine feasible.

The goal of HT treatment planning is to conform the spatial electromagnetic power deposition to the clinical target volume (selective heating), while at the same time minimizing treatment limiting hot spots in normal tissue. The application of treatment planning tools in the clinic has two major advantages. Firstly, the effects of a steering action or an adaptation of the heating technique can be visualised before it is actually applied to the patient. Secondly, as the number of temperature measurement points during clinical treatments is usually very limited, a potential benefit of model predictions is that they provide additional insight in the 3D temperature- and power absorption patterns in a patient.

A safe and effective integration of treatment planning in clinical routine requires that the clinicians know to what extent the predictions reflect reality. Therefore, quantitative validation of the SAR pattern predicted by an electromagnetic (EM) model of a hyperthermia applicator is an essential step in the development of a hyperthermia treatment planning system. High quality measurements that widely encompass the 3D applicator target volume are a prerequisite for model validation. Two aspects are especially of interest: the quality of the match between the measured and the predicted SAR distribution, and the relation between the model power and the real-world power. Further, quantitative validation involves the assessment of model performance using clear criteria, without human bias and interpretation.

The testing of EM models can be performed by several methods: (*i*) verification of model output with known analytical solutions, (*ii*) comparison between models, and (*iii*) validation with measurements, which is considered the ultimate test [5]. The number of published validation reports which compare measured SAR or E-field data with the output of electromagnetic models of hyperthermia applicators is fairly limited. Wust *et al.* [37] scanned the amplitudes and phases along two main directions of the SIGMA–Eye applicator, and compared these to finite element (FE) and finite-difference time-domain (FDTD) predictions. Wiersma and van Dijk [33] validated Conjugate Gradient FFT model predictions against amplitude and phase scans in two planes of the AMC-4 waveguide system. Samaras *et al.* [24] tested the ability of FDTD to predict SAR distributions for the conventional waveguide applicator, the Lucite applicator and the Lucite cone applicator, by

comparing the predicted distributions to infrared measurements of a transversal cross-section. Jacobsen *et al.* [15] verified FDTD results against E-field scans, and expressed the overall fit with a figure of merit. Wu *et al.* [34] compared E-field measurements and FE predictions for a phased array designed for hyperthermia treatments in the intact breast. Recently, Gellermann *et al.* [10] compared FDTD calculations with 3D SAR patterns derived from MR-thermographic measurements. These validations are subject to some limitations. Firstly, in all but the last study, the measurements cover only a subset of the 3D applicator target volume, i.e. 2D cross-sections or 1D tracks. Secondly, in all studies relative distributions are compared, and consequently the relation between model power and real-world power was not included in the model evaluation. Finally, in nearly all publications the performance of the model is expressed subjectively.

In this study, a quantitative validation was performed for the FDTD model of the Lucite cone applicator for superficial hyperthermia that has been used for the development of quality assurance guidelines [6,29] and for treatment planning. Using dosimetric nearfield measurement techniques, the 3D SAR distribution was measured of all Lucite cone applicators that are currently in use in our clinic. The gamma method [19,20] was used to objectively evaluate the match between measurement and model prediction. This method uses criteria for distance-to-agreement and dose-difference, so that validation results can be compared and interpreted. This validation approach accounts for the whole 3D applicator target volume, addresses the relation between model power and real-world power, and expresses the match between measurements and model prediction using clear, quantitative criteria.

Materials and Methods

Lucite cone applicator

The Lucite cone applicator (LCA) [31] is a 433 MHz water-filled horn applicator designed for external heating of superficial malignancies (superficial hyperthermia). The applicator target volume of a single LCA is $10\times10\times4$ cm³. LCAs can be combined in array configurations to effectively cover the whole radiotherapy field (from 10×10 to 20×30 cm²). There are seven LCAs available for treatments in our clinic.
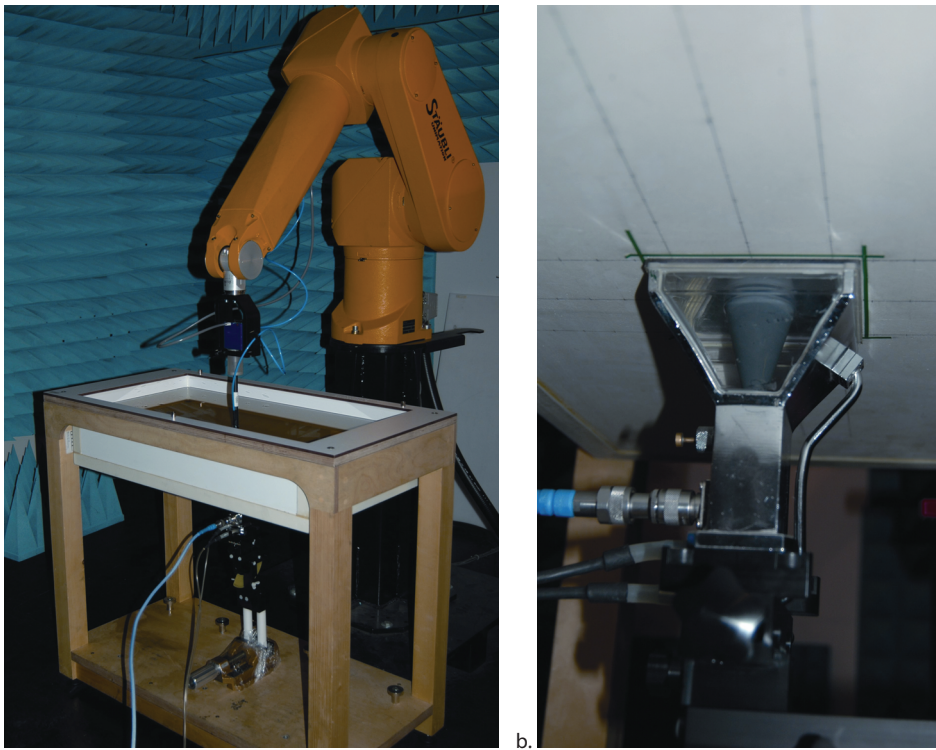
SAR measurements

The 3D SAR distribution of an LCA placed centrally below a flat phantom was measured. Figure 1 shows an overview of the measurement set-up. The phantom consisted of a rectangular phantom bath (Flat Phantom 4.4, SPEAG, Zürich, Switzerland) filled with HSL450 tissue simulating liquid (SPEAG, Zürich, Switzerland), which is a mixture of de-ionized water, sugar, salt, cellulose, and bactericide [22]. The dielectric properties of the HSL450 liquid were measured before the experiment, and are listed in Table 1. The conductivity of this phantom liquid falls well within the range reported for muscle tissue in

the literature, and its permittivity is comparable to that of muscle [8,17]. The inner dimensions of the bath were 700×600×170 mm³ and its shell thickness was 6.0 ± 0.2 mm. The liquid level was 140 mm during all experiments, which is > 5 times the half power penetration depth of the phantom liquid ($\delta_{\frac{1}{2}}$ = 0.024 m).

Table 1. Relative permittivity (ε_r) , effective conductivity (σ), and density (ρ) of the materials (f = 433 MHz).

Material	ε_r	σ (S/m)	ρ (kg/m³)
HSL450	45.9	0.91	1000
Phantom bath	3.7	0.04	
Lucite	2.59	0.003	
PVC	2.2	0.004	
De-ionized water	80.0	3.9×10^{-2}	

Figure 1. Measurement set-up. (a) The DASY4 system, consisting of a phantom shell filled with tissue-simulating liquid, and a robot arm holding the E-field probe. (b) Close-up of the LCA clamped to the bottom of the phantom shell.

The E-field was scanned with the DASY4 dosimetric assessment system (SPEAG, Zürich, Switzerland) [25], which is depicted in Figure 1. It consists of a miniature isotropic

E-field probe, a robot arm, a data acquisition unit and a computer running the data acquisition and control software. The probe (type ET3DV6; tip diameter 6.8 mm, dynamic range 5 W/kg – 100 mW/kg, linearity better than ±0.2 dB, deviation of axial isotropy < ±0.05 dB, deviation of spherical isotropy < ±0.20 dB) [23] was calibrated in the phantom liquid. The positioning accuracy of the probe was 0.1 mm. The measurement volume (*M*, dimensions 140×160×50 mm³) was chosen such that it widely encompassed the target volume of the LCA, and that the normalized SAR at 10 mm depth was less than 10% outside the measurement area. As shown in Figure 2, the measurement grid was centrally aligned above the LCA aperture. It consisted of 15×17×6 points (total 1530), with a sampling interval of 10 mm in all directions. The first horizontal scan plane was 4 mm from the inner phantom shell. The total measurement time required to obtain a 3D SAR scan of one antenna was about 75 minutes (scan time ~2.7 s per measurement point). One SAR scan was performed for every LCA.

Before scanning the SAR, the LCA was tuned such that the forward power was ≥ 18 dB over the reflected power. To feed the LCA with a known power level of 1.0 Watt, the procedure described in IEEE Standard 1528-2003 [3] was followed. This low power input to the antenna prevents heating of the phantom liquid. Before the start of the experiments, it was checked that the measurement system met the validated target reference specifications issued by the manufacturer (overall accuracy within 10%), by measuring the SAR profile from a calibration dipole antenna (D450V2; SPEAG, Zürich, Switzerland).
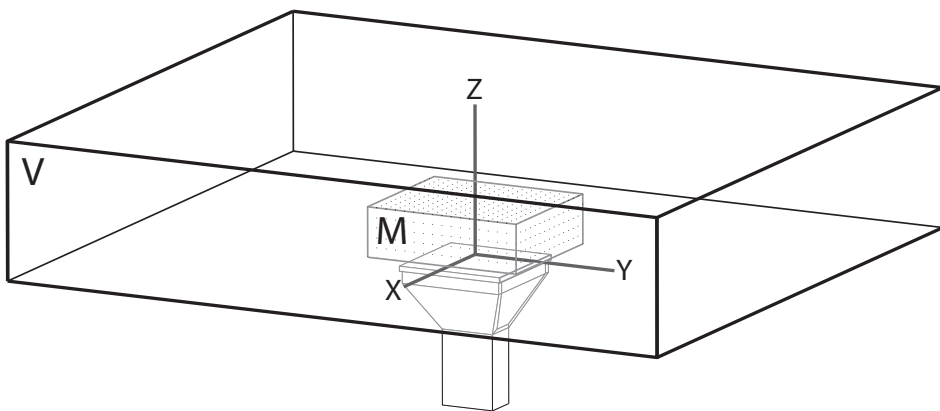
Figure 2. Schematic representation of the measurement set-up. The large block (black lines, *V*) is the phantom liquid volume inside the phantom bath. The smaller rectangular volume (grey lines, *M*) indicates the measurement volume; the dots are the scan points. For ease of reference, the position of the LCA below the phantom bath is indicated.

FDTD computations

The SAR distribution was simulated using the finite-difference time-domain (FDTD) method, implemented in the SEMCAD X simulation software [28]. The phantom and applicator were discretized in a non-uniform rectilinear grid (145×166×122 voxels), allowing local refinement and placement of gridlines at the boundary of objects. To minimize effects of staircasing, voxel dimensions were limited to less than 2 mm within the LCA volume. A minimum mesh step size of 1 mm was used near the source pin of the LCA. Voxel dimensions in the phantom varied between 1-2 mm ($\lambda/50$) below the footprint of the applicator. Outside the applicator target volume, the gridstep gradually increased to 6.8 mm ($\lambda/15$) in the phantom and surroundings. An edge source element bridging the gap between the source pin and the waveguide wall performed the excitation of the applicator. The predicted SAR was normalized to 1.0 W source power. The parameters of the materials are given in Table 1. A perfectly matched layer absorbing boundary condition [4] with a layer thickness of six cells terminated the simulation domain.

Relation between model SAR and real-world SAR

Simplification of the finer details of the coaxial feed and connector plug reduces model size and simulation time, but hinders a direct comparison of measured to predicted SAR. The relation between model SAR and real-world SAR was assessed by calculating the ratio of the absorbed power in the measurement domain $P_{\mathrm{abs}}^{\mathrm{M}}$ for both distributions. This ratio R_a for applicator a (a = 1 .. 7) is given by:

$$R_a = \frac{P_{\mathrm{abs,meas}_a}^{\mathrm{M}}}{P_{\mathrm{abs,model}}^{\mathrm{M}}} \tag{1}$$

For each LCA and for the model output, the absorbed power $P_{\mathrm{abs}}^{\mathrm{M}}$ was calculated by interpolating the SAR distributions to a uniformly spaced grid points of 1 mm³ resolution using cubic spline interpolation, and subsequent integration of SAR over the measurement volume:

$$P_{\mathrm{abs}}^{\mathrm{M}} = \sum_{M} SAR_i \cdot \rho \cdot \Delta v \tag{2}$$

where M is the measurement volume (140×160×50mm³), SAR_i is the SAR value in grid element i, Δv is the volume of that element (1mm³ by definition), and ρ is the density of the phantom liquid.

Applicator efficiency

The efficiency of the applicator is the ratio between the power absorbed in the whole phantom and the net power delivered at the applicator connector plug. In all cases the

power delivered at the plug ($P_{connector}$) was 1.0 W. To estimate the efficiency of the applicator, the model data was used to translate the absorbed power in the measurement domain (M) to the absorbed power in the whole domain (V) (Figure 2). The predicted power absorption in the whole phantom, $P_{\mathrm{abs,\,model}}^{\mathrm{V}}$, was computed by integrating SAR over the whole phantom volume (700×600×140 mm³) using the method described in the previous section. The applicator efficiencies η_a are obtained by multiplying this value with the ratios R_a:

$$\eta_a = \frac{P_{\mathrm{abs,model}}^{\mathrm{V}}}{P_{\mathrm{abs,model}}^{\mathrm{M}}} \cdot \frac{P_{\mathrm{abs,meas}_a}^{\mathrm{M}}}{P_{\mathrm{connector}}} = P_{\mathrm{abs,model}}^{\mathrm{V}} \cdot R_a \tag{3}$$

Gamma method

In this study, the gamma method is used to quantify the match between the 3D measured and calculated SAR distributions. This method has been applied extensively for explicit verification of radiotherapy plans [1,7,11,20,21,30,32]. The gamma method performs a dose distribution comparison in both dose and spatial domains: it combines distance-to-agreement (DTA) and dose-difference (DD) analyses, and requires a pass-fail criterion value for both DTA and DD. The γ distribution indicates the magnitude of passing or failure of these criteria: γ ≤ 1 in regions where the criteria are met, while γ > 1 in regions that fail the criteria. Details about the gamma method and its development can be found in Low and Dempsey [19] and Low *et al.* [20].

A γ value is calculated independently for each point in the measurement distribution. In this analysis the measurement dataset SAR_{meas} is the benchmark, and the model prediction SAR_{model} is the evaluated distribution. As a first step, the spatial distance r between a measurement point $\vec{r}_{\mathrm{meas},i}$ and its surrounding points in the model distribution $\vec{r}_{\mathrm{model}}$ is calculated:

$$r\left(\vec{r}_{\mathrm{model}}, \vec{r}_{\mathrm{meas},i}\right) = \left|\vec{r}_{\mathrm{meas},i} - \vec{r}_{\mathrm{model}}\right| \tag{4}$$

In addition, the difference between the measured SAR at position $\vec{r}_{\mathrm{meas},i}$, and the scaled model SAR in its surroundings is assessed:

$$\delta\left(\vec{r}_{\mathrm{model}}, \vec{r}_{\mathrm{meas},i}\right) = SAR_{meas,a}\left(\vec{r}_{\mathrm{meas},i}\right) - R_a \cdot SAR_{\mathrm{model}}\left(\vec{r}_{\mathrm{model}}\right) \tag{5}$$

where R_a is the power absorption ratio of the applicator at hand, which compensates for differences in efficiency between the model implementation of the LCA and the real-world applicator (see above).

Next, the generalized Γ function relates these distances and dose differences to the acceptance criteria:

$$\Gamma\left(\vec{r}_{\text{model}}, \vec{r}_{\text{meas}, i}\right) = \sqrt{\frac{r^2\left(\vec{r}_{\text{model}}, \vec{r}_{\text{meas}, i}\right)}{\Delta d^2} + \frac{\delta^2\left(\vec{r}_{\text{model}}, \vec{r}_{\text{meas}, i}\right)}{\Delta D^2}} \tag{6}$$

with Δd the acceptance criterion for DTA, and ΔD the criterion for DD .

Finally, the γ value at point $\vec{r}_{\text{meas}, i}$ is the minimum of the generalized Γ function:

$$\gamma\left(\vec{r}_{\text{meas}, i}\right) = \min\left\{\Gamma\left(\vec{r}_{\text{model}}, \vec{r}_{\text{meas}, i}\right)\right\} \forall \vec{r}_{\text{model}} \tag{7}$$

The model distribution was resampled on a finer grid using cubic spline interpolation, to prevent artefacts in the γ distribution due to grid steps that are too coarse relative to the DTA criterion value. The interpolation grid was centrally aligned to the evaluated measurement point, and extended 2·Δd in all directions. We used an interpolation grid step of Δd/6, because the effect of further refinement on the γ distribution was negligible, see Figure 3. This value is in line with the recommendation by Low *et al.* [19] to use a grid refinement of Δd/3 or finer in order to prevent artefacts in γ distributions.
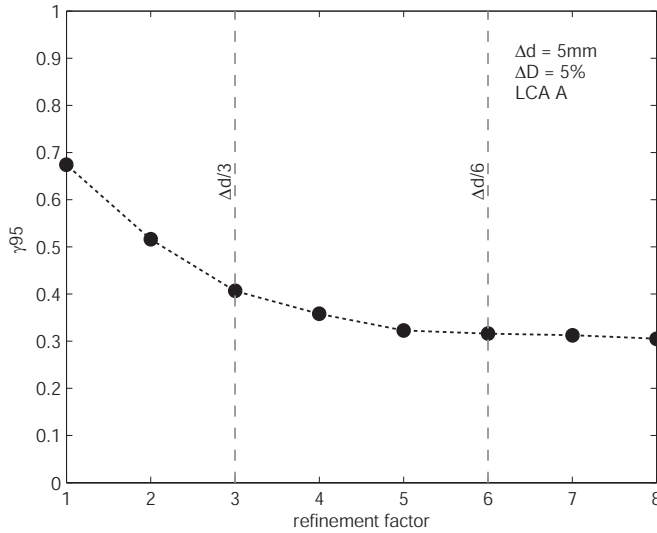
Figure 3. Illustration of the influence of model grid refinement on gamma evaluation: the 95th percentile of the γ distribution (γ95) stabilizes at a interpolation grid step of about Δd/6, indicating that at that level of refinement artefacts due to a coarse model distribution no longer persist. Δd/3 indicates the minimum refinement proposed by Low *et al.* [19]; Δd/6 indicates the refinement level applied in this study.

Because the gamma method has not been applied for the validation of hyperthermia applicator models before, DTA criterion values of 1 to 10 mm (step size 1 mm), and DD criterion values of 1 to 10% (step size 1%) were tested for each LCA. DD criterion values expressed in percent relate to the maximum value of the measured SAR distribution, and it

was verified that the maxima were no outliers. For comparison, acceptance criteria in the order of 3 mm / 3% are commonly considered feasible in radiotherapy [7,11,20,21,30,32].

The overall match between measurement and model was expressed with γ95, the 95th percentile of the γ distribution. The match was considered good given the selected tolerances, if at least 95% of the measurement points met the acceptance criteria, that is γ95 < 1. For evaluation of the match between the model distribution and those measured for all individual LCAs, cumulative histograms of the γ distributions were plotted.

Results

Table 2 shows the measured absorbed power for all applicators, and the predicted absorbed power in the measurement volume. The power absorbed in the measurement volume differed per applicator ($P_{abs,meas}^{M} = 232 - 285\,\text{mW}$) and was lower than predicted by the FDTD model ($P_{abs,model}^{M} = 310\,\text{mW}$). This resulted in power absorption ratio's ranging from $R_a = 0.75 - 0.92$ (mean 0.85). In the model prediction, the absorbed power in the *whole* phantom was $P_{abs,model}^{V} = 468\,\text{mW}$, which is 151% of the absorbed power in the measurement volume. This implies that the efficiency of the LCAs falls within the range of $\eta_a = 35 - 43\%$ (mean 40%).

The contour plots of the γ95 value for a wide range of DTA and DD criterion values are shown in Figure 4 for all applicators. From the plots it is clear that acceptance criteria 2mm / 2%, and less stringent criteria, were met (γ95 < 1) by all applicators. The cumulative histograms of the γ distributions for these acceptance criteria are shown in Figure 5. From the histograms, and from the γ95 contour plots it follows that two applicators (LCA 4 and LCA 6) limited the overall performance of the model, as they did not pass the 1mm / 1 to 4%, and 2mm / 1% tests. One applicator (LCA 1) matched the model exceptionally well: it met all tested acceptance criteria, except 1mm / 1%.

Table 2. Absorbed power in the measurement domain ($P_{\mathrm{abs}}^{\mathrm{M}}$) for all applicators, and for the FDTD model. The resulting power absorption ratio's ($R_a = P_{\mathrm{abs,meas}_a}^{\mathrm{M}} / P_{\mathrm{abs,model}}^{\mathrm{M}}$), and the efficiencies (η) are given as well.

Item	$P_{\mathrm{abs}}^{\mathrm{M}}$ (mW)	R_a (-)	η (-)
LCA 1	267	0.86	0.40
LCA 2	271	0.87	0.41
LCA 3	232	0.75	0.35
LCA 4	285	0.92	0.43
LCA 5	282	0.91	0.43
LCA 6	249	0.80	0.38
LCA 7	264	0.85	0.40
FDTD model	310	-	0.47
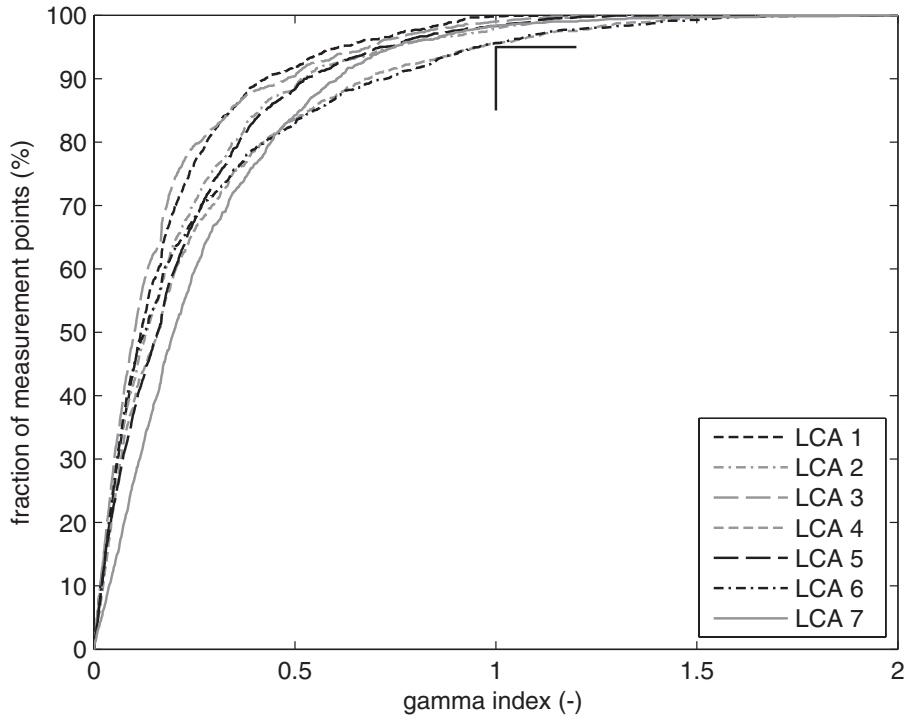
Figure 5. Cumulative histograms of the γ distributions of all applicators, for acceptance criteria DTA = 2mm / DD = 2%. None of the histograms crosses the angular shape (γ95 < 1), indicating that all LCAs meet these criteria.
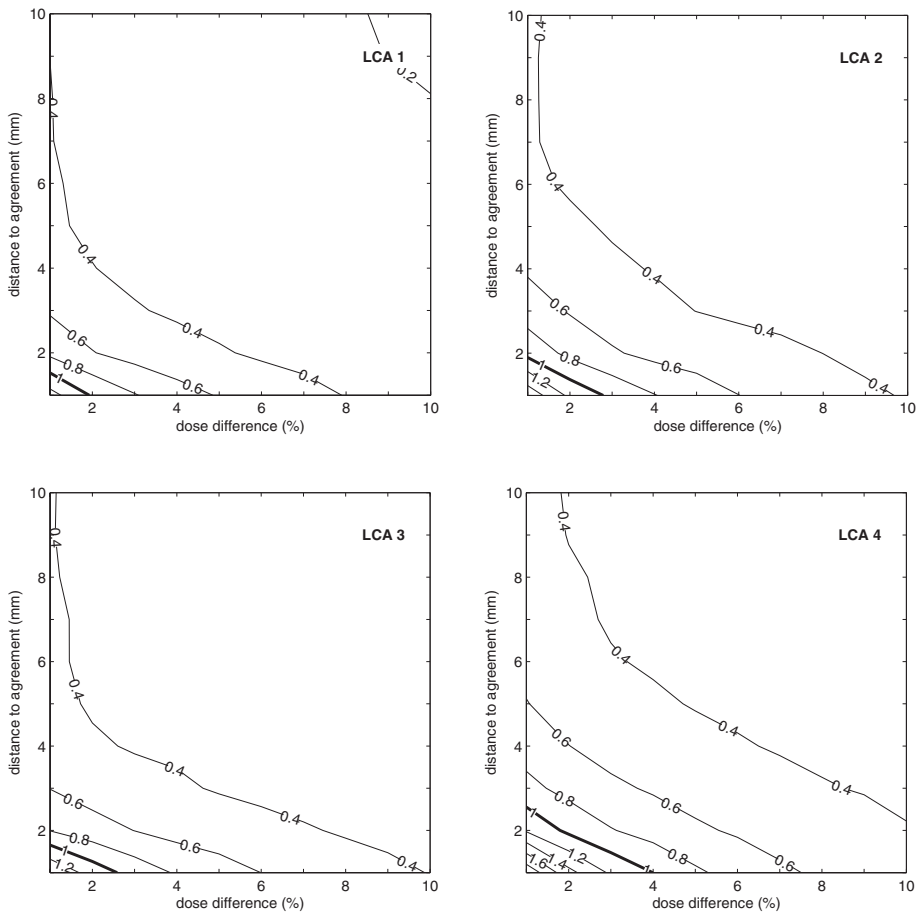
Figure 4. Contour plots of γ95 as a function of DTA and DD criteria, for applicators 1-4. The bold line is the γ95 = 1 contour; in the area where γ95 < 1, the acceptance criteria are met.
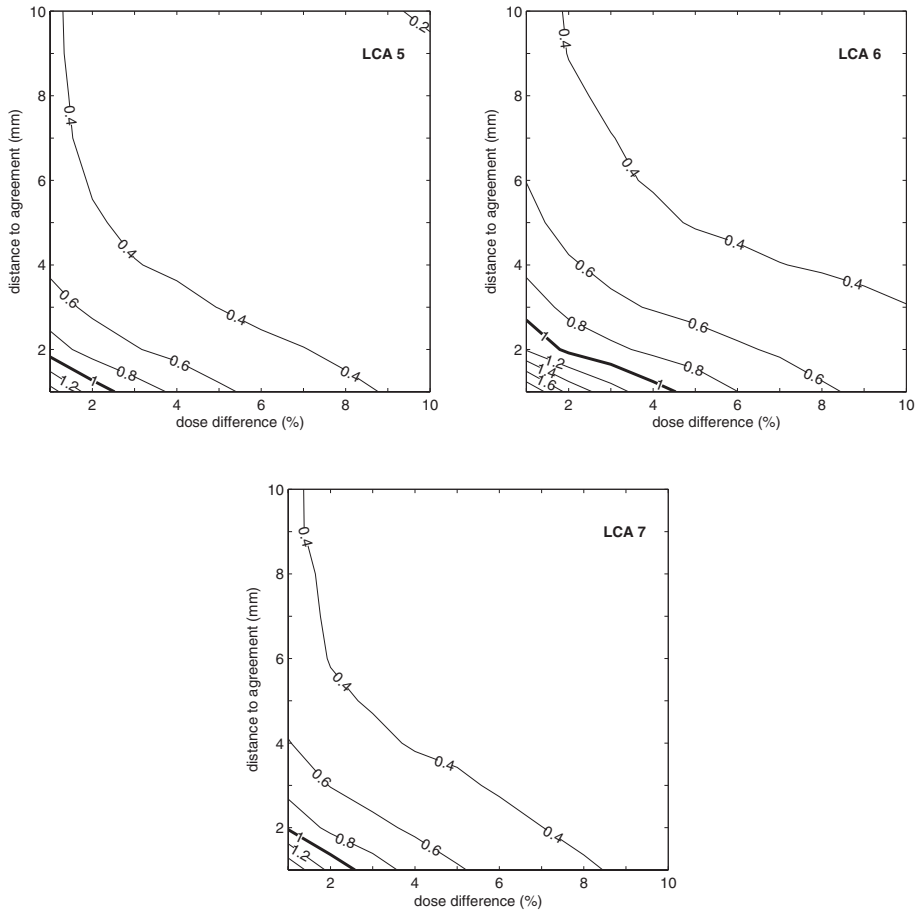
Figure 4. (*continued*) Contour plots of γ95 as a function of DTA and DD criteria, for applicators 5-7. The bold line is the γ95 = 1 contour; in the area where γ95 < 1, the acceptance criteria are met.

Discussion

This study applies the gamma method as a tool for quality assurance in hyperthermia. With the gamma method, the performance of an EM antenna model can be judged objectively against clear criteria, and validation efforts by different institutes become comparable. The current results show that acceptance criteria 2 mm / 2% are feasible, when state-of-the-art measurement techniques and refined FDTD models are used. General criteria for validation of predicted SAR and E-field distributions using the gamma method can be assessed as soon as quantitative validations of other EM models and of other hyperthermia applicators are executed.

Error sources for FDTD predictions usually relate to an imperfect representation of an object's geometry in the rectilinear grid, and limitations inherent to the numerical method (e.g. phase distortion, domain truncation and source modelling). Especially the simplified representation of the source (the omission of the C female receptacle connector and tuning pin), and the staircased representation of the flared horn are of interest for the FDTD model of the LCA. Given these potential sources of error, the predicted SAR distributions matched the measurements remarkably well ($\gamma95 < 1$ for acceptance criteria 2 mm / 2%, see Figure 4). However a higher efficiency was predicted by the model (model efficiency 0.47 vs. mean measured efficiency 0.40, see Table 2), which may relate to ohmic losses at the metallic surface of the LCA waveguide and source pin, while in FDTD perfect electric conductors (PEC) were assumed. Two additional simulations were performed to investigate the effect of the properties of metal, and of extending the staircased implementation to a computationally more expensive conformal model. Firstly, these revealed that implementing the metal structures with high-conducting media instead of PEC lowered the predicted efficiency by only 1%, see Table 3. Secondly, simulating the set-up using conformal FDTD did not lower the predicted efficiency (Table 3). Therefore, we would rather attribute the higher predicted SAR to the simplification of the source in the model, and to the use of a coaxial N/C adapter during the measurements. Experimental work has shown that the N/C adapter introduces a power loss of up to 0.2 dB (5%). Knowledge of the applicator-specific ratio of measured and predicted SAR (R_a) is needed for quantitative SAR planning, where real-world power is translated to model power and vice versa, e.g. when treatments are replayed in a model, and for thermal modelling based on a realistic heat balance.

The efficiency of the applicators could be calculated based on the SAR scans, because SAR was measured with a calibrated E-field probe, in a liquid of known dielectric properties and at an input power level where thermal effects can be neglected. The efficiency of the LCAs determined in this research (mean 40%, range 35–43%), was somewhat lower than the 50 ± 8% (mean ± 1 std) efficiency measured calorimetrically by van Rhoon *et al.* [31] for a prototype LCA. The current results show that for applicators of the same type and design, the efficiency varied per applicator, the maximum difference being 8% (Table 2). Although the efficiency differences are within the overall accuracy of the measurement system, they

can be attributed to the applicators themselves. As they were made by the hand, piece by piece, and have a different history of use and maintenance, their effective output may be slightly different. Although the efficiencies were measured for one specific load case, they can serve as an estimate of the applicator's efficiency in the clinic.

Table 3. Overview of power loss in the simulation domain per component, for different model implementations: the original (staircased) model, the original model implementing conducting media instead of PEC for metal structures, and a conformal FDTD implementation.

Solid	Power loss (W) per 1 W source power		
	Original model	Non-PEC*	Conformal FDTD
Phantom			
liquid	0.47	0.46	0.49
shell	0.026	0.026	0.026
LCA			
De-ionized water	0.38	0.39	0.38
Lucite cover	0.027	0.026	0.027
PVC cone	2.5×10^{-3}	2.5×10^{-3}	2.6×10^{-3}
Lucite window	4.4×10^{-4}	4.6×10^{-4}	4.6×10^{-4}
Lucite window	4.4×10^{-4}	4.6×10^{-4}	4.6×10^{-4}
metal housing	-	3.1×10^{-5}	-
source pin	-	1.4×10^{-5}	-
Total	0.91	0.91	0.93

*) Implements $\sigma = 14.5$ MS/m for metal (similar to brass).

The flat phantom shell provides a basic shape for the validation of an HT applicator model, which was the primary aim of this study. For more exhaustive performance tests of applicators and HT treatment planning models, anthropomorphic and/or heterogeneous phantoms should be included. For example, different superficial hyperthermia applicators can be tested on a mould of a mastectomy chest wall filled with a phantom liquid. Moreover, the site-specific performance of an (array of) applicators can be assessed when several target areas are defined on such a mould. This may facilitate the selection of the appropriate applicator for a specific site, which is conventionally based on practical experience [14]. Also, in deep hyperthermia, the steering capabilities of phased arrays can be tested in an anthropomorphic torso phantom. The used scanning system is capable of measuring SAR in phantoms of arbitrary shape, and under oblique angles, although for large set-ups an extended probe is needed. Several "man like" phantoms have been proposed over the years for comparative tests and quality assurance. Examples are the CDRH phantom [2], the elliptical standard phantom with fat-equivalent walls [35], and the elliptic phantom with skeleton insert [9]. Development of a set of highly standardized anthropomorphic phantoms, including a CAD dataset for manufacturing and model implementation, (e.g. analogous to the Specific Anthropomorphic Mannequin (SAM) head phantom used in compliance testing of wireless devices [3]), would allow pertinent and reproducible assessment of applicator performance, and provide excellent datasets for validation of treatment planning models in clinically relevant configurations.

Application of the gamma method is not limited to validation of SAR models of applicators for superficial hyperthermia, as it can be used to compare distributions of any origin and dimensionality, and defined on any mesh. In the light of further professionalization of hyperthermia equipment, normalization of hyperthermia quality, and integration of treatment planning in clinical practice, potential other applications of this method are:

– *Phase and amplitude validation of array elements.* To validate a model of a phased array, two separate γ evaluations (one for the phases and one for the amplitudes of the E-field) may be performed for each array element. Alternatively, but less thorough, a single γ evaluation may validate the interference pattern (superimposed E-fields) of multiple array elements.
– *Monitoring of the stability of the antenna profile.* Changes of the antenna profile can easily be identified and quantified with the gamma method, by comparing the 3D SAR profile of an antenna measured just after fabrication with profiles measured after major revisions and repairs, and at regular intervals.
– *Model verifications.* Model-to-model comparisons, and expression of model quality when comparing to standard test cases (e.g. analytical solutions). Also it provides a quantitative method to assess differences resulting from basic and detailed tissue segmentations.
– *Validation of thermal models used in hyperthermia treatment planning.* Like SAR distributions, the match between measured and predicted temperature distributions can be quantified with the gamma method.

General adoption of quantitative 3D validation of applicator models may be limited by the fact that in general hyperthermia centres are not equipped to scan absolute SAR levels in 3D. Most measurement facilities readily available at HT centres were developed for the slightly less demanding purpose of characterisation of antenna patterns, comparisons between applicators, and qualitative comparisons with model output (e.g. IR thermography [12], LED matrix [26], lamp phantom [35], Schottky diode sheet [18], and scanning E-field probes [13,16,27,36]). However, high quality scans can be obtained from third party institutes. Ultimately, the manufacturer of a HT applicator could decide to supply a high-quality SAR or E-field scan with the equipment, and include regular scans in a service contract. This will enable a clear specification of the system's performance, and provide a dataset for the validation of a treatment planning model.

Conclusion

This paper introduced the gamma method for quantitative validation of hyperthermia treatment planning models. In this case, a quantitative validation of the 3D SAR distribution predicted by a FDTD model of the Lucite cone applicator was performed, and the ratio of predicted and measured power was assessed. The validation data were obtained with a high-quality dosimetric assessment system, which provided a set of SAR scans that encompassed the whole 3D applicator target volume. To quantify the match between model prediction and measurement, various distance-to-agreement and dose-difference criteria were tested. A quantitatively good match was observed: all applicators passed the acceptance criteria 2 mm / 2% for DTA and DD, respectively. It was shown that a quantitative validation of HT antenna models is feasible, and is worth to be considered as a part of hyperthermia quality assurance procedures.

References

[1]   Agazaryan N, Ullrich W, Lee SP, Solberg TD. A methodology for verification of radiotherapy dose calculation. J Neurosurg 2004;101:356-61.

[2]   Allen S, Kantor G, Bassen H, Ruggera P. CDRH RF phantom for hyperthermia systems evaluations. Int J Hyperthermia 1988;4;17-23.

[3]   American National Standards Institute (ANSI). IEEE Recommended Practice for Determining the Peak Spatial-Average Specific Absorption Rate (SAR) in the Human Head from Wireless Communications Devices: Measurement Techniques. IEEE Std 1528-2003. New York: The Institute of Electrical and Electronics Engineers; 2003.

[4]   Berenger JP. A perfectly matched layer for the absorption of electromagnetic waves. J Comput Phys 1994;114:185-200.

[5]   COMAC BME Task Group. Treatment planning and modeling in hyperthermia. A Task Group Report of the European Society for Hyperthermic Oncology in cooperation with a COMAC-BME Concerted Action (4th Medical and Health Research Programme of the European Commission). Rome: Tor Vergata Medical Physics Monograph Series; 1992. p 49-51.

[6]   De Bruijne M, Samaras T, Bakker JF, Van Rhoon GC. Effects of waterbolus size, shape and configuration on the SAR distribution pattern of the Lucite cone applicator. Int J Hyperthermia 2006;22:15-28.

[7]   Franken EM, De Boer JC, Heijmen BJ. A novel approach to accurate portal dosimetry using CCD-camera based EPIDs. Med Phys 2006 ;33:888-903.

[8]   Gabriel S, Lau RW, Gabriel C. The dielectric properties of biological tissues: II. Measurements in the frequency range 10 Hz to 20 GHz. Phys Med Biol 1996;41:2251-69.

[9]   Gellermann J, Wlodarczyk W, Ganter H, Nadobny J, Fahling H, Seebass M, Felix R, Wust P. A practical approach to thermography in a hyperthermia/magnetic resonance hybrid system: validation in a heterogeneous phantom. Int J Radiat Oncol Biol Phys 2005;61:267-77.

[10]   Gellermann J, Weihrauch M, Cho CH, Wlodarczyk W, Fahling H, Felix R, Budach V, Weiser M, Nadobny J, Wust P. Comparison of MR-thermography and planning calculations in phantoms. Med Phys 2006;33:3912-20.

[11]   Gillis S, De Wagter C, Bohsung J, Perrin B, Williams P, Mijnheer BJ. An inter-centre quality assurance network for IMRT verification: results of the ESTRO QUASIMODO project. Ratiother Oncol 2005;76:340-53.

[12]   Guy AW. Analysis of electromagnetic fields induced in biological tissues by thermographic studies on muscle equivalent phantom models. IEEE Trans Microwave Theory Tech 1971;19:205-14.

[13]   Gross E, Raskmark P. Phased array hyperthermia, an experimental investigation. In: ed Sugahara T, Saito M, editors. Hyperthermic Oncology 1988 vol 1. London: Taylor & Francis; 1988. p. 724-5.

[14]   Hand JW, Lagendijk JJW, Bach Andersen J, Bolomey JC. Quality assurance guidelines for ESHO protocols. Int J Hyperthermia 1989;5:421-28.

[15]   Jacobsen S, Rolfsnes HO and Stauffer PR. Characteristics of microstrip muscle-loaded single-arm Archimedean spiral antennas as investigated by FDTD numerical computations. IEEE Trans Biomed Eng 2005;52:321-30.

[16]   Johnson JE, Neuman DG, Maccarini PF, Juang T, Stauffer PR, Turner P. Evaluation of a dual-arm Archimedean spiral array for microwave hyperthermia. Int J Hyperthermia 2006;22:475-90.

[17]   Joines WT, Zhang Y, Li C and Jirtle RL. The measured electrical properties of normal and malignant human tissues from 50 to 900 MHz. Med Phys 1994;21:547-50.

[18]   Kaatee RSJP, Van Rhoon GC. An electric field measurement system, using a two-dimensional array of diodes. Int J Hyperthermia 1999;15:441-54.

[19]   Low DA, Dempsey JF. Evaluation of the gamma dose distribution comparison method. Med Phys 2003;30:2455-64.

[20]   Low DA, Harms WB, Mutic S, Purdy JA. A technique for the quantitative evaluation of dose distributions. Med Phys 1998;25:656-61.

[21] McDermott LN, Wendling M, Van Asselen B, Stroom J, Sonke JJ, Van Herk M, Mijnheer BJ. Clinical experience with EPID dosimetry for prostate IMRT pre-treatment dose verification. Med Phys 2006;33:3921-30.

[22] Means DL, Chan KW. Evaluating Compliance with FCC Guidelines for Human Exposure to Radio Frequency Electromagnetic Fields: Additional Information for Evaluating Compliance of Mobile and Portable Devices with FCC Limits for Human Exposure to Radio Frequency Emissions. Supplement C, Edition 01-01, to OET Bulletin 65, Edition 97-01. Washington DC: Federal Communications Commission (FCC); 2001.

[23] Meier K, Burkhardt M, Schmid T, Kuster N. Broadband calibration of E-field probes in lossy media. IEEE Trans Microwave Theory Tech 1996;44:1954-62.

[24] Samaras T, Rietveld PJM, Van Rhoon GC. Effectiveness of FDTD in predicting SAR distributions from the lucite cone applicator. IEEE Trans Microwave Theory Tech 2000;48:2059-63.

[25] Schmid T, Egger O, Kuster N. Automated E-field scanning system for dosimetric assessments. IEEE Trans Microwave Theory Tech 1996;44:105-13.

[26] Schneider C, Van Dijk JD. Visualization by a matrix of light-emitting diodes of interference effects from a radiative four-applicator hyperthermia system. Int J Hyperthermia1991;7:355-66.

[27] Schneider CJ, Kuijer JP, Colussi LC, Schepp CJ, Van Dijk JD. Performance evaluation of annular arrays in practice: the measurement of phase and amplitude patterns of radio-frequency deep body applicators. Med Phys 1995;22:755-65.

[28] SEMCAD X Reference Manual. Zurich, Switzerland: SPEAG – Schmid & Partner Engineering AG; 2006. Available online at: http://www.semcad.com

[29] Van der Gaag ML, De Bruijne M, Samaras T, Van der Zee J, Van Rhoon GC. Development of a guideline for the water bolus temperature in superficial hyperthermia. Int J Hyperthermia 2006;22:637-56.

[30] Van Esch A, Depuydt T, Huyskens DP. The use of an aSi-based EPID for routine absolute disometric pre-treatment verification of dynamic IMRT fields. Radiother Oncol 2004;71:223-34.

[31] Van Rhoon GC, Rietveld PJM, Van der Zee J. A 433 MHz Lucite cone waveguide applicator for superficial hyperthermia. Int J Hyperthermia 1998;14:13-27.

[32] Van Zijtveld M, Dirkx ML, De Boer HC, Heijmen BJ. Dosimetric pre-treatment verification of IMRT using an EPID; clinical experience. Radiother Oncol 2006;81:168-75.

[33] Wiersma J, Van Dijk JDP. RF hyperthermia array modelling; validation by means of measured EM-field distributions. Int J Hyperthermia 2001;17:63-81.

[34] Wu L, McGough RJ, Arabe OA, Samulski TV. An RF phased array applicator designed for hyperthermia breast cancer treatments. Phys Med Biol 2006;51:1-20.

[35] Wust P, Fahling H, Jordan A, Nadobny J, Seebass M, Felix R. Development and testing of SAR-visualizing phantoms for quality control in RF hyperthermia. Int J Hyperthermia 1994;10:127-42.

[36] Wust P, Meier T, Seebass M, Fahling H, Petermann K, Felix R. Noninvasive prediction of SAR distributions with an electro-optical E field sensor. Int J Hyperthermia 1995;11:295-310.

[37] Wust P, Beck R, Berger J, Fahling H, Seebass M, Wlodarczyk W, Hoffmann W, Nadobny J. Electric field distributions in a phased-array applicator with 12 channels: Measurements and numerical simulations. Med Phys 2000;27:2565-79.

8

Benefits of superficial hyperthermia treatment planning: five case studies

Abstract

Purpose: To demonstrate the benefits of treatment planning in superficial hyperthermia.

Materials and Methods: Five patient cases are presented, in which treatment planning was applied to troubleshoot treatment limiting hot spots, to select the optimum applicator type and orientation, to assess the risk associated with metallic implants, to assess the feasibility of heating a deeper-seated tumour, and to analyse the effective SAR coverage resulting from arrays of applicators. FDTD simulation tools were used to investigate treatment options, either based on segmented or simplified anatomies.

Results: The background, approach and model implementation are presented per case. SAR cross-sections, profiles and isosurfaces were visualised to predict the effective SAR coverage of the target and the location of the maximum power absorption. In addition, the followed treatment strategy and the implications for the clinical treatment are given: e.g. higher temperatures, relief of treatment limiting hot spots or increased power input.

Conclusions: Treatment planning in superficial hyperthermia can be applied to improve clinical routine. Its application supports the selection of the optimum technique in non-standard cases, leading to direct benefits for the patient. In addition, treatment planning has shown to be an excellent tool for education and training for hyperthermia technicians and physicians.

Introduction

Hyperthermia treatment planning tools have a significant potential to further improve the quality of hyperthermia treatments. The principal advantage of treatment planning systems (TPS) is that they provide insight in the 3-D absorbed power (SAR) and temperature distributions that could not be observed otherwise. The fields of application of TPS are manifold [1-5]. TPS are an important tool to identify optimal settings for a specific patient anatomy, in anticipation of a hyperthermia (HT) treatment. During treatments, a TPS may support the steering task by complementing the sparse clinical thermometry, and by visualising the effect of the applicator settings on the SAR or heating patterns, before they are actually applied to the patient. Other clinical fields of application are post-treatment troubleshooting of acute limiting factors, evaluation of the clinical indications for hyperthermia treatments, development of standard settings for certain tumour locations, definition of contraindications for HT and investigation of feasibility to heat a specific target volume. For research purposes, TPS are a valuable tool to evaluate thermal goals and predictive parameters. Finally, TPS may aid the technical improvement and design of antenna systems [6-9].

Over the years, the development of various dedicated 3-D hyperthermia treatment planning systems [6,10-13] has evolved in the clinical application of hyperthermia treatment planning at multiple centres [4,14-15]. To date, the focus in hyperthermia treatment planning and its clinical application has primarily been on deep hyperthermia. To the best of our knowledge, only Kumaradas and Sherar [16] have reported the application of 3-D treatment planning tools to a patient case in superficial hyperthermia (SHT). The large number of degrees of freedom (phases and amplitudes) in phased-array systems probably explains this focus on deep hyperthermia: optimization modules in TPS may provide settings resulting in maximum target heating without unwanted side effects, which can hardly be found intuitively. In contrast, superficial hyperthermia applicator systems uses non-coherent powers sources, and in principle are easier to control. Nevertheless, treatment planning in superficial hyperthermia may prove to be very useful.

The goal of this paper is to demonstrate the benefits of treatment planning in superficial hyperthermia. The main benefits are the enhanced insight in the SAR coverage of the target in specific anatomies, and adaptation of the heating strategy for a specific patient. In addition, treatment plans of (abstractions of) clinical cases provide excellent means for education for the hyperthermia team. Five cases of patients with non-standard treatment fields are presented, in which treatment planning tools were successfully used to support decision making with regard to the treatment strategy.

Materials and methods

Applicator system

The Lucite cone applicator (LCA) is the standard applicator for superficial hyperthermia at the Rotterdam hyperthermia unit. The LCA is a water-filled 434 MHz horn applicator featuring Lucite windows and a PVC cone to enhance its effective field size. The LCA and the Lucite applicator (LA) are evolutions of the conventional waveguide applicator (CWA) [17]. A picture of an LCA and its principle E-field direction are given in Figure 1. The dimensions of the footprint of a single applicator are 10×10 cm². The applicators are always used in combination with a circulating waterbolus [18-19]. Up to six applicators, each with an independent power supply, can be combined in an array to cover larger treatment fields.
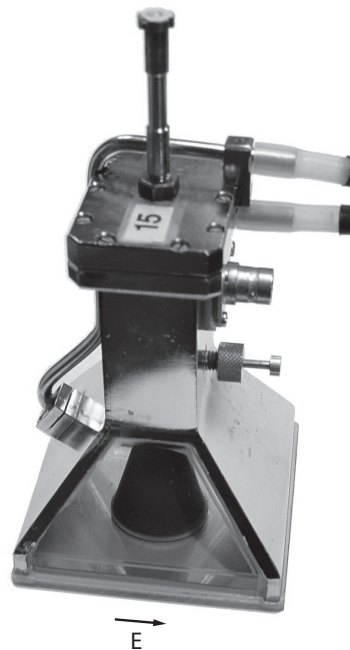
Figure 1. Picture of the Lucite cone applicator indicating its principal E-field direction (arrow). The .PVC cone in the horn aperture can be seen through the Lucite window.

Model implementation

Modelling of the 3D SAR distributions was performed using the finite-difference time-domain (FDTD) method. The models included one or multiple horn applicators (LCA/LA/CWA), a waterbolus, and the patient anatomy or abstracted anatomy. The SAR distributions were computed in the SEMCAD FDTD simulation environment (versions 1.8

and X) [20]. This tool features graded grids, such that the details of the applicator (e.g. the thin walls, source wire and flared horn) can be accurately resolved in the grid implementation of the model. While in all media at least 20 cells per wavelength were applied, the grid was refined to $\leq$ 2 mm in the applicator volume, and to $\leq$ 1 mm near the source. The computational domain was terminated with uniaxial perfectly matched layer (UPML) or Mur 2nd order boundaries. The dielectric properties of the tissues and applicator materials are listed in Table 1 [21-24]. The feasibility of simulating the LCA, LA and CWA horn applicators in a rectilinear grid using the FDTD method was demonstrated by Samaras *et al.* [24]. A quantitative validation of the current FDTD implementation of the LCA was performed by De Bruijne *et al.* [25].

In homogeneous tissue configurations (case 4), the SAR distributions were normalised to the maximum SAR. In inhomogeneous tissue configurations 100% SAR was the maximum of the 10 g spatial peak averaged (IEEE-1529) SAR distribution, to prevent effects of local outliers (case 1 and 3), or SAR was determined per 1 Watt of source power (case 2 and 5).

Cases

To demonstrate the benefits of treatment planning in SHT five cases are presented in this work. The cases address: (*i*) troubleshooting of treatment limiting hot spots, (*ii*) treatment of a patient with implants, (*iii*) heating of a deeper-seated tumour, (*iv*) targeting a saddle-shaped neck field, and (*v*) analysis of the effective SAR coverage resulting from a multi-applicator array. The background, approach, model implementation and the results are described per case in a separate section. The focus is on the selection of the appropriate technique in non-standard cases to obtain an optimum treatment strategy; the effect on clinical response is beyond the scope of this work. The cases are followed by a general discussion and conclusion.

Table 1. Properties of the tissues and applicator materials applied in the models.

Material	ε_r (-)	σ_{eff} (S/m)	ρ (kg/m^3)
Fat	5.6	0.04	888
Muscle	56.9	0.80	1050
Bone	13.1	0.09	1595
lung (inflated)	23.6	0.38	750
mammary tumour	57.9	0.85	1040
de-ionized water	80	0.04	-
Lucite	2.6	0.003	-
PVC	2.2	0.004	-

Case 1: Melanoma on lower leg

An 89-year old woman with three melanoma lesions on the lower leg (Figure 2(a)) was referred for irradiation (3×8 Gy, 1/wk) plus hyperthermia (1 hr/wk). The first hyperthermia treatment was problematic: the power input was greatly limited by pain from hot spots at the side of the leg. Consequently, tumour temperatures remained low (mean < 40°C) and the treatment was adjourned after 45 minutes. Treatment planning was used to analyse the problem and to propose an alternative treatment strategy. The parameters under study were the applicator type and the direction of the E-field. Three applicators were considered: the Lucite cone applicator (LCA), the Lucite applicator (LA) and the conventional waveguide applicator (CWA). In addition, E-field directions parallel and perpendicular to the lower leg were studied.

As a first step, a simplified model consisting of a muscle cylinder, an elliptic bone and a tumour knob was implemented, see Figure 2(b). At a later stage CT images of the lower leg were available; these were segmented using basic Hounsfield unit thresholding, and implemented in the model, see Figure 2(c). The analysis focused on the largest (central) melanoma lesion. The power absorption pattern resulting from the six combinations of applicator type and orientation were computed and visualized. The selection of applicator type and orientation was based on visual inspection of the SAR data volumes.

The results from the simplified anatomy are shown in Figure 3. For the set-up of the first treatment (LCA, E-field parallel) the simulated SAR distribution indicates hot spots at the side of the lower leg, identical to the location where the patient indicated pain during the treatment. In addition, the model indicates low power absorption in the centre of the tumour, in correspondence with the low measured temperatures during the first HT. The results show that the hot spots are less severe for the LA, and practically disappear for the CWA. The maximum SAR coverage of the tumour was obviously observed for the CWA with the E-field perpendicular to the lower leg. However, this configuration also possibly involves hot spots at the skin-tumour and tumour-bone interfaces. The CWA with the E-field parallel to the lower leg was considered the preferable configuration. Here, the maximum power deposition is at the tumour base, where high perfusion was expected, while no hot spots at the tumour-skin interface were expected. It was anticipated that the necrotic mass at the tumour top would be sufficiently heated by thermal conduction.

For the segmented anatomy, the simulated power absorption patterns are shown in Figure 4. These results confirmed that for the CWA applicator with the E-field directed parallel to the lower leg, there is an optimal power absorption in the tumour and no hot spots at the skin. Based on the treatment planning, the HT was continued using this configuration, with good results: during the second and third HT session the tumour temperatures were significantly higher (Figure 5), the treatment sessions were completed, and the patient reported no hot spots.

Case 2: Sternum cerclage

Implants are often considered a contraindication for hyperthermia. Depending on the type of implant, several interactions with the E-field are possible. In general we may discriminate three types: metallic implants, active implantable medical devices, and other (non-metallic and passive) implants. In the vicinity of metallic devices such as artificial hips, surgical clips and -wires, intrauterine devices and screws. this interaction may lead to local SAR enhancement. The interaction will highly depend on the electrical dimensions of the device and the strength and direction of the E-field. So far, published investigations have been limited to the risks associated with metallic surgical clips. Lee *et al.* [26] concluded that in an EM field, metallic objects that have dimensions that are much shorter than the wavelength can cause significant changes in the power deposition. Boll *et al.* [27] reported that radiofrequency ablation can be safely performed in patients with implanted clips, if a certain distance to the RF electrode is kept. For active implantable medical devices (like cardiac pacemakers) the risk of malfunctioning will depend on their electromagnetic compatibility (EMC). However, this type of susceptible implants is generally considered a contraindication for hyperthermia. For other implants, like silicone implants and Port-A-Cath systems, interaction with the E-field may lead to enhanced risk of hot spot formation, and there may be a health risk associated with e.g. deterioration of the implant or leakage.

In this case a patient was referred for reirradiation plus hyperthermia for breast cancer recurrences following a radical mastecomy. A complicating factor was that the patient had a sternum cerclage after open-heart surgery. The cerclage wires were suspected to behave like primitive loop antennas in the human body. Since the literature provides no guidelines for metallic implants other than surgical clips, we studied the possible effects of cerclage wires in a model to see if the patient could be treated with cerclage wires, or that removal of the wires should be considered. The goal in this case was to assess whether cerclage wires are a strict contraindication for SHT treatment. From the X-thorax of the patient (Figure 6(a)) it followed that 7 cerclage wires had been placed around the sternum. Because no CT data was available, general dimensions were assessed and the sternum cerclage was simplified to a flat bone structure (width 30 mm, height 10 mm, round edges) with a single metallic ring (cross-section 1 mm²) embedded in muscle tissue, 3 mm below the surface (see Figure 6(b)). The LCA and waterbolus were placed centrally above the ring. In total four configurations were simulated. To test minimum and maximum excitation of the wire loop, E-field directions parallel and perpendicular to the sternum were studied. Further, to assess the risk of hot spots induced by sternum cerclage, the SAR distribution resulting from a sternum with a perfectly electrically conducting ring was compared to that of a sternum without a ring for both field directions.

The SAR cross-sections through the sternum at the position of the ring are shown in Figure 7. The simulation results show that for an E-field direction parallel to the sternum, a conducting wire hardly changes the SAR distribution in the volume. However, for an E-field direction perpendicular to the sternum, the addition of a cerclage wire results in much

higher SAR near the sternum, and a 35-fold increase of the maximum SAR (4 without vs. 139 W/kg with ring, per 1 W of source power). Based on the calculations it was concluded that cerclage wires are no hard contraindication for superficial hyperthermia, provided that the E-field is parallel to the sternum. For E-field directions perpendicular to the sternum severe hot spots near cerclage wires should be expected.

The power was increased cautiously during the treatments with the advised configuration. It appeared that the total power input was not limited by pain complaints at the sternum (total end power during the four treatments: 220, 300, 260, 275 W for 6 applicators), and normal therapeutic temperatures were measured (steady-state mean interstitial temperatures of 41.4, 40.7, 41.1 and 42.1°C). The patient did however report pain complaints near the sternum, when the E-field direction of the two LCAs above the sternum was perpendicular. These observations are in line with the modelling results.

Case 3: Tumour covered by thick fat layer

A 47-year old woman with a history of locally advanced mamma carcinoma presented with an infraclavicular locoregional recurrence, mimicking a brachial plexus lesion. She was referred for reirradiation (8×4 Gy) plus hyperthermia. From the transverse CT slice shown in Figure 8 it followed that the recurrence laid at 3.7–5.4 cm below the skin, which is beyond the LCAs empirically derived standard maximum target volume depth of 4 cm. However, from the CT data it also became clear that the tumour was covered by an above-average fat layer (thickness ~2.9 cm). Because the effective conductivity of fatty tissue is low compared to muscle and tumour tissue (see Table 1), it could be anticipated that power absorption from the E-field at the depth of the tumour was still significant. Also, research by Van der Gaag et al. [19] revealed that in a three-layer anatomy (skin-fat-muscle) an increase in the fat layer thickness moves the heat focus to a greater depth, if sufficient waterbolus cooling is applied at the skin. A model was set up to evaluate the SAR coverage of the tumour and to consider treatment of the patient. A precondition to start HT treatments was the full enclosure of the tumour by the 25% SAR isosurface. This criterion is based on results by Myerson et al. [28] and Lee et al. [29], who demonstrated that coverage by the applicator's 25% iso-SAR contour was the most important factor to predict treatment outcome in recurrent breast carcinoma of the chest wall.

The CT dataset of the thorax was segmented in the tissue types fat, muscle, tumour, bone, and lung. In the model, the LCA was aligned centrally above the tumour, with a waterbolus thickness of at least 1 cm, see Figure 9(a). Orientations of the E-field parallel and perpendicular to the median plane were investigated. The 25%, 50% and 75% SAR isosurfaces were visualised.

The SAR volumes resulting from E-fields parallel with and perpendicular to the longitudinal axis are depicted in Figure 10. Figure 9(b) shows that, in accordance with the expectations, the peak SAR values were located in the muscle/tumour interface, with a secondary peak at the body surface. For the E-field parallel (Figure 10, top row), the main

SAR focus was located at the shoulder, possibly leading to a power limiting hotspot. Also, the tumour area was not fully covered by the 25% SAR volume. In contrast, for the E-field perpendicular (Figure 10, bottom row), the main SAR focus was at the tumour surface, while the 25% SAR volume did fully cover the tumour. Based on these observations, it was decided to treat this patient with the E-field direction perpendicular to the longitudinal axis. Two interstitial catheters were placed by ultrasound guidance to measure the temperature at two locations in the tumour at depth, about 1.5 cm apart. The measured temperatures are listed in Table 2. During the first treatment, no therapeutic temperatures ($T < 40°C$) were measured in the tumour due to a too conservative power build up. The next treatments showed that therapeutic temperatures could be reached in the tumour, however inhomogeneity was substantial: high tumour temperatures (steady-state mean 40.7 – 43.6 °C) were measured by one probe, while the temperatures in the other lagged behind by 2 – 4 °C. This temperature inhomogeneity is probably caused by distinct differences in local perfusion.

Table 2. Mean (range) steady-state temperatures measured in the tumour of case 3.

	Temperatures (°C)			
	Treatment 1	**Treatment 2**	**Treatment 3**	**Treatment 4**
Probe 1	37.8 (37.4 - 38.0)	39.1 (38.7 - 39.5)	37.8 (37.7 - 38.0)	39.1 (38.6 - 39.4)
Probe 2	38.3 (37.7 - 38.6)	43.6 (43.1 – 44.1)	40.7 (40.4 - 41.0)	41.9 (40.9 - 42.6)

a.   b.   c.
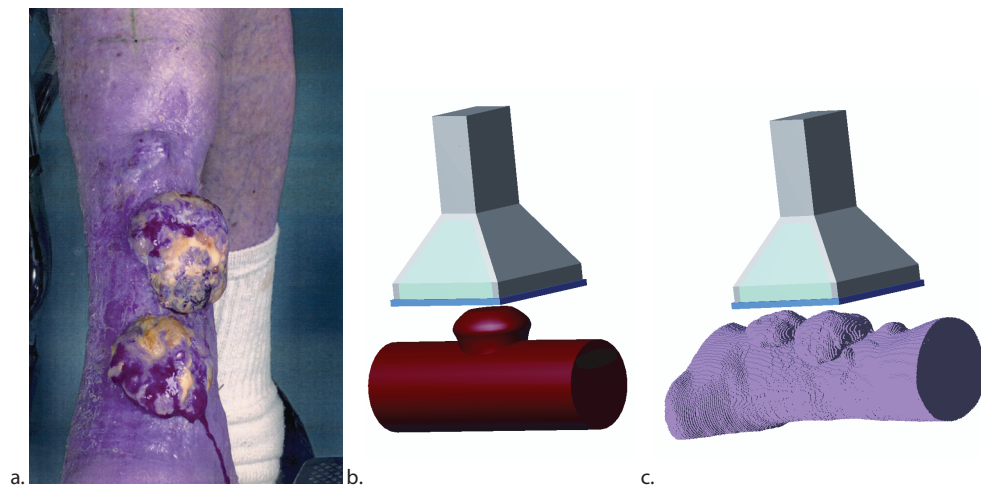
Figure 2. (a) The melanoma lesions of case 1. (b-c) Model implementation: LCA applicator and (b) simplified anatomy, or (c) segmented anatomy (waterbolus not shown).
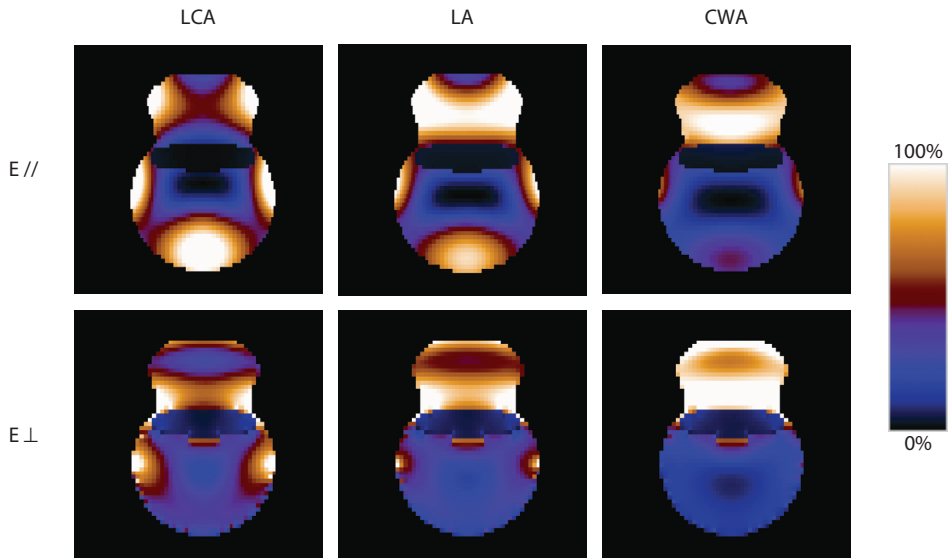
Figure 3. Results for the simplified anatomy: absorbed power in a transverse cross-section through the tumour, for three different applicators (LCA, LA, CWA) and two orientations of the electric field (parallel (//) or perpendicular (⊥) to the lower leg).
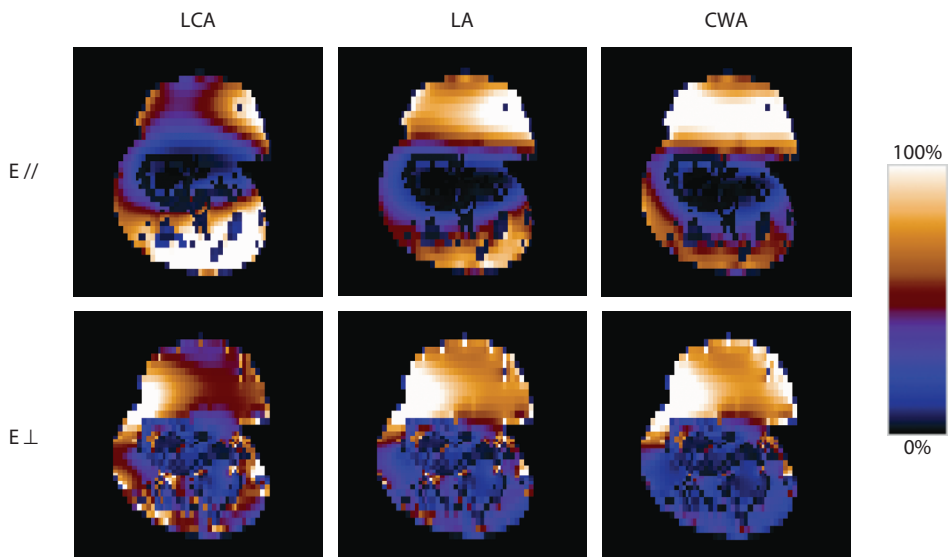

Figure 4. Results for the segmented anatomy: absorbed power in a transverse cross-section through the tumour, for three different applicators (LCA, LA, CWA) and two orientations of the electric field (parallel (//) or perpendicular (⊥) to the lower leg).
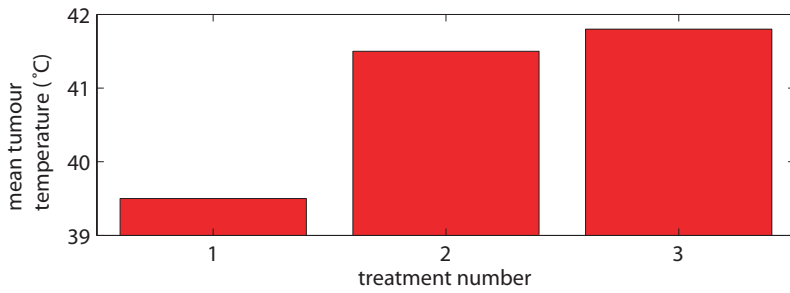
Figure 5. Mean tumour temperatures during the hyperthermia treatments. After the first treatment, the applicator set-up was changed based on treatment planning.
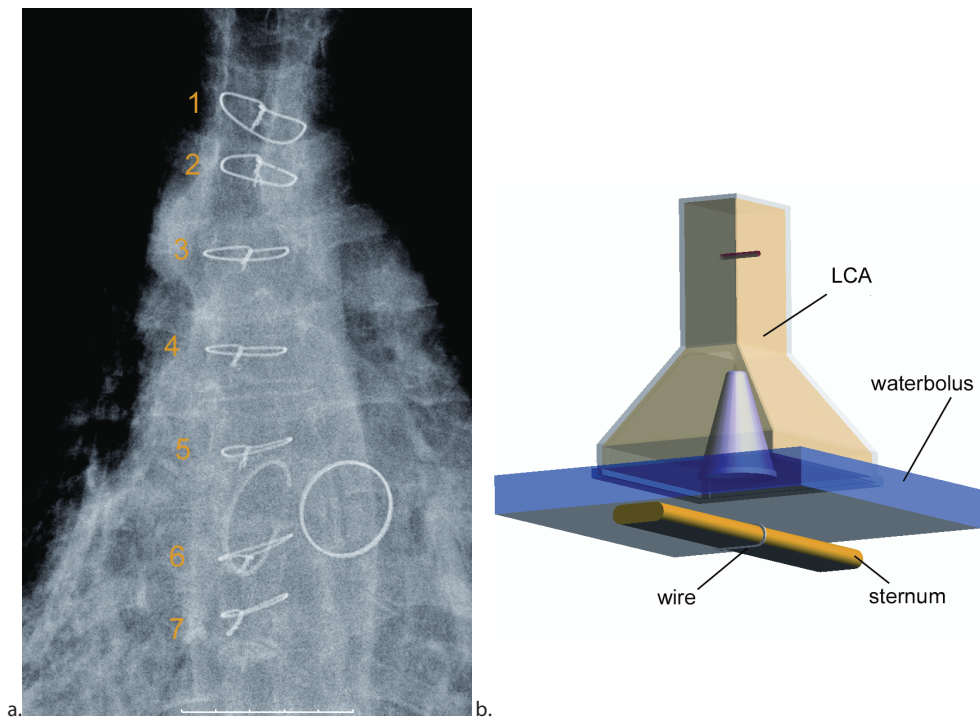
Figure 6. (a) X-thorax of the patient in case 2. The cerclage wires are numbered 1-7. The deeper seated heart valves are also visible. (b) Overview of the abstract model: LCA with a waterbolus placed above an elliptic bone with a metallic ring (muscle volume not shown).
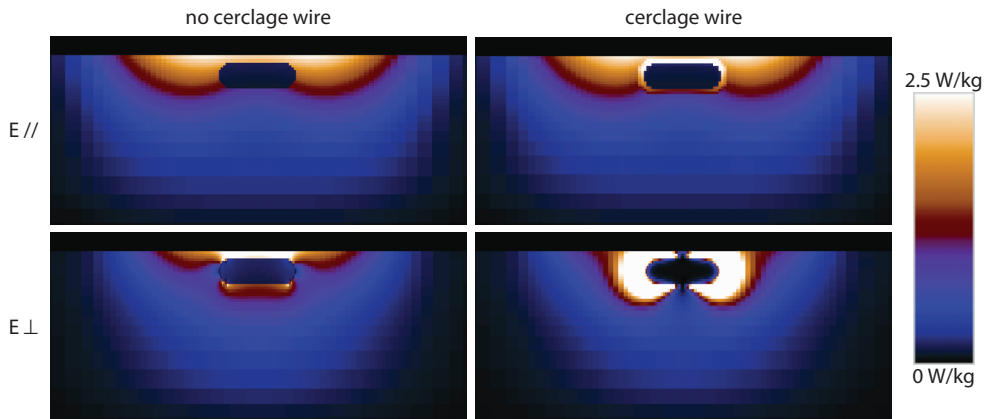
Figure 7. SAR cross-sections for a sternum without (left) and with a sternum cerclage wire (right), for E-field directions parallel (top, E//), and perpendicular (bottom, E⊥) to the sternum.
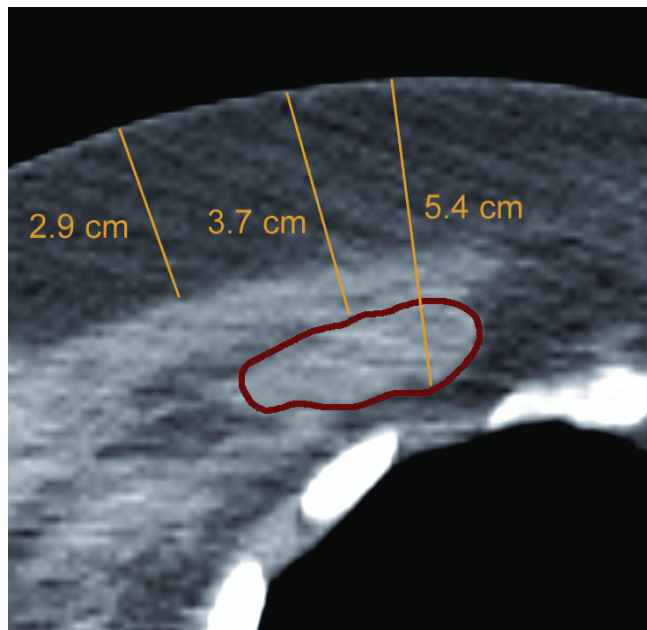
Figure 8. Transverse CT slice through the centre of the tumour of case 3. The tumour outline is indicated with a contour. The arrows show the tumour depth (3.7–5.4 cm) and the thickness of the fat layer (2.9 cm).
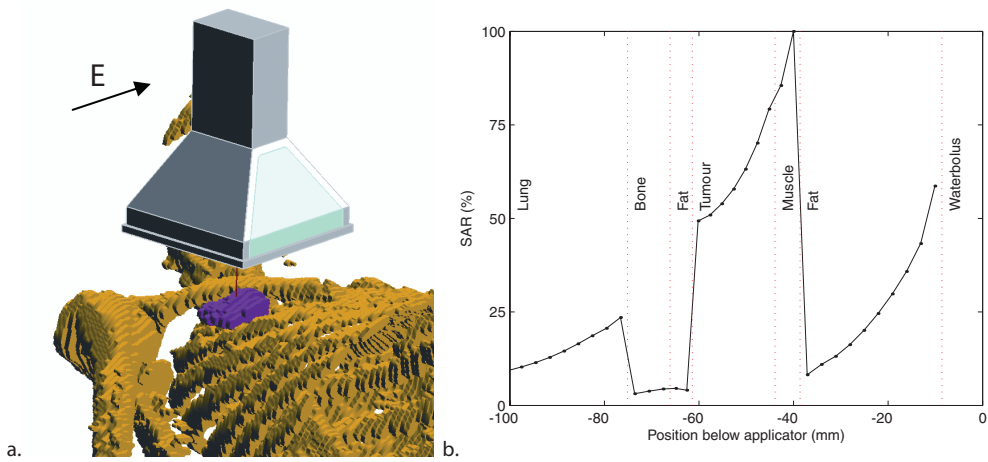
Figure 9. (a) Position of the LCA centrally above the tumour. Here, the E-field direction is perpendicular to the body axis. (b) Normalized SAR profile centrally below the applicator (E-field direction perpendicular), showing the main SAR peak at the muscle and tumour.
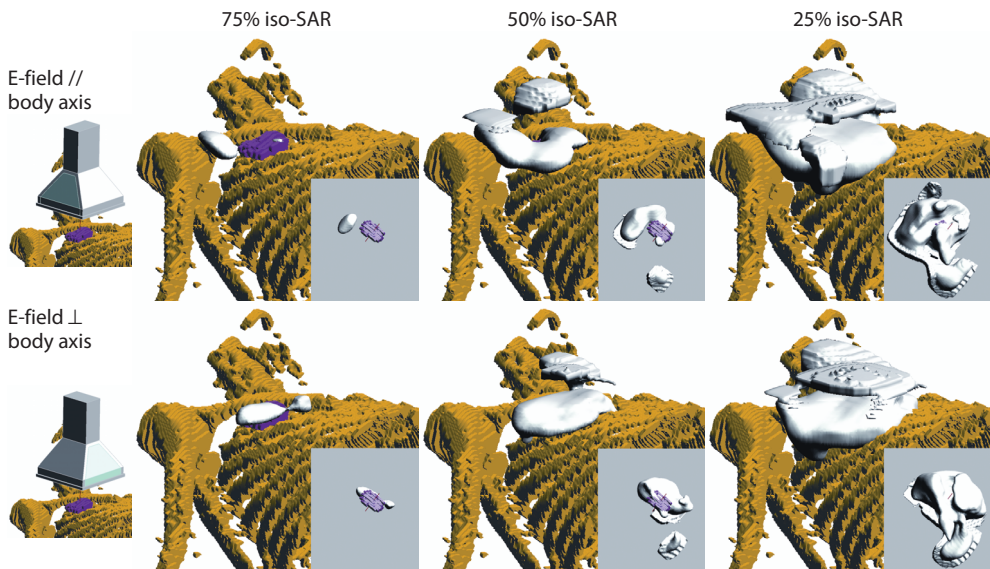
Figure 10. SAR coverage for E-field directions parallel (top) and perpendicular (bottom) to the body axis. The 75%, 50%, and 25% iso-SAR surfaces are depicted. The insets show the inferior view of the tumour's SAR coverage.

Figure 11. Local supraclavicular schwannoma recurrence (case 4).
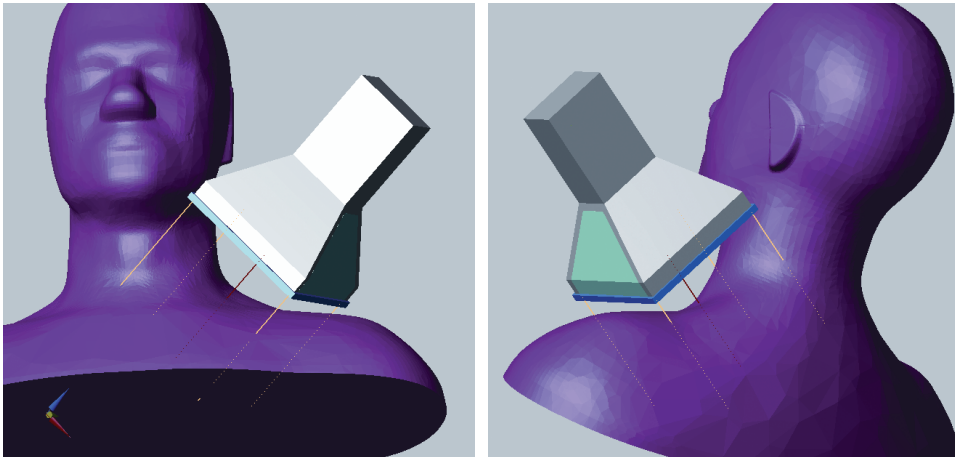
Figure 12. Overview of the model configuration: the LCA is targetet at the posterior triangle of the neck of the SAM phantom (waterbolus not shown). The lines show the projection of the centre and extent of the applicator horn on the anatomy.
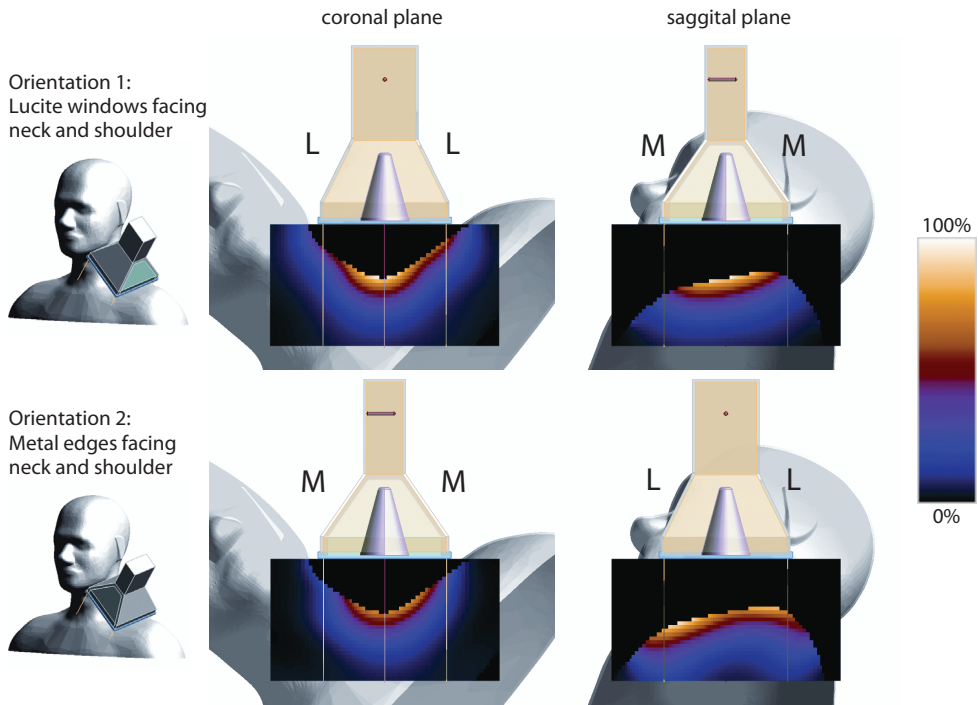
Figure 13. Normalized SAR in the SAM phantom, centrally below the applicator. SAR cross-sections for two orientations of the LCA are shown: in the top row the Lucite windows (L), and in bottom row the metal edges (M) face the shoulder and the neck.
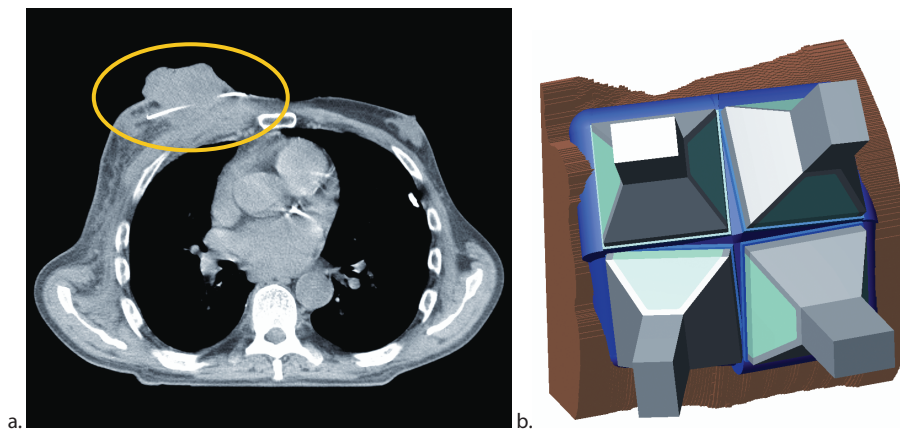
Figure 14. (a) Transverse CT slice of the thorax showing the exophytic Merkel cell carcinoma of case 5. The white line at the base of the tumour is one of the thermometry catheters. (b) Overview of the 2-by-2 umbrella-style LCA array placed onto the anatomy.

a.

b.

c.

d.
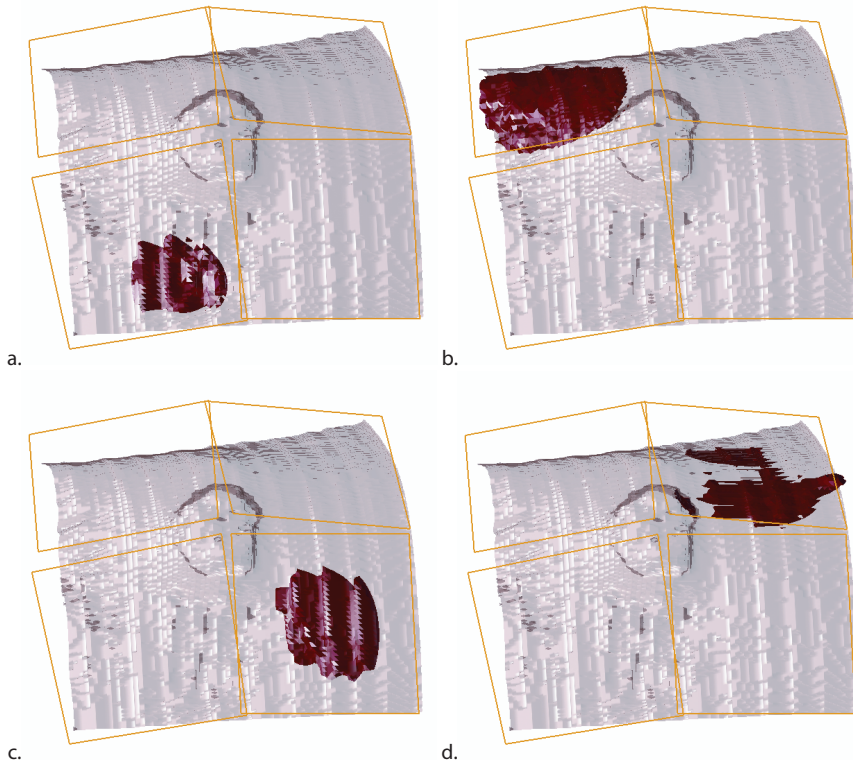
Figure 15. Individual SAR contribution of the applicators. Relative scaling: (a) [5 0 0 0], (b) [0 5 0 0], (c) [0 0 5 0] and (d) [0 0 0 5]. Isosurface at 10 W/kg. The applicators are represented schematically by their square aperture of 10×10 cm².
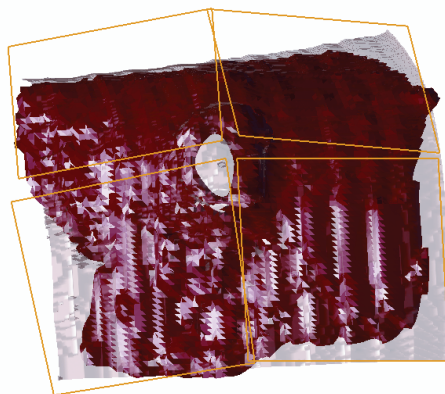
Figure 16. The 5 W/kg SAR isosurface resulting from scaling factors [4.25, 3, 3.5, 4.25]. The hole in the isosurface at the tumour centre is clearly visible.

Case 4: SAR coverage of a neck field

The feasibility of treatment was investigated for a 54-year old woman with a malignant schwannoma recurrence in the left supraclavicular fossa (see Figure 11). After initial surgical treatment plus 60 Gy radiotherapy post-operatively seven years earlier, and two more extensive local resections of recurrences, a new local recurrence could not be resected without unacceptable morbidity. Thus, reirradiation (28×1.8 Gy, 5/wk) plus HT (1 hr/wk) was considered. The recurrence was a subcutaneous 2–3 cm diameter nodule.

A complicating factor in this case was the significant pain associated with pressure on the target area and with lateroflexion of the neck. During the intake, it was assessed that the pressure from the waterbolus was tolerable. However, the patient's comfort did not allow lateral movement of the neck. Consequently, placement of the LCA at the posterior triangle of the neck resulted in a large distance from the skin to the centre of the applicator base, and short distance (~1 cm) from the applicator edges to the skin. As it was unclear what SAR distribution could be expected from an LCA opposing an angled tissue volume and a large distance of the central area of the applicator to the tumour location, a treatment plan was made. Because no CT dataset was available for this patient, a generalised anatomy of the head and neck (the Standard Anthropomorphic Model (SAM) phantom) was scaled to the proportions of the patient to investigate SAR coverage, see Figure 12. The phantom volume was assigned muscle tissue properties. The central axis of the applicator was directed at the centre of the tumour, and two applicator orientations were tested in which (*i*) the Lucite windows, and (*ii*) the metal edges faced the neck and shoulder.

The simulation results in Figure 13 show that when the Lucite windows face the neck and the shoulder, the SAR focus is centrally below the applicator at the site of the tumour. Placing the metal edges near the neck and the shoulder however resulted in less optimal SAR coverage, with the SAR maximum outside the central plane of the applicator. Both orientations did not result in hot spots at the shoulder or neck, despite the short distance between the horn edges and the skin.

During the treatments, the LCA was placed with the Lucite windows facing the neck and shoulder. It was decided to treat the patient without interstitial tumour measurements, because of tumour-induced pain. The power input to the applicator was not limited by local hot spots at the neck or shoulder, and the levels achieved in steady-state were such that therapeutic temperatures could be expected (100–140 Watts). Clinical results were satisfactory: no tumour progression in the treated volume was observed during follow-up (10+ months).

Case 5: Four-applicator umbrella array on exophytic tumour

A 79-year old man presented with a large (diameter 60 mm, height 20 mm) exophytic Merkel cell carcinoma on the thoracic wall which also involved the surrounding skin, see

Figure 14(a). The dimensions of the radiotherapy field (80×115 mm) were larger than the footprint of a single LCA, so a 2-by-2 "umbrella-style" LCA array was considered to heat the whole target volume. This set-up however implies that the exophytic tumour is not centrally below one applicator, but below the corners of four applicators. The question was whether effective heating of this specific target volume by an umbrella-style LCA array could be expected. A model was set up to visualise the effective SAR coverage.

Figure 14(b) shows the model configuration: four applicators placed in an umbrella set-up over the segmented anatomy. The computation of the total SAR involved four simulation runs, in which the source of one of the four applicators was driven. For each applicator the SAR values were normalized to 1 Watt input power. Thereafter, the total SAR (SAR_{tot}) from the non-coherently driven applicators was calculated by summing their relative contributions:

$$SAR_{tot}\left(\vec{r}\right) = \sum_{i=1}^{4} sf_i \cdot SAR_i\left(\vec{r}\right)$$

where i is the index of an LCA, sf_i is the power scaling factor of an applicator, and $\vec{r}$ is a point in the common grid.

To investigate the contribution of the individual applicators to the total SAR volume, the scaling factor of one was set to five and the others to zero, see Figure 15. Hereafter, the powers were scaled such that the size of the peak SAR (10W/kg) volumes of the applicators were similar, resulting in the scaling vector [4.25, 3, 3.5, 4.25]. The final treatment plan, depicted in Figure 16, revealed a hole in the 5 W/kg iso-SAR volume (approximately 50% normalized SAR) at the centre of the exophytic tumour, when at the same time it did cover the whole surrounding surface. This indicates that heating of the tumour centre would primarily occur by conduction from surrounding tissue. It was expected that this "heating the base" approach can be successful, provided that enough power is delivered to the target area, and can further be enhanced by tumour necrosis. During the first two treatments the mean steady-state temperatures measured at the tumour base were 40.7 and 41.8 °C, respectively. During the last (third) treatment the catheters were removed due to infection. However, there was a progressive trend in the applied total steady-state power (150, 400, 460 Watts), suggesting that also in the last treatment therapeutic temperatures (40–43°C) were reached.

Discussion

The cases presented in this work illustrate the use of treatment planning as a tool for decision support in superficial hyperthermia, more specifically to: (*i*) troubleshoot problems that rise during clinical application of SHT, (*ii*) guide the selection of applicator type and direction of the E-field, (*iii*) analyse the SAR coverage of a target volume in non-standard cases, and (*iv*) investigate to what extent potential contraindications obstruct

treatment. In some cases, abstractions of the patient's anatomy were exploited to speed up the process of decision making, or because 3D medical images were not available in an early stage. The understanding gained, even from simplified anatomies, has proved valuable in determining the treatment strategy and was of direct benefit for the patient. The main strength of input from simulations is that the effectiveness of different scenarios can be judged in advance of a HT session. In contrast, without input from simulations, decisions regarding the treatment approach are based on previous experiences and intuition, and their efficacy only becomes clear during the course of a treatment.

Another area where treatment planning plays an important role is the education and training of hyperthermia technicians and physicians. Traditionally, the mental image of the SAR pattern below an applicator is based on the patterns measured in flat phantom set-ups for quality assurance purposes [30]. In the clinical situation this mental picture does not always apply, as SAR patterns in patients are largely determined by the anatomy. Here, treatment plans critically refine insight in the real 3-D energy distribution, especially in non-standard cases. For educational purposes, treatment plans based on simplified anatomies are the best, because the connection between the main anatomical features, the applicator set-up, and the resulting SAR pattern is optimal and distractions from influences of small anatomical features are limited. In our experience both patient-specific and generalized treatment plans tend to feed interdisciplinary discussions and thus provide an excellent means of continuous training.

It is important to note that despite the close similarity between deep and superficial hyperthermia treatment planning, SHT-TP is a horse of a different colour. The different demands on a TPS originate from basic differences in equipment and steering. For the heating of deep-seated tumours, a phased array of dipoles (e.g. BSD-2000) or parallel-plate waveguides (AMC-4, AMC-8) is generally used. Here, the main steering parameters are the amplitudes and phases of the array elements, and optimization can be based on precomputed electric field distributions for the array elements to be considered [3]. In contrast, applicator systems for SHT (horn- and microstrip applicators) use non-coherent sources, thereby restricting the steering possibilities to power variations alone. Here, optimization of the heating technique involves the applicator type and orientation, and the placement of applicators relative to the patient's anatomy. Consequently, in SHT-TP each variation in an optimization parameter involves the generation and simulation of a separate model. In addition, SHT-TP is computationally demanding. Firstly, the 5–10 times higher frequencies applied in SHT (433 or 915 MHz) as compared to DHT (70-100 MHz) lead to smaller grid steps. Secondly, where in DHT voxels of about 1 cm are generally applied for EM simulations, the simulation of SHT applicators requires grid steps of 1 mm and less to accurately resolve the antenna structure in a mesh [18,31-32]. Therefore, fully fledged optimization in SHT-TP includes high-speed simulation tools which allow scripted model generation and simulation.

The tools for simulation of an array of applicators placed around a realistic anatomy are now available. This opens up new areas of research. One future benefit of SHTP is the

improvement of the observability of patient temperatures, by supplementing interstitial thermometry with temperature predictions based on treatment plans. The work by Kumuradas and Sherar [16] already aimed in this direction. For SHT the means to improve temperature monitoring are restricted. In general, the problem of interstitial thermometry persists: neither the patient nor the clinician appreciates increasing the density of interstitial temperature measuring points. Non-invasive thermometry (NIT) by MRI is not realistic for SHT, and NIT by microwave radiometry or ultrasound has not been demonstrated to provide the required spatial resolution and temperature sensitivity. Over time, predicted temperatures may even replace interstitial thermometry. However, accurate prediction of temperature distributions requires the calculation of absolute SAR levels, thus extensive knowledge of the relation between model SAR and real-world SAR. First steps in this direction have been taken by quantitative validation of the FDTD model of the LCA applicator [25]. Moreover, accurate thermal modelling requires a more extensive knowledge of tissue parameters and of a patient's perfusion characteristics than is available today.

Another potential benefit of SHT treatment planning tools is that calculated 3D SAR and temperature distributions provide a means to analyse the correlation between SAR coverage, cumulative equivalent minutes, or any other proposed prognostic parameter, and treatment outcome. A study investigating the prognostic value of 3D SAR coverage for breast cancer recurrences of the chest wall is currently in preparation at the Rotterdam hyperthermia unit. In this respect, superficial hyperthermia treatment planning is a gateway to an improved hyperthermic dosimetry.

Conclusion

Treatment planning in superficial hyperthermia is feasible and available for routine clinical use. Superficial hyperthermia treatment planning has been successfully applied to select the applicator type and the polarization of the E-field, to assess the risk associated with metallic implants, and to analyse the effective SAR coverage resulting from multi-applicator arrays. Apart from clinical benefits like higher tumour temperatures and relief of limiting hot spots, treatment planning in superficial hyperthermia provides a means to improve temperature monitoring and to proceed in hyperthermia dosimetry.

References

[1] Lagendijk JJW, Crezee J, Mooibroek J. Principles of treatment planning. In: Seegenschmiedt MH, Fessenden P, Vernon CC, eds. Thermo-radiotherapy and Thermo-chemotherapy. Volume 1. Biology, Physiology, and Physics. Berlin: Springer-Verlag, 1995, pp. 439-451.

[2] Wust P, Seebass M, Nadobny J, Felix R. Electromagnetic deep heating technology. In: Seegenschmiedt MH, Fessenden P, Vernon CC, eds. Thermo-radiotherapy and Thermo-chemotherapy. Volume 1. Biology, Physiology, and Physics. Berlin: Springer-Verlag, 1995, pp. 219-247.

[3] Paulsen KD, Geimer S, Tang J, Boyse WE. Optimization of pelvic heating rate distributions with electromagnetic phased arrays. Int J Hyperthermia 1999;15:157-186.

[4] Gellermann J, Wust P, Stalling D, Seebass M, Nadobny J, Beck R, Hege HC, Deuflhard P, Felix R. Clinical evaluation and verification of the hyperthermia treatment planning system Hyperplan. Int J Radiation Oncology Biol Phys 2000;47:1145-1156.

[5] Lagendijk JJW. Hyperthermia treatment planning. Phys Med Biol 2000;45:R61-R76.

[6] Wust P, Seebass M, Nadobny J, Deuflhard P, Monich G, Felix R. Simulation studies promote technological development of radiofrequency phased array hyperthermia. Int J Hyperthermia 1996;12:477-94.

[7] Kroeze H, Van de Kamer JB, De Leeuw AAC, Lagendijk JJW. Regional hyperthermia applicator design using FDTD modelling. Phys Med Biol 2001;46:1919-1935.

[8] Seebass M, Beck R, Gellermann J, Nadobny J, Wust P. Electromagnetic phased arrays for regional hyperthermia: optimal frequency and antenna arrangement. Int J Hyperthermia 2001;17:321-336.

[9] Paulides MM, Bakker JF, Zwamborn APM, Van Rhoon GC. A head and neck hyperthermia applicator: Theoretical antenna array design. Int J Hyperthermia 2007;23:59-67.

[10] Sullivan DM, Ben-Yosef R, Kapp DS. The Stanford 3-D hyperthermia treatment planning—Technical review and clinical summary. Int J Hyperthermia 1993;9:627–643.

[11] Das SK, Clegg ST, Anscher MS, Samulski TV. Simulation of electromagnetically induced hyperthermia: A finite element gridding method. Int J Hyperthermia 1995;11:797–808.

[12] Hornsleth SN, Seebass M, Mella O, Dahl O. Patient specific treatment planning in regional hyperthermia: practical experience in Bergen. In: Hornsleth SN, editor. Radiofrequency regional hyperthermia (dissertation). Aalborg University, Denmark; 1996.

[13] Van de Kamer JB, De Leeuw AAC, Hornsleth SN, Kroeze H, Kotte ANTJ, Lagendijk JJW. Development of a regional hyperthermia treatment planning system. Int J Hyperthermia 2001;17:207-220.

[14] Sreenivasa G, Gellermann J, Rau B, Nadobny J, Schlag P, Deuflhard P, Felix R, Wust P. Clinical use of the hyperthermia treatment planning system Hyperplan to predict effectiveness and toxicity. Int J Radiation Oncology Biol Phys 2003;55:407-419.

[15] Kok HP, van Haaren PM, van de Kamer JB, Zum Vorde Sive Vording PJ, Wiersma J, Hulshof MC, Geijsen ED, van Lanschot JJ, Crezee J. Prospective treatment planning to improve locoregional hyperthermia for oesophageal cancer. Int J Hyperthermia 2006;22:375-389.

[16] Kumaradas JC, Sherar MD. Edge-element based finite element analysis of microwave hyperthermia treatments for superficial tumours on the chest wall. Int J Hyperthermia 2003;19:414-430.

[17] Van Rhoon GC, Rietveld PJ, Van der Zee J. A 433 MHz Lucite cone waveguide applicator for superficial hyperthermia. Int J Hyperthermia 1998;14:13-27.

[18] De Bruijne M, Samaras T, Bakker JF, Van Rhoon GC. Effects of waterbolus size, shape and configuration on the SAR distribution pattern of the Lucite cone applicator. Int J Hyperthermia 2006;22:15-28.

[19] Van der Gaag ML, De Bruijne M, Samaras T, Van der Zee J, Van Rhoon GC. Development of a guideline for the water bolus temperature in superficial hyperthermia. Int J Hyperthermia 2006;22:637–656

[20] SEMCAD X Reference Manual. Zürich, Switzerland: Schmid & Partner Engineering AG; 2006. Accessed 20 January 2007. Available online at: http://www.semcad.com

[21] Gabriel S, Lau RW, Gabriel C. The dielectric properties of biological tissues: III. Parametric models for the dielectric spectrum of tissues. Phys Med Biol 1996;41:2271–2293.

[22] Joines WT, Zhang Y, Li C, Jirtle RL. The measured electrical properties of normal and malignant human tissues from 50 to 900 MHz. Med Phys 1994;21:547-550.

[23] COMAC BME Task Group 1992 Treatment planning and modeling in hyperthermia. A Task Group Report of the European Society for Hyperthermic Oncology in cooperation with a COMAC-BME Concerted Action (4th Medical and Health Research Programme of the European Commission) (Rome: Tor Vergata Medical Physics Monograph Series). pp 12, 135-6

9

General discussion and future outlook

General discussion and future outlook

The goal of this thesis is to investigate several quality factors in superficial hyperthermia. This was done by means of theoretical modelling and model validation, development of guidelines, equipment and evaluation tools, and analysis of clinical data. These aspects were detailed in the previous chapters, and were discussed at the end of each chapter. In this chapter, several aspects addressed in the previous chapters will be combined, additional comments will be made, and the most important aspects of the research will be drawn together. The value of the work will also be discussed, and some future perspectives for quality assurance in superficial hyperthermia will be considered. This general discussion focuses on the following topics: (*i*) the waterbolus, (*ii*) characterisation of applicators, (*iii*) modelling and treatment planning, (*iv*) thermal dose, and (*v*) human factors and practice variation. The quality of current treatments can be strongly enhanced by implementing the results obtained for these factors.

Influence of the waterbolus on treatment quality

It was shown in Chapter 4 that waterbolus dimensions are a critical factor for the effective field size of the LCA. To control the effective field size in the clinic, a clear guideline for the application of waterboli with LCA arrays was derived from the extensive modelling study in the same chapter. The shrinkage of SAR contours when a too limited watervolume exists outside the LCA array can be considered a SAR perturbation. In the literature, SAR pattern perturbations are often related to resonance effects (so-called spurious oscillations) in waterbolus layers, for which Gelvich *et al.* [1] set up a theoretical framework. According to Gelvich's theory, spurious oscillations cannot occur if a water-filled waveguide like the LCA is applied [1]. So, there are at least two mechanisms which may lead to SAR pattern perturbations: spurious oscillations, and field shaping due to an unfavourable water layer volume. For quality assurance, full investigation of these effects should be done for each applicator system.

Once the field shaping effect of the waterbolus has been characterised, one can also take advantage of it in some cases, e.g. to move the maximum of the SAR distribution, or to create an asymmetric SAR distribution. Other options to influence the field shape are to include lossy enclosures, or enclosures with a different permittivity in the waterbolus [2-4]. This option was not explored here: although the idea is attractive, the enclosures increase the complexity of the waterbolus system and will affect its robustness in the clinical setting.

The guideline for waterbolus dimensions, as presented in Chapter 4, triggered a re-design of the waterbolus to embed the optimal functioning of the LCA in the hardware ("quality by design"). The new waterbolus features a transparent stretchy polyurethane membrane envelope, an open-cell, low-density foam insert, and partitions. Four standard waterbolus sizes were defined, to accomodate different array dimensions. The foam insert

(*i*) makes the waterbolus dimensionally stable, (*ii*) assures a waterlayer thickness and extension of the bolus outside the array in conformity with the new Rotterdam QA guideline, and (*iii*) facilitates the correct placement of the applicators (tactile feedback and visual clues). The partitions improve shape stability. They also direct the flowpath of the water, thereby effectively cooling the whole skin-waterbolus interface. The polyurethane envelope enhances patient's comfort.

The waterbolus has two functions: to couple EM waves into the patient, and to cool the skin surface. Therefore, another point of consideration was to assess the cooling effect of the waterbolus on the temperature distribution in a patient. This research led to a new guideline for the waterbolus temperature, which is presented in Chapter 5. Quantification of the cooling effect is complex: the effective heat transfer depends on the waterbolus/recirculator combination, and may vary across the waterbolus area. The approach used in the the analysis presented in Chapter 5 is therefore practical: the effective heat transfer was derived from measurements, and this was done for each waterbolus dimension separately. This way, the waterbolus temperature guideline is specific for each waterbolus size. This implies that the guideline is not indicative for other applicator systems, unless it is clear from measurements that those other systems have comparable heat transfer coefficients.

The measured heat transfer coefficients can also be applied in thermal simulations in treatment planning. As discussed in Chapter 5, the convective boundary is a better choice than the alternative, a constant temperature boundary, in SHT treatment planning. The latter is tricky because it fixes the temperature distribution at the skin surface, assuming an unlimited heat flux through the waterbolus/skin interface, which in reality is limited. In short, knowledge of the effective heat transfer of a waterbolus is esential for steering as well as treatment planning.

Characterisation of applicators for superficial hyperthermia

Measurements of SAR patterns for many different applicator systems for superficial hyperthermia have been published over the last 25 years. By far the majority of measurements were performed by the group who developed the applicator, with the locally available tools (e.g. infrared camera or E-field sheet and flat phantoms, scanning E-field probe and phantom bath). Several limitations exist here:

- The measurement data usually consist of a set of normalised 2D SAR profiles, which cover only part of the 3D applicator target volume. The SAR values are seldomly related to input powers.
- The measurement set-up (flat phantom tissue, or rectangular liquid phantom) has limited relevance for the clinical situation. Target volumes may have flat, convex, concave, cylindrical, and uneven/irregular shapes in the clinic.

- Applicator efficiency and performance at significant power levels is hardly ever measured. Efficiency is a quality indicator for a HT applicator. Inefficient applicators tend to self-heat and to overload the amplifier system, which may put the system out of order within the timeframe of a treatment. Moreover, clinically applied powers cannot be compared between applicator types if their efficiencies are not quantified.
- An evaluation of performance by the developers of an applicator system may lead to a biased interpretation of results.

For a more objective comparison and appropriate selection of applicators in the future, the following points are recommended (see Chapter 7 for more details):

- Evaluations preferably by a third party, using high-level standardized equipment.
- Quantification of the full 3D SAR distribution in the applicator target volume at a fixed power input, and quantification of the applicator efficiency.
- Development of several anthropomorphic phantom shapes to qualify applicators for specific applications.
- Inclusion of measurements after running the equipment for 1 hour at maximum power.

Note that high-quality measurements of the full 3D SAR distribution also contribute to a more profound validation of treatment planning models.

The measurements presented in Chapter 7 implement part of these items, by adopting methods and tools from the IEEE-1528 standard. A limited set of anthropomorphic phantom shapes for superficial hyperthermia should be developed. It may not be feasible for research groups to test their (pre-)clinical applicators using state-of-the-art equipment. However, commercial parties selling superficial hyperthermia systems must be prepared to fully assess the quality of their equipment for clinical treatment sites and to extensively communicate this to their users.

The role of modelling and treatment planning

Models are simplifications of reality to gain insight. In this thesis, models serve three main purposes: (*i*) the development of new systems, (*ii*) optimization, and (*iii*) exploration of new applications. Within the scope of this thesis, models were used to support the development of a new waterbolus for LCA arrays. Following on the assessment of critical waterbolus dimensions in Chapter 4, the effect of waterbolus edge shape on the SAR distribution was explored in its redesign (Figure 1).

The use of modelling for optimization of treatments was applied in Chapter 8. It must be stated that the scope of the optimizations were somewhat limited, because the iterations were implemented manually. The optimization parameters in superficial hyperthermia include applicator type and orientation, placement of applicators onto the patient, and

power variations. Except for power variations, each optimization iteration requires the generation and simulation of a separate model. Therefore, a fully-fledged optimization procedure requires automatic model generation, which was not available at the time of the research. Chapter 8 also demonstrates the use of treatement planning to explore new applications, especially to check the feasibility of heating non-standard target volumes, and to reconsider contraindications (e.g. metallic implants, tumour depth beyond standard maximum target volume depth).
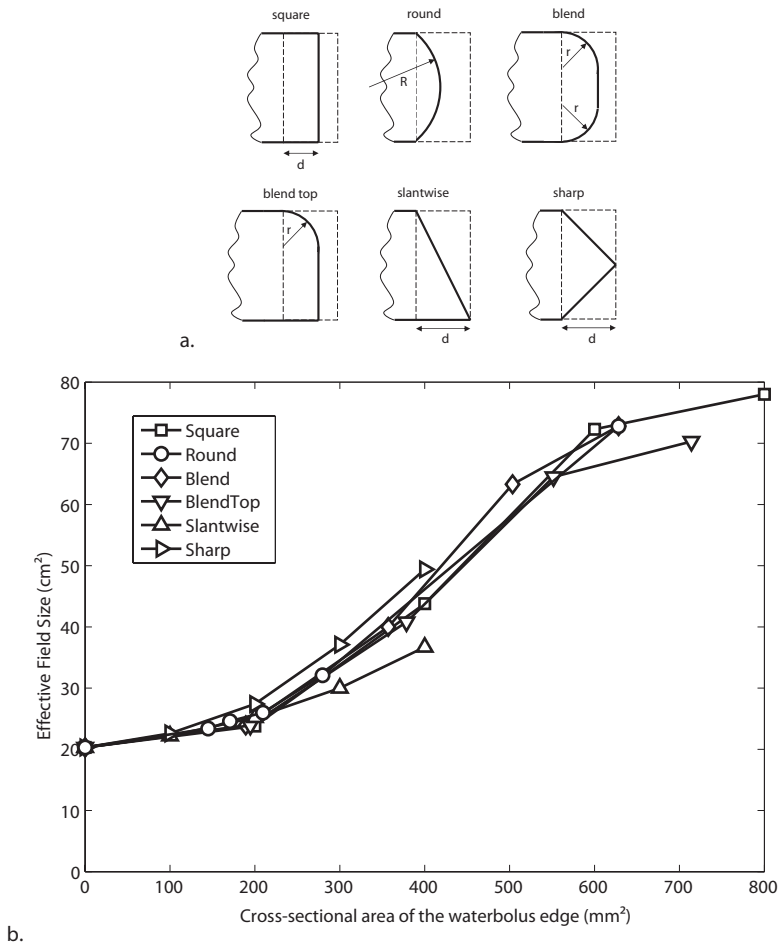
Figure 1. The effect of waterbolus edge shape on the effective field size (EFS) of the LCA. A single LCA was tested with a 10×10×4 cm³ waterbolus, to which different edges were added. The maximum edge extension was 2 cm. (a) The six edge shapes that were tested. The dashed lines indicate the maximum edge extension. (b) The effective field size of the LCA as a function of the cross-sectional area of the waterbolus edge. Edge shapes that add significant waterbolus volume prevent squeezing of the SAR distribution and thus low EFS values. Also, an enlarged waterbolus/tissue contact area does not guarantee optimal EFS.

Modelling with the purpose to explore the appropriate or optimal treatment approach is especially useful because a major problem in clinical hyperthermia is the limited observability: the electromagnetic field is invisible for humans, and its effect –the heating of tissue– can only sparsely be observed through thermometry. Here, model predictions can provide valuable insight before, during and after treatments. Visualisation of EM fields and SAR patterns enhances understanding. This way, models provide valuable backup for decisions that would otherwise be based on intuition. Also models form a great support to demonstrate the effects of steering and set-up on SAR patterns for educational purposes.

In this thesis, treatment planning was done off-line. The functionality of treatment planning models and the speed of simulation platforms continue to increase dramatically, allowing a further integration of the tools in the clinic to fully exploit their benefits. In Chapter 8 the focus was on the demonstration of feasibility and benefits of treatment planning in SHT. The value of treatment planning in terms of improved clinical response has not been assessed within the scope of this research. This can be demonstrated in a clinical study as soon as the tools are ready for routine planning. Currently, the relation between treatment outcome and parameters derived from calculated 3D SAR distributions is tested in a clinical study which includes 70 patients with a breast cancer recurrence at the chest wall. The ultimate goal here is to abandon the cumbersome and painful interstitial thermometry.

For a correct interpretation of results, validation of models is mandatory and should be considered a prerequisite for integration of a hyperthermia treatment planning system in clinical practice. A first set of validation experiments was presented in Chapter 4, to check whether the waterbolus effects were predicted correctly by the model. In Chapter 7 the LCA applicator model was validated more thoroughly against state-of-the-art SAR measurements. In radiotherapy, one of the commonly applied validation techniques is the gamma method. This method has now been introduced in hyperthermia, to move from a subjective interpretation of findings to an objective comparison between model prediction and measurement. A single quantity (γ_{95}) indicates the quality of the overall match, given a set of distance-to-agreement and dose-difference criteria. Now that treatment planning is increasingly applied in the clinic, quantitative model validation should become part of general hyperthermia quality assurance protocols.

Some additional comments on the use of a thermal dose as a quality indicator

The CEM43°CT90 thermal dose parameter has a long history. In 1991, Perez *et al.* [5] reported that their randomized phase III trial showed no significant overall difference in tumour response rates of superficial tumours treated with irradiation alone or combined with hyperthermia. The problems to demonstrate the effectiveness of hyperthermia in this clinical trial triggered a QA discussion [6], which culminated in the famous quote: "If we can't define the quality, can we assure it?" [7]. Starting from the observation that tumour temperature distributions predicted the hyperthermia effect [8], unambiguous thermal

dosimetry [9] was seen as the solution by the leading North-American hyperthermia group. Therefore a system to convert time-temperature relationships to a thermal dose (expressed in cumulative equivalent minutes) was set up [10,11], with the endpoint of setting a thermal goal for treatments [12,13].

Two phase III trials in which the prescribed thermal doses were tested, were published in 2005 [14,15]. The first was a study by Thrall *et al.* who treated canine sarcomas with radiotherapy plus hyperthermia. The dogs were randomized to receive either a low or a high thermal dose. The second was the study by Jones *et al*, who treated superficial tumours with thermoradiotherapy. Here all patients received a 1-hour hyperthermia test treatment and, if passed the test, were randomized for no further hyperthermia or a target dose of 10 equivalent minutes thereafter. Both trials clearly demonstrated the clinical benefit of adding hyperthermia to radiotherapy. However the advantage of thermal dose prescription was not convincingly demonstrated. The main criticisms are:

- Patients who had "unheatable" tumours were excluded in both trials. Still, these patients may well benefit from hyperthermia treatments, because the different hyperthermia mechanisms (direct cell kill at higher temperatures, enhancement of radiotherapy, improvement of oxygenation, stimulation of the immune system) come into play at different temperatures [16].
- In the study by Jones *et al.* two separate thermal dose categories were planned: ≤ 1 equivalent minutes for the no further HT group, and > 10 equivalent minutes for the HT group. However, the actual thermal dose ranges of these groups overlapped: 0.07 - 1.49 eq.min. for no further HT, and 0.57 - 36.21 eq.min. for the HT group. Further, the difference in CR rate was not statistically significant for patients without prior radiotherapy. Also, the tumour size and number of measurement points were not considered in the analysis.
- In the study by Thrall *et al.*, the difference in local control duration was only significant after correction for several prognostic factors, amongst which total treatment duration. This cumulative duration of all hyperthermia treatments is a confounding factor, as it will be influenced by tumour characteristics [17]. Also, the factor time is already taken into account in the thermal dose equation.
- Thrall *et al.* treated anaesthetized dogs with a single tumour mass, which is a distinctly different clinical setting than the treatment of non-anaesthetized human patients with single or multiple tumour sites.

Because CEM43°CT90 has been declared a dose parameter that should be prescribed and has been proclaimed "the key to hyperthermia's future" [18] after these trials, it should be tested whether it meets the principal requirements of a dose. The analysis of Rotterdam clinical data in Chapter 3 indicates that CEM43°CT90 is not a generally applicable dose parameter for reirradiation plus hyperthermia in recurrent breast cancer: it was shown that

no benefit should be expected from setting a thermal dose target, or from selecting patients by a heatability test.

The basic problem of the CEM43°CT90 parameter is that its formulation is based on cell heating experiments looking at direct heat cytotoxicity in the laboratory, whereas in the clinic many other mechanisms act at the tumour/patient level, and measurement and control of temperatures is more complex. Two examples of issues are: (*i*) hyperthermia anti-tumour mechanisms other than direct heat cytotoxicity are not in its formulation, and (*ii*) measured temperatures interact with tumour properties such as perfusion and size. The concerns are not new: already in early analyses of thermal parameters it was noted that much is arbitrary in the computation of thermal dose, and the applicability of thermal isoeffect dose formulae to treatment of human tumours is controversial [12,19]. Nowadays, the topic is still controversial. In Europe, the need for thermal dose prescription and its general applicability is questioned. In the USA, groups seem to embrace thermal dose as an important QA tool, and discussions on the appropriateness of the thermal dose concept are considered potentially harmful for the renewed acceptance of hyperthermia in the USA due to the two succesful randomized trials.

Apart from scientific considerations, there are also practical objections to the use of CEM43°CT90 prescription. First, thermal dose prescription basically implies varying treatment duration, because tissue temperatures are limited by patient's tolerance and hot spots. Introducing a variable treatment duration substantially decreases the clinical capacity, because time slots can be less efficiently used. For the Rotterdam clinic, at least a five-fold reduction of the clinical capacity would be expected[1]. Second, a thermal dose regime requires extensive thermometry. It therefore excludes patients who, for medical or practical reasons, have no or very limited thermometry.

For the future of hyperthermia it is important that a well-defined clinical approach is selected which is proven effective, has the lowest price and complexity and is the least burden on the patient. The approach may differ between centres, depending on local protocols, equipment, logistics, etc. For the Rotterdam clinic this seems to be a fixed-schedule approach with about one 60-minute treatment per week, a focus on appropriate applicator selection and placement to achieve optimal SAR coverage, and a minimum invasive thermometry.

---

[1] Dose target is 10 CEM43°CT90. Actual dose delivery: median 4.8 CEM43°CT90 for 8×1 hr HT (Chapter 3). Current HT schedule is 4×1 hr (Chapter 2). Expected median 2.4 CEM43°CT90 for 4×1 hr HT, so setting the dose target implies a 4.2 times increase in net treatment time. Expected inefficiency due to flexible treatment duration: 30% (two instead of three treatment slots per day). Overall 5.4 times increase in clinical capacity needed.

Human factors and practice variation in day-to-day application of hyperthermia

Early pictures of the intended clinical set-up for superficial hyperthermia (e.g. Perez *et al.* [20]) show a feedback device that controls the power supply based on measured temperatures, see Figure 2. As described in Chapter 6, the clinical reality today is that automatic feedback control is still not applied. Instead, the control task is performed by a human operator. As a consequence, human performance may be one of the key determinants in clinical quality assurance. The question is how to deal with the human factor.
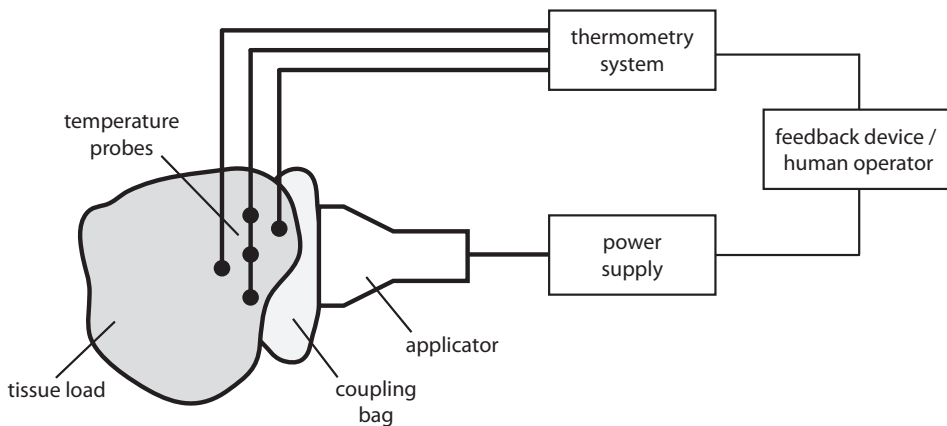
Figure 2. Schematic drawing of a typical hyperthermia clinical set-up, after [20]. The feedback loop is on the right: a 'feedback device' sets applicator powers based on measured temperatures; in practice this is a human operator.

The motivation of hyperthermia personnel plays a key role in delivering quality treatments. The motivation to push for maximum quality is especially relevant for the human controller in the clinic, because it is far more easy to reduce the power so that the patient does not complain, than to deal with the stress of frequent pain complaints when the power is pushed to obtain optimal heating. Or, as Clemenhagen [21] puts it: a lack of commitment is far more injurious to a quality assurance program than any technical flaws. In that sense, quality assurance guidelines can do little to guarantee everyday application of hyperthermia – it might even be frustrating for hyperthermists to be confronted with too much paperwork.

Practice variation is another critical factor [22]. Practice variation is evident in superficial hyperthermia, and can exist at the level of individuals and centres. The variation among hyperthermia technicians and its effect on clinical outcome has not been investigated scientifically. The review in Chapter 2 indicates that clinical results vary between treatment centres, suggesting that some practices are better at delivering hyperthermia. A big difference in the definition of the treatment goal (thermal dose

prescription vs. fixed schedule), which directly translates into practice variation, was highlighted in Chapter 3.

Transparency, exchange of information, peer review and open discussion may reduce practice variation between centers and within centres. In this light, Chapters 2 and 6 detail the clinical approach of the Rotterdam unit and the routine evaluation of treatments and steering performance in multidisciplinary discussions. Also, given the significant influence of the human factor in hyperthermia treatments, it makes sense to introduce a more formal and standardized training of clinical staff.

Final remarks

Apart from the topics addressed in this discussion, some final remarks will be made about the neccesary developments in the near future of clinical hyperthermia.

Currently there is no objective, proven quality indicator for superficial hyperthermia treatments. Quality indicators have been suggested, like SAR coverage of the target volume and CEM43°CT90 thermal dose derived from measured temperatures. Temperatures cannot be prescribed in the clinic with the current equipment, so thermal dose prescription basically boils down to a variation of treatment duration. In contrast, SAR patterns of applicator systems can be objectively determined and SAR coverage can be predicted. Therefore, SAR coverage currently is the most promising generally applicable quality indicator, and clinical testing of SAR prescription can be the next break through in hyperthermia.

Treatment planning may show the effect of virtually all factors that can be changed intentionally during treatments. Treatment planning tools should therefore be fully employed in clinical hyperthermia to identify the quality determinants for treatments, so that attention and efforts can be effectively focused. At the same time, the value of treatment planning and the colour pictures it produces should not be over-estimated. To allow transfer of modelling results to the clinic and vice versa it is essential that treatment planning tools are thoroughly validated, like any other clinical tool.

Nowadays hyperthermia is a recognized treatment and DBC-codes for insurance reimbursement have been defined for six indications in The Netherlands in 2009. This may attract new (commercial) hyperthermia initiatives and allows hyperthermia to move out of the academic context. Two hazards pop up here: (*i*) base quality levels for hyperthermia clinics have not been defined and (*ii*) formal HT training does not yet exist. These issues should be addressed to make it absolutely clear for patients (and insurance companies) what quality of treatment they can expect in a specific clinic. A logical next step to further professionalise clinical hyperthermia is to set up training programs for HT professionals (physicians, physician-assistants, technicians, physicists, treatment planning staff, calibration and maintenance staff). The following aspects are relevant for the definition of quality levels in superficial hyperthermia:

- Tumours treated
- Treatment schedules applied (proven by clinical studies, or arbitrary)
- Clinical results obtained
- Applicator system specifications
- Thermometry system specifications
- Steering approach and clinical procedures
- Treatment planning approach
- Calibration and maintenance program
- Patient care and -informing
- Treatment evaluation and documentation
- Team composition and skills

It may be expected that extensive discussions will be required in order to reach a consensus on the definition of the minimum acceptable quality, additional quality standards and audit procedures. The topics addressed in this thesis will provide a basis for the further professionalisation of clinical hyperthermia.

References

[1]   Gelvich EA, Mazokhin VN. Resonance effects in applicator water boluses and their influence on SAR distribution patterns. Int J Hyperthermia 2000;16:113-128.

[2]   Kroeze H, Van Vulpen M, De Leeuw AAC, Van De Kamer JB, Lagendijk JJW. The use of absorbing structures during regional hyperthermia treatment. Int J Hyperthermia 2001;17:240-257.

[3]   Kroeze H, Van Vulpen M, De Leeuw AAC, Van De Kamer JB, Lagendijk JJW. Improvement of absorbing structures used in regional hyperthermia. Int J Hyperthermia 2003;19:598-616.

[4]   Rossetto F, Stauffer PR, Manfrini V, Diederich CJ, Biffi Gentili G. Effect of practical layered dielectric loads on SAR patterns from dual concentric conductor microstrip antennas. Int J Hyperthermia 1998;14:553-571.

[5]   Perez CA, Pajak T, Emami B, Hornback NB, Tupchong L, Rubin P. Randomized phase III study comparing irradiation and hyperthermia with irradiation alone in superficial measurable tumors. Final report by the Radiation Therapy Oncology Group. Am J Clin Oncol 1991;14:133-141.

[6]   Perez CA, Gelliespie B, Pajak T, Hornback NB, Emami B, Rubin P. Quality assurance problems in clinical hyperthermia and their impact on therapeutic outcome: a report by the radiation therapy oncology group. Int J Radiation Oncology Biol Phys 1989;16:551-558.

[7]   Oleson JR. If we can't define the quality, can we assure it? Int J Radiat Oncol Biol Phys 1989;16:879.

[8]   Oleson JR, Dewhirst MW, Harrelson JM, Leopold KA, Samulski TV, Tso CY. Tumor temperature distributions predict hyperthermia effect. Int J Radiat Oncol Biol Phys 1989;16:559-570.

[9]   Leopold KA, Dewhirst MW, Samulski T, Harrelson J, Tucker JA, George SL, Dodge RK, Grant W, Clegg S, Prosnitz LR, *et al.* Relationships among tumor temperature, treatment time, and histopathological outcome using preoperative hyperthermia with radiation in soft tissue sarcomas. Int J Radiat Oncol Biol Phys 1992;22:989-998.

[10] Sapareto SA, Dewey WC. Thermal dose determination in cancer therapy. Int J Radiat Oncol Biol Phys 1984;10:787-800.

[11] Leopold KA, Dewhirst MW, Samulski TV, Dodge RK, George SL, Blivin JL, Prosnitz LR, Oleson JR. Cumulative minutes with T90 greater than Tempindex is predictive of response of superficial malignancies to hyperthermia and radiation. Int J Radiat Oncol Biol Phys 1993;25:841-847.

[12] Oleson JR, Samulski TV, Leopold KA, Clegg ST, Dewhirst MW, Dodge RK, George SL. Sensitivity of hyperthermia trial outcomes to temperature and time: implications for thermal goals of treatment. Int J Radiat Oncol Biol Phys 1993;25:289-297.

[13] Thrall DE, Rosner GL, Azuma C, Larue SM, Case BC, Samulski T, Dewhirst MW. Using units of CEM 43 degrees C T90, local hyperthermia thermal dose can be delivered as prescribed. Int J Hyperthermia 2000;16:415-428.

[14] Thrall DE, LaRue SM, Yu D, Samulski T, Sanders L, Case B, Rosner G, Azuma C, Poulson J, Pruitt AF, Stanley W, Hauck ML, Williams L, Hess P, Dewhirst MW. Thermal dose is related to duration of local control in canine sarcomas treated with thermoradiotherapy. Clin Cancer Res 2005;11:5206-5214.

[15] Jones EL, Oleson JR, Prosnitz LR, Samulski TV, Vujaskovic Z, Yu D, Sanders LL, Dewhirst MW. Randomized trial of hyperthermia and radiation for superficial tumors. J Clin Oncol 2005;23:3079-3085.

[16] Wust P, Hildebrandt B, Sreenivasa G, Rau B, Gellermann J, Riess H, Felix R, Schlag PM. Hyperthermia in combined treatment of cancer. Lancet Oncol 2002;3:487–497.

[17] Van der Zee J, van Rhoon CG, Rietveld PJM. No universally applicable thermal dose descriptor. Clin Cancer Res 2006;12:1943-1944.

[18] Jones E, Thrall D, Dewhirst MW, Vujaskovic Z. Prospective thermal dosimetry: the key to hyperthermia's future. Int J Hyperthermia 2006;22:247-53.

[19] Kapp DS, Cox RS. Thermal treatment parameters are most predictive of outcome in patients with single tumor nodules per treatment field in recurrent adenocarcinoma of the breast. Int J Radiat Oncol Biol Phys 1995;33:887-899.

[20] Perez CA, Emami B, Nussbaum GH. Clinical experience with external local hyperthermia in treatment of superficial malignant tumors. Front Radiat Ther Onc 1984;18:83-102.

[21] Clemenhagen CJ. Quality assurance in the hospital – making it work. Can Med Assoc J 1985;133:17-19.
[22] Dilts DM. Practice variation: the Achilles' heel in quality cancer care. J Clin Oncol 2005;23:5881-5882.

General conclusions

The conclusions regarding the individual research topics were presented at the end of each chapter. The main conclusions regarding quality assurance in superficial hyperthermia treatments are summarized in this final chapter:

- The waterbolus is a quality determinant for the Lucite cone applicator. Clinical quality assurance guidelines have been defined for the waterbolus dimensions and temperature. In principle, the effect of waterbolus dimensions, shape and temperature should be checked for every applicator type.
- Treatment planning was proven valuable in superficial hyperthermia. The use of treatment planning allows the identification of appropriate treatment strategies, especially in non-standard cases.
- An analysis of Rotterdam clinical data has shown that no benefit should be expected from a proposed CEM43°CT90 target dose of 10 equivalent minutes. Also, the proposed heatability testing did not select the responders in the same data of recurrent breast cancer patients treated with reirradiation plus hyperthermia.
- The human factor strongly determines the quality of superficial hyperthermia treatments, because the technician closes the feedback loop. Therefore a methodological evaluation of treatments and standardized training is essential.
- Treatment planning tools should be thoroughly validated, like any other tool introduced into the clinic. The gamma method is well suited for the quantitative validation of the 3D SAR profiles of hyperthermia applicators as predicted by treatment planning tools.
- Replacement of the current quality assurance guidelines with a quality stamp, which identifies a clinic's quality level based on an audit procedure, will represent a major step forward in hyperthermia quality assurance.

11

Summary

Summary

Superficial hyperthermia is an adjuvant to radiotherapy or chemotherapy in the treatment of cancer. During superficial hyperthermia treatments, a tissue volume in or several centimetres below the skin is heated to 45°C maximum. Randomised trials have demonstrated that the addition of hyperthermia increases complete response rates, extends duration of local control, and is a valuable tool in palliative care. The history and details of superficial hyperthermia treatments at the Erasmus MC were reviewed in Chapter 2. The Rotterdam hyperthermia unit uses a custom-built multi-applicator multi-amplifier superficial hyperthermia system operating at 433MHz. Up to six Lucite cone applicators (LCAs) can be used simultaneously to treat an area of 600 cm². Temperatures are measured continuously with fibre-optic multi-sensor probes. For patients with non-standard clinical problems, hyperthermia treatment planning is used to support decision making with regard to treatment strategy. A complete response (CR) is achieved in 74% of our patients with recurrent breast cancer, treated with a reirradiation scheme of 8 fractions of 4 Gy in 4 weeks, combined with 4 or 8 hyperthermia treatments. This is approximately twice as high as the CR rate following the same reirradation alone. The CR rate in tumours smaller than 30 mm is 80–90%; for larger tumours this is 65%. Hyperthermia appears beneficial for patients with microscopic residual tumour as well. To achieve high CR rates it is important to heat the whole radiotherapy field and to use an adequate heating technique.

The goal of the research described in this thesis was to identify quality determinants of superficial hyperthermia treatments, and to develop guidelines and tools to optimise the quality of treatments. The research focused on: identification of treatment goals, optimal application of the waterbolus, reduction of inter-operator differences, validation of treatment modelling tools, and optimisation of treatments for a specific patient.

The goal of treatment differs between superficial hyperthermia centres. Most centres apply fixed treatment intervals, for example sessions of 1 hour, once weekly. Other centres propagate the use of a target dose of 10 CEM43°CT90 (cumulative equivalent minutes at 43°C) and apply a flexible treatment time. The prospective use of the CEM43°CT90 thermal dose parameter has been proposed by others as a quality assurance tool for hyperthermia treatments. Its virtue was evaluated in Chapter 3 by means of a retrospective analysis of data from recurrent breast cancer patients who received reirradiation plus hyperthermia in Rotterdam. The CEM43°CT90 thermal dose was calculated for 72 patients who received 8×4 Gy reirradiation plus 8×1 hour hyperthermia for adenocarcinoma recurrences at the chest wall. A highly significant inverse association between CEM43°CT90 and tumour maximum diameter ($p < 1e\text{-}6$) was found. The association between complete response and CEM43°CT90 was not significant ($p \geq 0.7$). CEM43°CT90 was associated with duration of local control. Both CEM43°CT90 and tumour maximum diameter had a significant association with survival ($p \leq 0.01$). When adjusted for tumour maximum diameter, the association with thermal dose was not significant for either complete response, duration of

local control, or overall survival ($p > 0.2$). In short, the Rotterdam data showed no clear associations of CEM43°CT90 thermal dose with the clinical endpoints.

The development of clinical guidelines for the optimal application of the waterbolus (the water bag which is placed between the LCA and the patient) was discussed in Chapters 4 and 5. The first study (Chapter 4) targeted the effects of waterbolus dimensions and configuration on the effective field size (EFS) of the LCA. The effects of variations in (*i*) waterbolus thickness, (*ii*) waterbolus area, (*iii*) waterbolus length/width ratio and (*iv*) eccentric placement of the applicator have been investigated in a finite-difference time-domain (FDTD) model study. The prominent effects were verified with infrared thermography measurements. It is evident that a small (10×10 cm^2) waterbolus area restricts the EFS to 25% of the optimal value. Eccentric placement of the LCA near the waterbolus edge reduces the EFS to up to 50% of its optimum. The sensitivity to sub-optimal waterbolus area and length/width ratio increases with waterbolus height. Based on the results, the following guidelines for the clinical application of the waterbolus have been defined: the waterbolus should extend the LCA aperture at least 2.5 cm, especially at the Lucite windows, and the height should not exceed 2 cm. The second study, described in Chapter 5, investigated the influence of the waterbolus temperature on the tissue temperature distribution during superficial hyperthermia treatments. The goal here was to develop a guideline for the selection of the waterbolus temperature. A 3D electromagnetic and thermal model was set up to simulate an abstraction of the treatment. The optimal waterbolus temperature was determined for the most common target depths (0-1, 0-2, 0-3, 0-4, 1-3, 1-4 and 2-4 cm) and applicator array configurations (1×1, 1×2, 2×2 and 2×3 LCAs). A convection coefficient for the waterbolus/skin interface was employed in the model. Convection coefficients were measured for the different waterbolus dimensions, and ranged from 70 - 152 W/(m^2 K). The optimum waterbolus temperature was selected for each case by evaluating temperature-volume histograms, also taking into consideration the effects of perfusion and fat layer thickness. The resulting table serves as a guideline for the selection of the waterbolus temperature as a function of target depth and applicator array configuration.

Chapter 6 addresses the development of tools and methods for effective and efficient treatment evaluations. Systematic evaluation in a multidisciplinary team is used to secure the quality of steering as well as to stimulate general quality awareness of the hyperthermia team. Steering of multi-element heating arrays for superficial hyperthermia can be a challenge because the technician has to deal with a multiple-input multiple-output system, varying tissue dynamics, and often sparse tissue temperature data. In addition, patient feedback needs to be taken into account. Effective management of the steering task determines the quality of heating. To facilitate factual discussions, a treatment evaluation sheet was introduced which presents the power and temperature data in a compact and intuitive manner. Trend lines and a temperature-depth plot allow a quick analysis of the steering parameter values and the heating profile within the target volume. In addition, the principal statistics of applicator power, waterbolus- and tissue temperature values are given.

The power steering data includes the number of switch-off events, interruption time and the number of steering actions. A list of basic checks and reference values for clinical data support further the treatment evaluation. These tools and the systematic treatment evaluations they facilitate, ultimately lead to consistent performance and fine-tuning of the set-up and steering strategy for the individual patient.

The following two chapters deal with superficial hyperthermia treatment planning. The quantitative validation of the electromagnetic model of an applicator is an essential step in the quality assurance of hyperthermia treatment planning systems. This is the topic of Chapter 7. Quantitative validation has been applied for the FDTD model implementation of the Lucite cone applicator. The validation involved (*i*) the assessment of the match between the predicted and measured 3D specific absorption rate (SAR) distribution, and (*ii*) the assessment of the ratio between model power and real-world power. The 3D SAR distribution of seven LCAs was scanned in a phantom bath using the DASY4 dosimetric measurement system. The same set-up was modelled in the FDTD simulation package SEMCAD X. The match between the predicted and the measured SAR distribution was quantified with the gamma method, which combines distance-to-agreement and dose-difference criteria. Good quantitative agreement was observed: more than 95% of the measurement points met the acceptance criteria 2 mm / 2% for all applicators. The ratio between measured and predicted power absorption ranged from 0.75 to 0.92 (mean 0.85). The study showed that quantitative validation of hyperthermia applicator models is feasible and is worth considering as a part of hyperthermia quality assurance procedures.

The benefit of treatment planning in superficial hyperthermia has been demonstrated for five patient cases in Chapter 8. Treatment planning was applied to (*i*) troubleshoot treatment-limiting hot spots, (*ii*) to select the optimum applicator type and orientation, (*iii*) to assess the risk associated with metallic implants, (*iv*) to assess the feasibility of heating a deeper-seated tumour, and (*v*) to analyse the effective SAR coverage resulting from arrays of multiple applicators. FDTD simulations based on segmented or simplified anatomies were used to investigate treatment options. Predictions of the effective SAR coverage of the target and the location of the maximum power absorption were visualised and an optimum treatment strategy was selected. The implications for the course of subsequent treatments were given, for example: higher temperatures, relief of treatment limiting hot spots, or increased power input. It was shown that treatment planning in superficial hyperthermia is a tool to improve clinical routine. Its application supports the selection of the optimum technique in non-standard cases, leading to direct benefits for the patient. In addition, treatment planning has shown to be an excellent tool for training of hyperthermia technicians and physicians.

The general discussion and future perspectives of the research are given in Chapter 9. Next to the topics discussed in the previous chapters, some additional topics are: the controversy on treatment approaches based on CEM43°CT90 thermal dose, and the opportunities for third-party quality audits and formal hyperthermia training.

The main conclusions regarding quality assurance in superficial hyperthermia treatments were summarized Chapter 10:

- The waterbolus is a quality determinant for the Lucite cone applicator. Clinical quality assurance guidelines were defined for the waterbolus dimensions and temperature.
- Treatment planning was proven valuable in superficial hyperthermia. The use of treatment planning allows the identification of appropriate treatment strategies, especially in non-standard cases.
- An analysis of Rotterdam clinical data has shown that no benefit should be expected from a proposed CEM43°CT90 target dose of 10 equivalent minutes.
- The human factor strongly determines the quality of superficial hyperthermia treatments, because the technician closes the feedback loop. Therefore a methodological evaluation of treatments and standardized training is essential.
- Treatment planning tools should be thoroughly validated. The gamma method is well suited for the quantitative validation of the 3D SAR profiles of hyperthermia applicators as predicted by treatment planning tools.
- Replacement of the current quality assurance guidelines with a quality stamp, which identifies a clinic's quality level based on an audit procedure, will represent a major step forward in hyperthermia quality assurance.

12
Samenvatting

Samenvatting

Oppervlakkige hyperthermie wordt in combinatie met radiotherapie of chemotherapie toegepast bij de behandeling van kanker. Tijdens een oppervlakkige hyperthermie behandeling wordt een weefselvolume in of enkele centimeters onder de huid verwarmd tot maximaal 45°C. Gerandomiseerde onderzoeken hebben aangetoond dat de toevoeging van hyperthermie de complete respons verbetert, de duur van locale controle verlengt, en dat het een waardevolle bijdrage levert in de palliatieve zorg. Hoofdstuk 2 geeft een overzicht van de ontwikkelingsgeschiedenis en details van oppervlakkige hyperthermie behandelingen. De Rotterdamse hyperthermie afdeling gebruikt voor het verwarmen een systeem met meerdere applicatoren (antennes) en meerdere versterkers die werken op 433 MHz. Tegelijkertijd kunnen er tot zes Lucite cone applicatoren (LCA's) worden gebruikt om een oppervlak van maximaal 600 cm² te behandelen. De weefseltemperatuur wordt continu gemeten met optische glasfiber thermometers met meerdere sensoren. Voor niet-standaard klinische gevallen wordt een hyperthermie planningssysteem ingezet om de besluitvorming rond de te volgen behandelstrategie te ondersteunen. Een complete respons (CR) wordt bereikt in 74% van de patiënten met recidief borstkanker, die behandeld zijn met een bestralingsschema van 8×4 Gy in 4 weken, plus 4 of 8 hyperthermie behandelingen. Dit responspercentage is ongeveer tweemaal zo hoog als bij herbestraling alleen. Het responspercentage voor tumoren kleiner dan 30 mm is 80-90%; voor grotere tumoren is dit 65%. Hyperthermie biedt ook voordeel voor patiënten met microscopische tumoren. Om een hoog responspercentage te bereiken is het van belang om het hele radiotherapieveld te verwarmen en om adequate verwarmingstechnieken toe te passen.

Het doel van het onderzoek beschreven in dit proefschrift is het identificeren van de factoren die de kwaliteit van oppervlakkige hyperthermie behandelingen bepalen, en om richtlijnen en gereedschappen te ontwikkelen om die kwaliteit te optimaliseren. Het onderzoek heeft zich toegespitst op: het bepalen van het behandeldoel, het optimaal toepassen van de waterbolus, het verminderen van verschillen tussen behandelaars, de validatie van modellen en het optimaliseren van behandelingen voor specifieke patiënten.

Het behandeldoel verschilt tussen oppervlakkige hyperthermie klinieken. De meeste klinieken passen een vaste behandelduur toe, bijvoorbeeld 1× per week 1 uur. Andere centra propageren het gebruik van een doeldosis van 10 CEM43°CT90 (cumulatief equivalente minuten op 43°C) en passen een flexibele behandelduur toe. Het voorschrijven van een CEM43°CT90 thermische dosis is - door anderen - voorgesteld als een middel voor kwaliteitsborging. In hoofdstuk 3 is de waarde van deze dosisparameter getest door middel van een retrospectieve analyse van data van borstkanker patiënten die in Rotterdam behandeld zijn. De CEM43°CT90 thermische dosis werd berekend voor 72 patiënten die 8×4 Gy herbestraling kregen en 8×1 uur hyperthermie voor terugkerend adenocarcinoom op de borstkas. Er was een zeer significant verband tussen CEM43°CT90 en de maximale tumor diameter ($p < 1e-6$). Het verband tussen CR en CEM43°CT90 was niet significant

(p > 0.7). CEM43°CT90 hing wel samen met de duur van locale controle. Zowel CEM43°CT90 als de maximale tumor diameter waren significant gerelateerd aan de overleving ($p \leq 0.01$). Na correctie voor maximum tumordiameter was er geen significant verband tussen thermische dosis en CR, duur van locale controle, of overleving (p > 0.2). Kortom, de Rotterdamse data toonde geen duidelijk verband tussen CEM43°CT90 thermische dosis en de klinische eindpunten.

In de hoofdstukken 4 en 5 wordt het ontwikkelen van klinische richtlijnen voor de optimale toepassing van de waterbolus (de waterzak die tussen de applicator en de patient wordt gelegd) behandeld. De eerste studie (hoofdstuk 4) richt zich op het effect van waterbolus afmetingen en configuratie op de effectieve veldgrootte (EFS). De effecten van (*i*) waterbolus dikte, (*ii*) oppervlak, (*iii*) lengte/breedte verhouding en (*iv*) excentrische plaatsing van de applicator zijn onderzocht met een finite difference time domain (FDTD) model. De voornaamste effecten zijn gevalideerd met infrarood temperatuur metingen. Het is duidelijk dat een klein waterbolus oppervlak (10×10 cm²) de EFS reduceert tot 25% van de optimale waarde. Wanneer de LCA bij de rand van de waterbolus wordt geplaatst, kan dit de EFS reduceren tot 50% van z'n optimum. De gevoeligheid voor een suboptimale grootte of lengte/breedte verhouding van de waterbolus neemt toe met de dikte van de waterlaag. De volgende richtlijnen voor klinische toepassing van de waterbolus zijn gedefinieerd: de waterbolus moet minimaal 2.5 cm uitsteken buiten de LCA's en de bolus moet niet hoger zijn dan 2 cm. De tweede studie (hoofdstuk 5) gaat in op de invloed van de waterbolus temperatuur op de temperatuurverdeling in het weefsel tijdens oppervlakkige hyperthermie behandelingen, met als doel een richtlijn voor de waterbolus temperatuur op te stellen. Om een abstractie van de behandeling te simuleren, is een 3D electromagnetisch en thermisch model opgesteld. De optimale waterbolus temperatuur werd bepaald voor de meest voorkomende doeldieptes (0-1, 0-2, 0-3, 0-4, 1-3, 1-4 en 2-4 cm) en applicator opstellingen (1×1, 1×2, 2×2 en 2×3 LCA's). In het model werd een convectie coefficient toegepast voor de waterbolus/huid interface. Convectie coefficienten zijn gemeten voor verschillende waterbolus afmetingen, en varieerden van 70-152 W/(m²K). De optimale waterbolus temperatuur werd gekozen door temperatuur-volume histogrammen te evalueren, waarbij ook de effecten van doorbloeding en dikte van de vetlaag zijn meegenomen. De resulterende tabel dient als klinische richtlijn voor de selectie van de waterbolus temperatuur, gegeven een diepte van het doelgebied en applicator configuratie.

Hoofdstuk 6 behandelt de ontwikkeling van hulpmiddelen en methodes voor effectieve en efficiente evaluaties van behandelingen. Systematische evaluatie in een multidisciplinair team wordt toegepast om de kwaliteit van sturen te borgen en om het algemene kwaliteitsbewustzijn van het team te stimuleren. Het sturen van een configuratie met meerdere antennes kan een uitdaging zijn, omdat de laborant te maken heeft met een multi-input multi-output systeem, varierende weefseldynamica en een vaak beperkt aantal temperatuur metingen. Daarbij moeten ook de signalen van de patient worden meegenomen. Het effectief uitvoeren van de stuurtaak bepaalt de kwaliteit van verwarmen. Om een op de feiten gerichte discussie te bevorderen is een evaluatiesheet geïntroduceerd

waarop de vermogens- en temperatuur data op een compacte en intuïtieve manier wordt weergegeven. Trendlijnen en een temperatuur-diepte diagram geven snel een beeld van de stuurparameters en van het verwarmingsprofiel in het doelvolume. Daarnaast worden de belangrijkste statistieken van de applicatorvermogens en de waterbolus- en weefseltemperaturen gegeven. Voor de applicatoren wordt ook het aantal keer dat het vermogen is uitgezet, de tijd dat het vermogen uit stond en het aantal stuuracties weergegeven. Verder wordt de evaluatie van behandelingen ondersteund met een lijst van basale checks en referentiewaardes. Deze middelen en de systematische evaluatie die zij ondersteunen moeten uiteindelijk leiden tot constante prestaties en het op de individuele patient afstemmen van de behandelstrategie.

Het onderwerp van de volgende twee hoofdstukken is behandelplanning in oppervlakkige hyperthermie. Kwantitatieve validatie (hoofdstuk 7) is een essentiele stap in de kwaliteitsborging van hyperthermie planningssystemen. Kwantitatieve validatie is toegepast voor de FDTD model implementatie van de LCA. De validatie omvat: (*i*) het vaststellen van de mate van overeenkomst van de voorspelde en de gemeten 3D SAR[1] verdeling en (*ii*) het bepalen van de verhouding tussen het vermogen in het model en dat in de echte wereld. De 3D SAR verdeling van zeven LCA's is gemeten in een fantoombad met het DASY4 dosimetrisch meetsysteem. Dezelfde configuratie werd gemodelleerd in het FDTD simulatiepakket SEMCAD X. De overeenkomst van de gemeten en de voorspelde SAR verdeling werd gekwantificeerd met de gamma methode, die de criteria afstand-tot-overeenkomst en dosisverschil combineert. Er werd een goede kwantitatieve overeenkomst gevonden: meer dan 95% van de meetpunten voldeed voor alle applicatoren aan de criteria 2mm / 2%. De verhouding van gemeten en voorspeld vermogen varieerde van 0.75 tot 0.92 (gemiddeld 0.85). De studie toont aan dat het kwantitatief valideren van modellen van hyperthermie applicatoren haalbaar is en dat het de moeite waard is om dit op te nemen in procedures voor kwaliteitsborging in de hyperthermie.

De meerwaarde van het toepassen van behandelplanning in oppervlakkige hyperthermie is aangetoond in hoofdstuk 8 aan de hand van vijf klinische voorbeelden. Behandelplanning werd toegepast om: (*i*) beperkende hot-spots te onderzoeken, (*ii*) het optimale applicatortype en de juiste orientatie te selecteren, (*iii*) het risico van metalen implantaten in te schatten, (*iv*) vast te stellen of dieper gelegen tumoren kunnen worden verwarmd, en (*v*) om de effectieve SAR bedekking bij meerdere incoherent gestuurde antennes te analyseren. Om de behandelopties te onderzoeken werden FDTD simulaties op basis van een gesegmenteerde of een gesimplificeerde anatomie uitgevoerd. Om een strategie te kunnen bepalen werden de voorspelde effectieve SAR bedekking van het doelgebied en de ligging van de pieken in vermogensabsorptie gevisualiseerd. De impact hiervan op volgende behandelingen was bijvoorbeeld: hogere temperaturen, het wegvallen van hot-spots die eerder de behandeling beperkten, of een verhoogd applicator vermogen.

---

[1] SAR = Specific Absorption Rate of absorptietempo, maat voor de absorptie van energie uit een electromagnetisch veld in het weefsel.

Aangetoond is dat behandelplanning het kiezen van een optimale behandelstrategie, met name in niet-standaard gevallen, in belangrijke mate ondersteunt. Dit leidt tot een directe winst voor de patient. Verder is gebleken dat behandelplanning een uitstekend hulpmiddel is voor de opleiding van laboranten en artsen.

Hoofdstuk 9 bevat een algemene discussie van het onderzoek en een schets van de toekomstperspectieven die het biedt. Behalve de onderwerpen die in eerdere hoofdstukken zijn bediscussieerd, komen hier nog aan bod: het verschil van inzicht over de behandelaanpak op basis van CEM43°CT90 thermische dosis en de mogelijkheden die er zijn voor kwaliteitsinspecties door onafhankelijke partijen en voor een meer formele opleiding.

De belangrijkste conclusies met betrekking tot kwaliteitsborging in oppervlakkige hyperthermie zijn samengevat in hoofdstuk 10:

- De waterbolus is een kwaliteitsbepalende factor voor de LCA. Klinische richtlijnen zijn opgesteld voor de waterbolus temperatuur en configuratie.
- Er is aangetoond dat behandelplanning waardevol is in oppervlakkige hyperthermie. Toepassing ervan maakt het vaststellen van de juiste behandelstrategie mogelijk, vooral in niet-standaard gevallen.
- Een analyse van Rotterdamse klinische data heeft laten zien dat er geen enkele meerwaarde hoeft te worden verwacht van het toepassen van de voorgestelde CEM43°CT90 doeldosis van 10 equivalente minuten.
- Menselijke factoren bepalen in sterke mate de kwaliteit van behandeling, omdat de laborant in de kliniek de terugkoppellus sluit. Daarom is het essentieel dat behandelingen goed worden geëvalueerd en dat opleiding wordt gestandaardiseerd.
- Planningssystemen voor hyperthermie moeten grondig worden gevalideerd. De gamma methode is prima geschikt om de 3D SAR verdeling van hyperthermie applicatoren, zoals voorspeld door modellen, te valideren.
- Het vervangen van de huidige kwaliteitsrichtlijnen door een keurmerk dat het kwaliteitsniveau van een kliniek aangeeft, zou een grote stap voorwaarts zijn in de kwaliteitsborging van hyperthermie behandelingen.

13

Publications and honours
Curriculum vitae
Acknowledgements

Publications in peer-reviewed journals

de Bruijne M, van der Zee J, Ameziane A, van Rhoon GC. Quality control of superficial hyperthermia by treatment evaluation. Int J Hyperthermia 2011;27:199-213.

de Bruijne M, van der Holt B, van Rhoon GC, van der Zee J. Evaluation of CEM43°CT90 thermal dose in superficial hyperthermia: a retrospective analysis. Strahlenther Onkol 2010;186:436-443.

van der Zee J, de Bruijne M, Mens JW, Ameziane A, Broekmeyer-Reurink MP, Drizdal T, Linthorst M, van Rhoon GC. Reirradiation combined with hyperthermia in breast cancer recurrences: overview of experience in Erasmus MC. Int J Hyperthermia 2010;26:638-648.

Franckena M, Fatehi D, de Bruijne M, Canters RA, van Norden Y, Mens JW, van Rhoon GC, van der Zee J. Hyperthermia dose-effect relationship in 420 patients with cervical cancer treated with combined radiotherapy and hyperthermia. Eur J Cancer 2009;45:1969-1978.

Fatehi D, van der Zee J, de Bruijne M, Franckena M, van Rhoon GC. RF-power and temperature data analysis of 444 patients with primary cervical cancer: deep hyperthermia using the Sigma-60 applicator is reproducible. Int J Hyperthermia 2007;23:623-643.

de Bruijne M, Wielheesen DH, van der Zee J, Chavannes N, van Rhoon GC. Benefits of superficial hyperthermia treatment planning: five case studies. Int J Hyperthermia 2007;23:417-429.

de Bruijne M, Samaras T, Chavannes N, van Rhoon GC. Quantitative validation of the 3D SAR profile of hyperthermia applicators using the gamma method. Phys Med Biol 2007;52:3075-3088.

van der Gaag ML, de Bruijne M, Samaras T, van der Zee J, van Rhoon GC. Development of a guideline for the water bolus temperature in superficial hyperthermia. Int J Hyperthermia 2006;22:637-656.

van der Zee J, de Bruijne M, van Rhoon GC. Thermal medicine, heat shock proteins and cancer. Int J Hyperthermia 2006;22:433-437.

Fatehi D, de Bruijne M, van der Zee J, van Rhoon GC. RHyThM, a tool for analysis of PDOS formatted hyperthermia treatment data generated by the BSD2000/3D system. Int J Hyperthermia 2006;22:173-184.

de Bruijne M, Samaras T, Bakker JF, van Rhoon GC. Effects of waterbolus size, shape and configuration on the SAR distribution pattern of the Lucite cone applicator. Int J Hyperthermia 2006;22:15-28.

Wielheesen DH, de Bruijne M, Graveland WJ, van Rhoon GC, van der Zee J. Leg coverage with towels during regional deep hyperthermia treatment and its effect on pelvic temperature and temperature distribution. Int J Hyperthermia 2005;21:77-87.

The QR codes in the right column provide direct links to the abstracts on PubMed.org.

Honours

International Journal of Hyperthermia Editor's Award for Best Paper in Physics and Engineering from a Young Investigator in 2007

Young Investigator Travel Award of the 9th International Congress on Hyperthermic Oncology (ICHO), 2004, St.Louis, USA

Curriculum Vitae

Maarten de Bruijne

Born January 5th, 1973 in Ede, The Netherlands

1985 – 1991	Secondary school (Gymnasium), Marnix College, Ede, The Netherlands.
1991 – 1999	Masters Degree in Mechanical Engineering at Delft University of Technology, The Netherlands. Thesis: "Design of an actuator- and control system for fresh finger specimens".
1999 – 2002	Engineering Consultant at The MathWorks BV, Gouda, The Netherlands.
2002 – 2007	Hyperthermia Research Physicist at Erasmus MC – Daniel den Hoed Cancer Center, Rotterdam, The Netherlands.
2007 – present	Process Systems Engineer at the Energy research Centre of the Netherlands, Petten, The Netherlands.

Acknowledgements

A word on the wordles

The cover and title pages of this thesis are illustrated with word clouds, also known as wordles. Wordles graphically represents the contents of a text. In the word cloud, the "importance" (frequency of occurrence) of a word determines its dimensions. Wordles provide a visual way to analyse texts. For the lazy reader, they offer a quick answer to the question: what is this all about?

Thanks to Jonathan Feinberg (www.wordle.net) for providing a nice wordle generator.